Molecular recognition of aberrant translation

Szymon Juszkiewicz

MRC Laboratory of Molecular Biology
and
St Catharine's College

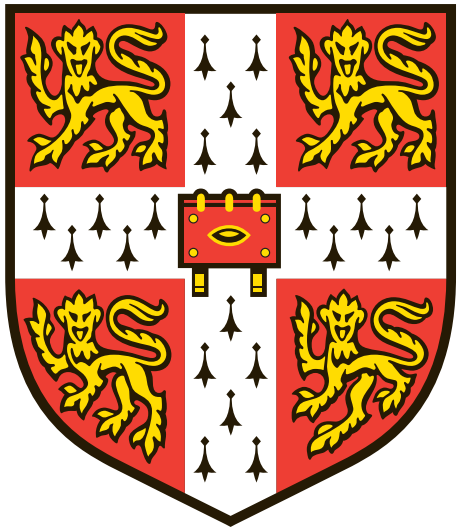

This dissertation is submitted for the degree of

Doctor of Philosophy

University of Cambridge
March 2019

For my parents

Declaration

This dissertation is the result of my own work and includes nothing which is the work done in collaboration except where specifically indicated in the text. It is not substantially the same as any that I have submitted, or, is being concurrently submitted for a degree or diploma or other qualification at the University of Cambridge or any other University or similar institution. It does not exceed the prescribed word limit for the Biology Degree Committee.

Szymon Juszkiewicz,
March 2019

Summary

Molecular recognition of aberrant translation

Szymon Juszkiewicz

Protein translation is a fundamental, demanding process which requires several million ribosomes and consumes as much as 75% of cellular energy. Because of its importance, translation is regulated at many levels to maintain its high fidelity, with both substrates and synthesized products monitored by numerous quality control mechanisms. While post-translational quality control of proteins has been studied extensively, the mechanisms of co-translational quality control of nascent polypeptides, mRNA and the ribosome itself have only recently been appreciated.

One of the major unanswered questions is how quality control mechanisms manage to specifically identify an aberrant event amid widely heterogenous normal physiologic states. This question forms the basis of this thesis, which is focused on understanding the molecular principles that determine accurate recognition of aberrantly slow ribosomes. To address this, we developed a novel flow cytometry-based assay to visualize terminal ribosome stalling at single cell resolution in mammalian cells. Using the assay, we firmly established that poly(A) messenger RNA (mRNA) is the most potent cause inducing terminal stalling. This system also led us to the identification and downstream characterization of a novel protein factor, the E3 ubiquitin ligase ZNF598, which we showed to be involved in triggering the quality control pathway during poly(A) translation. Subsequent *in vitro* ubiquitination experiments using purified ribosomes and ligase revealed molecular targets of ZNF598 - proteins eS10 and uS10 of the 40S ribosomal subunit. We further verified that ubiquitination of both targets is functionally important for poly(A)-mediated terminal stalling in cultured cells. Together, it led to the conclusion that ZNF598 recognizes excessively slow ribosomes and ubiquitinates them on the small subunit to initiate downstream quality control pathways responsible for the degradation of aberrant nascent proteins.

To further understand how ZNF598 specifically recognizes and ubiquitinates aberrantly translating ribosomes, we reconstituted its recruitment to poly(A)-stalled translation complexes in an *in vitro* translation system. Unexpectedly, these experiments

revealed that ZNF598 specifically associates with and ubiquitinates a sub-population of poly(A) stalled ribosomes consisting of closely-packed, collided di-ribosome species. This finding led to the general model of indirect detection of excessively slow ribosomes by ZNF598, whereby it recognizes ribosome collision events. We subsequently verified and generalised our proposed model using *in vivo* based experiments. In cultured cells, induction of stochastic ribosome collisions using sub-inhibitory doses of several unrelated translation elongation inhibitors led to the robust recruitment of ZNF598 to the sites of collisions, as manifested by ubiquitination of eS10.

Our results explain the mechanism for sensing excessively slow translation at the molecular level. Moreover, the proposed model has also profound implications for general cellular physiology. Most importantly, the use of ribosome collisions to infer stalling means the degree of slowdown tolerated on an mRNA is tuned by the frequency of translation initiation; hence, the threshold for triggering quality control is necessarily substrate-specific.

Publications

Volkmar, N., Thezenas, M.-L., Louie, S.M., **Juszkiewicz, S.**, Nomura, D.K., Hegde, R.S., Kessler, B.M., and Christianson, J.C. (2018). The ER membrane protein complex (EMC) promotes biogenesis of sterol-related enzymes maintaining cholesterol homeostasis. J. Cell Sci. 132, jcs223453.

Chitwood, P.J., **Juszkiewicz, S.**, Guna, A., Shao, S., and Hegde, R.S. (2018). EMC Is Required to Initiate Accurate Membrane Protein Topogenesis. Cell 175, 1507–1519.e16.

Juszkiewicz, S.*, Chandrasekaran, V.*, Lin, Z., Kraatz, S., Ramakrishnan, V., and Hegde, R.S. (2018). ZNF598 Is a Quality Control Sensor of Collided Ribosomes. Mol. Cell 72, 469–481.e7. (*These authors contributed equally to this work)

Juszkiewicz, S., and Hegde, R.S. (2018). Quality Control of Orphaned Proteins. Mol. Cell 71, 443–457.

Yanagitani, K., **Juszkiewicz, S.**, and Hegde, R.S. (2017). UBE2O is a quality control factor for orphans of multiprotein complexes. Science 357, 472–475.

Juszkiewicz, S., and Hegde, R.S. (2017). Initiation of Quality Control during Poly(A) Translation Requires Site-Specific Ribosome Ubiquitination. Mol. Cell 65, 743–750.e4.

Acknowledgements

This thesis and the incredible journey that led to it would not have been possible without the generous support and impact of numerous people.

First and foremost, I would like to thank my advisor and mentor Manu Hegde. I am, and always will be, grateful for the remarkable opportunity he gave me by taking me into his lab. He is an exceptional scientist, who by example taught me how to excel in all aspects of scientific work. What I cherish most is his incredible joy and passion for science. It has been an endless source of inspiration and motivation both in the lab and in my everyday life. These characteristics have made the last few years easily among the happiest and most rewarding time in my life.

I have also had the pleasure to work with a group of tremendous scientists. Collectively, they formed a unique, highly stimulating and interactive lab environment which made science even more exciting. I would specifically like to thank Kota Yanagitani and Susan Shao with whom I shared many valuable scientific insights and who introduced me to the wonderful world of *in vitro* biochemistry, Rebecca Voorhees for her insightful comments and suggestions, Eszter Zavodszky for sharing many handful tips and tricks (especially during the countless hours spent in the tissue culture room). More recently, John O'Donnell, a truly kindred spirit who quickly became one of my best friends and Zhewang Lin for his inspiring work ethics and great help with polysome profiling. Finally, my fellow graduate students Patrick Chitwood and Alina Guna for countless conversations in- and outside of the lab. Alina additionally deserves special thanks for her patient proofreading, which without a doubt has made this thesis much more comprehensible. I would also like to mention our collaborators and friends Vish Chandrasekaran and Sebastian Kraatz from the Ramakrishnan lab. We managed to tackle some challenging problems which would have been impossible without our effective teamwork.

The LMB as an institute is a unique place, where help is multi-faceted and generous. I would especially like to thank the in-house facilities, including the media kitchen, flow cytometry facility and mass spectrometry facility, which significantly contributed to the work presented in this thesis. I would also like to extend my gratitude to all my colleagues from the Cell Biology Division, but most importantly fellow students Stefano Giandomenico, Giulio Valperga and Patrick Hoffmann with whom I shared great

moments during our annual skiing trips and more regular stress-relieving sessions at the local climbing gym.

Finally, I want to thank my family for their continuous support and encouragement. My grandparents Krysia and Kazek are among my earliest fans who have always encouraged me to follow my dreams of a scientific career. It was as a result of our many discussions that I decided to pursue biotechnology instead of engineering. My parents deserve a very special thanks for providing me the most unimaginably best environment to grow up in. They gave me a complete freedom to pursue whatever I wished, and have continuously supported me even in my most inconceivable endeavours, like the attempt to do a PhD at the University of Cambridge. My brother Michał has been my staunch best friend that I can always count on, especially when I need a refreshing and truthful opinion. Last but not least, I would like to thank my dearest friend Marta, who has been and continues to be my greatest source of strength, support and inspiration. Through our companionship, we both embarked on this seemingly unthinkable journey and I could only hope we will continue to do so for years to come.

Abbreviations

aa-tRNA	aminoacyl-transfer ribonucleic acid
ABCE1	ATP-binding cassette sub-family E member 1
AP	arrested products
ASCC	Activating signal cointegrator 1 complex
A-site	acceptor site
ATP	adenosine 5’-triphosphate
CAT	C-terminal alanine tail
CHX	cycloheximide
CRISPR	clustered regularly interspaced short palindromic repeats
Cryo-EM	cryo electron microscopy
CUE	coupling of ubiquitin to ER degradation
DMSO	dimethyl sulfoxide
DNA	deoxyribonucleic acid
DTT	dithiothreitol
EDTA	ethylenediaminetetraacetic acid
eEF1	Eukaryotic elongation factor 1
eEF2	Eukaryotic elongation factor 2
EJC	exon junction complex
ER	endoplasmic reticulum
eRF1	Eukaryotic release factor 1
E-site	exit site
FACS	Fluorescence-activated cell sorting
FL	full length
GFP	Green fluorescent protein
GTP	guanosine 5’-triphosphate
HA	hemagglutinin
Hel2	Histone E3 ligase
HEPES	4-(2-hydroxyethyl)-1-piperazineethanesulfonic acid
kDa	kilodalton
KO	knockout
mRNA	messenger ribonucleic acid

NC	nascent chain
NEMF	Nuclear export mediator factor
NGD	no-go decay
NMD	nonsense-mediated decay
NSD	non-stop decay
PABP	Poly(A)-binding protein
PAGE	polyacrylamide gel electrophoresis
PBS	phosphate-buffered saline
Poly(A)	poly-adenosine
PSB	physiological salt buffer
P-site	peptidyl site
PTC	peptidyl transferase center
PTM	post-translational modifcations
RACK1	Receptor of activated protein C kinase 1
RFP	Red fluorescent protein
RING	really interesting new gene
RNA	ribonucleic acid
RNC	ribosome-nascent chain
RQC	ribosome-associated quality control
RRL	rabbit reticulocyte lysate
rRNA	ribosomal ribonucleic acid
SDS	sodium dodecyl sulfate
siRNA	small interfering ribonucleic acid
Slh1	Ski2-like helicase 1
SR	stalling reporter
TMT	tandem mass tagging
tRNA	transfer ribonucleic acid
Ub	ubiquitin
UTR	untranslated region
VCP	Valosin-containing protein
VHP	villin headpiece
WT	wild type
ZNF598	Zinc finger protein 598

Table of Contents

List of figures

Chapter 1: Introduction

The central dogma of molecular biology, as postulated by Crick in 1958, dictates that genetic information unidirectionally flows from nucleic acid to protein (Crick, 1958). A key step in this process is the translation of nucleic acid, at the stage of messenger RNA (mRNA), into an amino acid sequence. This essential task is performed by the ribosome, a large two subunit, highly conserved RNA-protein enzyme (Figure 1.1). The ribosome facilitates translation by creating a platform that allows transfer RNA (tRNA) to base pair with mRNA, which then results in the catalysis of a peptide bond between an incoming, tRNA-attached amino acid and the growing nascent polypeptide in the ribosome (Nissen et al., 2000).

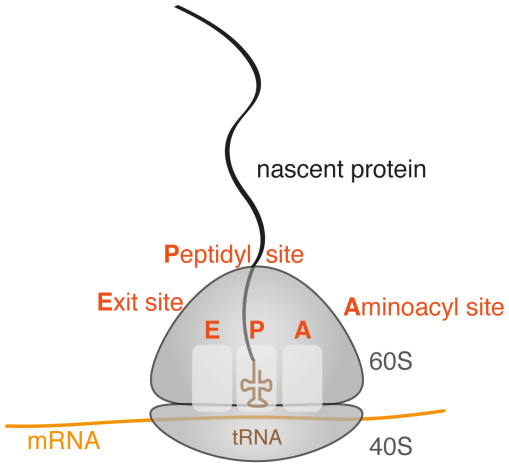

Figure 1.1 Overview of the ribosome. Ribosome consists of two subunits: 60S large subunit containing the active site of the enzyme and 40S small subunit, which binds the mRNA template. Protein synthesis occurs through binding of tRNAs and their associated amino acids to the ribosome as dictated by an mRNA template. tRNAs move sequentially through three ribosomal binding sites during translation: the aminoacyl (A), peptidyl (P), and exit (E) sites.

Protein translation is one of the most fundamental and energetically costly processes in the cell. In a typical mammalian cell, translation of the entire diverse proteome requires roughly 3 million ribosomes and amounts to as much as 75% of cellular energy expenditure (Wolff et al., 2014). In order to maintain faithful interpretation of the genetic code on such a large scale, cells have evolved multiple checkpoints to minimize the synthesis of faulty proteins. For example, tRNA synthetases often have proofreading activity to avoid tRNA mis-acylation (Ling et al., 2009), whereas kinetic proofreading enhances the accuracy of mRNA decoding at the ribosome

(Hopfield, 1974; Zaher and Green, 2009). The mRNA itself is also under stringent surveillance (Doma and Parker, 2007). In the nucleus, incompletely processed mRNAs lacking the essential poly(A) tail are effectively retained at the site of their transcription (Custodio et al., 1999), whereas mRNAs without 5' cap structure are exported to the cytoplasm and degraded by exonuclease (Schwer et al., 1998).

Despite these checks, the translation cycle is nevertheless prone to interruptions due to genetic mutations, mRNA maturation errors, damage to biosynthetic machinery, environmental stresses, and altered metabolic states. The timely detection and resolution of abnormal translation is essential for maintaining proteostasis and preventing disease (Chu et al., 2009; Ishimura et al., 2014; Lee et al., 2006). However, the molecular principles governing accurate recognition of aberrantly translating ribosomes amid millions of ribosomes translating at widely heterogenous speeds remain unknown.

1.1 Canonical translation cycle

Growing evidence suggests that the ribosome, as a central part of the translation cycle, can act as a recognition hub for the detection of aberrant translation (Shoemaker and Green, 2012), initiating downstream pathways of mRNA decay (Doma and Parker, 2006; Frischmeyer et al., 2002; Van Hoof et al., 2002), ribosome recycling (Pisareva et al., 2011; Shoemaker et al., 2010), nascent protein degradation (Ito-Harashima et al., 2007), stress responses (Brandman et al., 2012) and nutrient starvation (Marton et al., 1997). As such, it is essential to briefly discuss the major steps of protein synthesis.

The translational cycle is generally divided into four stages: initiation, elongation, termination and recycling (Figure 1.2). Initiation in eukaryotes is the most complicated step, but also has the least relevance for the work described in this thesis. It will be briefly discussed here; for more extensive background see (Hinnebusch, 2014; Hinnebusch and Lorsch, 2012). In short, initiation begins when the ternary complex, consisting of initiator methionyl-tRNA (Met-tRNA) and the GTP-bound form of eukaryotic initiation factor 2 (eIF2) binds to the small ribosomal subunit to form the 43S pre-initiation complex (43S PIC). This complex is additionally stabilised by eIF1, eIF1A, eIF5 and eIF3. 43S-PIC is recruited to the 5' end of the mRNA near the cap structure by more eIFs: 4A, 4B, 4E, 4G which together form a large complex which interacts with both the 5' cap and poly(A) binding protein (PABP). At this stage, the mRNA is in a characteristic 'closed-loop' structure. Once properly positioned near the cap, 43S PIC scans the mRNA for an AUG

start codon in a suitable sequence context, termed the Kozak consensus sequence (Kozak, 1986). AUG recognition leads to massive rearrangements within the 43S PIC which culminate in the recruitment of the 60S large ribosomal subunit. The meeting of 43S PIC and 60S forms the 80S ribosome, which is ready to begin the elongation cycle.

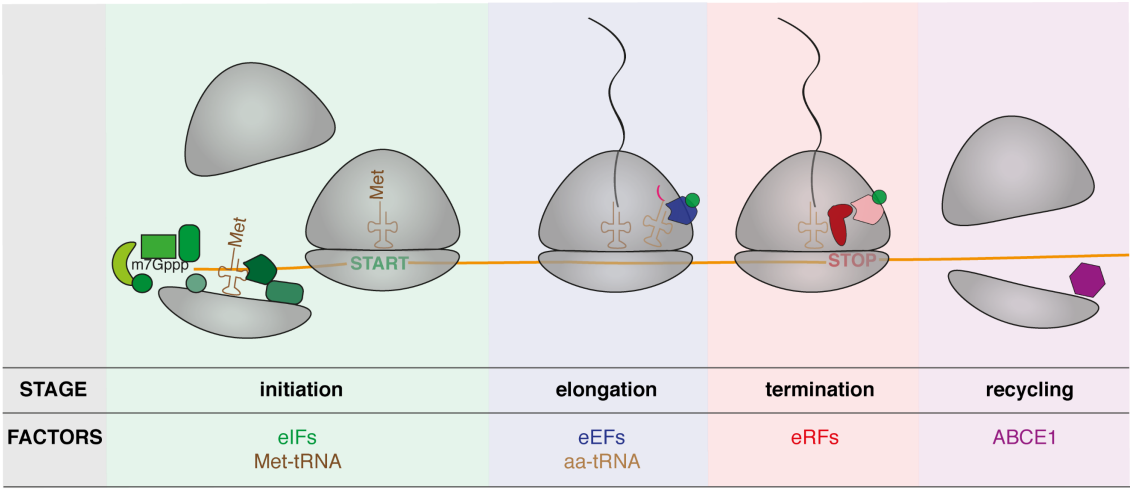

Figure 1.2 Overview of the canonical cycle of translation. Initiation begins when the small ribosomal subunit loaded with initiator methionyl-tRNA (Met-tRNA) assisted by other initiation factors (eIFs) is recruited to the mRNA near the 5' cap structure. After positive recognition of the start signal, the large subunit replaces eIFs and the resulting 80S ribosome is ready for the next stage of elongation. During elongation, the ribosome undergoes repetitive cycles of peptide chain synthesis through the coordinated actions of elongation factors (eEFs) and aminoacyl-tRNAs (aa-tRNAs) (see also Figure 1.3). Elongation lasts until the stop codon is recognized by the peptide chain release factors (eRFs), which terminate translation by release of the nascent protein. The last stage of this process involves recycling of the ribosomal subunits thereby allowing the process to start again.

The stage of elongation is highly conserved between eukaryotes and bacteria, with much of our mechanistic understanding of this process based on work in bacterial systems. Elongation begins with the recruitment of a ternary complex of aminoacyl-tRNA (aa-tRNA), elongation factor 1A (eEF1A; homolog of bacterial EF-Tu) and GTP, all required to decode the mRNA codon positioned within the first ribosomal binding site called aminoacyl site (A-site) (Figure 1.3) (Carvalho et al., 1984; Shao et al., 2016). Codon recognition triggers GTP hydrolysis by eEF1A and accommodation of the aa-tRNA into the A-site (Voorhees et al., 2010; reviewed in Zaher and Green, 2009). Peptide bond formation, which occurs spontaneously after accommodation of the aa-tRNA into the A-site, results in the transfer of the growing protein chain from the peptidyl site (P-site) tRNA to the A-site tRNA (detailed review in bacteria, Beringer and Rodnina, 2007). At the same time ribosomal subunits rotate with respect to one another, while the A- and

P-site tRNAs adopt a so called 'hybrid' conformation in which their anticodon loops remain in the A- and P-sites and the acceptor ends move to the P-site and exit site (E-site), respectively (Behrmann et al., 2015; Budkevich et al., 2011; Moazed and Noller, 1989). tRNAs in hybrid states are usually referred to as A/P-tRNA and P/E-tRNA, since they partially occupy both sites. Translocation, which is catalysed by elongation factor 2 (eEF2; EF-G in bacteria) and involves rotation of the 40S subunit into its canonical position, shifts the A/P and P/E- tRNAs to the P- and E-sites, respectively, preparing the ribosome for the addition of a subsequent amino acid (reviewed in Ling and Ermolenko, 2016).

When the ribosome reaches a stop codon at the A-site, a pair of termination factors, eRF1 and eRF3 in complex with GTP are recruited (Brown et al., 2015). The overall shape of the eRF1 resembles that of a tRNA, allowing it to analogously bind in the A-site, except it specifically recognizes a stop codon. Subsequently, GTP hydrolysis by eRF3 triggers a large conformational change within eRF1, which positions its conserved, catalytic glycine-glycine-glutamine (GGQ) motif in the PTC. This results in hydrolysis of the ester bond between the P-site tRNA and nascent polypeptide with the latter being released from the ribosome (Alkalaeva et al., 2006; Frolova et al., 1999; Salas-Marco and Bedwell, 2004). At this point eRF3 dissociates from the ribosome and ATP-binding cassette sub-family E member 1 (ABCE1), another NTPase, is recruited to initiate ribosome recycling by splitting the two ribosomal subunits (Khoshnevis et al., 2010; Pisarev et al., 2010; Shoemaker and Green, 2011). In addition to this role, recent evidence suggests that, by performing this action, ABCE1 can act as a missing link between recycling and initiation, preventing 60S rejoining and facilitating recruitment of eIFs for another round of translation (Heuer et al., 2017).

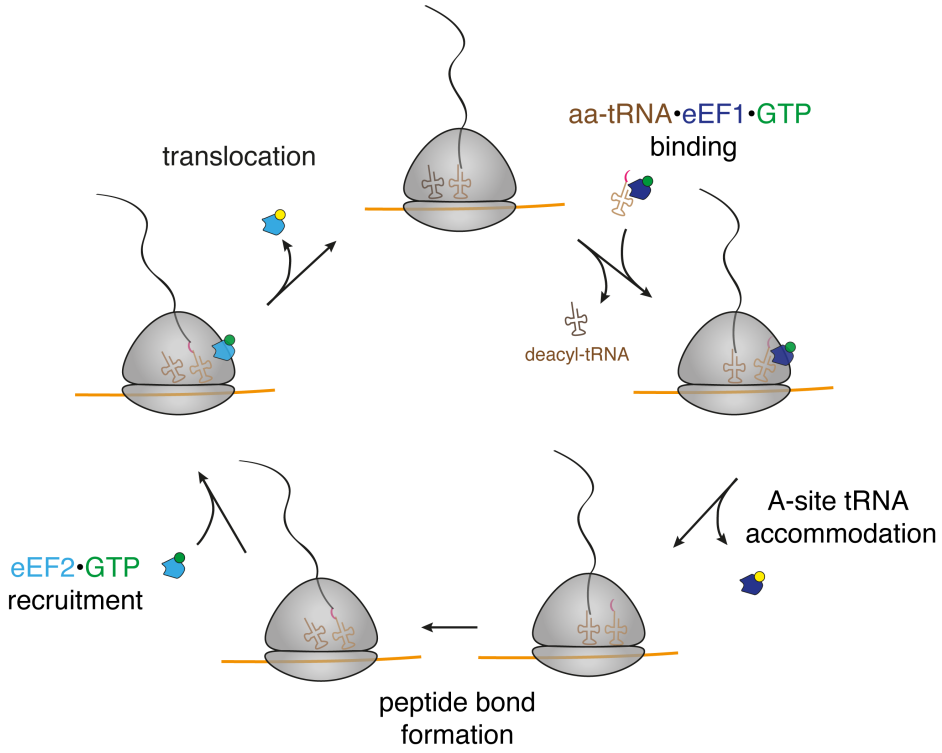

Figure 1.3 Overview of the translation elongation cycle. The first step of elongation involves selection of the appropriate aa-tRNA-eEF1-GTP within the A-site of the ribosome. GTP hydrolysis by eEF1 facilitates accommodation of the A-site tRNA, which becomes ready to accept growing polypeptide chain from the P-site tRNA. During peptide bond formation, tRNAs adopt 'hybrid' conformations. Ribosomes in a hybrid state revert to their canonical state upon translocation, which is induced by eEF2-GTPase activity.

1.2 mRNA maturation

Many interruptions to the normal translation cycle are caused by various defects within the major substrate of the ribosome: mRNA. In higher eukaryotes, mature mRNA is produced in a series of co-transcriptional processing events (Figure 1.4). Soon after transcription begins, pre-mRNA undergoes the first processing event which involves addition of the 7-methylguanosine cap to its 5' end (reviewed in Shuman, 2000). In mammals, bifunctional mRNA capping enzyme is recruited to the C-terminal domain (CTD) of the RNA polymerase II, which serves as a hub for many processing factors. Capping enzyme first acts on the terminal nucleotide of the pre-mRNA to remove γ phosphate and then catalyses transfer of the GMP from GTP to the terminal nucleotide of the pre-mRNA via 5'-5' linkage. A separate enzyme, guanine-7-methyltransferase, finishes capping by adding a methyl group to the guanine at position 7. The second processing event of the pre-mRNA is splicing. It involves excision of the intervening, non-coding sequences (introns) and ligation of the coding regions (exons). This process

consists of multiple steps and is catalysed by a large macromolecular RNA-protein complex called the spliceosome (reviewed in Scheres and Nagai, 2017). The final mRNA processing step involves endonucleolytic cleavage which occurs 20-30 nucleotides downstream of the conserved AAUAAA sequence, usually near the 3' end of the pre-mRNA. Cleavage is immediately followed by addition of a poly(A) tail. In mammals, cleavage is mediated by multiple protein factors, whereas poly(A) tail addition only requires poly(A) polymerase (reviewed in Proudfoot, 2004). Hence, mature mRNA consists of: a 5' cap structure; a 5' untranslated region (5' UTR); an open reading frame (ORF; defined by the start codon followed by the stop codon in the same reading frame); a 3' UTR and a poly(A) tail.

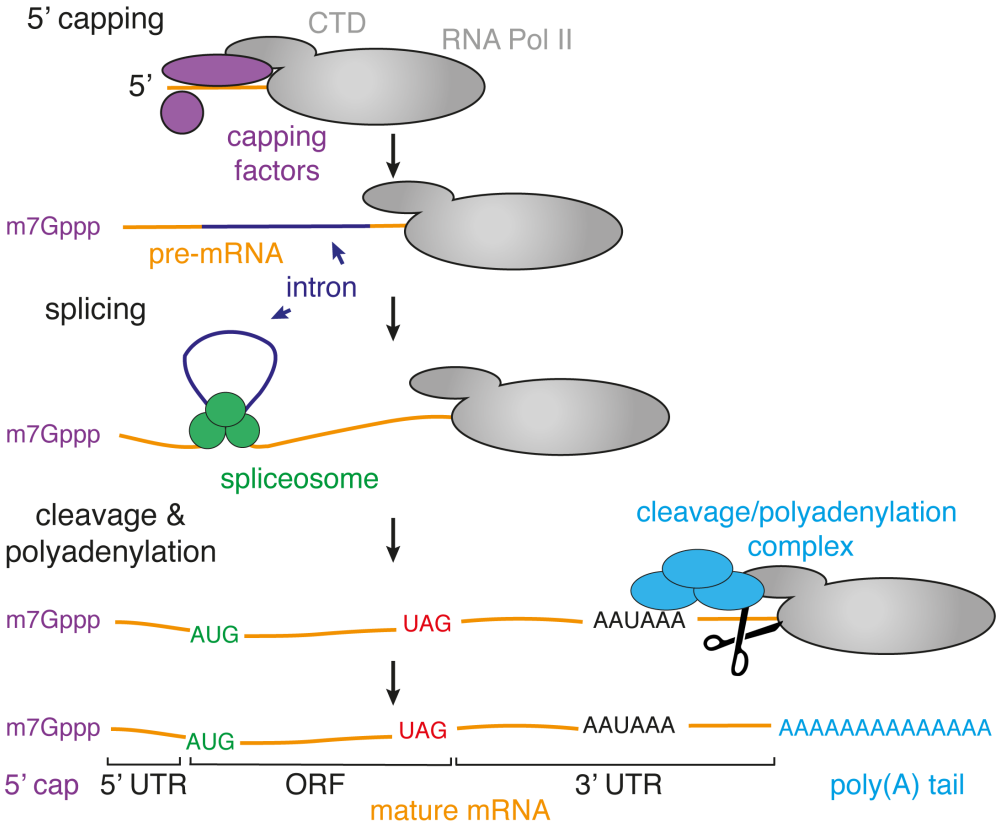

Figure 1.4 mRNA maturation process. RNA Polymerase II (RNA Pol II) synthesises pre-mRNA. The first processing event starts co-transcriptionally after 20-30 nucleotides of nascent transcript are already synthesised and involves addition of a 5' methylguanosine cap (m7Gppp) by capping factors, which directly bind to RNA Pol II C-terminal domain (CTD). The second processing event of splicing may also start co-transcriptionally and involves excision of non-coding sequences of the pre-mRNA (introns) and ligation of coding regions (exons) by RNA-protein machinery called the spliceosome. The final processing event starts with recognition of the conserved AAUAAA sequence by the cleavage/polyadenylation complex, which induces endonucleolytic cleavage 20-30 nucleotides downstream. Cleavage is immediately followed by addition of a poly(A) tail and the now mature mRNA is ready for export to the cytoplasm and translation.

1.3 Translation-coupled mRNA quality control

Major mRNA defects such as lack of the poly(A) tail or the 5' cap structure are readily recognized during the mRNA maturation process (Custodio et al., 1999; Schwer et al., 1998). However, there are infinite more subtle errors that can occasionally slip through the main early mRNA quality control mechanisms (Figure 1.5). Translation of such mRNAs would result in the production of an aberrant protein product, which could potentially endanger cellular homeostasis. Therefore, the cell has necessarily evolved additional quality control mechanisms in order to degrade defective transcripts. These processes usually operate in a translation-dependent manner and are collectively referred to as 'mRNA surveillance'.

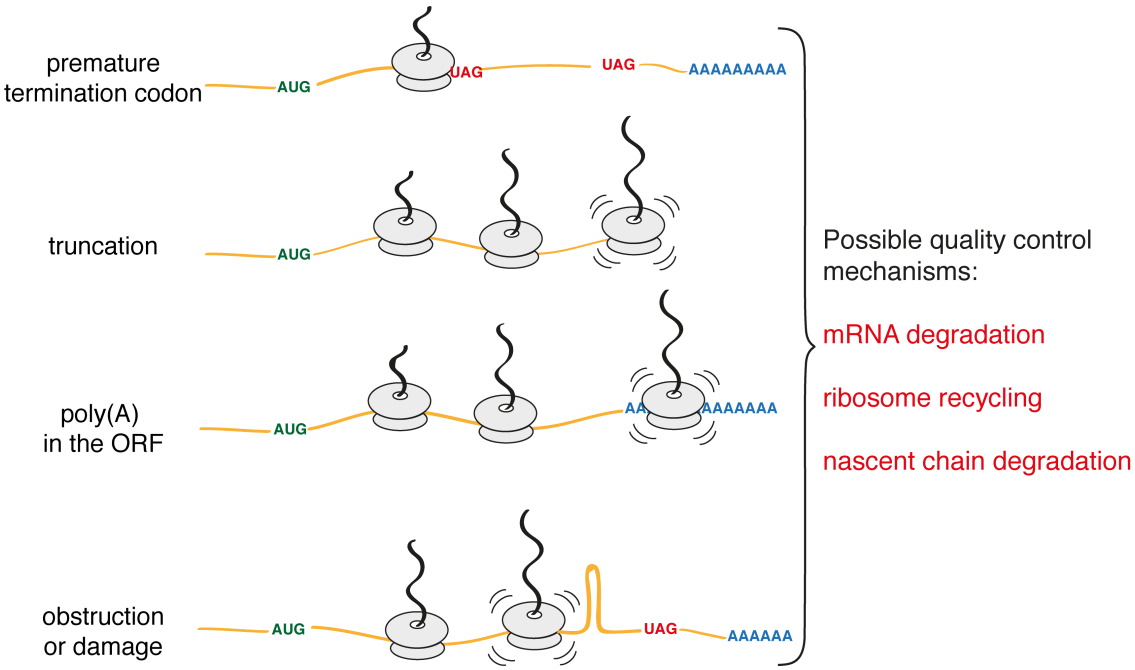

Figure 1.5 Causes of aberrant translation. Four different situations which cause interruptions to the canonical translation cycle. In each case the ribosome serves as a cue for recognition by one or more quality control pathways, which try and resolve either of these stalled translational events.

1.3.1 Nonsense-mediated decay (NMD)

The first realization that defective mRNA is specifically recognized as aberrant was made in the early 1980s. It was observed that globin-encoding mRNA derived from β^0-thalassemic patients is much more rapidly turned over than non-thalassaemic β-globin mRNA (Maquat et al., 1981). The source of this difference was traced to a single nucleotide deletion resulting in a premature termination codon (PTC) at codon 60

(Kinniburgh et al., 1982). This selective destabilization of PTC-containing mRNAs is now commonly referred to as nonsense-mediated decay (NMD). Another, even more intriguing observation was that such mutated mRNAs could be stabilised by inhibition of translation with antibiotics (Carter et al., 1995). Thus, degradation of PTC-containing mRNAs seemed to be strictly dependent on their translation. This raised the very important question of how can the cell sense that the stop codon is premature to induce degradation of aberrant mRNA, instead of releasing the nascent polypeptide and initiating another round of translation? Over the years a number of hypotheses have been put forward to address this issue (reviewed in: Chang et al., 2007; Karousis and Mühlemann, 2018). In higher eukaryotes, it is thought that proximity of the exon-junction complex (EJC) can serve as a signal for the induction of NMD (Le Hir et al., 2001; Lykke-Andersen et al., 2001; Nagy and Maquat, 1998). The EJC is a protein complex deposited on the exon junctions during splicing. In normal mRNA, the stop codon is usually present in the last exon, therefore presence of the EJC downstream of the stop codon immediately marks mRNA as suspicious. An alternative model suggests that the presence of an extended 3' UTR may sensitize mRNAs to NMD (Amrani et al., 2004; Hogg and Goff, 2010; Muhlrad and Parker, 1999). Whether an extended 3' UTR directly facilitates recruitment of the NMD trans-acting factors (Hogg and Goff, 2010) or promotes NMD by effective separation of positive termination effectors such as PABP from the site of termination (Singh et al., 2008) is currently unclear. Even though the exact combination of features sensed by NMD factors remains incompletely defined, the general theme remains: quality control machinery seems to be tweaked to monitor translational apparatus in the broader context of its surrounding protein and nucleic acid environment.

1.3.2 Non-stop decay (NSD)

mRNAs containing PTC are not the only mRNAs that are recognized in a translation-dependent fashion. It was observed that mRNAs lacking an in frame stop codon are also destabilized in a process called non-stop decay (NSD) (Frischmeyer et al., 2002; Van Hoof et al., 2002). Such mRNAs can exist due to mistakes in pre-mRNA processing such as premature cleavage and polyadenylation events (Kaida et al., 2010; Zhou et al., 2018) or post-transcriptional alterations such as endonucleolytic cleavage (Meaux and Van Hoof, 2006). It was originally assumed that for these mRNAs, due to a lack of a stop

codon, ribosomes would reach the end of a message and not be able to be recycled by the canonical, stop-codon dependent termination factors eRF1-eRF3. Indeed, studies in yeast *Saccharomyces cerevisiae* have shown that NSD relies on the recognition of ribosomes stalled at the end of truncated messages by Ski7 (Araki et al., 2001; Van Hoof et al., 2002), another member of the translational GTPases family which includes already mentioned eEF1A and eRF3. Ski7 can recruit and interact with the exosome complex, a major 3' to 5' exonuclease capable of degrading aberrant transcripts (Araki et al., 2001; Van Hoof et al., 2002). However, Ski7 does not have an obvious homolog in mammals, therefore its function is most likely compensated by the factors involved in the no-go decay pathway discussed below.

1.3.3 No-go decay (NGD)

Finally, translating ribosomes can encounter impediments within an mRNA sequence that lead to its terminal arrest before translation can be completed. The no-go decay (NGD) pathway effectively targets mRNAs containing stall-inducing features using arrested ribosomes as a cue for their degradation (Doma and Parker, 2006). The best described examples of stalling sequences involve stable mRNA secondary structures like hairpins or pseudoknots (Doma and Parker, 2006), chemical modifications of nucleobases which interfere with mRNA-tRNA base pairing (Simms et al., 2014), combinations of difficult to decode codons (Letzring et al., 2010, 2013) or nascent polypeptides inducing stalling through a strong interaction with the ribosome exit tunnel (Lu and Deutsch, 2008; Wilson et al., 2016). In yeast, it was shown that stem loop-containing mRNAs undergo endonucleolytic cleavage, creating substrates for the 5'-3' exonuclease exosome and the major 3'-5' exonuclease Xrn1 (Doma and Parker, 2006). This process is again strictly dependent on translation, as preventing the ribosomes from reaching the stem loop results in complete stabilisation of the aberrant message. Further studies implicated factors Dom34 (Pelota in mammals) and Hbs1 as instrumental for this endonucleolytic cleavage event (Doma and Parker, 2006; Passos et al., 2009). Because Dom34/Pelota and Hbs1 are close homologs of the canonical termination factors eRF1 and eRF3, respectively, it was immediately speculated that their function involved close interaction with the ribosome (Atkinson et al., 2008; van den Elzen et al., 2010; Graille et al., 2008; Kobayashi et al., 2010). Indeed, subsequent biochemical reconstitution experiments have shown that Dom34/Pelota-Hbs1 are able to split the ribosome in a

reaction which was later discovered to also involve the known ATPase ABCE1 (Rli1 in yeast) (Becker et al., 2011; Pisareva et al., 2011; Shao et al., 2016; Shoemaker et al., 2010). The major feature distinguishing Dom34/Pelota from eRF1 is its lack of a conserved GGQ motif, which is directly responsible for release of the peptide chain during termination (Figure 1.6) (Frolova et al., 1999). Splitting of the ribosomal subunits from these aberrant mRNAs would allow the small ribosomal subunit to re-engage with other messages, preventing the depletion of ribosomes from the translating pool. However, it would leave behind the 60S-attached peptidyl-tRNA species, which first has to be processed, before starting another round of translation. Recognition and processing of 60S-aminoacyl-tRNA species will be described in more details later in Chapter 1.4.

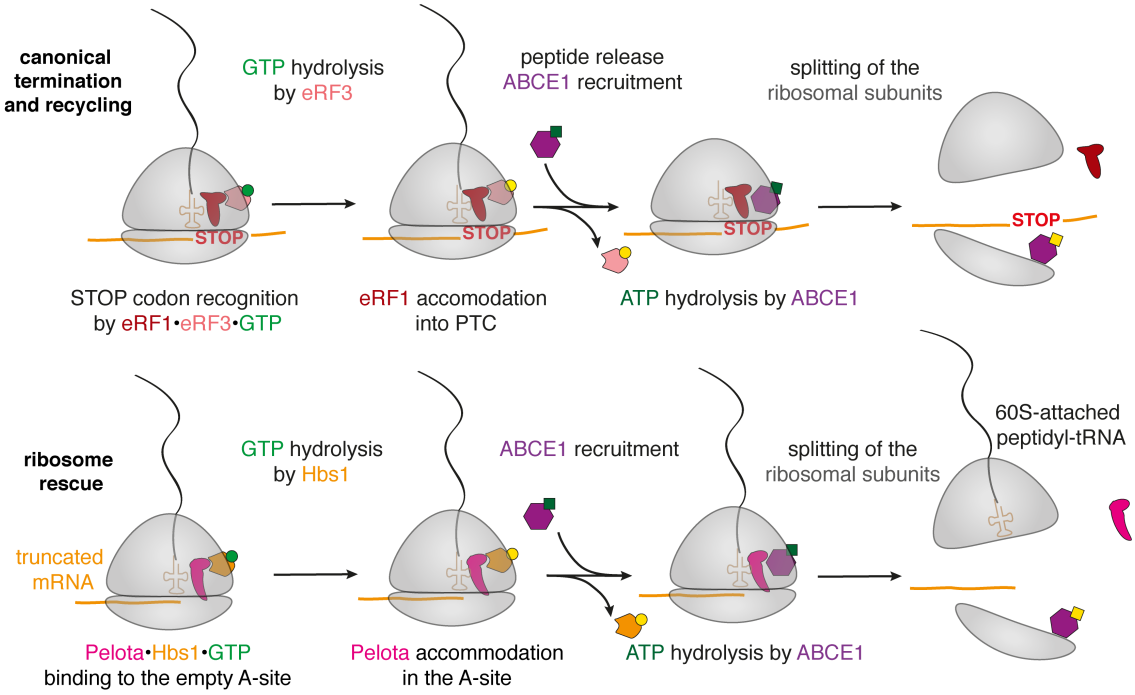

Figure 1.6 Comparison between canonical termination of translation and rescue of the stalled ribosome. Top, during canonical termination, the ternary complex eRF1-eRF3-GTP is recruited to a ribosome once it has reached a stop codon. Stop codon recognition triggers GTP hydrolysis by eRF3, which allows eRF1 to accommodate into the A-site and release the nascent polypeptide. GDP-bound eRF3 then dissociates from the ribosome and splitting factor ABCE1 is recruited in its place. Using energy from ATP hydrolysis, ABCE1 can push apart and split ribosomal subunits, allowing their use in subsequent round of translation. **Bottom**, Ribosomes stalled on truncated mRNA cannot be recognized by stop codon-dependent release factors, instead triggering the recruitment of rescue factors. These factors act similarly to the termination factors, except Pelota does not support nascent peptide release. Therefore, subsequent splitting reaction generates unique species of peptidyl-tRNA attached to the 60S ribosomal subunit.

1.3.4 Interplay between NSD and NGD

Historically NSD and NGD were presented as distinct processes, however increased mechanistic understanding makes it more difficult to clearly demarcate the two. Other than the obvious feature that stalled ribosomes act as a cue, these pathways are also intertwined at downstream steps.

Firstly, NGD induces endonucleolytic cleavage of the mRNA (Doma and Parker, 2006). This effectively generates a 3' end fragment which itself becomes a substrate for NSD. Therefore, it is hard to disentangle the contribution of each pathway to the overall destabilization of the stall-inducing mRNA. Secondly, Dom34-Hbs1 complex was shown to be functioning in both NSD and NGD, suggesting a similar mode of recognition in the case of either defect (Saito et al., 2013; Tsuboi et al., 2012). Finally, it was also observed that translation through the poly(A) tail leads to strong ribosomal arrest, a situation which will likely appear if the mRNA lacks a stop codon due to premature cleavage and polyadenylation (Ito-Harashima et al., 2007). Therefore, at least in the case of this one classical NSD substrate, the ribosome would effectively stall before reaching the end of the message, rendering an actual NGD substrate.

1.3.5 Ribosome is a hub for quality control pathways

Comparing different branches of mRNA surveillance, a common theme emerges that mRNAs are assessed for their integrity by ribosomes during the translation process, and interruptions to the normal translation cycle results in the recognition and degradation of aberrant mRNA. This model has several key implications. The first, already discussed, implies that ribosomes which are stalled during translation need to be rescued by specialized factors, since they become incompatible with canonical termination factors (Figure 1.6). Second, apart from the defective mRNA and stalled ribosome, the cell also needs to deal with the partially synthesized nascent protein. Well-designed studies using artificial reporters for mRNA surveillance pathways rigorously demonstrated that aberrant, truncated nascent chains are effectively degraded in a proteasome dependent manner (Dimitrova et al., 2009; Ito-Harashima et al., 2007; Kuroha et al., 2009; Wilson et al., 2007). Hence, it is now well established that mRNA surveillance is almost always accompanied by ribosome recycling and nascent protein degradation – events all centred on the ribosome.

1.4 Ribosome-associated quality control (RQC) of nascent proteins

1.4.1 Ubiquitin ligase responsible for proteasomal targeting of stalled nascent polypeptides

The key discovery that shed light on the degradation of arrested nascent proteins was the identification of a ubiquitin ligase that polyubiquitinates stalled truncated polypeptides, thereby committing them for rapid, proteasome-mediated degradation (Bengtson and Joazeiro, 2010). This ligase in yeast was termed Ltn1 (initially Rkr1) and was already found in a previous screen for factors which when mutated stabilised NSD protein products (Wilson et al., 2007). The Listerin gene, encoding the mammalian homologue of Ltn1, was initially identified in a mouse forward genetic screen for neurodegenerative disorders and derives its name from the characteristic 'listing' or 'tilting' phenotype of the homozygous *lister* mice (Chu et al., 2009). The mechanism of Listerin-mediated nascent protein ubiquitination will be discussed in detail in the following chapters.

1.4.2 The factors involved in RQC

Soon after identification of Ltn1's function, a number of other genes, found independently in two parallel genetic screens, were placed into the same pathway. One screen aimed to identify factors mediating the cytosolic heat-shock response (Brandman et al., 2012). Analysis of genetic interaction maps identified two factors with very similar profiles and therefore presumably similar roles in translation. The first was the already known Ltn1, and the second factor was a protein of unknown function, termed Rqc1. Native purification of Rqc1-associated complexes from yeast lysates yielded not only Ltn1, but also Rqc2 [initially Tae2, in mammals currently known as NEMF (Nuclear Export Mediator Factor)], the 60S ribosomal subunit and the AAA+ ATPase Cdc48 [in mammals known as Valosin-containing protein (VCP) or p97] with its cofactors Ufd1 and Npl4. A second screen searched for additional factors involved in the recognition and degradation of aberrant mRNAs or associated nascent peptides and found again the same set of genes: Rqc1, Rqc2 and Cdc48 complex which were also shown to be physically associated with 60S ribosomal subunits (Defenouillère et al., 2013). This large macromolecular assembly of Ltn1, Rqc1, Rqc2, Cdc48 complex bound to 60S ribosomal subunit was named the ribosome-associated quality control (RQC) complex.

Genetic studies allowed identification of the core set of components involved in degradation of stalled nascent polypeptides, however out of these only Ltn1 had been assigned the specific function of ubiquitinating stalled nascent proteins (Bengtson and Joazeiro, 2010). Additional biochemical experiments revealed that Rqc2, but neither Rqc1 nor the Cdc48 complex, was necessary for efficient ubiquitination of model stalled substrates (Brandman et al., 2012; Defenouillère et al., 2013). In turn, recruitment of Cdc48 complex to the ribosome was dependent on Rqc1 and ubiquitination of the nascent chain (Brandman et al., 2012; Defenouillère et al., 2013). Moreover, in the absence of Cdc48, tRNA-attached stalled nascent chains were observed in the ribosomal fractions (Verma et al., 2013). Together, these results suggested a model in which Rqc2 and Ltn1 promote nascent chain ubiquitination, whereas Rqc1 recruits Cdc48 complex. The Cdc48 complex then extracts ubiquitinated nascent chains from the ribosome using its pulling force, analogous to the other systems in which this function of Cdc48 was already firmly established (Stolz et al., 2011).

1.4.3 Sequence of events in the RQC pathway

Another key insight from these screens was that association of the RQC components occurred exclusively with the 60S ribosomal subunit (Bengtson and Joazeiro, 2010; Brandman et al., 2012; Defenouillère et al., 2013). This observation, combined with the discovery that rescue factors Dom34-Hbs1 are involved in NGD (Doma and Parker, 2006) suggested that ribosome splitting is an important pre-requisite for nascent chain targeting to the proteasome. However, the exact sequence of events involving these implicated factors was not clear. More importantly, it was unknown how the RQC system specifically recognizes stalled ribosomes and truncated nascent chains, avoiding the vast majority of normal heterogenous translating ribosomes.

An important clue came from a serendipitous observation made in a mammalian rabbit reticulocyte lysate *in vitro* translation system (Shao et al., 2013). Here, translation of truncated mRNAs, a trick which is usually used to generate defined ribosome-nascent chain complexes for studying protein translocation into organelles (Perara et al., 1986), resulted in efficient polyubiquitination of arrested nascent proteins. Moreover, these ubiquitinated, ribosome associated nascent chains co-migrated with the 60S ribosomal subunit when analysed using sucrose density gradients. Therefore, the observed phenomenon turned out to be the mammalian equivalent of the previously described

yeast RQC. In support of that, the nascent chain ubiquitination was also Listerin dependent and triggered by translation of other NGD substrates (Shao et al., 2013). Hence, it opened the possibility for mechanistic dissection of the RQC pathway using a biochemically tractable *in vitro* translation system. The first important discovery was the unambiguous establishment of the sequence of events preceding proteasomal degradation of stalled nascent proteins. Even though both Listerin and polyubiquitinated nascent peptides were observed comigrating with 60S ribosomal subunits, it was not clear if splitting of ribosomal subunits preceded ubiquitination or happened immediately afterwards. The issue was resolved by demonstrating that inhibition of splitting (through immunodepletion or use of a dominant-negative version of rescue factor Hbs1) abolished Listerin recruitment and ubiquitination of nascent polypeptide. Conversely, artificial splitting of stalled ribosomes reversed Listerin association with 60S ribosomes and permitted nascent chain ubiquitination (Shao et al., 2013). Thus, ribosome splitting turned out to be a prerequisite for subsequent Listerin-mediated polyubiquitination of nascent chain. Reconstitution experiments using purified components confirmed this hypothesis, additionally showing that Listerin alone can discriminate 60S-associated nascent proteins from 80S associated complexes (Shao and Hegde, 2014).

1.4.4 Assembly and structure of the RQC complex

In order to understand how Listerin can achieve the specificity for truncated nascent chains, a structural approach was used in combination with biochemical reconstitution experiments. As previously mentioned, the splitting reaction mediated by rescue factors Pelota-Hbs1 does not involve hydrolysis of the ester bond between the tRNA and the nascent polypeptide due to the lack of conserved GGQ motif in Pelota. If the truncated peptidyl-tRNA species is relatively short, it can drop off the 60S ribosomal subunit (Pisareva et al., 2011; Shoemaker et al., 2010). However, longer, folded nascent chains would be sequestered and remain attached to the 60S. In this instance, splitting would result in formation of a unique molecular species of a 60S-bound nascent polypeptide still attached to the P-site tRNA, which would now become exposed as an accessible unprotected inter-subunit interface (Figure 1.6). Hence, it was speculated that either the tRNA, the exposed part of the inter-ribosomal interface, or both could be sensed by Listerin (Rodrigo-Brenni and Hegde, 2012; Shao et al., 2013). This hypothesis was confirmed, when the first low-resolution structure of a nascent chain-60S-Listerin

complex was determined by cryo electron microscopy (cryo-EM). The structure revealed that part of the ligase occupied the intersubunit interface and would normally clash with 40S subunit, explaining why 80S ribosomes cannot be recognized by Listerin (Shao and Hegde, 2014). However, such peptidyl-tRNA-60S-Listerin complexes assembled *in vitro* rapidly re-associated with free 40S, unlike the same complexes assembled in complete cytosol (Shao et al., 2013). Therefore, an additional stabilising factor was postulated to exist in order to render stable RQC complexes. An obvious candidate was the poorly characterized protein NEMF, a mammalian homolog of yeast Rqc2 which was previously shown to be required for ubiquitination of stalled nascent chains in yeast (Brandman et al., 2012; Defenouillère et al., 2013). Addition of NEMF into reconstitution reactions not only prevented 40S re-joining, but also improved efficiency of Listerin-mediated ubiquitination by stabilizing the entire complex (Shao et al., 2015). Moreover, order of addition experiments revealed that NEMF recruitment precedes Listerin engagement, suggesting its primary role in discrimination of complexes selectively targeted for ubiquitination (Shao et al., 2015). These biochemical observations were further confirmed by structural analyses of peptidyl-tRNA-60S-RQC complexes in both yeast and mammalian systems (Lyumkis et al., 2014; Shao et al., 2015; Shen et al., 2015). Yeast RQC complexes were assembled *in vivo* and purified via epitope tags on Ltn1 or Rqc1 (Lyumkis et al., 2014; Shen et al., 2015). It is worth noting that yeast RQC complexes were further stabilized by use of mutant Ltn1, which does not support ubiquitination, thereby preventing downstream disassembly reactions. Mammalian complex was assembled *in vitro* from purified components (Shao et al., 2015). Both yeast and mammalian RQC complexes revealed that Rqc2/NEMF binds to the 60S ribosomal subunit in the region which ordinarily would be covered by the 40S ribosomal subunit (Lyumkis et al., 2014; Shao et al., 2015; Shen et al., 2015). As predicted, it forms contacts with both the 60S subunit and P-site tRNA (Lyumkis et al., 2014; Shao et al., 2015; Shen et al., 2015). Interactions with P-site tRNA are crucial for NEMF recruitment, explaining its high specificity only towards 60S-nascent chain-tRNA complexes formed after splitting by rescue factors (Shao et al., 2015).

Thus, Listerin's high specificity towards stalled nascent chains is encoded at multiple levels. First, Listerin binding alone is incompatible with the 80S ribosome. Second, it's efficient interaction with the ribosome requires an additional binding surface present in the NEMF-ribosome complex. Third, Listerin is only recruited to 60S subunits

containing tRNA-attached stalled nascent chains. This is important to avoid futile titration of the ligase to the empty 60S subunits, especially when we consider that Listerin's copy number in the cell is much lower than the number of ribosomes.

All pair wise interactions between components of the functional RQC complex are extremely weak individually. Only when combined is there enough avidity to render the complex stable and ubiquitination-competent. This implies that quality control is achieved entirely on the basis of the context, rather than a single aberrant recognition motif. This concept is very similar to the already described recognition of premature termination codon during NMD, which relies heavily on a combination of features encoded by the surrounding protein environment.

1.4.5 Carboxyl-terminal alanine and threonine (CAT) tails

The structure of the yeast RQC complex revealed one more unexpected and intriguing piece of biology (Shen et al., 2015). There was an additional tRNA positioned approximately where the A-site tRNA would be, except in the absence of 40S, there was no mRNA template that it could base-pair with. Instead, it was held in place by interactions with Rqc2. Sequencing of tRNAs from the purified RQC complexes revealed enrichment in alanyl- and threonyl-tRNAs (Shen et al., 2015). Alanine and threonine were also enriched in the total amino acid analysis of stalled, truncated nascent chains. Moreover, molecular weight of truncated peptides was larger than expected from previous studies (Brandman et al., 2012). This discrepancy between the predicted observed weight of the stalled amino acid sequence proved to be a result of C-terminal extension (Shen et al., 2015). Finally, this extension was strictly dependent on Rqc2 and could be enriched when the downstream events of ubiquitination or extraction of the nascent polypeptide were inhibited. Thus, it appeared that Rqc2 could mediate non-canonical, mRNA- and 40S- independent elongation of the stalled nascent chain using charged alanyl- and threonyl-tRNAs as a substrate (Shen et al., 2015). *In vitro* reconstitution experiments using a yeast cell-free system confirmed that the process of CAT tail formation relies on ribosome peptidyl-transferase activity, as antibiotics targeting the PTC abolished C-terminal extension (Osuna et al., 2017). Moreover, depletion of GTP or direct inhibition of elongation factors eEF1A and eEF2 using antibiotics had no effect on this activity, confirming its independence from canonical elongation machinery. Curiously, cycloheximide, an antibiotic which binds in the E-site

and prevents translocation of deacylated tRNA, also did not have any impact on the CAT tail formation, suggesting an alternative mechanism for the translocation of deacylated tRNA in the absence of 40S and mRNA (Osuna et al., 2017).

The major physiological role of CAT tails is still debatable. One proposed function could be a fail-safe mechanism, effectively pushing lysine residues out of the ribosomal exit tunnel in a situation when none are available for ubiquitination by Ltn1 (Kostova et al., 2017). In fact, the structure of the mammalian functional RQC complex revealed that Listerins' RING domain is positioned in close proximity to the ribosomal exit tunnel (Shao et al., 2015), implying that only a small fragment of arrested nascent polypeptide might be accessible for ubiquitination. In agreement with this, biochemical characterization determined the Ltn1-accessible window to be ~12 amino acids outside the exit tunnel (Kostova et al., 2017). Using artificial, stalled substrates containing lysine residues within the ribosomal exit tunnel, it was shown that CAT tail addition can convert RQC-resistant nascent chains into Listerin-accessible. Moreover, *in silico* genome wide analysis estimated that CAT-tailing would increase the fraction of RQC-degradable substrates from ~60% to ~95%, assuming stochastic ribosomal stalling along every open reading frame (Kostova et al., 2017). Similarly, CAT tails seem to facilitate Ltn1-mediated degradation of some folded nascent polypeptides, perhaps by increasing their mobility outside the ribosome exit tunnel, giving them a better chance to be ubiquitinated by the spatially restricted Ltn1 (Sitron and Brandman, 2018).

Finally, CAT-tails were proposed to be necessary for aggregation of stalled nascent chains that failed to be ubiquitinated by Ltn1 (Choe et al., 2016; Defenouillère et al., 2016; Yonashiro et al., 2016). Such CAT-tail dependent aggregates were shown to sequester multiple cytosolic chaperones leading to induction of proteotoxic stress. CAT-tail mediated aggregate formation also correlates with Rqc2-dependent induction of the heat shock response (Shen et al., 2015), suggesting that CAT-tailing may facilitate activation of stress responses to eliminate toxic species. Why cells have evolved a process which could potentially lead to a rapid collapse of cellular proteostasis merits further investigation. Future studies should reveal how cells coordinate RQC activity with CAT-tail formation in order to maintain the fine balance between selective degradation and induction of systemic stress responses.

1.4.6 Nascent chain extraction and degradation

Combined genetic, biochemical and structural efforts allowed for near-complete mechanistic dissection of the RQC pathway up to the point of Listerin-mediated polyubiquitination of the stalled nascent polypeptide. However, the molecular details of the following steps: peptidyl-tRNA hydrolysis, nascent chain extraction and delivery to the proteasome, are only beginning to emerge.

The major challenge after ubiquitination is the release of the nascent chain trapped in the ribosomal exit tunnel. This species would contain bulky polyubiquitin tags, perhaps also a folded domain on the N-terminus, and tRNA attached to the C-terminus. This situation efficiently prevents slipping of the nascent chain in either direction, effectively locking the substrate in place (Shao et al., 2013). Genetic studies suggested involvement of the AAA+ ATPase Cdc48 complex in the process of nascent chain extraction (Brandman et al., 2012; Defenouillère et al., 2013; Verma et al., 2013). However, without specific release of the tRNA, Cdc48 would not be able to thread the substrate through the ribosomal exit tunnel. Recently, several independent studies utilizing either genetic analyses or classical biochemical fractionation have identified another Cdc48 cofactor - Vms1 (ANKZF1 in mammals) thought to be involved in the specific release of the ubiquitinated nascent chain (Kuroha et al., 2018; Verma et al., 2018; Zurita Rendón et al., 2018). Genetic approaches combined several previous observations: first, Δvms1 mutations, like RQC-deficient mutations, cause a synthetic growth defect when combined with mutations that impair degradation of non-stop mRNAs (Defenouillère et al., 2013; Van Hoof et al., 2002), second Δvms1 mutations are sensitive to cycloheximide, an elongation inhibitor which was shown to induce the RQC pathway (Stapf et al., 2011), and finally, Vms1 was shown to protect cells from mitochondrial toxicity of ribosome-stalled nascent chains which are inaccessible for Ltn1 (Izawa et al., 2017). Analyses using model stall-inducing substrates confirmed that Vms1 deletion causes accumulation of tRNA-attached stalled nascent chains (Verma et al., 2018; Zurita Rendón et al., 2018). Vms1 was also shown to interact with ribosomes, a prerequisite for a factor involved in nascent chain release (Verma et al., 2018; Zurita Rendón et al., 2018). These observations prompted further structural (Zurita Rendón et al., 2018) and bioinformatics (Verma et al., 2018) analyses which revealed that Vms1 contains a conserved RNase H fold, which is similar to known peptidyl-tRNA hydrolases

like eRF1. Although Vms1 contains GSQ residues instead of the conserved GGQ residues required for hydrolysis of the ester bond between tRNA and peptide chain by eRF1 (Frolova et al., 1999), several different mutations of catalytic glutamate phenocopied a full Vms1 deletion (Verma et al., 2018; Zurita Rendón et al., 2018). Similarly, *in vitro* reconstitution experiments revealed effective release of the nascent chain from the stalled 60S-aminoacyl-tRNA species by wild type, but not catalytically inactive version of Vms1 and ANKZF1 (Verma et al., 2018; Zurita Rendón et al., 2018). Therefore, Vms1/ANKZF1 was provisionally assigned a function of peptidyl-tRNA hydrolase for 60S-attached aminoacyl-tRNAs.

An alternative approach to identify a relevant tRNA hydrolase involved a series of activity-based biochemical fractionations of rabbit reticulocyte lysate which yielded two potential candidates (Kuroha et al., 2018). The first was Ptrh1, a protein homologous to bacterial peptidyl-tRNA hydrolase Pth. It was shown to release both 60S-associated truncated nascent chains and, surprisingly, nascent chains attached to the stalled full 80S ribosomes. However, Ptrh1 could not release polyubiquitinated nascent chains. In turn, those were selectively cleaved off by the ANKZF1, which corresponded to the second identified activity. ANKZF1, consistent with previous studies, was only active on 60S attached-nascent chains. Moreover, careful analysis of ANKZF1-processed nascent chains revealed the presence of additional nucleotides left behind on the C-terminal portion of the truncated nascent chain. This could only be explained by endonuclease activity of ANKZF1 towards tRNA, instead of previously postulated peptidyl-tRNA hydrolase activity (Kuroha et al., 2018). Even though ANZKF1 was shown to be active only on the 60S-attached peptidyl-tRNA complexes with tRNA moiety successfully accommodated in the P-site, the molecular details of its recruitment and, more importantly, its interplay with Cdc48/p97 complex merits further investigation.

1.5 Ribosomal stalling triggers induction of the RQC

The RQC pathway, as described in the previous chapter, can be roughly divided into three separate phases: 1) splitting of the stalled ribosome into subunits; 2) RQC complex assembly and nascent-chain ubiquitination; 3) tRNA hydrolysis, nascent-chain release and degradation (Figure 1.7). Progression through these stages is reasonably well defined with each step biochemically reconstituted with purified components. Naturally, a few questions remain unanswered, such as the exact details of how the Cdc48/p97 complex

extracts the ubiquitinated nascent chain. However, the events leading up to the splitting of stalled ribosomes into subunits, including the very initial event of selective recognition of aberrantly translating ribosomes are much less clear.

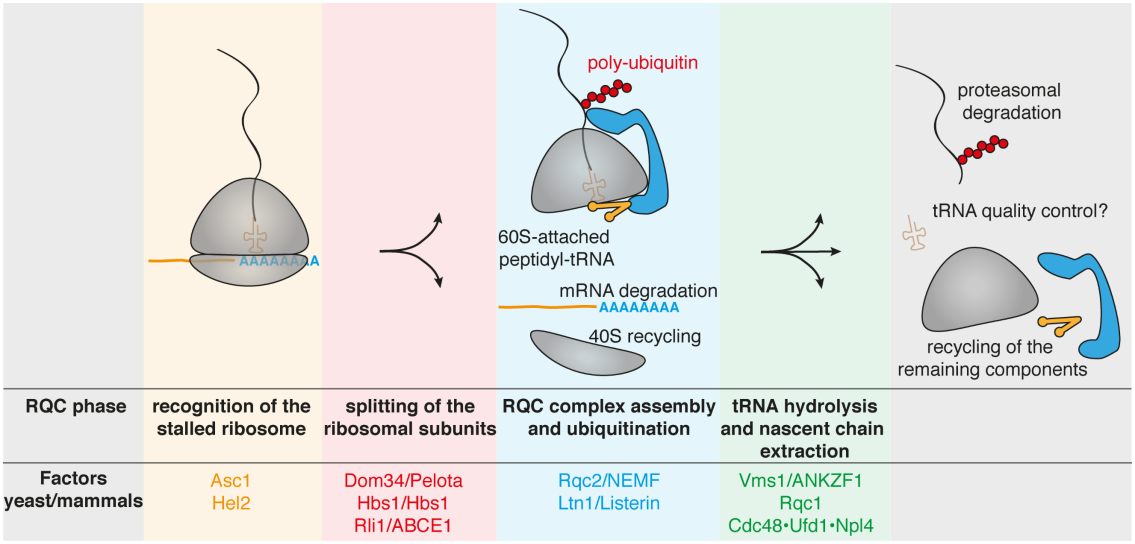

Figure 1.7 Major steps and factors of the RQC pathway. Ribosomes translating through stall-inducing mRNA sequences are recognized by a poorly understood mechanism thought to involve ribosomal protein Asc1 and an E3 ligase of unknown function Hel2. Recognition is followed by splitting of the ribosomal subunits by the rescue factors. As a result of their action, the peptidyl-tRNA-containing inter-subunit interface of 60S becomes exposed and acts as a cue for the assembly of the RQC complex, which facilitates poly-ubiquitination of the stalled nascent-polypeptide. The polyubiquitinated complex is then the substrate for disassembly factors, which cleave the tRNA and extract the polyubiquitinated nascent polypeptide to permit its degradation by the proteasome. The remaining components are likely being checked and/or recycled. Listed below are factors implicated at each step in both yeast and mammals.

The first problem is how aberrantly translating ribosomes are distinguished from physiologically valid translating ribosomes. In some cases, this is clear, such as when ribosomes reach the end of a truncated mRNA. Due to incompatibility with neither elongation factors nor termination factors, these ribosomes are effectively trapped and must eventually get recognized by rescue factors. However, the recognition task becomes non-trivial if we consider aberrantly translating ribosomes experiencing problems in the middle of the mRNA. In almost every cell, at any given time, millions of ribosomes are actively translating proteins. Moreover, elongation speed of individual ribosomes can vary dramatically (Ingolia et al., 2011), as it is under the influence of various fluctuating factors. Therefore, it becomes difficult to differentiate between physiologically slow or pausing ribosomes and ribosomes that are pathologically stalled and need to be rescued.

1.5.1 Translation speed and stall-inducing signals

To accurately define terminally stalled ribosomes, one needs to consider how elongation rate can be influenced by different factors. Firstly, the presence of certain encoded amino acid sequences can influence translation rate. This could be because of the inherent nature of the amino acids themselves, which directly affects the kinetics of peptide bond formation, or due to the inhibitory conformations of the nascent chains in the ribosomal exit tunnel. An example of the former is peptide bond formation between two prolines. Due to its chemical nature, proline-tRNA is both a poor peptidyl acceptor in the A-site and a poor donor in the P-site (Pavlov et al., 2009; Wohlgemuth et al., 2008). Hence, the overall kinetics of the proline-proline peptide bond formation is slow and mRNAs encoding relatively abundant polyproline stretches can pose a significant challenge for translating ribosomes. To avoid terminal stalling during poly-proline translation, specialized factor eIF5A (EF-P in bacteria) is employed (Doerfel et al., 2013; Gutierrez et al., 2013; Ude et al., 2013). eIF5A binds to the E-site of the ribosome and stabilizes P-site tRNA to facilitate nucleophilic attack by the aminoacyl-tRNA in the A-site (Schmidt et al., 2016).

An excellent example of a stalling induced by nascent polypeptide is the case of XBP1u mRNA. Upon endoplasmic reticulum (ER) stress, the ER-localized endoribonuclease IRE1α induces splicing of the precursor form of the XBP1u mRNA, which leads to translation of the active transcription factor XBP1s (Calfon et al., 2002; Yoshida et al., 2001). This splicing event occurs because the translation of unspliced XBP1u mRNA causes transient ribosomal stalling, most likely due to specific interactions of the nascent polypeptide with the ribosomal exit tunnel (Yanagitani et al., 2011). The pausing is sufficiently long, that it allows targeting of the ribosome-nascent chain complexes to the ER (Yanagitani et al., 2009, 2011). Hence, ribosomal pausing can sometimes be employed by cellular machinery to regulate physiological processes e.g. by targeting ribosome-nascent chain complexes to specific organelles.

Other factors besides amino acid sequence can affect translation rates. Another prominent example is the nucleotide sequence of the mRNA. In yeast, it was shown that the arginine CGA codon is very inefficiently decoded, with two CGA codons in a row sufficient to cause terminal ribosomal stalling (Letzring et al., 2010). This was later explained to be a result of inefficient decoding by non-Watson-Crick, purine-purine base

pairing between adenine in the wobble position of CGA codon and inosine in the corresponding tRNA (Letzring et al., 2013). Other codon choices can also have a less dramatic effect on translation rate. In yeast, certain pairs of codons arranged in a specific order can cause significant slowdown of translation elongation (Gamble et al., 2016). While for some pairs this slowdown can be explained by inefficient wobble decoding, it seems like additional interplay between adjacent tRNAs can further influence rate of decoding (Gamble et al., 2016). More broadly, codon optimality, which reflects the usage of certain codons in the transcriptome and the availability of the corresponding tRNA, was shown to correlate with the translation rate of an entire mRNA (Presnyak et al., 2015). Also more obvious problems, such as inefficient aminoacylation, which could result from insufficiency of a specific amino acid, can lead to ribosomal stalling due to unavailability of the cognate aminoacyl-tRNA species (Lareau et al., 2014). Finally, mRNA secondary structure can often form a roadblock for translating ribosomes (Doma and Parker, 2006; Hosoda et al., 2003). Viruses frequently exploit pseudoknots or stem-loop structures to induce transient ribosomal pausing which, when combined with additional 'slippery' sequence upstream, can lead to so called programmed ribosomal frameshifting, which results in production of multiple different protein products from a single mRNA template (Dinman, 2012). This adaptive strategy allows viruses to maintain a small genome size, without compromising on translational output.

As described above, there are many physiological situations in which ribosomes may transiently pause, but it is more beneficial to resume translation instead of inducing quality control pathways. The separate types of stall-inducing signals are related to various mRNA defects that could be encountered during translation. The common denominator for all such signals is the induction of quality control responses, including mRNA surveillance and RQC. Examples of mRNA defects such as truncations or chemical modifications of nucleobases were previously discussed in the context of NGD and NSD. However, in mammalian cells perhaps the most common defects result from mistakes made during mRNA processing. It is estimated that up to ~10% of human genes may contain alternative polyadenylation sites within their coding sequence (Kaida et al., 2010; Ozsolak et al., 2010). Moreover, it was also shown that premature cleavage and polyadenylation events may be upregulated in cancerous cells (Berg et al., 2012). Hence, mRNAs might frequently become polyadenylated within the open reading frame. Such mRNAs were shown to effectively trigger NSD and RQC pathways due to terminal

stalling of the ribosomes translating through poly(A) mRNA in both yeast (Ito-Harashima et al., 2007) and mammalian cells (Arthur et al., 2015). The molecular basis for stalling on poly(A) remains unclear, but two models have been proposed from *in vitro* studies. First, poly-basic residues, like the poly-lysine encoded by poly(A), might interact with the negatively charged ribosomal exit tunnel. Such electrostatic interactions were shown to slow elongation *in vitro* (Lu and Deutsch, 2008). In support of that, other combinations of codons encoding polybasic tracts (excluding repeated arginine-encoding CGA codons, which additionally stall translation due to wobble decoding) were also shown to induce RQC in yeast (Kuroha et al., 2010). A second, non-mutually exclusive mechanism involves intrinsically slow decoding of sequential AAA codons, which was proposed to result in ribosome sliding (Koutmou et al., 2015). This complication notwithstanding, the end result of translation through poly(A) is a ribosome stalled before reaching the end of poly(A), hence containing AAA codons in the A-site, P-site and E-site. Such a complex would not necessarily differ from actively elongating complexes, yet somehow it needs to be recognised by the rescue factors Pelota-Hbs1 to be effectively recycled, while both the aberrant mRNA and the truncated nascent chain need to be degraded.

Translation speed appears to be extremely heterogenous, including physiologically justified cases of transient ribosomal pausing. In light of that, terminal ribosome stalling, which could occur for many different reasons, could potentially result in a formation of macromolecular complexes indistinguishable from actively elongating complexes. Given the high energetic cost of protein translation (approximately 2000 ATP molecules per one molecule of protein) (Li et al., 2014), only specific recognition of terminally stalled complexes could warrant efficient maintenance of cellular homeostasis. How this selectivity is achieved is only beginning to emerge.

1.5.2 Recognition of ribosomes stalled at the end of truncated mRNAs

Perhaps the best understood example of recognition and resolution of terminally stalled ribosome is the case of truncated mRNA. When an 80S ribosome reaches the end of a truncated message, it stalls with the peptidyl-tRNA in the P-site and an empty A-site. Such a macromolecular assembly is acted upon by the rescue factors Pelota-Hbs1 (Becker et al., 2011; Shao et al., 2016). Hbs1, as already mentioned, is a translational GTPase belonging to the same family as eEF1A, eEF2 and eRF3 (Atkinson et al., 2008).

These proteins bind near the A-site of the ribosome in a GTP-dependent manner (Brown et al., 2015; Shao et al., 2016). Additionally, their respective binding partners (tRNA in case of eEF1A and eRF1 in case of eRF3) can 'read' the identity of the mRNA sequence in the A-site, providing further specificity (Brown et al., 2015; Shao et al., 2016). Recent high-resolution structures of mammalian Pelota-Hbs1 and yeast Dom34-Hbs1 complexes assembled on the ribosome stalled at the truncated mRNA explain the specificity of Pelota/Dom34 towards an empty A-site (Hilal et al., 2016; Shao et al., 2016). The structure revealed that b3'-b4' loop of Pelota extends from the N-terminus and protrudes into the mRNA channel taking the path which normally would be occupied by the A-site mRNA. This is in full agreement with previous *in vivo* and *in vitro* data from both mammalian and yeast systems suggesting activity of the ribosome rescue complex towards ribosomes stalled at the end of truncated mRNAs (Guydosh and Green, 2014; Pisareva et al., 2011; Shao et al., 2013; Shoemaker and Green, 2011; Shoemaker et al., 2010). However, the Pelota-Hbs1 complex was also successfully assembled on the ribosomes stalled by the poly(A) sequence (Shao et al., 2016). Surprisingly the b3'-b4' loop was in the exact same position as in the complex assembled on truncated mRNA, whereas the A-site mRNA was completely disordered. This observation supports previous results, which demonstrated that both yeast Dom34-Hbs1 and mammalian Pelota-Hbs1 complexes can also split internally stalled ribosomes *in vitro* (Pisareva et al., 2011; Shao and Hegde, 2014; Shoemaker et al., 2010). However, it does not explain how Dom34-Hbs1 can distinguish poly(A) stalled ribosomes from translating ribosomes in a physiological context. Moreover, ribosomes stalled due to the unavailability of the aminoacyl-tRNA or by the stem-loop-containing mRNA are also successfully engaged by Dom34-Hbs1. Hence, translation complexes which are likely to represent ribosomes in different rotation states, assembled on different mRNAs, can all be engaged by Dom34-Hbs1.

1.5.3 Recognition of internally stalled ribosomes

The simplest proposed model for selective recognition of internally stalled ribosomes involves competition of rescue factors with other translation factors (Brandman and Hegde, 2016). It relies on the assumption that initial interaction of Pelota-Hbs1-GTP complex with the ribosome is labile due to the presence of mRNA within the A-site. Only after GTP hydrolysis by Hbs1 can Pelota be properly accommodated into the A-site to

induce splitting. This gives enough time for competition from much more abundant tRNA-eEF1A or eRF1-eRF3 complexes. Competition is only possible if the correct codon is in the A-site and the appropriate decoding complex is available. In other cases, Hbs1 will eventually hydrolyse GTP and induce splitting. It is more difficult to apply this model to the poly(A) stalled ribosomes, as the appropriate tRNA-eEF1A complex is likely to be available. However, it is possible that the ribosome might be refractory to the elongation due to unfavourable architecture around the PTC. Alternatively, mRNA secondary structure within the A-site can interfere with the binding of the cognate tRNA-eEF1A. Therefore, unsuccessful rounds of tRNA-eEF1A engagement would eventually lead to Pelota-Hbs1 engagement and irreversible splitting of ribosomal subunits.

A different model involves participation of auxiliary components in this circumstance. Some evidence supporting this alternative came from a genetic screen in yeast aimed to identify factors involved in stalling on polybasic sequences (Kuroha et al., 2010). It revealed that deletion of ribosomal protein Asc1 [in mammals Receptor for Activated C-kinase 1 (RACK1)] resulted in increased readthrough of stretches of mRNA encoding 12 arginine residues. Asc1 deletion also allowed readthrough of the mRNA encoding poly-lysine tracts, which led to the general conclusion that Asc1 facilitates ribosomal stalling mediated by polybasic nascent chains (Kuroha et al., 2010). Another genetic screen designed to uncover additional factors involved in stalling on polybasic sequences was based on the double fluorescence reporter encoding GFP and RFP separated by polyarginine stretch (Brandman et al., 2012). By measuring GFP and RFP signals independently, factors involved in degradation of the polypeptide upstream of the stalling signal could be differentiated from the factors inducing stalling itself. Hence, Asc1 deletion resulted in increased levels of both RFP and GFP signals, which indicated increased readthrough of the polybasic stretch. In contrast, deletion of known RQC components like Ltn1 or Rqc1 resulted in selective increase of the GFP only, confirming the defect related to nascent polypeptide degradation occurring after the initial stalling event. Curiously, in this screen deletion of the RING-domain containing protein Histone E3 ligase 2 (Hel2) resulted in similar phenotype as an Asc1 deletion, which was increased readthrough of the polyarginine stretch (Brandman et al., 2012).

Together, these two screens suggest involvement of at least two additional factors - ribosomal protein Asc1 and putative E3 ubiquitin ligase Hel2 in the RQC-mediated degradation of stalled nascent polypeptides (Brandman et al., 2012; Kuroha et al., 2010).

Moreover, stabilisation of the entire, full length protein product translated from the stalling reporter likely implicates involvement of these factors at the stage upstream of the ribosome splitting. Understanding of the molecular details of how Hel2 and Asc1 cooperate to selectively induce RQC during translation through polybasic sequences is extremely important, as it will elucidate the commitment step which determines whether translation complex will be irreversibly split or not.

1.6 Overview of thesis

The goal of this thesis is to investigate how cells detect excessively slow translation. To address this problem, we use a combination of cell culture and *in vitro*-based approaches, supported by structural biology. In the next chapter, we present the development and characterization of a novel, flow cytometry-based reporter assay for studying translational stalling at single cell resolution. Using this reporter, we realize that long poly(A) stretches are a major stalling signal in mammalian cells. We also confirm the active role of the Zinc finger protein 598 (ZNF598) E3 ubiquitin ligase (mammalian homolog of yeast Hel2) in the induction of quality control during excessively slow translation.

In Chapter 3, we further pursue the biological role of ZNF598 and identify two ribosomal proteins of the 40S ribosomal subunit as its primary ubiquitination targets. We subsequently verify these targets *in vivo*, showing that site-specific, ZNF598-mediated ubiquitination of the core ribosomal proteins is functionally important for the induction of RQC.

In Chapter 4, we reconstitute ZNF598-mediated recognition of ribosomes translating through stall-inducing poly(A) mRNA in an *in vitro* translation system. We find that ZNF598 recognizes closely juxtaposed, collided di-ribosome species, which are formed as a consequence of excessively slow translation. We further characterize this species biochemically and structurally to describe its unique features. In Chapter 5, these features are then exploited to validate our *in vitro* results in the context of a living cell. Crucially, we confirm all of our *in vitro* findings, additionally showing that ZNF598 can act as a general sensor of excessively slow translation, as it is capable of detecting collisions induced by a variety of different pausing signals. Finally, we explore the physiological implications of our collision-based detection mechanism. We demonstrate that the threshold for the induction of quality control can be actively modulated, as it

integrates multiple parameters such as relative ribosome speeds and inter-ribosomal distances, which are shaped by cellular context.

In Chapter 6 we focus on the downstream steps immediately after ribosome ubiquitination. Exploiting our dual-fluorescence stalling reporter combined with genetics and *in vivo*-based biochemistry, we characterize mammalian helicase ASCC3 as a novel factor recently implicated in the early events of the RQC. Most importantly, we show that it binds to the ribosomes as a stable multi-protein complex, acting downstream of ZNF598.

Finally, in the last chapter we discuss the implications of our findings, and how they change our understanding of co-translational quality control mechanisms, as well as how they can be understood in the context of the broader field of translational control.

Chapter 2: Analysis of translational stalling in mammalian cells

The first hints that stalled translation is coupled to nascent protein destabilization came from experiments in yeast *S. cerevisiae*. Using cleverly designed reporter constructs, it was shown that translation through an mRNA consisting of a stretch of 36 adenines (poly(A)) led to translational stalling and rapid proteasomal degradation of the resulting truncated polypeptide (Ito-Harashima et al., 2007). In the decade following this initial observation, the pathway responsible for the degradation of these stalled nascent polypeptides has been described in great mechanistic detail [see Chapter 1.4, also reviewed in (Joazeiro, 2017)]. However, it remains unclear how cells detect these stalled ribosomes in the first place. Fundamental questions such as whether stalling itself is due to intrinsic properties of the poly(A) mRNA and/or the nascent peptide, or if it relies on the activity of trans-acting factors remain outstanding. Initial hypotheses posited that translational repression may be due to interactions between the positively charged lysine residues and negatively charged ribosomal exit tunnel (Lu and Deutsch, 2008), however this idea is certainly too simplistic in light of more recent observations. For example, experiments in mammalian cells showed that AAA codons lead to more severe stalling than synonymous AAG codons which should both result in a poly-lysine polypeptide, suggesting that the mRNA sequence may play a much more important role than previously anticipated (Arthur et al., 2015). Secondly, deletion of the ribosomal protein Asc1 or putative E3 ubiquitin ligase Hel2 permits readthrough of polybasic sequences, thereby implicating these factors as having essential roles in this process (Brandman et al., 2012; Kuroha et al., 2010; Letzring et al., 2013). Finally, the position of the polybasic sequence within the open reading frame (ORF) seems to influence dependence of stalling on the presence of Asc1 or Hel2. It was shown that polybasic sequences located near the start codon stall translation in a Hel2 and Asc1 independent manner, whereas the same sequences located downstream seem to be sensitive to deletion of both of those factors (Letzring et al., 2013). Together, these observations challenge any existent explanations as to why poly(A) sequences cause stalling and protein degradation. As such, we chose to develop a system to rigorously study the basis of ribosome stalling on these problematic mRNA sequences.

To understand how additional trans-acting factors may influence translation through poly(A) mRNA, we developed a flow-cytometry based reporter assay for studying translational stalling at single cell resolution. With this assay, we determined that long stretches of poly(A) mRNA (~60 adenines) are the most efficient signal for the induction of the RQC pathway in humans. Using poly(A) as a model stalling substrate, we were able to confirm involvement of RACK1 (human homolog of Asc1) in the induction of this quality control pathway. We also verified our *in silico* prediction that human protein ZNF598 is a functional homolog of the yeast Hel2. Cells lacking ZNF598 showed reduced amounts of stalling on poly(A) compared to wild type cells. Additional genetic rescue experiments using a ligase-deficient mutant version of ZNF598 showed that ubiquitin ligase activity is essential to induce stalling and trigger the RQC pathway on poly(A) sequences. Finally, genetic epistasis experiments allowed assignment of both genes RACK1 and ZNF598 in the same pathway, as no synergistic phenotype was observed upon their simultaneous depletion.

Cumulatively, our results suggest that ZNF598 and RACK1 are involved in the same process: facilitating identification of ribosomes translating poly(A) stretches and inducing the downstream events of the RQC pathway. The ubiquitin ligase activity of ZNF598, which proved to be essential for its function in this pathway, suggests a previously underappreciated role for post-translational modifications (PTMs) in modulating protein translation.

2.1 Fluorescence-activated cell sorting (FACS)-based assay for studying translational stalling

The hallmark definition of ribosomal stalling is the inability of the ribosome to terminate the canonical translation cycle. Therefore, a useful assay for monitoring translational stalling should indicate whether a ribosome can efficiently engage and translate mRNA upstream of a test stalling sequence and subsequently show whether the ribosome is then capable of reaching the stop codon. Such an assay would be able to parse between direct effects of a stalling sequence on translation elongation from other types of translational repression (e.g. inhibition of translation initiation by systemic stress response or mRNA degradation). Previous assays for studying translational stalling in yeast were mostly based on reporters encoding fusions of two different fluorescent/luminescent proteins separated by a test stalling sequence (Brandman et al., 2012; Letzring et al., 2010). In

theory, the amount of stalling can be deduced from quantitating the ratio between fluorescence/luminescence downstream versus upstream of the stall. However, while theoretically appealing, in practice interpreting the results from these reporters is complicated by the fact that translational stalling induces degradation of the mRNA (Doma and Parker, 2006), as well as the truncated nascent polypeptide (Ito-Harashima et al., 2007). Therefore, effective terminal stalling inevitably results in the complete repression of the entire reporter.

In order to circumvent this complication, we designed a reporter assay which would allow us to decouple translational stalling from the degradation of the protein product upstream of the stall. We took advantage of a double fluorescent reporter system encoding GFP on the N-terminus and RFP on the C-terminus separated by a stalling reporter (SR). The stalling reporter backbone consisted of an N-terminal 3xFLAG tag and the previously described autonomously folding villin headpiece (VHP) domain fused with the test stalling sequence by an unstructured linker derived from the cytosolic fragment of Sec61β (Shao et al., 2013) (Figure 2.1A). Importantly, both fluorescent proteins are insulated from the SR by two viral P2A sequences, which cause skipping of the peptide bond formation without interrupting translation elongation (Lin et al., 2013). Hence, successful translation of the entire cassette should result in the production of equal amounts of three separate protein products: GFP, 3xFLAG-SR and RFP. In contrast, terminal stalling induced by the test sequence encompassed by the SR should interrupt translation before RFP synthesis, resulting in unequal amounts of RFP relative to GFP. Both fluorescent proteins have long half-lives and are not attached to any potential degron sequences, allowing the relative ratio of the two to be detectable by fluorescence-activated cell sorting (FACS) for a significant period following their initial translation. This ratio would then act as an indicator of the amount of terminal stalling induced by the test sequence. Moreover, the level of the N-terminal GFP would also be an indirect measure of mRNA abundance. This permits western blot analysis of 3xFLAG-SR levels normalised to GFP level, therefore controlling for mRNA abundance while reporting on stall-induced degradation by cellular quality control pathways.

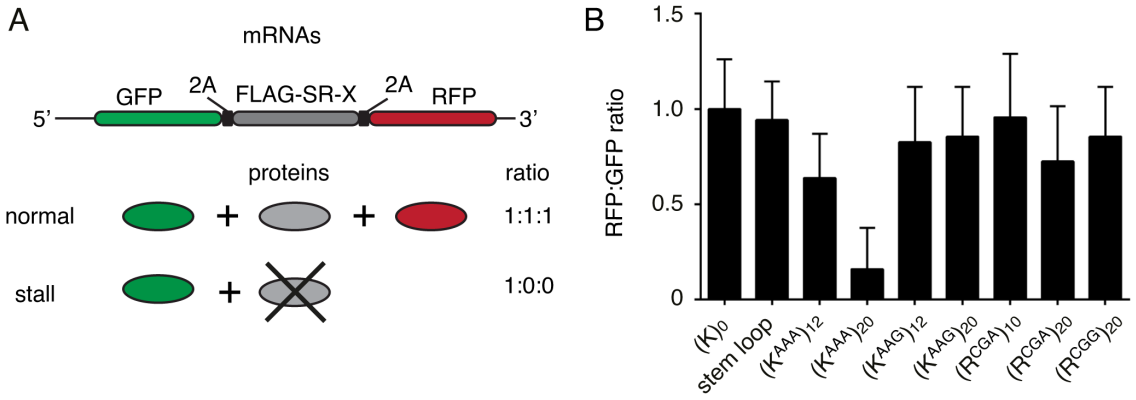

Figure 2.1 FACS-based assay for studying translational stalling in mammalian cells. (A) Schematic representation of the reporter construct and expected protein products in the absence or presence of terminal stalling; X in "FLAG-SR-X" indicates tested stalling sequence. **(B)** Median RFP:GFP ratio of cells transiently transfected with indicated stalling reporters ('X'). Error bars represent 68% of the events around the median (n=20,000).

2.2 Poly(A) is the major signal for stalling in mammalian cells

Our first experiment aimed to assess the stalling potential of different mRNA sequences previously implicated in translational repression in yeast and mammalian *in vitro* systems. We sampled a number of different examples, including a stem-loop sequence (Doma and Parker, 2006), stretches of 12 or 20 lysine residues encoded by either AAG or AAA and poly-arginine (10 or 20 residues) encoded by CGA or CGG. To this end, we transiently transfected HEK 293 cells with different stalling reporters in our cassette and quantified the RFP:GFP ratio. For all subsequent FACS-based experiments, instrument settings (including voltage on both GFP and RFP channels) were adjusted to produce RFP:GFP ratio of 1 when the control sequence $(K)_0$ (containing no additional elements besides the universal 3xFLAG-SR backbone) was analysed.

Our analysis of different putative stalling sequences yielded interesting results. For example, an mRNA stem-loop sequence previously shown to induce translational stalling and trigger the no-go decay pathway in yeast (Doma and Parker, 2006) failed to induce any appreciable stalling (Figure 2.1B). This discrepancy could be due to the more processive activity of mammalian versus yeast ribosomes. Similarly, stretches of two different poly-arginine tracts encoded by codons CGG and CGA of up to 20 repeats also failed to result in stalling when analysed in our mammalian system. This indicates that inefficient wobble decoding of CGA codons, previously described as being problematic for translation in yeast (Letzring et al., 2013), does not have a significant impact on mammalian translation machinery. Indeed, only stretches of polylysine encoded by AAA

codons, [depicted as $(K^{AAA})_n$, where n represents the number of codons], showed appreciable decrease in the RFP:GFP ratio. The $(K^{AAA})_{12}$ construct reduced the ratio to about 60% of the control sequence, whereas translation of $(K^{AAA})_{20}$ construct resulted in a dramatic ~8-fold decrease in RFP:GFP ratio. At the same time, stretch of polylysine encoded by a different codon $(K^{AAG})_{20}$ showed only a very slight decrease in RFP:GFP ratio.

Previous reports suggested possible frameshifting events which can occur during translation through iterated AAA codons (Arthur et al., 2015; Koutmou et al., 2015). We therefore decided to investigate the possibility and extent of frameshifting for our reporters. For this, we designed additional constructs in which a single nucleotide was introduced or deleted immediately preceding RFP, changing its reading frame relative to the remainder of the construct (Figure 2.2A). Flow cytometry analysis revealed that for the control $(K)_0$ construct RFP is present only in its native frame, as expected. In contrast, for both $(K^{AAA})_{12}$ and $(K^{AAA})_{20}$ significant amounts of RFP signal were detectable in all three reading frames, with a slightly lower preference for the +1 frame (Figure 2.2B). This analysis indicates that our reporters are consistent with previous reports of frameshifting through poly(A) stretches. Therefore, we reasoned that the RFP:GFP ratio in our original experiments likely underestimate the actual amount of poly(A) readthrough. In order to correct for this effect, the RFP:GFP ratio observed at the peak of each histogram showed in Figure 2.2B (i.e. median value of RFP:GFP ratio for -1, 0 and +1 RFP constructs) was used as an indicator of read-through into that frame. The sum of the values for all reading frames was used to estimate the net read-through (i.e., the RFP:GFP ratio that would have been seen if there was no frameshifting). This analysis shows that the compensated RFP:GFP ratio for $(K^{AAA})_{12}$ is ~90% of that seen for $(K)_0$, whereas the compensated ratio for $(K^{AAA})_{20}$ is ~40% of that seen for $(K)_0$. Correcting for frameshifting we see that $(K^{AAA})_{12}$ and $(K^{AAA})_{20}$ constructs show ~10% and ~60% stalling relative to the control $(K)_0$ sequence, respectively.

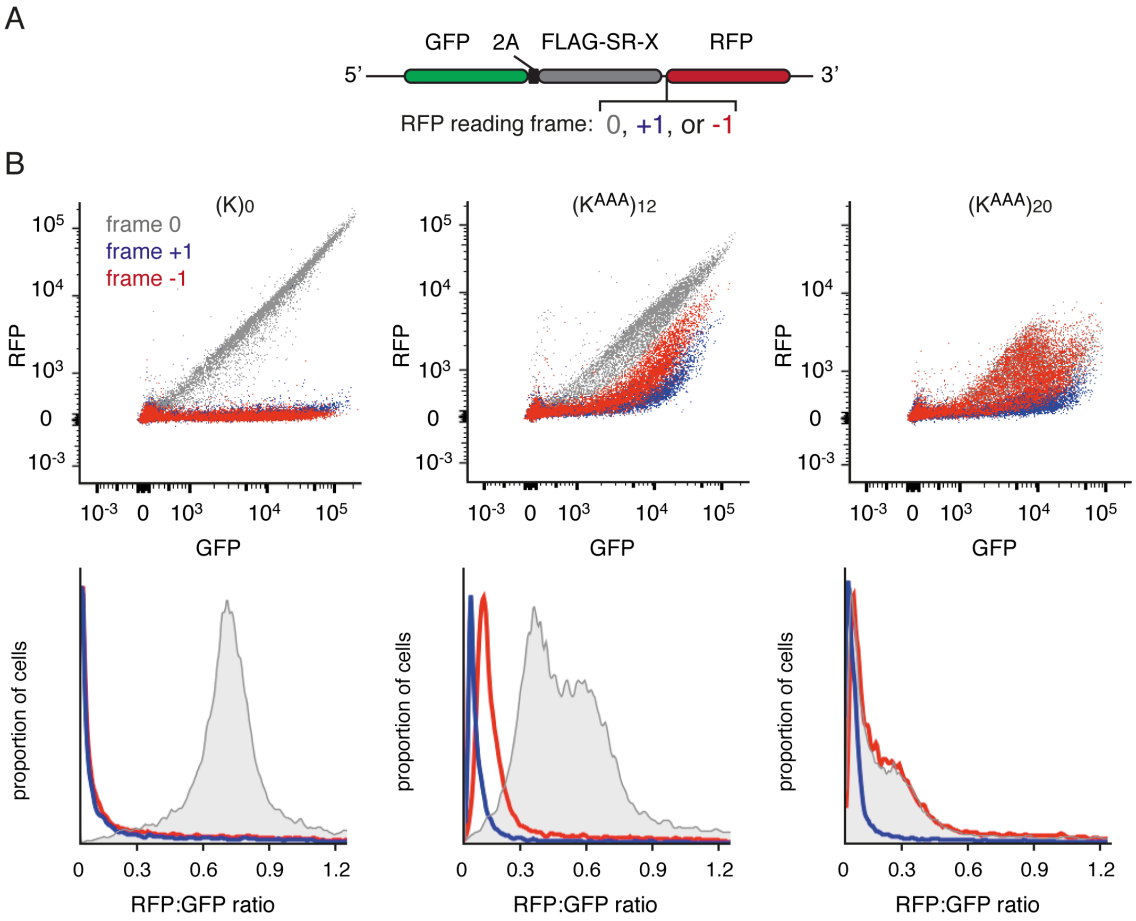

Figure 2.2 Analysis of frameshifting during translation through poly(A). (A) Schematic representation of constructs used for monitoring frameshifting. Single nucleotide insertions or deletions were introduced just preceding RFP to change its reading frame relative to the remainder of the construct. **(B)** HEK 293 cells were transfected with either $(K)_0$, $(K^{AAA})_{12}$ or $(K^{AAA})_{20}$ constructs in each of the three RFP reading frames and analysed by flow cytometry after 24 hours. Shown below each scatter plot of GFP and RFP levels are the corresponding histograms of the RFP:GFP ratio. Grey is the native frame where RFP is in frame with GFP. Red and blue are constructs with RFP in the -1 and +1 frames relative to GFP, respectively.

Our results are generally in agreement with the only currently available study of translational stalling in mammalian cells (Arthur et al., 2015). Arthur et al. studied translation of polybasic sequences (including poly(A) encoded poly-lysine) using neonatal human fibroblasts as a model system. Their reporter differed substantially from ours, as it contained the test sequence near the 5' end of the ORF and did not account for mRNA degradation. This detail notwithstanding, they do report that poly(A) is a much more effective signal for stalling than other polybasic sequences. Curiously however, they observe a different threshold for stalling, with six AAA codons sufficient to see a ~ 4-fold reduction in test construct expression, while we only see a substantial difference at 12 and more codons. This disparity may be due to differences in the cell type used or

the nature of the reporter itself. That being said, the major conclusion from our results is that mammalian cells, unlike yeast, evolved to induce stalling within mRNA containing long poly(A) stretches. Given that the poly(A) sequences which induced terminal stalling in our system are much longer than any poly(A) region encoded within human genome, it seems plausible that this pathway is likely tuned to identify mRNAs that are prematurely polyadenylated within the coding region. This would trigger stalling before the aberrant and unnecessary synthesis of ~20 lysine residues.

2.3 Translation through poly(A) in mammals induces RQC-mediated degradation of nascent protein

To characterize poly(A) mediated stalling in more detail, we generated stable isogenic cell lines using the Flp-In 293 T-Rex system integrating either control $(K)_0$ or stall-inducing $(K^{AAA})_{21}$ reporters under a doxycycline inducible promoter. Flow cytometry analysis showed the expected correlation between GFP and RFP levels across a broad range of expression in control $(K)_0$ cells. By contrast, $(K^{AAA})_{21}$ cells showed dramatically reduced levels of RFP, without an appreciable decrease in the GFP. As a consequence, the $(K^{AAA})_{21}$ expression resulted in a ~8-fold decrease in the RFP:GFP ratio compared to $(K)_0$ expression (Figure 2.3A).

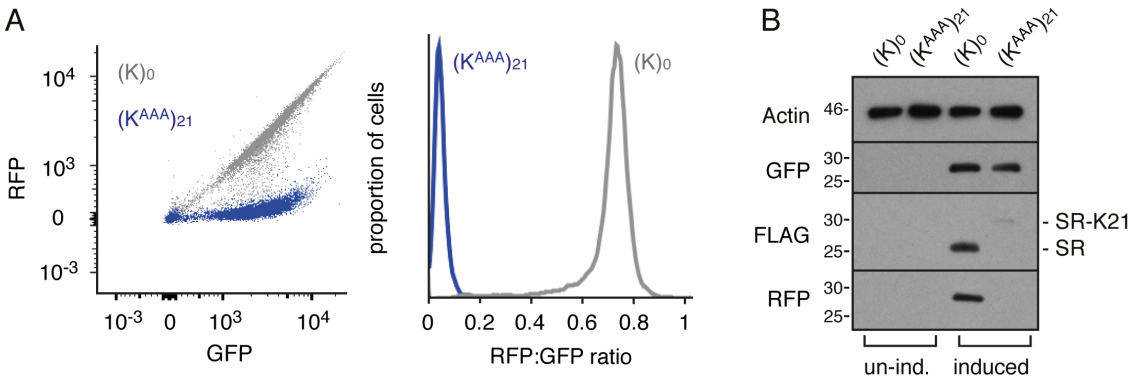

Figure 2.3 Stable cell line expressing the $K(^{AAA})_{21}$ stalling reporter recapitulates terminal stalling observed with transient transfection. (A) Isogenic cell lines expressing control $(K)_0$ (in gray) or $(K^{AAA})_{21}$ (in blue) reporter constructs for 24h following doxycycline induction were analysed by FACS. A scatter plot of individual events (left) and a cumulative histogram representing RFP:GFP ratio (right) are shown. **(B)** Whole cell lysates from $(K)_0$ and $(K^{AAA})_{21}$ cells with or without induction with doxycycline for 24h were analysed by western blotting. Note the absence of RFP and dramatic decrease in FLAG-tagged SR in $K(^{AAA})_{21}$ cell line upon induction, indicative of terminal stalling. For reference, the levels of upstream GFP are equal in both control and stalling reporter cell lines. SR and SR-K21 indicate positions of the stalling reporter on the blot (see Figure 2.1A).

Western blot analysis of lysates from both cell lines showed loss of RFP expression in the $K(^{AAA})_{21}$ cell line, without any changes to upstream GFP expression, confirming flow cytometry results (Figure 2.3B). Moreover, we saw significantly decreased levels of the 3xFLAG-SR in $(K^{AAA})_{21}$ cells compared to the $(K)_0$ control. The small amount of signal observed in the $(K^{AAA})_{21}$ cells seen as higher molecular weight bands (Figure 2.3B, lane 4), corresponds to the expected size of the 3xFLAG-SR-K_{21} readthrough product. This is consistent with low levels of RFP observed in those cells.

To determine whether the stalling-specific decrease in 3xFLAG-SR in $(K^{AAA})_{21}$ cells was due to proteasome-mediated degradation, we treated cells with the proteasome inhibitor MG132. This resulted in a small increase of the full length 3xFLAG-SR-K_{21} (Figure 2.4A). Moreover, longer exposure of the western blot revealed the existence of smaller molecular weight, heterogenous products that migrated as a smeary pattern on the gel specifically in the MG132-treated sample (second lane). These heterogenous products correspond to the truncated nascent polypeptides and are referred to henceforth as arrested products (AP). Consistent with this interpretation, only the arrested products were selectively stabilised in cells treated with siRNA targeting NEMF, an essential component of the RQC-mediated nascent protein degradation pathway (Figure 2.4B, lane 3) (Shao et al., 2015).

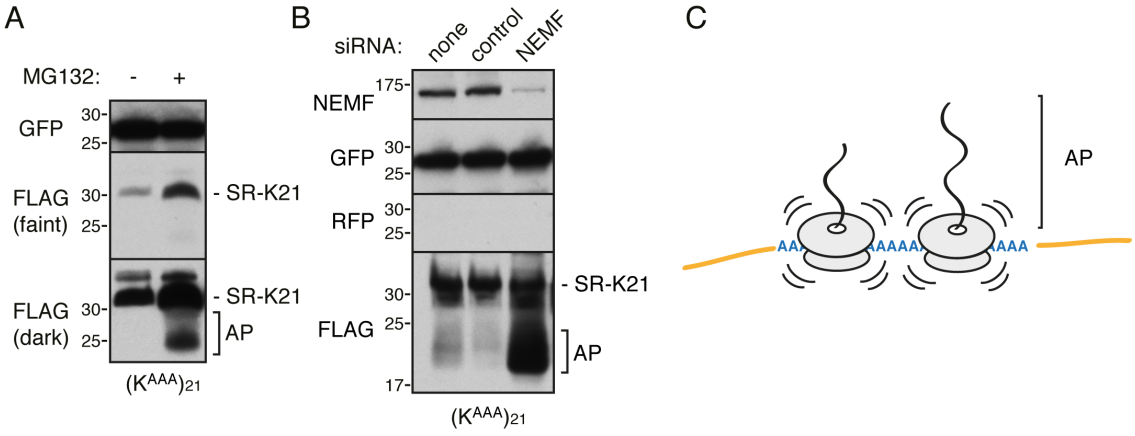

Figure 2.4 Arrested nascent polypeptides are targeted to the proteasome by RQC pathway. **(A)** Cells expressing $(K^{AAA})_{21}$ stalling reporter for 24h were treated with 20 µM proteasome inhibitor MG132 for 4h. Cell lysates were collected and analysed by western blotting for expression of GFP and RFP as indicated. **(B)** $(K^{AAA})_{21}$ cells were subjected to indicated siRNA treatment for 72h, expression of the reporter was concurrently induced for 24h and resulting cell lysates were analysed by western blotting. **(C)** Schematic representation of the ribosomes stalled on the poly(A) exposing arrested products of different lengths (AP).

This result indicates that most ribosomes translating through poly(A) stall terminally, while resulting arrested translation products are effectively targeted for degradation by the known RQC pathway (Figure 2.4C). The small number of ribosomes that readthrough the poly(A) generate full-length 3xFLAG-SR-K_{21} peptide. This product itself is targeted for proteasomal degradation by other quality control pathways, most likely recognizing long, polybasic stretch of lysines, which might serve as a degron sequence. This highlights the importance of insulating the stalling sequence from fluorescent proteins, which allowed us to decouple any protein-degradation events from translational stalling.

Closer inspection of the higher molecular weight domains of the western blots, like in the one in Figure 2.4B, revealed that skipping of the peptide bond at the P2A sequence sometimes fails (Figure 2.5A). Especially after NEMF knockdown one can see small amounts of the fusion products, instead of separate proteins. However, this species was minor and did not affect the interpretation of flow cytometry results and cumulative fate of the FLAG-SR.

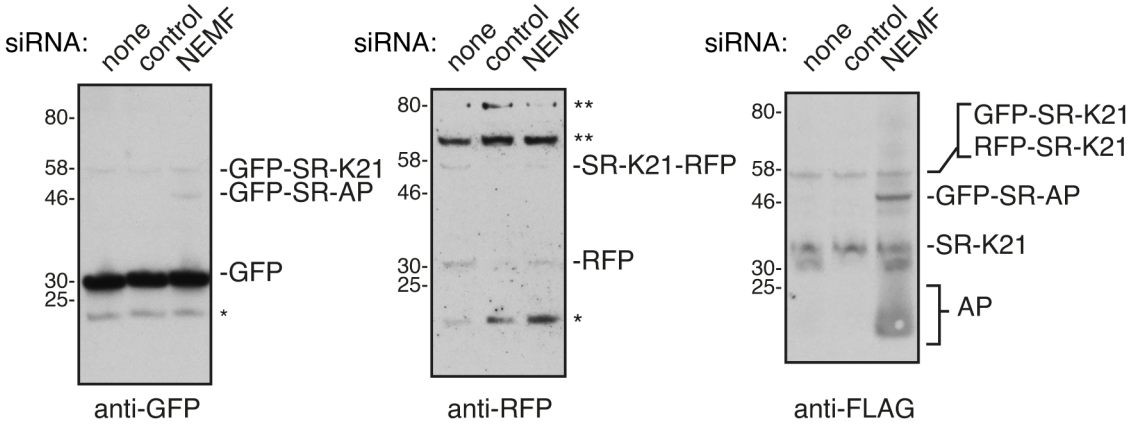

Figure 2.5 Skipping of the peptide bond on the P2A sequences sometimes fails. Lysates from $(K^{AAA})_{21}$ cells subjected to indicated siRNA treatment for 72h and induced with doxycycline for another 24h were analysed by western blotting. Full western blots probed against GFP, RFP and FLAG are shown. Note that small amounts of the fused products are indicated in the upper parts of the membranes. Asterisks indicate non-specific products

Finally, both FACS and western blot results (Figures 2.3A, B) do not show any difference in GFP expression between $(K)_0$ containing control cells and $(K^{AAA})_{21}$ cells. This indirectly reflects equal mRNA levels of both reporters and argues against appreciable mRNA degradation induced by stalling. It also means that, at least in HEK 293 cells, RQC-mediated protein degradation is not always accompanied by mRNA degradation. This argues that the endonucleolytic cleavage of the aberrant mRNA

induced by terminal ribosomal stalling (Doma and Parker, 2006; Kuroha et al., 2010; Tsuboi et al., 2012) is not required for initiation of the RQC pathway, meaning that these two pathways can be decoupled.

2.4 40S ribosomal protein RACK1 facilitates stalling on poly(A) sequences

Having established a quantitative assay and validated a model stalling substrate, we decided to investigate the role of auxiliary components in terminal ribosomal stalling. It was previously reported that the yeast Asc1 stimulates ribosomal arrest on iterated CGA codons (Brandman et al., 2012; Kuroha et al., 2010; Letzring et al., 2013), as well as other polybasic sequences, including poly(A) encoded poly-lysine (Kuroha et al., 2010). Given our results, we set out to investigate whether the 40S ribosomal protein RACK1, the human homolog of Asc1, is also mediating stalling on poly(A) sequences in mammalian cells. For this, we used siRNA-mediated gene silencing to efficiently knock down RACK1 in our characterised $K(^{AAA})_{21}$-expressing stable cell line (Figure 2.6A). Flow cytometry analysis showed that RACK1 knockdown results in an increase in the RFP:GFP ratio, indicative of increased readthrough the stalling sequence. This suggests that in humans, as in yeast, RACK1 seems to facilitate stalling on poly(A) sequences, suggestive of a broadly conserved role in translational arrest.

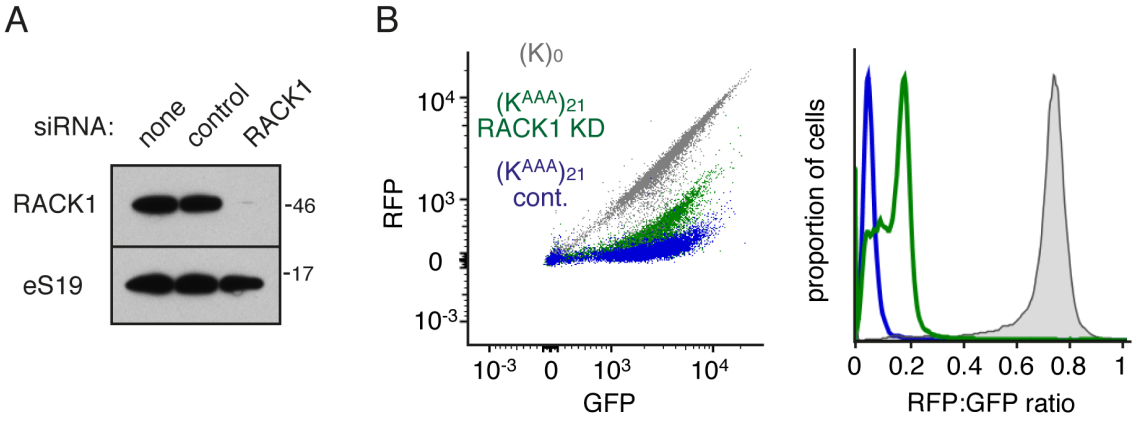

Figure 2.6 Human RACK1 facilitates stalling on poly(A) sequences. $(K^{AAA})_{21}$ cells were treated with nothing, control or RACK1 targeting siRNAs for five days and analysed by **(A)** western blotting and **(B)** flow cytometry; scatter plot representing individual events (left) and histogram depicting calculated RFP:GFP ratio (right) are shown.

2.5 ZNF598 is a human homolog of Hel2

RACK1 is a ribosomal protein belonging to the WD40 protein family. Members of this family, including RACK1, are known to act as a scaffolding proteins mediating numerous interactions within complex networks of signalling pathways (Gallo and Manfrini, 2015). Therefore, it is likely that RACK1 will play more passive, structural role in mediating quality control response during translation through stall-inducing sequences. However, alongside Asc1, another candidate protein Hel2, a putative E3 ubiquitin ligase, was previously implicated in mediating stalling on iterated CGA codons in yeast (Brandman et al., 2012; Letzring et al., 2013). This suggested the exciting possibility of a ubiquitin-mediated mechanism of translational regulation. We sought to explore this possibility in a mammalian system in the context of our reporter construct. Our attempts to find a mammalian homolog using regular homology BLAST searches failed, however the Ensembl Biomart tool (Flicek et al., 2014) uncovered ZNF598 as a putative homolog. ZNF598 is a RING domain-containing protein which shares 15% homology with Hel2. In order to see whether this candidate may also have a role in the translation stalling process, we knocked it down in the stable cell line expressing the $(K^{AAA})_{21}$ reporter using siRNA (Figure 2.7A). Quantitative analysis using FACS revealed an increase in the RFP:GFP ratio upon ZNF598 depletion, attributable to increased readthrough the poly(A) stalling sequence (Figure 2.7B). This conclusion is further supported by the increased levels of both full-length FLAG-SR-K_{21} and RFP downstream of the stall sequence, but not GFP which is upstream of the stall (Figure 2.7C).

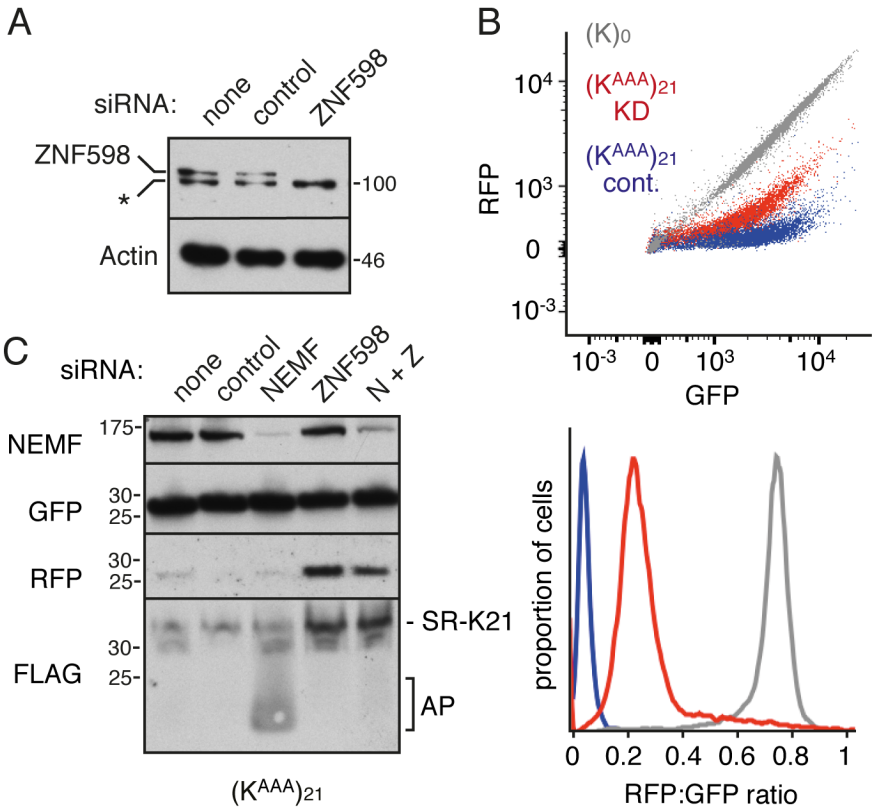

Figure 2.7 ZNF598 is required to initiate RQC pathway during translation through poly(A) sequences. $(K^{AAA})_{21}$ cells were treated with nothing, control or ZNF598 targeting siRNAs for 72h, induced for the expression of the reporter for 24h and analysed by western blotting **(A)** or flow cytometry **(B);** $(K)_0$ cells (in grey) served as a reference. **(C)** $(K^{AAA})_{21}$ cells were treated with indicated siRNAs for 72h and analysed by western blotting for depicted proteins; N+Z indicates combined knockdown of both NEMF and ZNF598. Asterisk indicates non-specific band detected by anti-ZNF598 antibody.

As was already shown in Figure 2.4B, NEMF knockdown in $(K^{AAA})_{21}$ cells resulted in the stabilisation of heterogenous arrested products, which were a consequence of failed RQC-mediated degradation. Combined knockdown of NEMF and ZNF598 abolished formation of those arrested products, which implies that ZNF598 must act upstream of NEMF and therefore initiate the RQC pathway (Figure 2.7C).

In order to generate a more reliable tool for studying the specific function of ZNF598, we knocked out ZNF598 in stable cells bearing the $(K^{AAA})_{21}$ reporter using CRISPR-Cas9 technology (Figure 2.8A) (Ran et al., 2013). ZNF598 knockout (KO) cells recapitulated the phenotype observed with siRNA knockdown (Figure 2.8B).

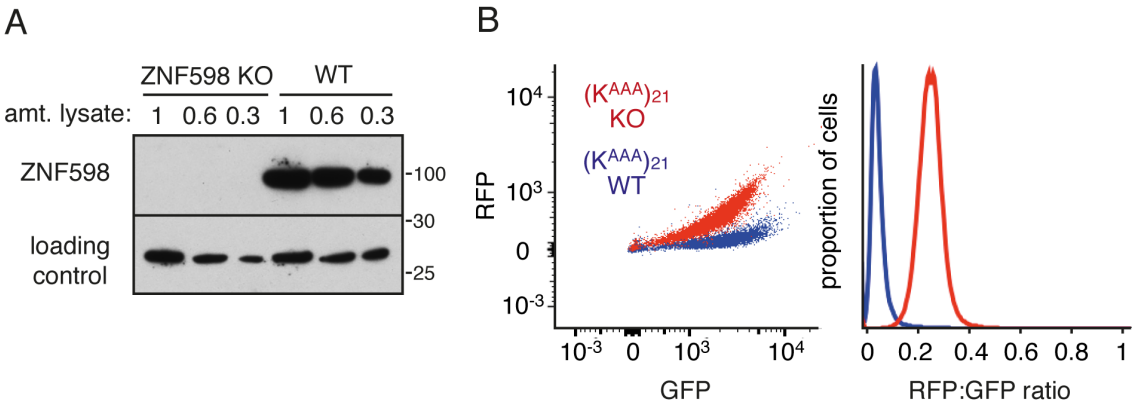

Figure 2.8 ZNF598 knockout cells recapitulate the poly(A) readthrough phenotype. (A) Serial dilutions of lysates from WT and ZNF598 KO cells were analysed by western blotting. **(B)** Same WT and KO cells as in (A) were induced for the expression of the reporter for 24h and analysed by flow cytometry.

Analysis of transiently expressed reporters of poly(A) frameshifting in the ZNF598 knockout cells confirmed a significant amount of translation downstream of the $(K^{AAA})_{21}$ in all three frames, with +1 frame being less preferred (Figure 2.9A, B). After correcting for frameshifting, it was estimated that ZNF598 deletion results in readthrough of the $(K^{AAA})_{21}$ reporter, which is up to 90% of what is observed for the control $(K)_0$ construct. Collectively, these results indicate that in cells lacking ZNF598 there is almost no terminal stalling or RQC mediated degradation.

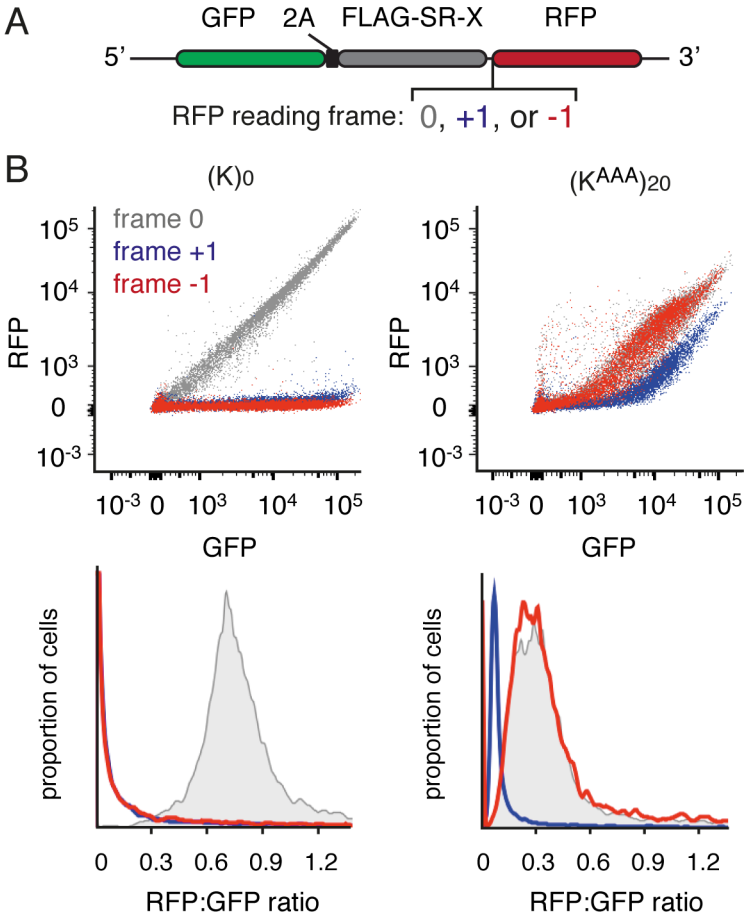

Figure 2.9 Analysis of frameshifting in ZNF598 KO cells. (A) Schematic representation of constructs used for monitoring frameshifting. **(B)** ZNF598 KO cells were transfected with either $(K)_0$ or $(K^{AAA})_{20}$ constructs in each of the three RFP reading frames and analysed by flow cytometry after 24 hours. Shown below each scatter plot of GFP and RFP levels are the corresponding histograms of the RFP:GFP ratio. Grey is the native frame of RFP relative to GFP. Red and blue are constructs with RFP in the -1 and +1 frames, respectively.

2.6 Ligase activity of ZNF598 mediates its function within the RQC pathway

ZNF598, similarly to Hel2, contains a conserved RING domain near its N-terminus, which suggests that it may act as a RING-type E3 ubiquitin ligase (Figure 2.10A). In order to test whether the ZNF598's RING domain (and therefore possible ligase activity) is necessary to mediate terminal stalling during poly(A) translation, we overexpressed either wild type or mutant ZNF598 lacking the RING domain (ΔRING-ZNF598) in our ZNF598 KO cells at similar levels (Figure 2.10B). Induction of the $K(^{AAA})_{21}$ reporter and subsequent analysis of GFP and RFP levels by FACS allowed us to conclude that only WT ZNF598 but not ΔRING-ZNF598 can reverse RFP:GFP ratio to the levels observed

in WT (not ZNF598 KO) cells (Figure 2.10C, D). Thus, it appears that ZNF598's ability to induce quality control during poly(A) translation is completely dependent on its ubiquitin ligase activity.

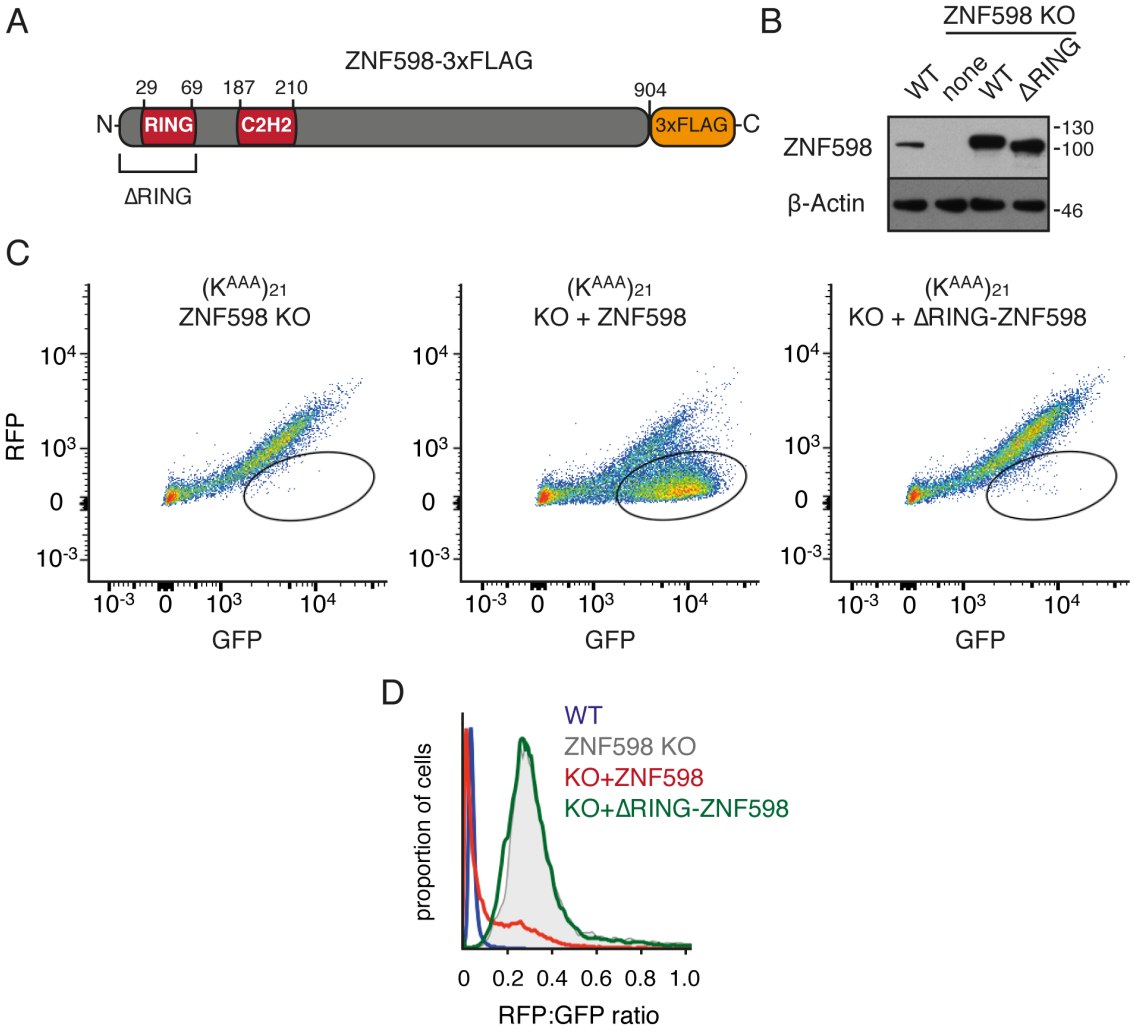

Figure 2.10 ZNF598 induces quality control during poly(A) translation through its RING domain. (A) Schematic representation of ZNF598 constructs used in genetic rescue experiments illustrating the position of the affinity tag and region deleted to generate ligase-deficient mutant. **(B)** ZNF598 KO cells were transiently transfected with WT or ΔRING-ZNF598 and after 24h analysed by western blotting to confirm similar expression levels of both proteins. **(C)** ZNF598 KO cells were transiently transfected with WT or ΔRING-ZNF598 (as judged by expression of co-transfected BFP) and analysed by FACS 24h after induction of the reporter with doxycycline. The majority of cells expressing WT ZNF598 displayed restored ribosomal stalling as indicated by reduced RFP expression levels (marked with black circle). **(D)** Histograms of the RFP:GFP ratio for cells analysed in (C) are plotted in comparison to WT cells.

2.7 RACK1 and ZNF598 act within the same pathway

Deletion of either RACK1 or ZNF598 resulted in a similar phenotype as manifested by increased RFP:GFP ratio in the $(K^{AAA})_{21}$ construct. Moreover, this effect could be

attributed mainly to increased expression of RFP positioned downstream of the stall-inducing poly(A) tract (as a result of the failure in the induction of quality control response). These observations allowed us to conclude that in mammals, as in yeast, both RACK1 and ZNF598 (or their homologs) are involved in induction of the RQC during translation through stall-inducing sequences. We next wondered whether these proteins act independently as part of separate pathways or if they cooperate within the same pathway. To address this, we knocked down RACK1 in the existing ZNF598 KO reporter cell line. When analysed by FACS, cells depleted of both RACK1 and ZNF598 showed higher expression of GFP (but not RFP) when compared to ZNF598 KO cells (Figure 2.11A). Hence, double deletion resulted in a lower overall RFP:GFP ratio (Figure 2.11B). This result indicates that both proteins must act in the same pathway as double deletion shows no additive effect when considering readthrough the stalling sequence. The small increase in GFP expression observed upon RACK1 knockdown is probably due to disruption of other functions of RACK1 outside RQC, whereas incomplete readthrough the poly(A) could be explained by frameshifting (as previously described).

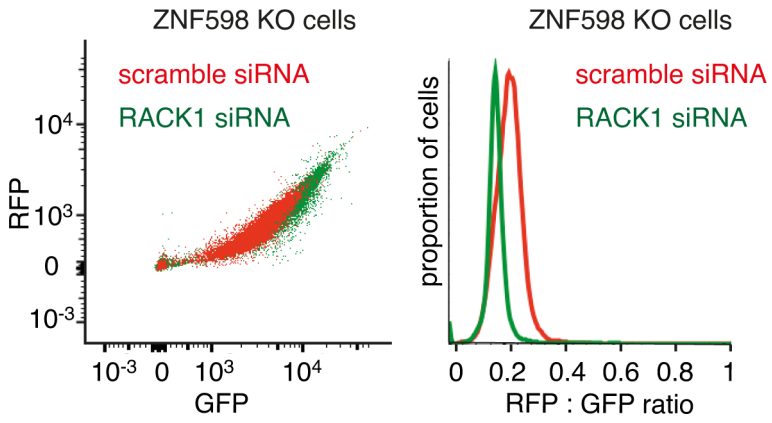

Figure 2.11 ZNF598 and RACK1 act within the same pathway to induce quality control during poly(A) translation. ZNF598 KO cells bearing the $(K^{AAA})_{21}$ reporter were treated with siRNA targeting RACK1 (green) or scrambled siRNA (red) for 5 days, induced for the expression of reporter for 24h and analysed by flow cytometry. Scatter plot representing individual events (left) and histogram depicting calculated RFP:GFP ratio (right) are shown.

2.8 Discussion

We have developed a robust, *in vivo* single cell resolution assay for studying translational stalling in mammalian cells. This assay allowed us to probe multiple different mRNA sequences previously reported to induce stalling in yeast. These include RNA stem-loop

sequences (Doma and Parker, 2006) and sequences encoding stretches of polybasic amino acids such as polyarginine and polylysine of varying lengths (up to 20 iterated codons) (Brandman et al., 2012; Ito-Harashima et al., 2007; Kuroha et al., 2010). To our surprise, out of the whole panel of tested sequences (Figure 2.1B) only long stretches of poly(A) (more than 40 adenines) were able to stall translation to an appreciable level. Our results are largely inconsistent with the previous simplistic model explaining stalling on polybasic sequences through electrostatic interactions in the ribosomal exit tunnel (Lu and Deutsch, 2008). Although it is still possible that polybasic sequences can slow down translation speed, this seems insufficient to induce terminal ribosomal stalling in mammals as evidenced by our data (at least in human HEK 293 cells). The threshold for stalling observed in our analyses (~40 adenines) is much longer than the longest stretches of adenines natively occurring within the open reading frames of the human genome (Arthur et al., 2015). This implies that the quality control system responsible for detection of ribosomal stalling is tuned to specifically recognise translation through the poly(A) tail. This is important, as it might reflect an evolutionary adaptation of higher eukaryotes to a much more complicated and therefore error prone system of mRNA processing, which includes a significant amount of gene splicing. Occasional mistakes during mRNA maturation, such as mis-splicing or premature cleavage and polyadenylation events could lead to generation of transcripts containing long poly(A) tails within the open reading frame. In humans, the average length of the poly(A) tail is ~250 nucleotides, hence translation through it would result in the production of a nascent chain containing ~80 lysines. Of those, even up to 50 would be exposed outside of the ribosomal exit tunnel before the ribosome reaches the end of the transcript. Highly basic stretches usually serve as a nuclear/nucleolar localisation signal (Kalderon et al., 1984b, 1984a). Therefore, such nascent polypeptides could improperly engage nuclear import factors. Once in the nucleus, polybasic peptides could interfere with RNA biogenesis, as was already shown for short poly-dipeptide repeats (glycine arginine or proline-arginine) encoded by the neurodegeneration-associated expansion repeats of the *c9orf72* gene (Kwon et al., 2014; Mizielinska et al., 2014). We speculate that synthesis of long stretches of lysines could potentially be detrimental to the cell, putting it under negative selective pressure. At the same time, the evolution of quality control pathways capable of preventing broad scale negative cellular consequences of mRNA processing mistakes seems to be facilitated.

Exactly how poly(A) mRNA can stall translation is currently unclear. However, it appears that in mammals induction of the quality control response during poly(A) translation seems to require additional trans-acting factors, as reported previously for yeast (Brandman et al., 2012; Kuroha et al., 2010). Using a cell line with a stably integrated, inducible reporter cassette containing $(K^{AAA})_{21}$ sequence, we were able to show that deletion of RACK1, the mammalian homolog of yeast Asc1, leads to increased readthrough of the stall-inducing poly(A) sequence, indicative of the failure of premature termination on the stall-inducing sequence. Moreover, we were also able to identify ZNF598 as a mammalian homolog of yeast Hel2, a putative E3 ubiquitin ligase previously implicated to be involved in the early events of the RQC pathway. Deletion of the ligase resulted in a similar readthrough phenotype as RACK1 deletion. This was due to a loss of ZNF598's ubiquitin ligase activity, as mutant version of the protein without the RING domain was not able to restore terminal ribosomal stalling on poly(A) when re-expressed in ZNF598-deficient cells. Additional genetic analyses allowed us to conclude that both RACK1 and ZNF598 most likely operate within the same pathway. The most intuitive model that could be drawn on the basis of this data involves RACK1 as a recruitment/binding element for ZNF598 ligase, which in turn should induce downstream events of the quality control pathway, ultimately leading to the degradation of the nascent polypeptide and recycling of the ribosomal subunits.

In light of our discovery and a recent report on regulatory ribosomal ubiquitination, which was observed to be induced by various stresses including inhibition of translation elongation (Higgins et al., 2015), it is tempting to speculate that ZNF598 can directly modify ribosomes with ubiquitin moieties. Hence, the ZNF598 E3 ligase could potentially act as a translational modulator which selectively recognizes ribosomes translating through poly(A) sequences and marks them with ubiquitin. This ribosomal ubiquitination event can in turn serve as a signal for downstream components of the quality control pathway. Investigation of this hypothesis as well as identification of the molecular targets of the ZNF598 are the subjects of the following chapter.

2.9 Materials and methods

Plasmids, siRNA and antibodies

Reporter constructs for transient expression were generated using the mGFP-N1 plasmid (Clontech) as a backbone. This was first modified by an RFP sequence appended to the

N-terminal P2A downstream of the multi cloning site (MCS). Next, the MCS of the backbone was replaced with the second P2A sequence followed by a 3xFLAG and previously described VHPβ sequence (Shao et al., 2013). Finally, the universal backbone was cut with SalI and KpnI restriction enzymes and various stalling sequences (see Table 2.1) were inserted as a double-stranded oligonucleotides using standard ligation. Design and generation of the original constructs was a collaborative effort between Manu Hegde, Kota Yanagitani, Verena Bittl and the author of this thesis. Constructs used for generation of the stable cell lines were obtained by cloning of the entire reporter cassettes into the pcDNA 5/FRT/TO vector. Constructs for expression of C-terminally 3xFLAG-tagged ZNF598 were in a pcDNA3.1 vector. The ΔRING-ZNF598-3xFLAG mutant was generated using site directed mutagenesis. For CRISPR-Cas9 mediated knockout of ZNF598 in reporter cell lines, guide RNA targeting exon 1 of ZNF598 (5'-TAGAGCAGCGGTAGCACACC-3') was designed using the CRISPR design tool at crispr.mit.edu and cloned into the px330-U6 plasmid (Ran et al., 2013). Most of the described constructs are available through addgene including: pmGFP-P2A-K0-P2A-RFP #105686, pmGFP-P2A-K(AAA)12-P2A-RFP #105687, pmGFP-P2A-K(AAA)20-P2A-RFP #105688, pmGFP-P2A-K(AAG)20-P2A-RFP #105689, pcDNA3.1-ZNF598-TEV-3xFLAG #105690. Silencer Select Pre-designed siRNAs were from Life Technologies: anti-ZNF598 #s40509, anti-NEMF #s17483, anti-RACK1 #s20342. Rabbit polyclonal antibodies against ZNF598 were from GeneTex #GTX119245 and Abcam #ab80458, mouse monoclonal antibody against β-actin conjugated to HRP was from SIGMA #A3854, mouse monoclonal anti-FLAG M2 antibody was from SIGMA #F3165, rabbit polyclonal anti-eS19 antibody was from Bethyl Labs #A304-002A, rabbit polyclonal anti-RACK antibody was from Bethyl Labs #A302-545A, HRP-conjugated goat anti-rabbit (#111-035-003) and anti-mouse (#115-035-003) antibodies were from Jackson Immunoresearch, rabbit polyclonal antibody against NEMF was previously described (Shao et al., 2015) and rabbit polyclonal antibodies against GFP and RFP were also custom made as described in (Chakrabarti and Hegde, 2009).

NAME	SEQUENCE (5' -> 3')
K0	CGCCATGGCGACCCCCGGGGGATCC
K12 (AAA)	CGCCATGGCGACCAAAAAAAAAAAAAAAAAAAAAAAAAAAAAAAAAA CCCGGGGGATCC
K20 (AAA)	CGCCATGGCGACCAAAAAAAAAAAAAAAAAAAAAAAAAAAAAAAAAA AAAAAAAAAAAAAAAAAAAAAAAAACCCGGGGGATCC
K12 (AAG)	CGCCATGGCGACCAAGAAGAAGAAGAAGAAGAAGAAGAAGAAGAAGAAG CCCGGGGGATCC
K20 (AAG)	CGCCATGGCGACCAAGAAGAAGAAGAAGAAGAAGAAGAAGAAGAAGAAG AAGAAGAAGAAGAAGAAGAAGAAGCCCGGGGGATCC
R10 (CGA)	CGCCATGGCGACCCGACGACGACGACGACGACGACGACGACGACCCGGGG GATCC
R20 (CGA)	CGCCATGGCGACCCGACGACGACGACGACGACGACGACGACGACGACGAC GACGACGACGACGACGACGACCCGGGGGATCC
R20 (CGG)	CGCCATGGCGACCCGGCGGCGGCGGCGGCGGCGGCGGCGGCGGCGGCGGC GGCGGCGGCGGCGGCGGCGGCGGCCCGGGGGATCC
STEM-LOOP	CGCCCTGTTCCACTATAGGGCACCTCCCCGCGCACCACCGCCGACGTCGGC GGTGGTGCGCGGGGAGGTGCCCTATAGCGGTAC

Table 2.1 Nucleotide sequences of the stalling reporters used in this study.

Cell Culture

HEK 293 T cells (ATCC CRL-3216) were cultured in Dulbecco's Modified Eagle's Medium (DMEM) containing 10% Fetal Calf Serum (FCS). Flp-In 293 T-Rex cells (Thermo Fisher) were cultured in DMEM containing 10% tetracycline-free FCS in the presence of 15 µg/ml blasticidin and 100 µg/ml hygromycin. Stable cell lines were generated using pcDNA5/FRT/TO-based reporter constructs in the Flp-In system according to the manufacturer's protocol (Invitrogen). CRISPR-Cas9 mediated knockout of ZNF598 was performed in the stable cell line bearing $(K^{AAA})_{21}$ reporter using standard protocol (Ran et al., 2013). In brief: cells were transiently transfected with px330 plasmid encoding the sgRNA targeting exon 1 of ZNF598 gene. Three days after transfection, cells were trypsinized and subcloned into 96-well plate at a density of 0.5 cell per well to obtain single cell clones, which were allowed to grow for two weeks. Individual clones were then expanded and screened for the expression of ZNF598 protein by western-blotting of serial dilutions of the total cell lysates relative to the starting cell line. Multiple clones showing no detectable expression of ZNF598 (even with long over-exposure) were selected for further studies. Expression of transgene in stable cell lines was induced with 1 µg/ml of doxycycline for 24-48h. MG132 treatment was at 20 µM for 4h, as indicated. Transient transfections were performed using TransIt-293 reagent (Mirus) according to the manufacturer's protocol. siRNA silencing was performed using Lipofectamine RNAiMAX reagent (Life Technologies) using standard protocol for the

duration indicated on the figures. In case of RACK1 silencing, a second transfection of siRNA was performed 3 days after the first in order to obtain efficient knockdown.

Flow Cytometry

Cells from 24-well plates were trypsinized, sedimented in a tabletop centrifuge at 1,000 rpm for 5 min at room temperature, washed twice with PBS and resuspended in 0.5 ml of PBS. Flow cytometry data were collected on the Beckton Dickinson LSR II instrument and analysed in FlowJo software. The quantitative value for RFP:GFP ratio showed in Figure 2.1B represents the median for 20,000 GFP positive events normalized to the value observed for the control, non-stalling construct [$(K)_0$]. Error bars represent "robust SD" value calculated in FlowJo, which represents 68.26% of the events around median.

Western Blot Analysis

For western blot analysis, cells were firstly washed with PBS twice and directly lysed with 100 mM Tris pH 8.0 containing 1% SDS, then boiled for 10 min with occasional vortexing to shear genomic DNA. For loading, protein concentration of all samples was adjusted using NanoDrop-based measurements of the absorbance at 280 nm. SDS-PAGE sample buffer was added to the samples for a final concentration of 50 mM Tris, 1% SDS, 10% glycerol and 10 mM DTT. Samples were analysed using 10% Tris-Tricine based gels and transferred to a 0.2 μm nitrocellulose membrane (BioRad). Incubations with primary antibodies were for 1h in room temperature (RT) or overnight at 4°C. For detection, membranes were incubated with HRP-conjugated secondary antibodies for 1h in RT, whereas SuperSignal West Pico reagent (Thermo Fisher) was used as a chemiluminescent substrate.

Chapter 3: Initiation of quality control during poly(A) translation requires ZNF598-mediated site-specific ribosome ubiquitination

The recent discovery that ribosomes can be ubiquitinated in response to different stress conditions, including the inhibition of translation elongation, raised the exciting possibility that translation can be influenced by post-translational modifications of specific ribosomal proteins (Higgins et al., 2015). Our observation that ZNF598, an E3 ubiquitin ligase, is required to initiate the RQC pathway during poly(A) translation suggests the first direct link between such a ubiquitination event and translation elongation.

In order to confirm this putative mechanism in molecular detail, we set out to reconstitute ZNF598-mediated ubiquitination of the ribosomes *in vitro*. Our first goal was to identify which ribosomal (or ribosome-associated) proteins are specifically modified by ZNF598. We found the 40S subunit proteins eS10 and uS10 to be the primary and secondary targets, respectively. Both of these proteins were mainly mono-ubiquitinated on two neighbouring lysine residues, sites which were identified using mass spectrometry. These ubiquitination sites were further validated *in vivo* in a mammalian cell system. In wild type HEK 293 cells ubiquitinated forms of both eS10 and uS10 can be detected by western blotting under steady state conditions. By contrast, ZNF598-deficient cells have undetectable levels of either modified eS10 or uS10. Finally, we showed that these ZNF598 mediated ubiquitination events are functionally important for induction of the RQC during poly(A) translation. Cumulatively, in this chapter we establish a causal link between site-specific ubiquitination on the small ribosomal subunit and regulation of translation at an early stage of the RQC pathway. This discovery will pave the way for further dissection of the molecular mechanisms governing the initial recognition of aberrantly translating ribosomes.

3.1 ZNF598 ubiquitinates purified ribosomes *in vitro*

To determine potential target(s) of ZNF598, we made use of a versatile *in vitro* reconstitution approach. We first considered the possibility that ZNF598 directly ubiquitinates one of the ribosomal or ribosome-associated proteins. To test this, we purified ZNF598 from mammalian cells using an affinity-based approach. For this we used our well-expressed C-terminally 3xFLAG tagged ZNF598 construct (see Figure 2.10A). Our standard purification procedure allowed us to obtain a relatively pure preparation of recombinant ZNF598-3xFLAG at a concentration of ~2 μM (Figure 3.1A). We then set up an *in vitro* ubiquitination assay with the minimal necessary components. This contained our purified ZNF598, partially-purified ribosomes derived from rabbit reticulocyte lysate, an ATP-regeneration system, and ubiquitination machinery consisting of ubiquitin, an E1 enzyme and an E2 enzyme (UbcH5a). We found that ZNF598 is capable of adding tagged ubiquitin to the purified ribosomes with high efficiency (Figure 3.1B, C). We also saw high molecular weight bands corresponding to polyubiquitin conjugates likely added by other ribosome-associated ligases. However, critically, there were two major bands specific to the ZNF598-containing reactions. These ZNF598-specific bands migrated exclusively in ribosome-containing fractions when analysed on a sucrose gradient (Figure 3.1B). Collectively, our results strongly suggest that the *bona fide* molecular target(s) of ZNF598 are either the ribosome itself or tightly associated ribosomal factors.

3.2 ZNF598 primarily targets 40S ribosomal proteins eS10 and uS10

The appearance of two specific bands in our *in vitro* ubiquitination reactions suggested that ZNF598 is either targeting two separate proteins or a single protein which gets modified on two distinct lysine residues. To determine which of these scenarios was the case, we scaled up the *in vitro* ubiquitination reaction and purified ubiquitinated proteins from ribosomal fractions using a ubiquitin-conjugated affinity tag. When analysed on a Coomassie stained gel, the eluate from our purification yielded two distinct bands, which collapsed into one single band of around 20 kDa upon digestion of the sample with catalytic domain of the promiscuous de-ubiquitinating enzyme USP2 (Figure 3.2A). Mass spectrometry analysis revealed that this product is the 40S ribosomal protein eS10.

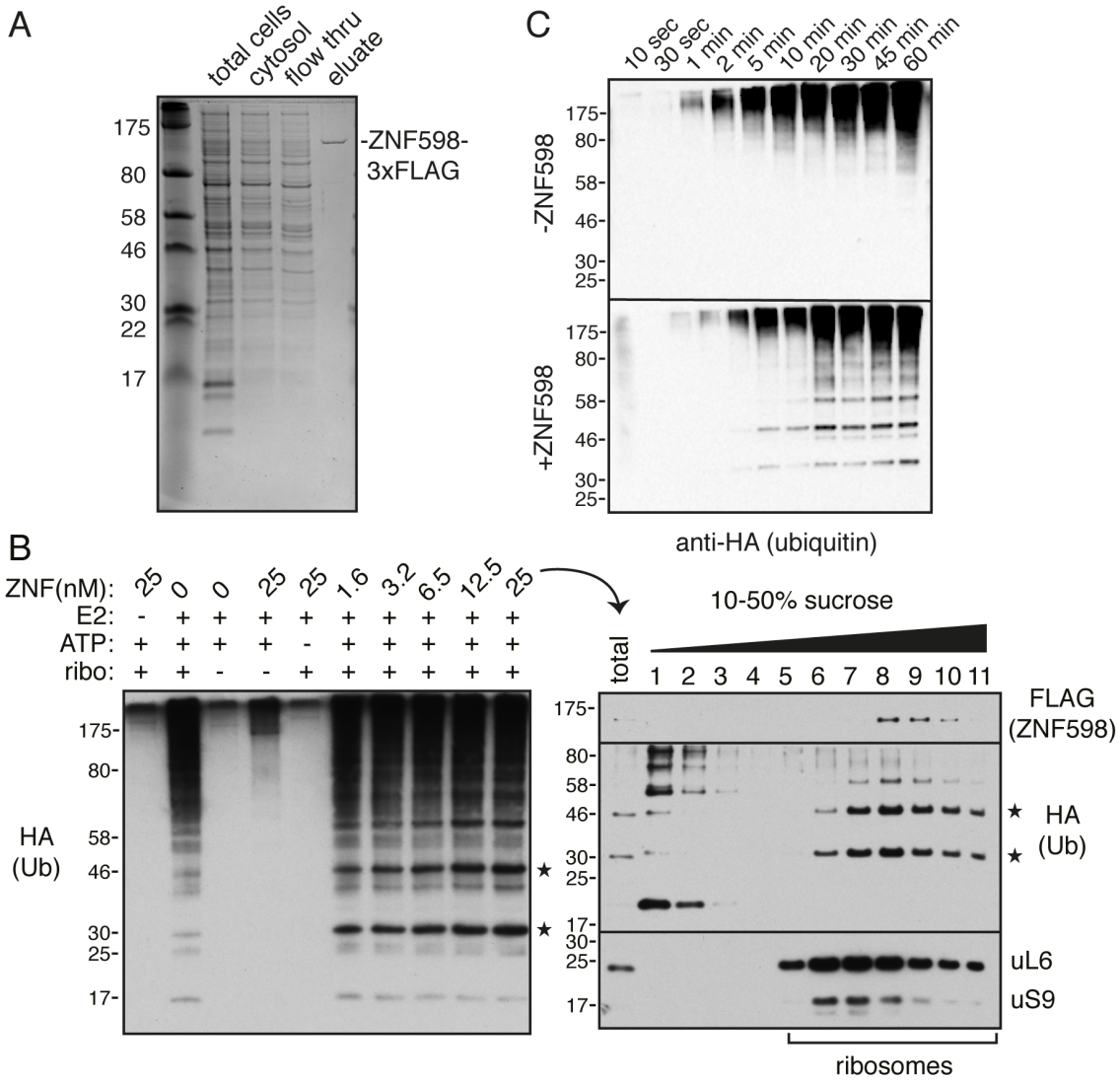

Figure 3.1 ZNF598 ubiquitinates purified ribosomes *in vitro*. (A) Purification of ZNF598-3xFLAG from cultured cells stained by Coomassie blue. **(B)** *In vitro* ubiquitination reactions of ribosomes in the presence of the indicated factors were analysed by western blotting by probing against the ubiquitin HA-tag**.** The last reaction was subsequently separated on a 10-50% sucrose gradient and analysed by immunoblotting. Primary ubiquitinated products are indicated by asterisks. **(C)** Immunoblotting analysis of a time course of an *in vitro* ubiquitination reaction with or without recombinant ZNF598 at 50 nM. Membranes were probed as in (B).

Additional analysis of eS10 di-Gly modified peptides allowed identification of lysine residues K138 and K139 as a primary ubiquitination sites. Even though other ubiquitinated products were not sufficiently strong to be visualized on the gel, mass spectrometry analysis identified ZNF598-ubiquitinated sites on proteins uS10 (K4 and K8) and uS3 (K214) (Table 3.1).

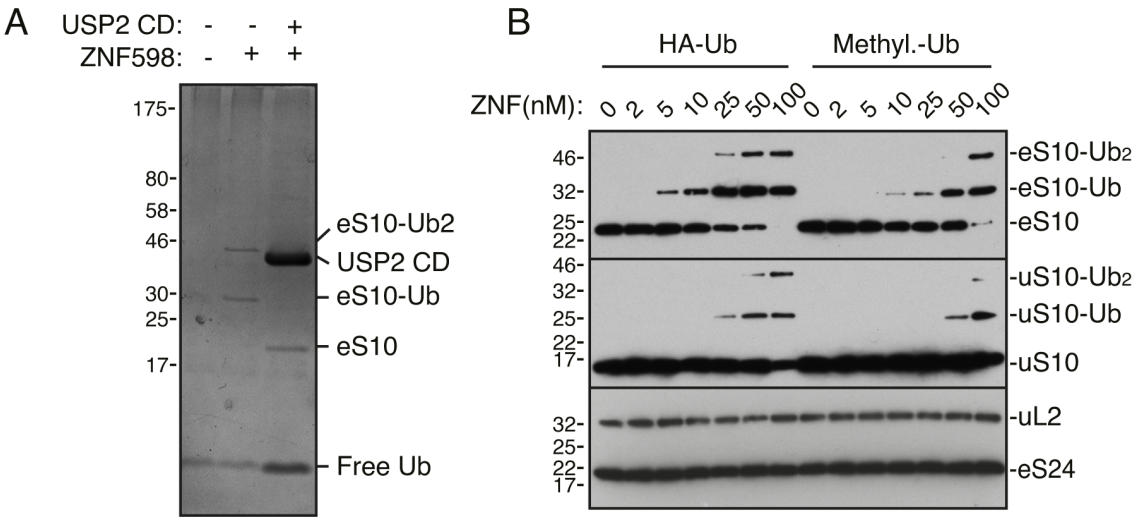

Figure 3.2 ZNF598 ubiquitinates eS10 and uS10 *in vitro*. (A) *In vitro* ubiquitination reactions with (+) or without (-) recombinant ZNF598 performed in the presence of His-ubiquitin were fractionated on a sucrose gradient. Ribosome-containing fractions were pooled and denatured to purify ubiquitinated core ribosomal proteins via His-pulldown. Some eluates were then treated with the catalytic domain (CD) of the promiscuous deubiquitinating enzyme USP2 and all samples were analysed by SDS-PAGE and Coomassie blue staining. The major ZNF598-dependent ubiquitinated products were identified by mass spectrometry. **(B)** *In vitro* ubiquitination reactions containing increasing amounts of ZNF598 and HA-tagged ubiquitin or methylated-ubiquitin were analysed by immunoblotting for the indicated ribosomal proteins.

	total spectral counts	
protein	-ZNF598	+ZNF598
eS10	5	50
uS3	4	35
uS10	0	20
eS4	12	19
uS5	7	15
eL13	5	15
eL8	9	14
eS7	5	11
eS6	4	10
eS1	4	9
uL30	10	9
eL24	6	9
eL19	6	9
eL6	3	7
eEF1	4	7
eS8	4	6
uL2	7	6
uL3	5	6
eL14	4	6
uL5	5	5

Western blot analysis of the *in vitro* ubiquitination reaction products confirmed ZNF598-mediated modification of eS10 and uS10 with mono-ubiquitin on up to two separate residues, whereas other ribosomal proteins like uL2 or eS24 remained unmodified (Figure 3.2B). Even though we detected ubiquitination of eS3 by mass spectrometry, appreciable ubiquitination was not seen when samples were analysed by immunoblotting (data not shown).

Table 3.1 Results of the mass spectrometry analysis of the ubiquitinated products recovered from the reaction depicted in Figure 3.2A. Proteins in red showed at least 5-fold enrichment in the sample containing ZNF598.

3.3 ZNF598 ubiquitinates eS10 and uS10 in cultured cells

To verify that our *in vitro* identified targets of ZNF598 (eS10, uS10 and uS3) are also modified *in vivo*, we analysed totals cell lysates from both WT and ZNF598-deficient Flp-In 293 T-Rex cells by immunoblotting. Using eS10-, uS10- and eS3-specific antibodies, we could detect additional, ~10 kDa bigger product for each of the analysed targets. These products were clearly diminished (uS3, uS10) or completely absent (eS10) in cells lacking ZNF598 (Figure 3.3A, B). In the case of another ribosomal protein, uS5, which was previously reported to be ubiquitinated under conditions of stress (Higgins et al., 2015), we found no such mark in our system (Figure 3.3B). The higher molecular weight products were confirmed to be ubiquitin marks based on the appearance of another, even slower migrating band in cells transiently transfected with hemagglutinin (HA)-tagged ubiquitin (Figure 3.3C). Additionally, HA-ubiquitinated versions of eS10 (Figure 3.3C), uS10 and uS3 (data not shown) were selectively recovered after immunoprecipitation with an antibody against HA.

It was previously shown that treatment of cells with the translation elongation inhibitor cycloheximide (CHX) or the ER stress inducing dithiothreitol (DTT) resulted in regulatory ubiquitination of several ribosomal proteins (Higgins et al., 2015). When we performed similar treatments in cells lacking ZNF598, it affected each of the targets in a somewhat different way (Figure 3.3 C). The small increase in ubiquitination upon CHX treatment observed in the WT cells was attenuated (in case of uS10 and uS3) or completely abolished (eS10) in ZNF598-deficeint cells. However, ubiquitination of uS3 and uS10 induced by DTT was ZNF598-independent. In contrast, ubiquitination of uS5 which is not targeted by ZNF598 was not affected in either case. Hence, it appears that multiple different ribosomal proteins can be ubiquitinated during various stress conditions, yet only some of those are targeted by ZNF598 E3 ligase. Additionally, both *in vitro* and *in vivo*, eS10 seems to be the most specific target of ZNF598.

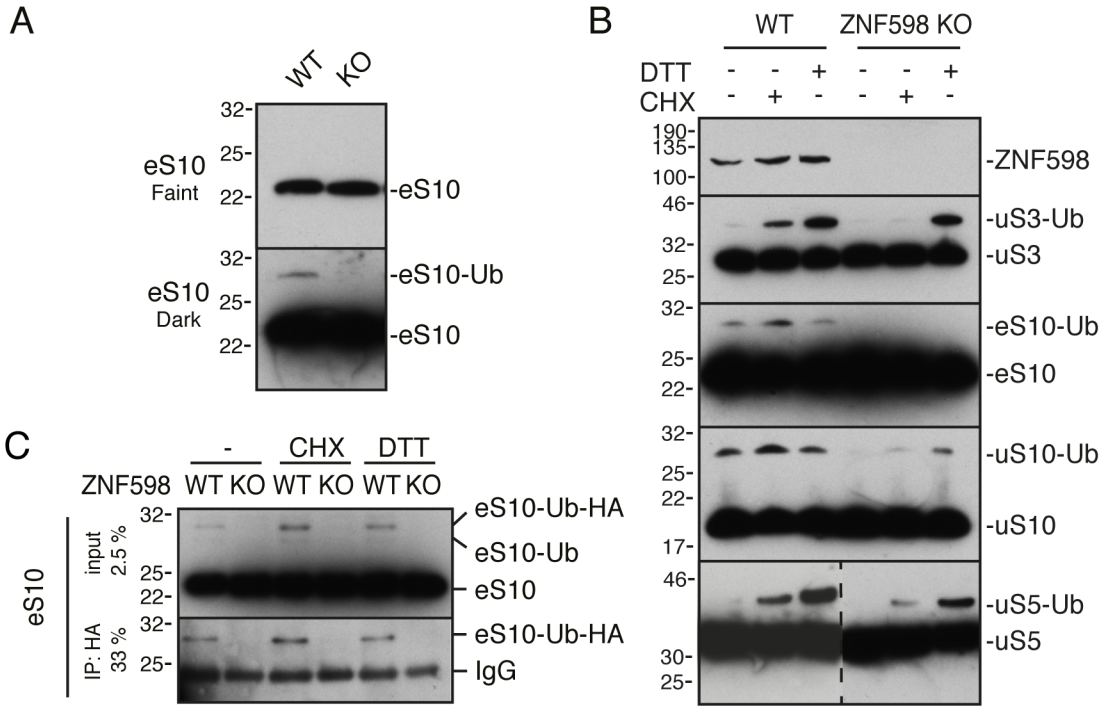

Figure 3.3 Ribosomal proteins eS10, uS10 and to some extent uS3 are ubiquitinated in a ZNF598-dependent manner in cultured cells. (A) Total cell lysates from WT or ZNF598-deficient (KO) cells were analysed by immunoblotting with an antibody against eS10. Faint (upper panel) and dark (lower panel) exposures are shown. **(B)** WT and KO cells were treated with nothing, 100 µg/ml cycloheximide (CHX) or 1 mM DTT for 2h and total cell lysates were collected and analysed by immunoblotting against indicated proteins. **(C)** WT and KO cells were transiently transfected with HA-ubiquitin and treated as in (B). Total cell lysates and HA-affinity purified products were analysed by immunoblotting with antibody against eS10. Bands corresponding to unmodified, Ub-modified and HA-Ub-modified eS10 are indicated. Additional band corresponding to Immunoglobulin light chain (IgG) is also indicated.

3.4 ZNF598-mediated ubiquitination of eS10 and uS10 is essential for efficient induction of the quality control during poly(A) translation

We have robustly demonstrated that ZNF598 ubiquitinates specific ribosomal proteins both *in vitro* and *in vivo*. This in hand, we set out to show that the same ubiquitination events are functionally relevant in inducing the RQC. To this end, we generated matched stable cell lines using the Flp-In 293 T-Rex system expressing HA-tagged eS10 either in its nature form, or with arginine substitutions at the previously identified residues K138 and K139. Constitutive induction of the transgenes resulted in all HA-tagged versions of eS10 expressed at the similar levels and constituting ~70% of the total eS10 pool, which

remained constant (Figure 3.4A). Sucrose gradient fractionation confirmed that double K138/139R mutant of eS10 (Figure 3.4B) as well as single K139R mutant (data not shown) were successfully incorporated into assembled ribosomes. To test the functional implications of abolishing the capacity to ubiquitinate eS10, we transiently expressed the $(K^{AAA})_{20}$ stalling reporter in each of our mutant cell lines (Figure 3.4C). Flow cytometry analysis revealed a small increase in the RFP:GFP ratio in single K139R mutant and further increase in double K138/139R mutant.

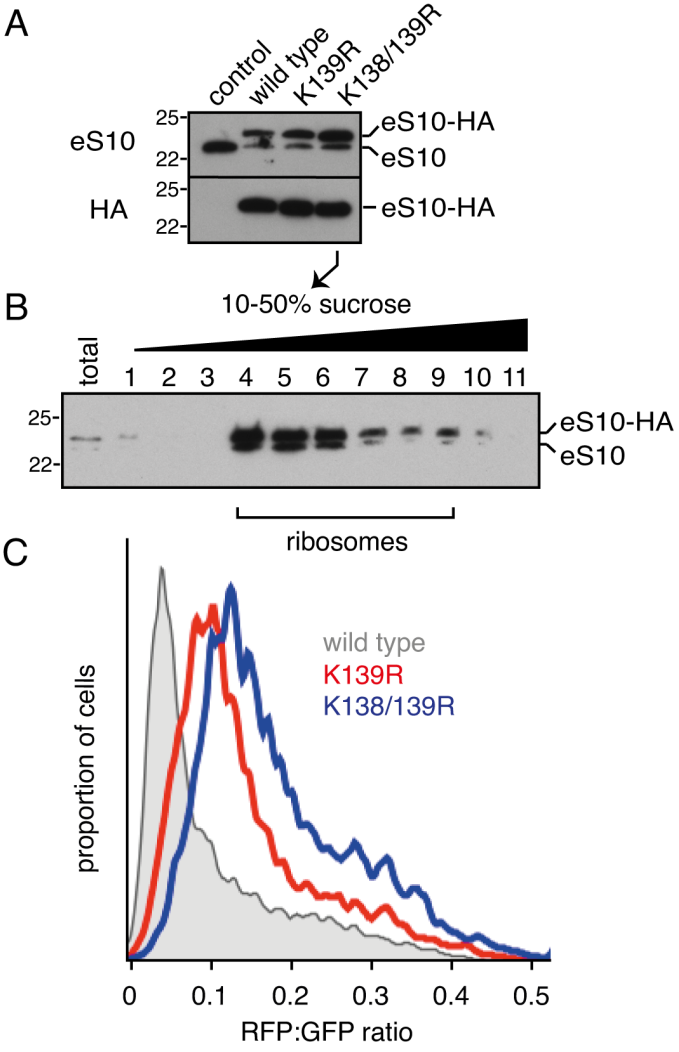

Figure 3.4 eS10 ubiquitination facilitates induction of RQC during poly(A) translation. (A) The cytosolic fractions from stable cell lines expressing HA-tagged versions of eS10 were analysed by immunoblotting with indicated antibodies. **(B)** Cells expressing the K138/139R mutant of eS10 were fractionated on 10-50% sucrose gradient and analysed by immunoblotting probing with the anti-eS10 antibody. Fractions containing ribosomes are indicated. Similar results were obtained with other mutants (data not shown). **(C)** Stable cells expressing the indicated eS10-HA mutant were transiently transfected with the $(K^{AAA})_{20}$ reporter and analysed after 24h by FACS. Histograms showing RFP:GFP ratio are shown for eS10-HA (grey) eS10-HA K139R single mutant (red) and eS10-HA K138/139R double mutant (blue).

Sucrose gradient fractionations also confirmed efficient ribosomal incorporation of the uS10-HA K4/8R (Figure 3.5B) as well as other mutants (data not shown). Analysis of the expression of the $(K^{AAA})_{20}$ construct revealed no increase in RFP:GFP ratio in K8R single mutant and a small increase when K4/8R double mutant was analysed.

To conclude, mutation of the most efficient ZNF598 ubiquitination sites on the ribosome partially phenocopies ZNF598 deletion, resulting in increased readthrough of the stall sequence of $(K^{AAA})_{20}$ reporter construct. Mutation of two lysine residues on eS10 resulted in better readthrough of the $(K^{AAA})_{20}$ reporter, than mutation of only one lysine residue. Thus, it is reasonable to assume that other ubiquitin molecules positioned near the mutated site can partially compensate for the lack of primary targets. In support of that, mutation of the uS10 ubiquitination sites, which spatially can be close to the primary ubiquitination sites on eS10, also resulted in small increase in RFP:GFP ratio when poly(A) reporter was analysed.

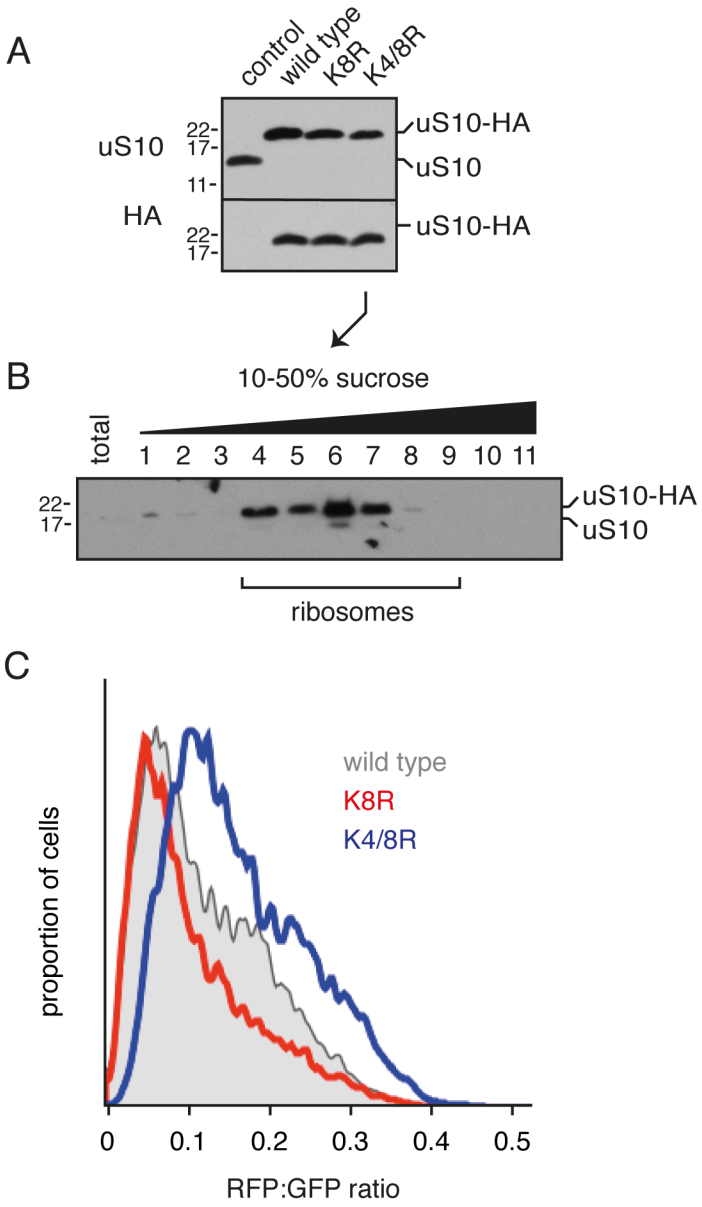

Figure 3.5 uS10 ubiquitination facilitates induction of RQC during poly(A) translation. (A) The cytosolic fractions from stable cell lines expressing HA-tagged versions of uS10 were analysed by immunoblotting with indicated antibodies. **(B)** Cytosol isolated from cells expressing K4/8R mutant of uS10 was fractionated on 10-50% sucrose gradient and analysed by immunoblotting with anti-uS10 antibody. Fractions containing ribosomes are indicated. Similar results were obtained with other uS10 mutants (data not shown). **(C)** Stable cells expressing indicated mutants of uS10-HA were transiently transfected with the $(K^{AAA})_{20}$ reporter and analysed after 24h by FACS. Histograms showing RFP:GFP ratio are shown for uS10-HA (grey) uS10-HA K8R single mutant (red) and uS10-HA K4/8R double mutant (blue).

3.5 Discussion

We have characterized mammalian protein ZNF598 and established its function as a ribosomal ubiquitin ligase. Through a combination of *in vitro* reconstitution and cell culture experiments, we have identified the 40S-ribosomal proteins eS10 and uS10 as major targets of ZNF598. Finally, our double-fluorescence reporter for studying translational stalling allowed us to demonstrate that ubiquitination on ZNF598-targeted residues is functionally important for the induction of RQC during poly(A) translation. Our findings have important implications for establishing how quality control of nascent chains is governed and provides several new avenues for future study.

We find that mutation of primary (K138 and K139 of eS10) or secondary (K4 and K8 of uS10) ubiquitination sites targeted by ZNF598 results in increased readthrough of the poly(A) stalling sequence. We cannot exclude the possibility that the mutation from lysine to arginine would have a ubiquitination-independent effect, however similarity of the lysine mutation and ZNF598-deletion phenotypes strongly supports the role for ubiquitin in RQC induction. The fact that we observe effects with either eS10 or uS10 mutants suggests that exact position of the ubiquitin molecule does not seem to be important, as long as there is another functional ubiquitination site in close proximity. In support of this notion, both eS10 and uS10 are spatially proximal on the surface exposed side of the 40S subunit, with their ubiquitination sites located on their protruding flexible tails. Therefore, we would like to propose a model in which the ubiquitin molecule on the surface of the 40S ribosomal subunit ultimately leads to terminal stalling and induction of the quality control. Given that the regions functional for elongation, such as the PTC, A-, P-, E-sites or mRNA entry channel are relatively distant from the ubiquitination sites, it is less likely that ubiquitin can directly inhibit elongation through simple obstruction of the biochemical reaction. A more plausible mechanism is one where other factors may sense and signal ZNF598 mediated ubiquitination events to downstream components of the RQC. Our dual fluorescent reporter assay (described in Chapter 2) should facilitate genome-wide genetic screens to identify additional machinery involved in ubiquitin-mediated induction of the RQC.

Recently, two independent studies confirmed our discovery of ZNF598 as a ribosome ubiquitin ligase involved in the early events of RQC. The group of Eric Bennett performed quantitative proteomic profiling of total and ubiquitin modified proteins in

ZNF598-deficient cells, which confirmed that eS10, uS10 and uS3 were among the most strongly affected proteins (Sundaramoorthy et al., 2017). Additionally, a study from Sonenberg group reported the same targets of ZNF598, also showing that ZNF598 can crosslink to mRNA, rRNA and tRNA, as judged by the PAR-CLIP experiment (Garzia et al., 2017). Interestingly, crosslinks to AAA-decoding $tRNA_{Lys}$(UUU) were 10-fold enriched over its cellular abundance, suggesting specific engagement of ZNF598 with AAA-decoding ribosomes.

The mechanism of RQC induction through site-specific ribosome ubiquitination is also conserved in yeast. Hel2, the yeast homolog of ZNF598 which was originally implicated in stalling on polybasic sequences (Brandman et al., 2012), was also shown to be directly involved in ribosome ubiquitination (Matsuo et al., 2017). Since yeast do not have the C-terminal part of eS10, which contains K138 and K139, the primary target of Hel2 is uS10, which gets modified on K6 and K8 residues (corresponding to K4 and K8 residues in mammalian uS10, which we also observed to be ubiquitinated by ZNF598). As predicted, the same sites were functionally important for the quality control induction during translation through difficult to decode polybasic stretches (Matsuo et al., 2017).

Our discovery has also more general implications for the field of translational regulation. It is the first report of a site-specific ubiquitination event on the ribosome that is linked to a specific function within the quality control pathway. It is important to note that deletion of ZNF598 affected only a subset of previously reported regulatory ubiquitination events induced by different stressors (Higgins et al., 2015). In this regard, future studies should link the remaining sites of ubiquitin-modification to specific ribosome-associating ligases and physiologic responses.

Taking a broader perspective, our pioneering finding of a functional, site specific ribosome ubiquitination event represents an example of a previously unappreciated mechanism of translational control. Indeed, several recent studies have identified other modifications of core ribosomal proteins which may also be of similar importance in terms of their functional relevance. Some disease related modifications include the Parkinson's-related phosphorylation of uS19 (Martin et al., 2014) or ufmylation on uS3, uS10 and uL16 (Simsek et al., 2017). As for our described ubiquitination event, these other modifications await further characterization to identify the important molecular players involved in these processes and their biological relevance.

3.6 Materials and methods

Constructs, antibodies, purified proteins

All of the constructs used in this chapter, including fluorescent reporter constructs and plasmids for expression of recombinant ZNF598 were described in Chapter 2. The following antibodies were used: rabbit polyclonal antibody against ZNF598 from Abcam #ab80458, rabbit monoclonal antibody against eS10 from Abcam #ab151550, rabbit monoclonal antibody against uS10 from Abcam #ab133776, rabbit polyclonal antibody against uS3 from Bethyl Labs #A303-840A, rabbit polyclonal antibody against uS5 from Bethyl Labs #A303-794A, rabbit polyclonal antibody anti-uS9 from Santa Cruz Biotechnology #sc-102087, rabbit polyclonal antibody anti-uL6 from Santa Cruz Biotechnology #sc-102085, rabbit monoclonal anti-uL2 antibody from Abcam #ab169538, rabbit monoclonal anti-eS24 antibody from Abcam #ab196652, mouse monoclonal anti-HA antibody from Covance #MMS-101P, mouse monoclonal anti-FLAG M2 antibody from SIGMA #F3165 and HRP-conjugated goat anti-rabbit and anti-mouse antibodies from Jackson Immunoresearch #111-035-003 and #115-035-003 respectively. Proteins used in the *in vitro* ubiquitination reactions were from Boston Biochem: His-Ubiquitin #U-530, HA-Ubiquitin #U-110, Methylated Ubiquitin #U-501, UbcH5a #E2-616, GST-UBE1 (human) #E-306, USP2-CD #E-504, ZNF598-3xFLAG was purified as described below.

Cell culture, flow cytometry, western blotting

All cell culture-based experiments, including flow cytometry and western blotting analyses were performed as described in Chapter 2. Treatments with cycloheximide (CHX) and DTT were performed in regular DMEM with 10% FCS as described in detail in figure legends.

Ribosomes purification

Ribosomes were purified from 25 ml of rabbit reticulocyte lysate (RRL; Green Hectares) by ultracentrifugation in a TLA100.4 rotor at 100,000 rpm for 40 minutes at 4°C. The supernatant was removed and ribosomes were briefly washed with Ribosome Wash Buffer (RWB) (20 mM HEPES pH 7.5, 100 mM K(OAc), 1.5 mM $Mg(OAc)_2$, 0.1 mM EDTA). Ribosome pellets were resuspended in 0.8 ml of RWB and homogenized with a

glass dounce. Once completely resuspended, 2 ml of ribosomes were layered over a 1 ml sucrose cushion (RWB with 1 M sucrose and 1 mM DTT) and centrifuged using a TLA100.4 rotor at 100,000 rpm at 4°C for 1h. Ribosome pellets were finally resuspended in total volume ~2.2 ml of dialysis buffer (20 mM HEPES pH 7.4, 100 mM K(OAc), 1.5 mM $Mg(OAc)_2$, 10% glycerol). Purified ribosomes were flash frozen in liquid nitrogen and concentration was estimated from the absorbance at 260 nm, with the assumption that that 1 A_{260} unit corresponds to 16 nM ribosomes.

Recombinant ZNF598-3xFLAG protein purification

C-terminal 3xFLAG-tagged ZNF598 was transfected into HEK 293 cells using TransIT 293 reagent (Mirus), and purified two days after. Sixteen 10 cm dishes of confluent ZNF598-expressing cells were harvested in ice cold PBS and lysed in ~1 mL 50 mM HEPES pH 7.4, 100 mM K(OAc), 5 mM $Mg(OAc)_2$, 100 µg/mL digitonin, 1 mM DTT, 1X EDTA-free protease inhibitor cocktail (Roche) for 20 min on ice. The lysates were then spun in a tabletop centrifuge at 4°C for 10 minutes. The resulting supernatant was incubated with 100 µL of packed anti-Flag resin for 1-1.5 hour at 4°C. The resin was washed three times with lysis buffer, three times in 50 mM HEPES pH 7.4, 400 mM K(OAc), 5 mM $Mg(OAc)_2$, 100 µg/mL digitonin, 1 mM DTT buffer, and three times in 50 mM HEPES pH 7.4, 100 mM K(OAc), 5 mM $Mg(OAc)_2$ buffer. Elutions were carried out with one column volume of 0.2 mg/ml 3X-Flag peptide in the final wash buffer at room temperature for 30 minutes. Two sequential elutions were combined to form the final fraction.

In vitro ubiquitination of ribosomes

In vitro ubiquitination reactions contained the following components at indicated final concentration: ATP 1 mM, Creatine Phosphate (CP) 10 mM, Creatine Kinase (CK) 40 ng/ml, His-Ub/HA-Ub/methylated-Ub 10 µM, rhGST-UBE1 100 nM, UbcH5a 200 nM, ZNF598 (1.6 – 100 nM as indicated), ribosomes 220 nM in physiological salt buffer (PSB) (100 mM K(OAc), 50 mM Hepes, pH 7.4, 5 mM $Mg(OAc)_2$). Assembled reactions were incubated at room temperature for 15 min, ribosomes and ZNF598 were then added and the reaction was incubated for an additional hour at 32°C.

Large scale ubiquitination reactions (200 µl) used for downstream analysis by mass spectrometry were first separated on 10-50% sucrose gradient for 1h at 55,000 rpm, at 4°C using TLS-55 rotor (Beckman). Eleven fractions, 200 µl each, were removed numbering from the top and ribosomal fractions (4-11) were pooled together. 1.6 ml of ribosome-containing fractions were mixed with 400 µl of 5x SDS containing buffer (500 mM Tris pH 8.0 with 5% SDS) and samples were denatured for 5 min at 95°C. Next, 8 ml of Triton buffer (1xPBS, 0.5% Triton-X100, 250 mM NaCl, 20 mM imidazole) was added to dilute SDS, followed by addition of 20 µl of NiNTA-agarose resin and incubation of the samples overnight with end-over-end rolling at 4°C. Beads were spun, supernatant aspirated and washed trice with 1 ml of Triton buffer. Elution was done with 2.5x sample buffer containing 50 mM EDTA (for direct SDS-PAGE analysis and mass spectrometry) or PBS with 50 mM EDTA for de-ubiquitination with 10 µM USP2 CD for 1h at 32°C.

Sucrose gradient fractionation

Small 0.2 ml gradients were prepared in 7 x 20 mm centrifuge tubes (Beckman 343775) by successively layering 40 µl each of 50%, 40%, 30%, 20%, and 10% sucrose (w/v) in PSB. Gradients were then allowed to stand for 1-2 h at 4°C. *In vitro* ubiquitination reactions (20 µl) were loaded on top of the gradients, and the samples centrifuged in a TLS-55 rotor at 55,000 rpm for 30 min at 4°C with the slowest acceleration and deceleration settings. Eleven 20 µl fractions were successively collected from the top and used directly for western blot analysis. For purification using NiNTA resin as well as cytosol separation, 10-fold larger gradients were prepared in exactly the same way using 11 x 34 mm tubes (Seton 5011), but centrifuged at 55,000 rpm in the TLS-55 rotor for 1 h.

Cytosol fractionation

Actively growing Flp-In HEK 293 T-Rex cells expressing eS10-K138/139R-HA (~80% confluent) in 6-well plates were first washed with PBS and the cytosolic fractions were extracted with digitonin-containing buffer (25 mM Hepes, pH 7.4, 125 mM K(OAc), 15 mM $Mg(OAc)_2$, 100 µg/ml digitonin, 40 U/ml RNase inhibitor, 50 µg/mL CHX, 1 mM DTT, 1X protease inhibitor cocktail) on ice for 5 min. The lysates were spun at maximum

speed in a benchtop microcentrifuge for 10 min at 4°C, and the supernatant was separated on a 2 ml 10-50% sucrose gradient as detailed above. Fractions were collected and subjected to TCA precipitation for downstream analysis by immunoblotting.

Chapter 4: ZNF598 recognizes and selectively ubiquitinates collided di-ribosome species

Thus far, our data strongly support a model in which induction of the RQC during translation through stall-inducing sequences is facilitated by trans-acting factors ZNF598 and RACK1. Of these, ZNF598 seems to be the factor which is actively responsible for specific recognition of aberrant translation and catalysing site-specific ribosome ubiquitination. Our model assumes that ZNF598 selectively recognizes and modifies only stalled ribosomes, however the basis of this selectivity is currently unclear. Moreover, we have thus far not definitively demonstrated that stalled ribosomes are indeed ubiquitinated. This technical challenge is largely due to the low abundance of such species and the inherently transient nature of the regulatory ubiquitination event in actively growing cells.

In this chapter, we exploited a rabbit reticulocyte lysate (RRL) *in vitro* translation system to reconstitute ZNF598-mediated recognition and ubiquitination of ribosomes translating through stall-inducing poly(A) sequences. Unexpectedly, we found that ZNF598 did not engage single stalled mono-ribosomes. Instead, it selectively recognized and efficiently ubiquitinated collided ribosomes. Collided ribosomes are a result of a trailing ribosome encountering the leading, stalled ribosome. Specific ZNF598-mediated recognition of collided ribosomes was confirmed using an orthogonal method of induced stalling. This method involved using a mutant version of eRF1 incapable of peptide release, which we added to the native, non-nuclease digested RRL. As a result, we selectively stalled ribosomes terminating at the stop codon of the highly abundant, naturally occurring globin mRNA, which allowed us to generate large quantities of collided poly-ribosomes. Depending on the number of ribosomes translating a particular mRNA molecule, we obtained collided poly-ribosomes consisting of 2-6 ribosomes. All of those were efficiently recognised and targeted by ZNF598, with the minimal unit still efficiently ubiquitinated consisting of only 2 ribosomes. When we further characterized this di-ribosome species biochemically, we found that it is completely nuclease resistant, which distinguished it from other poly-ribosome species not targeted by ZNF598. A collaboration with members of Venki Ramakrishnan's group allowed us to obtain a high-

resolution structure of the collided di-ribosome. The structure nicely revealed the unique molecular architecture of this species, allowing us to place biochemical, genetic, and functional data into a physical framework.

4.1 ZNF598 engages a sub-population of poly(A)-stalled ribosomes

Resolution of translational stalls *in vivo* is extremely efficient. This indicates that intermediate steps are rapid and transient, and would therefore be difficult to capture and characterize biochemically. This complication also applies to the initial recruitment and ubiquitination of stalled translation complexes by ZNF598. Therefore, we decided to reconstitute this process in a system subject to more control, and turned to looking at ZNF598 recruitment to poly(A)-stalled ribosomes in a rabbit reticulocyte lysate (RRL)-based *in vitro* translation system. A recently published proteomic analysis of human erythropoiesis showed that ZNF598 was almost undetectable in reticulocytes (Gautier et al., 2016). Indeed, our initial characterization of ZNF598 levels in RRL showed its extremely low level compared to HEK 293 cells (Figure 4.1). Hence, RRL provided an ideal blank slate which we could exploit by adding recombinant ZNF598 in order to interrogate its function. In all subsequent experiments, RRL was supplemented with recombinant, 3xFLAG-tagged ZNF598 at low nanomolar range mimicking physiological concentrations observed in cultured cells.

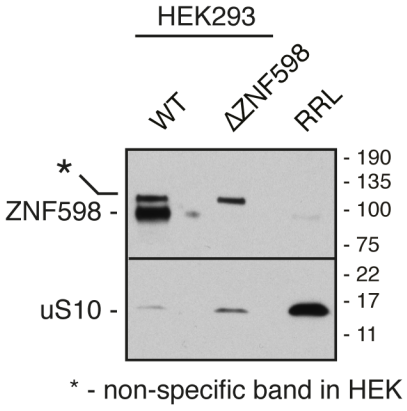

Figure 4.1 ZNF598 is downregulated in reticulocytes. Lysates from WT or ZNF598-deficient cells (ΔZNF598) as well as rabbit reticulocyte lysate (RRL) were analysed by western blotting for ZNF598 and uS10 levels. Note that ZNF598 is barely detectable, even though the RRL was massively overloaded (as judged by uS10 levels) and more sensitive, custom-made antibody against ZNF598 was used. Asterisk indicates non-specific band detected by the antibody in HEK cells.

We programmed our ZNF598-supplemented RRL with an mRNA encoding an N-terminal twin-strep tag (TST), followed by a VHP domain and $(K^{AAA})_{20}$ stalling sequence (Figure 4.2A). We then purified translational complexes via the nascent chain and separated them on a 10-50% sucrose gradient (see Figure 4.2B). Immunoblotting of isolated sucrose gradient fractions revealed that ~70% of ZNF598 comigrated with fractions containing ribosomes (Figure 4.2C). A small proportion of ZNF598 was observed at the top of the gradient, most likely due to dissociation, which might have occurred during fractionation. Off note, ZNF598 was not recovered in the controlled reaction when the nascent chain did not have an epitope tag (data not shown).

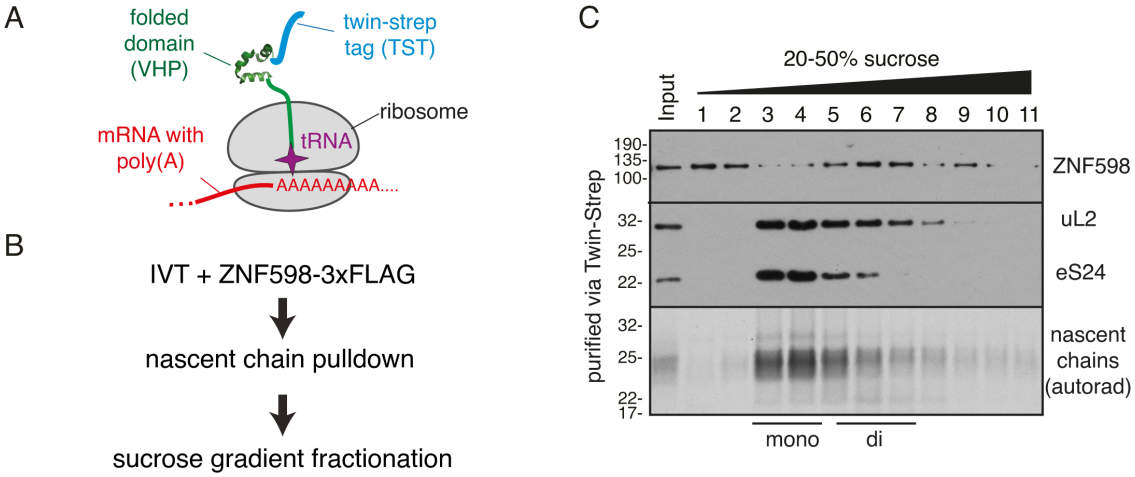

Figure 4.2 ZNF598 co-purifies with sub-population of poly(A) stalled ribosomes. (A) and **(B)** Schematic representation of the strategy used to generate and analyse poly(A)-stalled ribosome-nascent chain complexes in an *in vitro* translation system **(C)** *In vitro* translated ribosome-nascent chain complexes were purified via twin-strep tag (TST), separated on a 10-50% sucrose gradient and analysed by autoradiography (nascent chain) or immunoblotting (with indicated antibodies). Mono- and di- ribosome containing fractions are indicated.

Autoradiography analysis revealed that the majority of poly(A)-stalled nascent chains were in the 80S mono-ribosome fractions (fractions 3-4). This is expected as our *in vitro* translation system can generally support only a single round of translation initiation. However, very little ZNF598 was observed in these same fractions. This rather unexpected result argues against the possibility that ZNF598 detects a feature of a single stalled mono-ribosome. In turn, the majority of ZNF598 cofractionated with a small population of nascent chains found deeper in the gradient. We suspected that these fractions contained di-ribosome species, formed when a trailing ribosome collides with a stalled, leading ribosome. To confirm this suspicion, we added an inhibitor of translation initiation shortly (two minutes) after the start of the reaction to further

minimize multiple rounds of initiation in our system (Figure 4.3A). As expected, analysis of these reactions by fractionation on a sucrose gradient showed a reduction in both the di-ribosome population and ZNF598 recruitment (Figure 4.3B). Therefore, we concluded that ZNF598 recognizes di-ribosome species more effectively than stalled 80S mono-ribosomes.

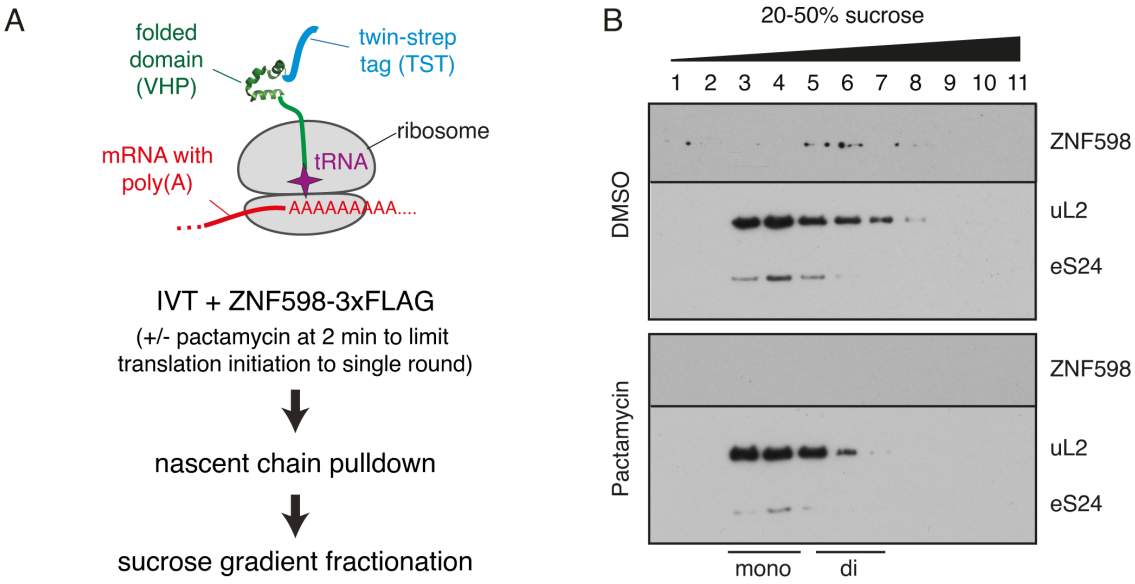

Figure 4.3 ZNF598 effectively engages di-ribosomes, but not stalled 80S monosomes. (A) Schematic representing strategy to limit translation initiation (note similarity to method described in Figure 4.2A, except pactamycin was added 2 min after start of reaction). **(B)** Ribosome nascent chain complexes from the reactions generated as in (A) were treated with DMSO (top panel) or pactamycin (bottom panel), isolated via TST on the nascent chain, normalized based on ribosomal content (as judged by absorbance at 260 nm) and separated on a 10-50% sucrose gradient. Each fraction from the gradients was analysed separately by immunoblotting for recombinant ZNF598 and ribosomal proteins uL2 and eS24. Positions of mono-ribosomes and di-ribosome containing fractions are indicated.

To orthogonally verify ZNF598-specificity towards di-ribosome species, we purified poly(A)-stalled translational complexes via a 3xFLAG tag on our recombinant ZNF598 (Figure 4.4A). Consistently with the previous experiment, ZNF598 precipitated stalled nascent chains of two specific sizes (Figure 4.4B). We reasoned that those two products might correspond to the nascent chains attached to the lead (stalled) and trailing ribosomes from the di-ribosome species. Importantly, lower molecular weight species which were underrepresented in the input, became enriched to about 50% of the total signal in ZNF598 precipitated sample. In support of our interpretation, sucrose gradient fractionation of both the input and ZNF598-precipitate confirmed that the lower

molecular weight species migrated exclusively in di-ribosome fractions (Figure 4.4C). Thus, it appears that ZNF598 selectively precipitated di-ribosome species, explaining the strong enrichment in shorter nascent chains. Quantification of radioactive signal after sucrose gradient fractionation confirmed, that ZNF598-recovered nascent chains had the same migration profiles as di-ribosome specific short nascent chains (Figure 4.4D). We conclude that ZNF598 is incapable of recognizing poly(A) stalled 80S mono-ribosomes. In turn, it seems to preferentially engage the minor population of higher order translation complexes consisting of di-ribosomes.

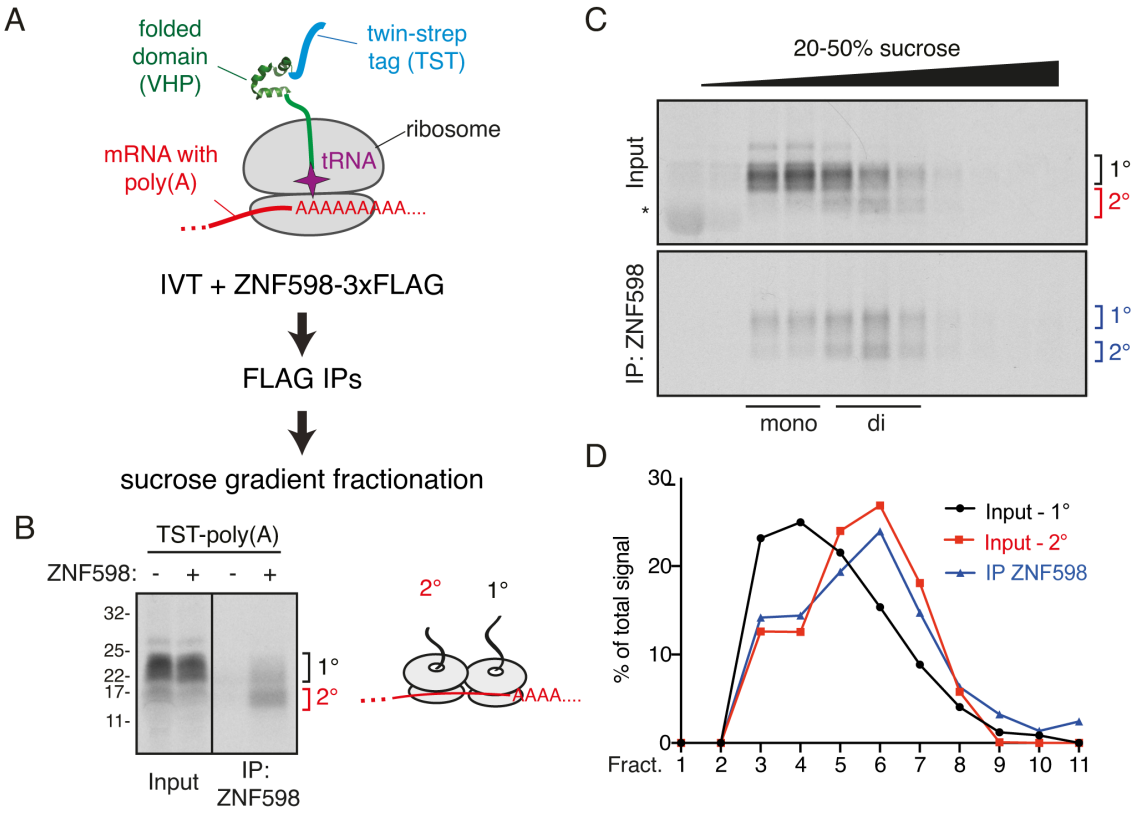

Figure 4.4 ZNF598 selectively precipitates higher-order translation complexes. (A) Experimental strategy to analyse ZNF598-associated translation complexes. **(B)** Translation complexes stalled on the poly(A) from reactions with (+) 5 nM 3xFLAG-tagged or without (-) ZNF598 were immunoprecipitated using anti-FLAG antibodies and analysed by autoradiography. 1° and 2° correspond to the nascent chains associated with the first stalled ribosome and the trailing ribosome, respectively (see diagram on the right). **(C)** Total reactions (Input) and ZNF598-precipitated complexes prepared as in (B) were fractionated on a sucrose gradients and nascent polypeptides visualized by autoradiography. 1° (black) indicates nascent chains associated with mono-ribosomes and 2° (red) indicates nascent chains associated with the second, trailing ribosome in the input sample. 1° and 2° (blue) represents di-ribosome associated nascent chains recovered after ZNF598 IP. **(D)** Autoradiograms from (C) were analyzed by densitometry and the relative distribution of the signal corresponding to nascent chains associated with mono-ribosomes (black), trailing ribosomes (red) and ribosomal complexes recovered with ZNF598 (blue) was plotted.

4.2 Stalling of ribosomes at the stop codon triggers efficient ZNF598 recruitment

As shown above, *in vitro* translation of exogenously added mRNA yields very low quantities of higher-order ribosome complexes. This is a significant limitation of our system when considering our interest in further biochemical and structural characterization of translational stalling. Hence, we sought to develop an alternative strategy to generate large amounts of site-specifically stalled ribosomes. For this we took advantage of endogenous translation complexes in our lysate system. Native reticulocyte lysate predominantly contains two homologous mRNAs coding for α- and β-hemoglobin (henceforth collectively referred to as globin). This provides an abundant, near-homogeneous source of native poly-ribosomes which can be used as substrates for generating aberrant translation complexes and assessing their recognition by ZNF598. To mimic stalling at a terminal poly(A), we needed a means to induce a localized stall on globin-translating poly-ribosomes. We made use of eRF1^{AAQ}, a dominant-negative mutant release factor that traps translation complexes at a termination codon (Brown et al., 2015; Shao et al., 2016). eRF1^{AAQ} would only stall ribosomes at a stop codon while permitting elongation of other ribosomes (Figure 4.5A), analogous to what would happen on non-stop mRNAs. As expected, the primary products of eRF1^{AAQ}-containing *in vitro* translation reactions were full-length (FL) globin nascent chains (Figure 4.5B). When analysed on a sucrose gradient, at least ~60% of FL globin migrated in the ribosomal fractions. These products represent ribosome-associated nascent chains which did not terminate due to eRF1^{AAQ} engagement. The remainder ~40% of the FL products migrated in non-ribosomal fractions and represent nascent chains terminated by endogenous eRF1. The vast majority of ribosome-associated nascent chains migrated in fractions 6-9, which correspond to di-, tri- and bigger poly-ribosome assemblies. The lower molecular weight species present in these fractions correspond to the nascent chains attached to the ribosomes queued behind the stalled, terminating ribosome.

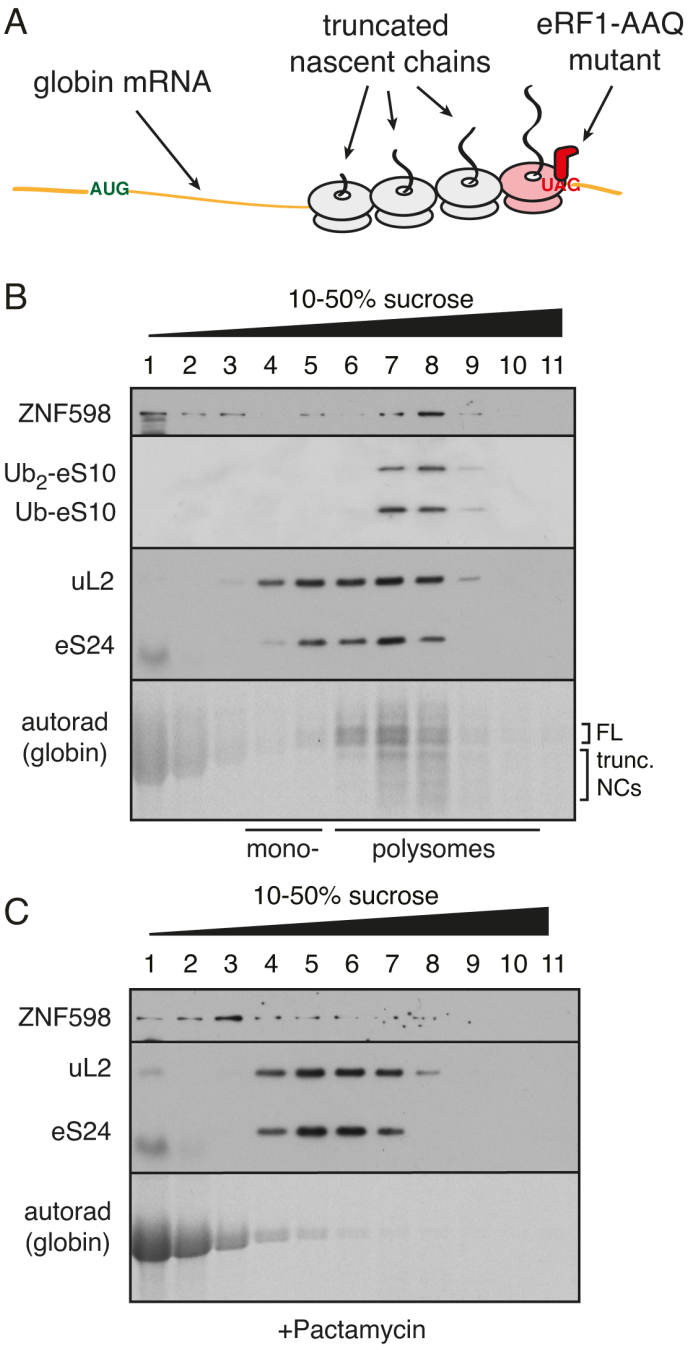

Figure 4.5 Poly-ribosomes stalled at a stop codon are recognized by ZNF598 (A) Schematic representation of the strategy used to generate ribosomes site-specifically stalled at the stop codon of the globin mRNA using mutant termination factor eRF1^{AAQ}. **(B)** An *in vitro* translation reaction of native globin mRNA was supplemented with 5 nM of 3xFLAG- tagged recombinant ZNF598, 1 µM eRF1^{AAQ} and 10 µM His-tagged ubiquitin and allowed to proceed. After sucrose gradient fractionation, nascent globin peptides were visualized by means of autoradiography and subjected to immunoblotting to detect the presence of specific factors. To detect ubiquitinated eS10, each fraction was precipitated via His-ubiquitin and the eluate was probed with an antibody against eS10. **(C)** An *in vitro* translation reaction was performed and processed as in (B), except in the absence of eRF1^{AAQ} and the presence of pactamycin in order to allow complete run-off of the ribosomes on the globin mRNA. FL corresponds to the full-length nascent polypeptides; "trunc. NCs" stands for "truncated nascent-chains".

In the control reaction in which eRF1^{AAQ} was omitted and pactamycin was added to limit additional rounds of initiation, these products were no longer seen (Figure 4.5C). Here, the majority of the signal corresponded to the FL globin, which migrated at the top of the gradient in non-ribosomal fractions.

Recombinant ZNF598 was added to the eRF1^{AAQ}-containing reaction and was shown to migrate predominantly in poly-ribosome containing fractions along with the truncated nascent chains (Figure 4.5B). Small amounts of ZNF598 were detected in the top fractions, most likely due to dissociation during sucrose gradient fractionation. Importantly, ubiquitin-modified versions of ribosomal protein eS10, the major target of ZNF598, were observed in fractions 7-9 comigrating with both ZNF598 and truncated nascent chains (Figure 4.5B). In a control reaction (without eRF1^{AAQ}) ZNF598 was not associated with ribosomes (Figure 4.5C) and eS10 ubiquitination was not detected (data not shown). In conclusion, native poly-ribosomes stalled at the stop codon by means of eRF1^{AAQ} form higher-order translational complexes, which are effectively recognized by ZNF598 which then ubiquitinates eS10. This system therefore recapitulates key aspects of stalling on poly(A) sequences.

4.3 ZNF589 selectively recognizes and ubiquitinates nuclease-resistant di-ribosome species

To gain insight into the cue for ZNF598 engagement, we uncoupled stalling and ubiquitination reactions in our *in vitro* system. This allowed us to manipulate the stalled complexes prior to assessing their competence for ZNF598 recognition. To do this, we first purified ribosomes from the eRF1^{AAQ}-containing reaction and then set up ubiquitination reactions by adding ZNF598 along with all of the essential components for ubiquitination. As expected, post-translational addition of the ligase resulted in efficient ubiquitination of eS10, comparable to its co-translational activity. This reaction was completely dependent on eRF1^{AAQ}-induced stalling, as ribosomes isolated from the control reaction where run-off was permitted were not recognized by ZNF598. To further verify that higher-order ribosome complexes are indeed the target for ZNF598, we added nuclease to the stalled polysomes to digest the mRNA and disassemble ribosomes before addition of ZNF598. To our surprise, eS10 ubiquitination was not affected by nuclease pre-treatment (Figure 4.6A).

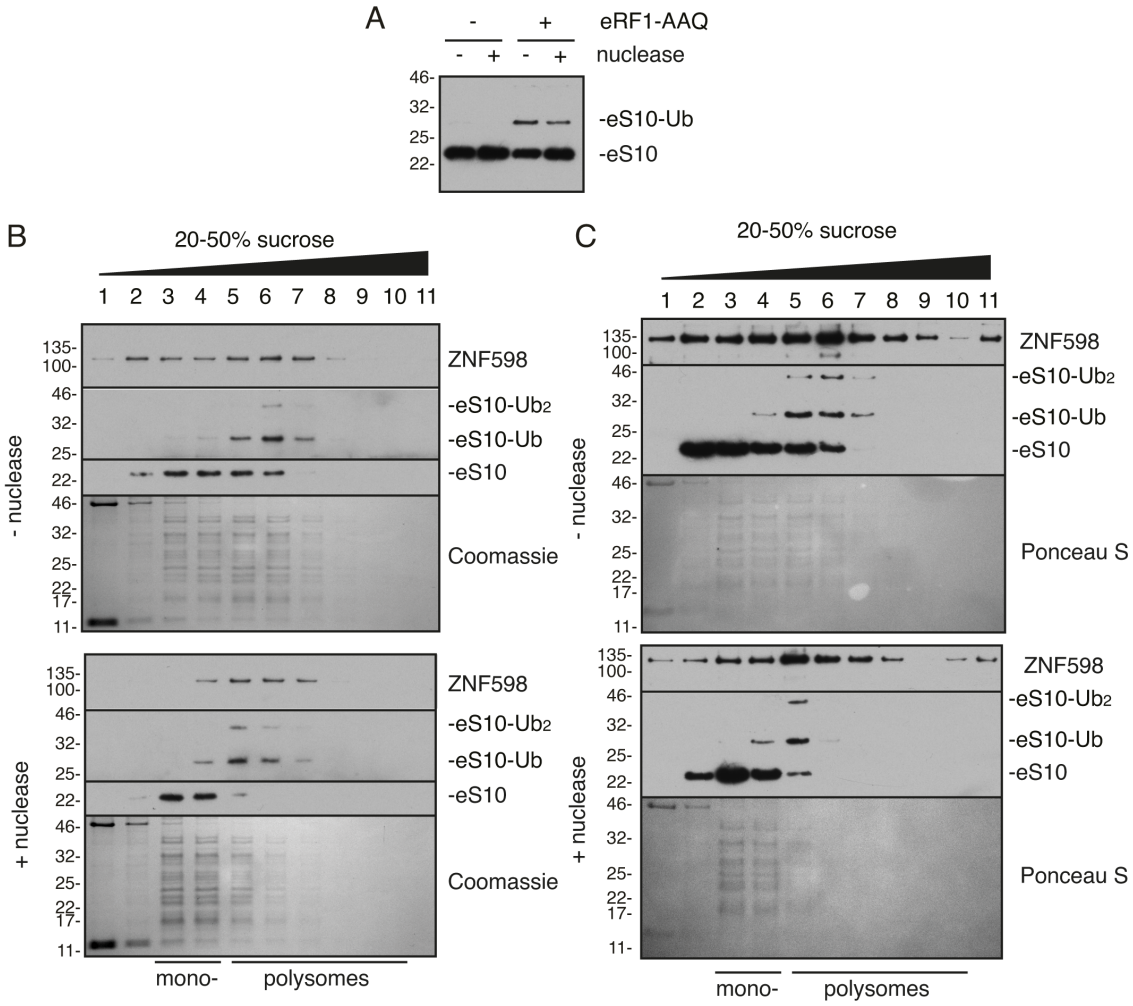

Figure 4.6 ZNF598 selectively recognizes and ubiquitinates nuclease-resistant, di-ribosome species. (A) Polysomes purified from native *in vitro* translations of globin mRNA lacking (-) or containing (+) 1 μM eRF1^{AAQ} and pre-treated with nothing (-) or micrococcal nuclease (+) were incubated in ubiquitination reactions with ZNF598 and analysed by immunoblotting. In **(B)** and **(C)** Ribosomes from reactions containing eRF1-AAQ described in (A) were fractionated on a high-resolution sucrose gradient (20-50%) and analysed by immunoblotting, Coomassie staining and Ponceau staining. Note that in (B) unmodified and ubiquitinated forms of eS10 were detected separately on two different pieces of the blot, whereas in (C) both forms were detected on one piece of the blot.

To ensure that the nuclease was digesting properly, we analysed *in vitro* ubiquitinated ribosomes (same as lane 4 on Figure 4.6A) as well as control, non-nucleased ribosomes (same as lane 3 on Figure 4.6A) on a 20-50% sucrose gradient (Figure 4.6B, C). As judged by both Coomassie stained-gel and immunoblotting, the majority of the poly-ribosomes were converted into monosomes upon nuclease digestion (Figure 4.6B). However, a small population of poly-ribosomes still migrated deeper into

the gradient, proving to be nuclease resistant. This population was selectively recognized and ubiquitinated by ZNF598 as it and ubiquitinated eS10 were detected in the same fractions by immunoblotting (Figure 4.6B). When both unmodified and ubiquitinated eS10 were analysed simultaneously on the same strip of blotted membrane we noticed that almost all of eS10 was modified with ubiquitin in the fractions containing nuclease resistant di-ribosomes, whereas essentially no modification was detected in the monosome-containing fractions (Figure 4.6C). These data collectively suggest that site-specific stalling at the stop codon results in the formation of tightly-packed (and so nuclease-resistant) poly-ribosomes. These species, unlike stalled individual 80S monosomes or loosely-packed poly-ribosomes, appear to be the preferred target of the ZNF598 E3 ligase.

We next wanted to see whether this observation held true for native ribosomes which had not been potentially damaged by nuclease treatment. For this, an eRF1^{AAQ}-stalled lysate was separated on a sucrose gradient and fractions enriched in complexes containing mono and poly-ribosomes were further purified by sedimentation (Figure 4.7A). Treatment of ribosomes from each fraction with ZNF598 showed that di- to penta-ribosome complexes were effectively targeted by ZNF598 as judged by eS10 ubiquitination, while monosomes remained unmodified (Figure 4.7B). Moreover, the proportion of ubiquitin-modified eS10 increased for complexes containing more ribosomes, with penta-ribosomes more efficiently ubiquitinated than di-ribosomes. This observation is consistent with a model where ZNF598 modifies queued trailing ribosomes rather than the first, stalled ribosome.

A number of conclusions are supported by our *in vitro* experiments with heterologous and endogenous translation complexes. First, a stalled translation complex consisting of mono-ribosome is not in and of itself detected or ubiquitinated effectively by ZNF598. Hence, the major 80S ribosome complexes stalled on poly(A) or at the stop codon of globin mRNAs are not targets of ZNF598. Second, while the preferred targets of ZNF598 seem to contain two or more ribosomes, not all poly-ribosomes are ZNF598 targets. The targeted and non-targeted populations of poly-ribosomes can be experimentally distinguished by their differential sensitivity to nuclease digestion. Because ubiquitinated eS10 is essentially absent in the monosome fraction after nuclease digestion (Figure 4.6C), we can deduce that ribosomes in nuclease-sensitive poly-ribosome complexes were not modified by ZNF598. By contrast, nearly all ribosomes in

the nuclease-resistant population are ubiquitinated, indicating that it is collided ribosomes in a tightly packed queue which are the preferred substrate for ZNF598.

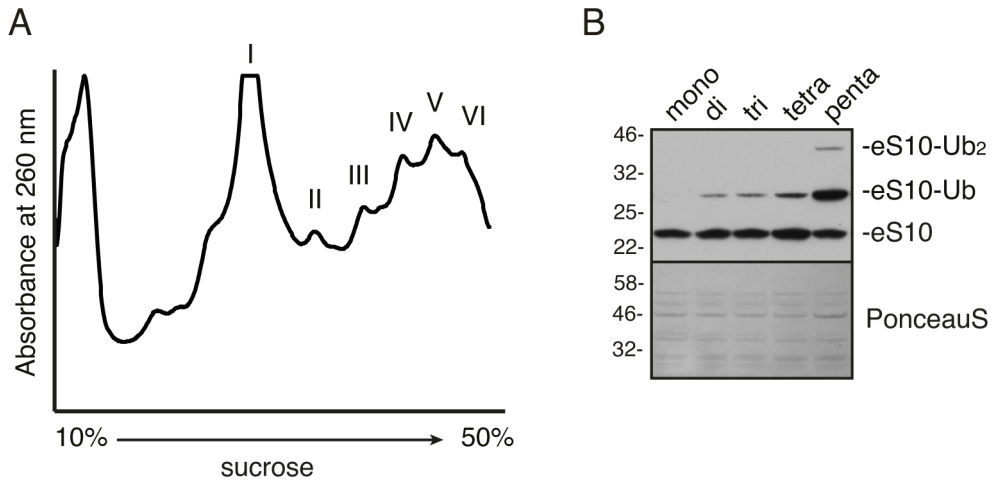

Figure 4.7 The collided di-ribosome is the minimal unit for ZNF598 recognition. (A) Native RRL translating globin mRNA in the presence of eRF1^{AAQ} was fractionated on a sucrose gradient. The profile of absorbance at 260 nm is shown with peaks corresponding to mono- (I), di- (II), tri- (III), tetra- (IV), penta- (V) and hepta- (VI) ribosomes as indicated. **(B)** Ribosomes from fractions enriched in mono- and poly-ribosomes were purified and normalized to contain equal amounts of ribosomes, as judged by absorbance at 260 nm. Each species was separately subjected to *in vitro* ubiquitination in the presence of 10 nM ZNF598 and analysed by probing for eS10 ubiquitination. Ponceau S staining of the blot is shown to verify equal input of ribosomes in each sample. Ribosome fractionation was performed with help from Sebastian Kraatz and Vish Chandrasekaran.

4.4 Cryo-EM structure of a stalled di-ribosome reveals unique inter-ribosomal interface

Identification and isolation of queued ribosomes stalled with eRF1^{AAQ} provided a means to generate sufficient sample such that the target of ZNF598 could be investigated by single particle cryo-EM. Sample preparation started with native polysomes from the *in vitro* translation reaction of globin mRNA performed in the presence of eRF1^{AAQ} (but in the absence of ZNF598) being separated on a sucrose gradient as shown on Figure 4.7A. Fractions corresponding to tetra-ribosomes were pooled together, ribosomes were concentrated by ultracentrifugation and deposited on grids for cryo-EM.

Cryo-EM analysis of di-ribosome species described in this section (including sample preparation, data processing and model building) was performed entirely by Vish Chandrasekaran with help from Sebastian Kraatz, whereas interpretation of the structure

was a result of collaboration between Vish Chandrasekaran, Ramanujan Hegde and the author of this thesis. Technical details related to data collection, data processing as well as model building are therefore omitted for clarity while the final structure will be discussed in the context of the *in vitro* biochemistry described above. For technical details on the cryo-EM analysis please refer to Juszkiewicz et al., 2018.

Guided by the biochemistry, the first step of cryo-EM analysis involved identification of the leading (stalled) ribosome, which contained eRF1^{AAQ} and ABCE1. This was achieved by focused classification with partial signal subtraction. From this subset of ribosomes, the population that contained additional signal corresponding to the trailing (collided) ribosome was identified, re-extracted, re-centered and used to generate an initial map of a collided di-ribosome. Further analysis revealed degrees of flexibility between the two adjacent ribosomes, necessitating additional multi-body refinement to improve resolution to around 6.8Å and 6.5Å for stalled and collided ribosomes, respectively. Finally, using all the particles from the same data set as a starting point, higher resolution maps were generated from the two major classes of particles: eRF1^{AAQ}- and ABCE1- containing ribosomes and ribosomes in a rotated state containing tRNAs in hybrid positions. These maps proved to be higher resolution versions of the stalled and collided ribosomes from the initial collided ribosome map. This is consistent with the fact that all of these particles originated from the collided complexes, which disassembled during the vitrification process. Hence, high resolution versions of the maps were used to generate atomic models. These were docked into the collided di-ribosome map to yield the consensus structure of the collided di-ribosome (Figure 4.8A).

The structure revealed that the leading ribosome is in a canonical state with the peptidyl-tRNA in the P-site, eRF1^{AAQ} occupying the A-site and ABCE1 interacting at the factor binding site. The E-site remained unoccupied and the L1 stalk displayed an ‘open’ conformation. That is a significant difference in comparison to the earlier published monosome 80S•eRF1^{AAQ}•ABCE1 structure which contained E-site tRNA (Brown et al., 2015). The collided ribosome is observed in a rotated state, with A/P and P/E hybrid tRNAs and an empty factor binding site. This is notable as this conformation should be compatible with eEF2 binding, however no extra density in the factor binding site was observed even after focused classification.

Finally, the two ribosomes interact with each other only via their small subunits. The two regions of close juxtaposition between the small subunits of the stalled and

collided ribosomes, which we define as interface 1 (Figure 4.8B) and 2 (Figure 4.8C), are noteworthy as they help to explain previous genetic, functional and biochemical data on ribosomal stalling. The first interface is formed by proteins eS1, uS11, eS26 and eS28 which are surrounding the mRNA exit channel of the stalled ribosome and protein uS4 and helix 16 from the 18S rRNA, which are at the mouth of mRNA entrance channel of the collided ribosome (Figure 4.8B). Hence, the mRNA path connecting mRNA channels of stalled and collided ribosomes is completely surrounded by the ribosomal proteins and rRNA elements forming the interface 1. This explains our previous observation that mRNA occupied by collided di-ribosomes is resistant to nuclease treatment (Figure 4.6).

Interface 2 is formed by ribosomal protein RACK1 of the stalled ribosome and proteins eS10, uS3 and uS10 of the collided ribosome (Figure 4.8C). Each of these proteins were previously implicated in the early events of RQC. Since the RACK1 on the stalled ribosome mediates all of the contacts with collided ribosome, its depletion would most likely affect the stability of di-ribosome architecture. This could explain the observation that in mammals, as well as in yeast, RACK1/Asc1 deletion affects the recognition of ribosomal stalling and results in readthrough of stall-inducing sequences (see Chapter 2, Figure 2.6) (Kuroha et al., 2010; Matsuo et al., 2017; Sitron et al., 2017; Sundaramoorthy et al., 2017).

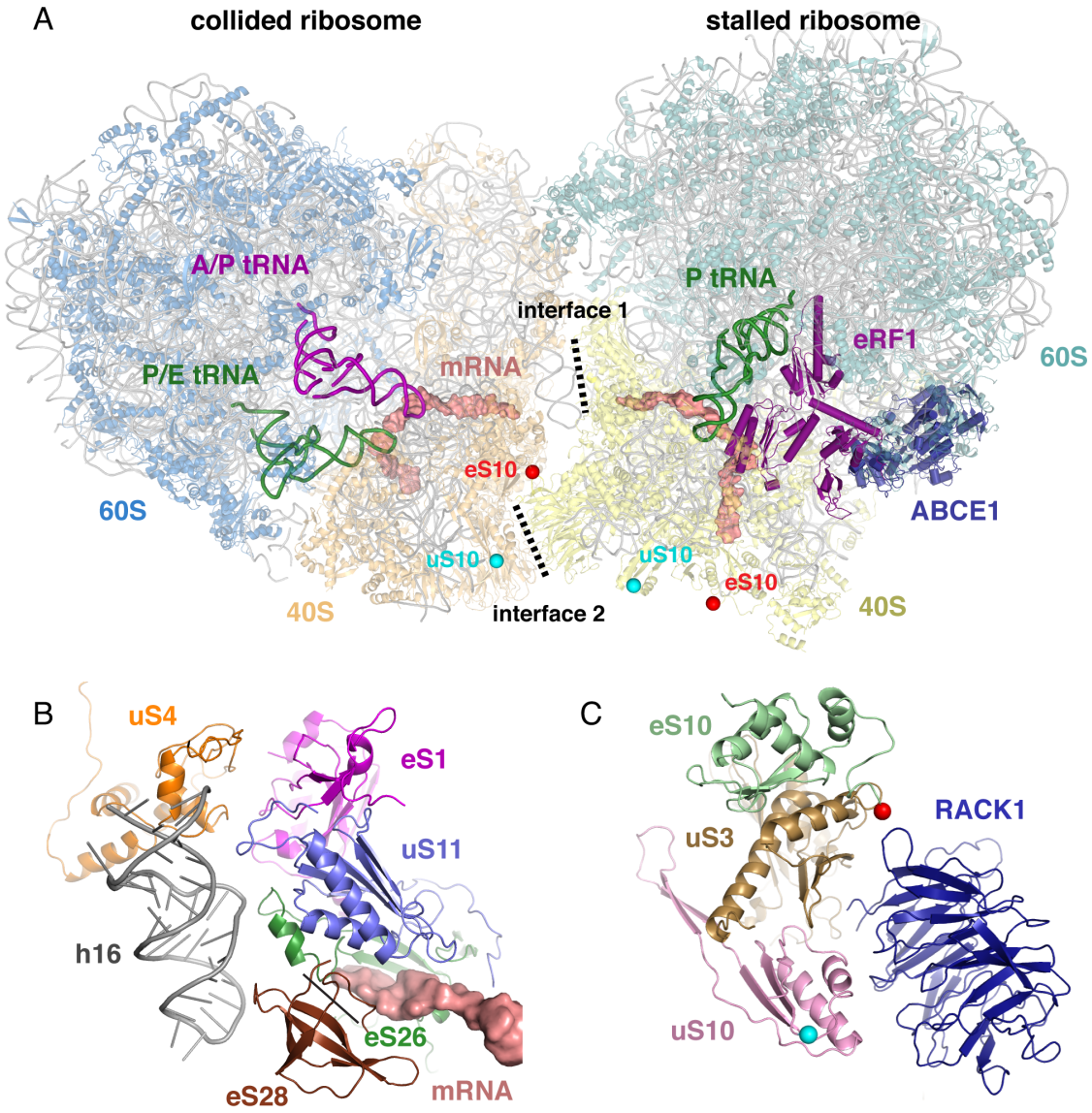

Figure 4.8 The consensus structure of the collided di-ribosome and molecular interfaces between 40S subunits. (A) Overview of the consensus structure of the collided di-ribosome. Black dashed lines indicate two primary interfaces between the small subunits of stalled and collided ribosomes. Spheres represent the approximate site of the ubiquitination on eS10 (red) and uS10 (cyan). The ubiquitinated residues are not modelled, so the most proximal visible residues are indicated. **(B)** Close-up of interface 1. Proteins uS4 and h16 of the 18S rRNA are from the collided ribosome, whereas proteins eS1, uS11 eS26 and eS28 are from the stalled ribosome. The mRNA (pink) in the mRNA channel of the stalled ribosome is shown. **(C)** Close-up view of interface 2. Proteins eS10, uS3 and uS10 are from the collided ribosome and RACK1 is on the stalled ribosome. Spheres represent ubiquitination sites, as in (A) (red – eS10; cyan – uS10). Structural analysis was performed by Vish Chandrasekaran and rendering by Manu Hegde.

We and others have previously shown that ZNF598 primarily ubiquitinates eS10 (Chapter 3, Figures 3.2, 3.3) (Garzia et al., 2017; Sundaramoorthy et al., 2017), whereas yeast Hel2 was reported to ubiquitinate uS10 (Matsuo et al., 2017). Although the primary

residues targeted by ZNF598 and Hel2 are not visible in our structure, the most proximal residues that we can identify in the collided ribosome are near interface 2 (Figure 4.8C). In contrast, the same residues on the stalled ribosome are distant from the interface. Based on the ZNF598's selectivity towards closely packed di-ribosomes over mono-ribosomes, it is reasonable to speculate that the inter-ribosomal interface serves as an initial recognition signal for ZNF598 recruitment. Therefore, we favour a model in which ZNF598 binds in the region defined by the inter-ribosomal interface and ubiquitinates eS10 or uS10 on the collided ribosome to induce downstream quality control pathways.

4.5 The inter-ribosomal interface of the collided di-ribosome is compatible with different types of stalls

The described general mechanism for the detection of ribosomal stalling should allow recognition of various types of stalls independent of cause. The ribosome stalled with eRF1^{AAQ} exists in the canonical conformation. To test whether stalls which trap the ribosome in an alternative, rotated state would result in the formation of a similar type of inter-ribosomal interface, we computationally replaced the stalled ribosome in a collided di-ribosome model with a ribosome in the rotated state. We observed no obvious clashes between the large ribosomal subunits while the small subunits changed very little, maintaining the near intact 40S-40S interface (Figure 4.9A). This suggests that the described collided state, and therefore ZNF598 recognition, should be compatible with ribosome stalling independent of translation cycle step. In agreement with this conclusion, we observed that collided penta-ribosome seems to be ubiquitinated more efficiently than the collided di-ribosome (Figure 4.7B). As the second ribosome of the tri-ribosome is in a rotated state, the interface between the second and the third ribosome must be different than the interface between the first and the second ribosome. Therefore, in order to explain more efficient ubiquitination of the tri-ribosome, one needs to assume that ZNF598 can efficiently recognize both types of interfaces.

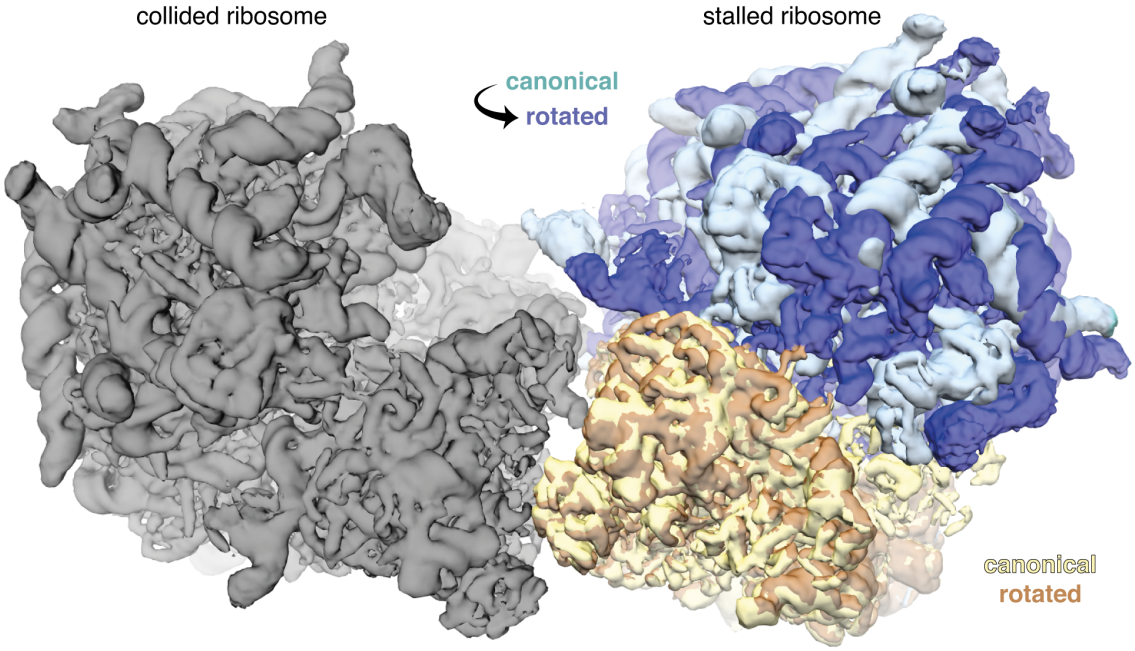

Figure 4.9 Tolerance of the collided di-ribosome. Maps of ribosomes in a canonical state (pale cyan/yellow) and in a rotated state (blue/orange) are superimposed in the "stalled" position of the collided di-ribosome structure relative to the rotated-state collided ribosome (grey). Structural analysis as well as maps rendering was performed by Vish Chandrasekaran with help from Manu Hegde.

4.6 Discussion

Our data cumulatively suggest that ZNF598 recognizes aberrant translation by specifically recognizing ribosome collisions. These collisions occur when a faster moving, trailing ribosome "catches up" with a slower (or stalled) leading ribosome. This is supported by the fact that the collided di-ribosome species acquires a well-defined, unique molecular architecture. The collided ribosomes have their 40S ribosomal subunits in close juxtaposition while their 60S subunits are facing opposite directions. This conformation is sufficiently flexible and tolerant to accommodate different rotation states of the stalled ribosome. Hence, it appears that many different types of stalls should be recognized by the same unifying mechanism.

We and others have previously shown that ZNF598 can ubiquitinate eS10, uS10 and to some extent uS3 (see Chapter 3: Table 3.1, Figure 3.3) (Garzia et al., 2017; Sundaramoorthy et al., 2017). All three of these ribosomal proteins are located at the interface of the collided di-ribosome. Given that the interface is the most distinctive feature of the di-ribosome, it is reasonable to speculate that it would contain the ZNF598-

binding site. However, a structure containing ZNF598 bound to the collided di-ribosome is required to confirm this and to understand this putative interaction in molecular detail.

The structure also sheds light on the potential role of Asc1/RACK1, another factor previously implicated in stalling on polybasic sequences (Chapter 2: Figure 2.6) (Kuroha et al., 2010; Sitron et al., 2017; Sundaramoorthy et al., 2017). Since RACK1 is a crucial part of our described interface 2 of the collided di-ribosome (Figure 4.8C), its absence would most likely destabilize the di-ribosome architecture and therefore result in inefficient ZNF598 recognition and ubiquitination. Consistently with this hypothesis, genetic analyses in mammals suggest that both RACK1 and ZNF598 are acting within the same pathway (see Chapter 2: Figure 2.11). Moreover, deletion of yeast Asc1 was dominant to Hel2 perturbation (Sitron et al., 2017) which suggests that it must be involved in the step upstream of the ubiquitination.

Ribosome collision events were recently reported to be important for the induction of endonucleolytic cleavage on stall-containing mRNAs in yeast (Simms et al., 2017). Therefore, it appears that both nascent chain quality control and mRNA decay rely on ribosome collisions. The most parsimonious explanation is that ZNF598/Hel2 acts as a universal sensor of ribosome collisions and deposits a ubiquitin mark on the key residues of the 40S ribosomal subunit. The ubiquitin mark then serves as a signal for factors that induce mRNA cleavage, similar to its behaviour in inducing ribosome splitting and nascent protein degradation as part of the RQC pathway. In support of this idea, the most recent study from Inada group reported that Hel2 deletion abolishes primary endonucleolytic cleavage events observed within the di-ribosome unit (Ikeuchi et al., 2019).

The molecular mechanism by which ZNF598/Hel2-mediated ubiquitination induces downstream RQC events remains unknown. Other factors such as the helicase ASCC3 (Slh1 in yeast) were previously implicated in nascent protein quality control however their exact role remains unknown (Ikeuchi et al., 2019; Matsuo et al., 2017; Sitron et al., 2017). The ability to assemble a defined substrate consisting of ubiquitinated di-ribosomes in an *in vitro* system should facilitate the discovery of downstream steps in this process. Crucially, how signalling occurs between ubiquitin to downstream factors that disassemble the di-ribosome, induce subunit splitting and mRNA cleavage remains to be investigated.

It was previously shown both *in vitro* and *in vivo* that polysomes can be arranged in a variety of different conformations including spirals, circles, beads-on-a-string and other closely-packed structures of unknown biological relevance (Afonina et al., 2014; Brandt et al., 2009, 2010; Christensen and Bourne, 1999; Myasnikov et al., 2014). The collided di-ribosome described in this chapter is one such, as ribosomes are arranged in a helical manner (Myasnikov et al., 2014). Although the functional relevance of this helical assembly was not analysed in its initial report, we would like to propose that it might actually represent the stalled ribosome, followed by an array of collided ribosomes. In support of this interpretation, such helical poly-ribosomes were characterized by lower translation activity and were preferentially observed at later stages of translation (Afonina et al., 2015), when mRNA damage could induce ribosome arrest while the disassembly pathways got saturated or lost their activities.

With parallels to how 60S-peptidyl-tRNA sub-ribosomal species are being selectively recognized by the NEMF-Listerin complex, the supra-molecular assembly of the collided di-ribosome appears to be similarly recognized by another factor monitoring translation – ZNF598. Therefore, it is very likely that other previously described ribosome configurations (Afonina et al., 2014; Brandt et al., 2009, 2010; Christensen and Bourne, 1999) or yet uncharacterized ribosome-associated complexes might also represent biologically-relevant configurations. These conformations may be sensed by different factors to initiate crucial processes such as a quality control or translational regulation.

4.7 Materials and methods

Constructs, antibodies, purified proteins

Constructs used for *in vitro* translation in RRL were based on the pSP64 vector. The constructs were designed to have an N-terminal epitope tag (Twin-strep) followed by the previously described cytosolic domain of Sec61β into which an autonomously folding domain VHP was inserted between amino acids 13 and 14 (Shao et al., 2013), a stretch of 20 AAA codons and a C-terminal 3F4 tag. Construct for expression of recombinant, C-terminally tagged with 3xFLAG ZNF598 was described in Chapter 2. Purified $eRF1^{AAQ}$ was a gift from V. Chandrasekaran. All of the antibodies as well as purified proteins used in the *in vitro* ubiquitination reactions were described in Chapters 2 and 3.

In vitro transcription and translation

In vitro transcription reactions were performed as previously described (Sharma et al., 2010). Briefly, transcription reactions contained 10 ng/µl PCR product in 40 mM HEPES pH 7.4, 6 mM $MgCl_2$, 10 mM reduced glutathione, 20 mM spermidine, 0.1 mM GTP, 0.5 mM ATP, 0.5 mM CAP structure (NEB), 04-0.8 U/µl RNasin (NEB) and 0.4 U/µl SP6. Transcriptions were performed at 37°C for 1h. *In vitro* translations were performed as described (Sharma et al., 2010). In short, the translation system was based on RRL (Green Hectares). Two different types of lysates were employed: for translation of exogenously added mRNAs, native lysate was pre-treated with micrococcal nuclease to digest endogenous mRNA molecules (Sharma et al., 2010). To generate native polysomes stalled on endogenous mRNA (predominantly α- and β-globin), non-nucleased, native RRL was used. A typical translation reaction contained 33% of RRL (by volume) of crude RRL, 20 mM HEPES, 10 mM KOH, 50 mM K(OAc) 1 mM ATP, 1 mM GTP, 2 mM $MgCl_2$, 1 mM reduced glutathione, 0.3 mM spermidine, 40 µM of each amino acid except methionine, 40 µg/ml creatine kinase, 12 mM creatine phosphate and 20 µg/ml of tRNA from pig liver. When the exogenous mRNA was translated, the transcription reaction (without purification) was added to 5% by volume to the translation reaction. Translations were performed at 32°C for 20-45 min, unless specifically indicated in the figure legends.

Affinity purification of complexes from in vitro translation reactions

For affinity purifications, 200 µl or 400 µl reactions supplemented with recombinant ZNF598-3xFLAG at 2.5-10 nM were carried out for 25 min at 32°C. To stop the reaction, samples were transferred to ice with the rest of the experiment performed at 4°C. Next, 15 µl of packed StrepTactin High Performance Sepharose (GE Healthcare) or 15 µl of packed anti-FLAG resin (SIGMA) was added directly to the reaction and samples were incubated for 1.5h with end-over-end mixing at 4°C. After incubation the resin was washed briefly 5 times with RNC buffer (50 mM HEPES pH 7.6, 100 mM K(OAc), 5 mM $Mg(OAc)_2$). For the elution of StrepTactin-bound complexes, the resin was incubated with RNC buffer containing 50 mM D-biotin for 30 min on ice. FLAG-tagged complexes were eluted off the resin with RNC buffer containing 0.2 mg/ml 3xFLAG peptide for 30 min in RT.

His-ubiquitin pulldowns under denaturing conditions

When purification of ubiquitinated products was necessary, His-tagged ubiquitin (Boston Biochem) was added to the translation reactions to a final concentration of 10 μM. For purification purposes, samples were first adjusted to 100 mM Tris pH 8.0 with 1% SDS in a final volume of 100 μl, boiled for 5 min at 95°C, cooled to RT and diluted with 900 μl of pulldown buffer [PBS, 0.5% Triton-X100, 250 mM NaCl, 20 mM imidazole)]. To each sample, 10 μl of packed Ni-NTA (QIAGEN) resin was added and samples were incubated for 1.5h at 4°C with end-over-end rolling. The resin was washed 4 times with pulldown buffer and elution was with SDS-PAGE sample buffer supplemented with EDTA at 50 mM.

Sucrose gradient fractionations

Sucrose gradient fractionations were performed as described in Chapter 3 with minor modifications. Higher resolution sucrose gradients (20-50%) were used as indicated in individual figures. For analysis of the radiolabeled nascent chains, each of the 11 fractions recovered from the sucrose gradient was digested with 0.15 mg/ml of RNAse A for 30 min on ice to cleave off the associated tRNA.

Ribosome purification and ubiquitination analysis

Purification of collided di-ribosomes for biochemical analysis (including ubiquitination) used as a starting point 500 μl of *in vitro* ubiquitination reaction using native, non-nucleased RRL supplemented with $eRF1^{AAQ}$ at 1 μM. The reaction was allowed to proceed for 20 min at 32°C. As indicated, some samples were subjected to nuclease digestion (or mock treatment without nuclease) which involved addition of $CaCl_2$ to 0.5 mM and S7 micrococcal nuclease (Roche) to 150 U/ml for 10 min at 25°C. Reactions were quenched by the addition of EGTA to 1 mM. To sediment ribosomes, reaction mixtures were layered onto 250 μl of 20% sucrose cushion in RNC buffer and spun for 1h at 100,000 rpm at 4°C in TLA-120.2 rotor (Beckman Coulter). Ribosomal pellets were washed once with 200 μl of RNC buffer and resuspended in 50 μl of RNC buffer for subsequent analyses. Ubiquitination reactions were performed as described in Chapter 3, except that ZNF598 concentrations were adjusted to 2.5-10 nM, as indicated in the text and in the individual figure legends.

Western blot analysis and ZNF598 purification

All the western blots as well as the purification procedure for 3xFLAG tagged ZNF598 were as described in previous chapters.

Purification of stalled poly-ribosomes for cryo-EM

Four 1 ml in vitro translation reactions performed in non-nucleased RRL supplemented with 500 nM $eRF1^{AAQ}$ were incubated at 32°C for 25 min. Ribosomes from each reaction were pelleted through a 2 ml cushion of 15% (w/v) sucrose in 1xPS buffer (50 mM HEPES, 100 mM KOAc, 2 mM $Mg(OAc)_2$, 0.5 mM TCEP, pH 7.4) by centrifugation at 100,000 rpm for 1 hr at 4°C in a TLA-100.3 rotor (Beckman). The pellets were resuspended by soaking and repeated pipetting in 800 µl PS buffer supplemented with 1 U/ml RNasin inhibitor and carefully loaded onto two 14 ml sucrose gradients (10%–50%) in PS buffer supplemented with 20 U/ml RNasin inhibitor (Promega). The gradients were centrifuged at 40,000 rpm for 2 hr at 4°C in an SW 40 Ti rotor (Beckman) and fractionated at 30 s per fraction (~0.65 ml each) using a peristaltic pump setup connected to a UV absorbance reader at 260 nm (Gilson). Fractions corresponding to tetra-ribosomes were pooled, diluted to 3 ml in PS buffer and the ribosomes pelleted by centrifugation at 100,000 rpm for 1 hr at 4°C in a TLA-100.3 rotor. The pellets were resuspended in 25 µl of PS buffer supplemented with 1 U/ml RNasin inhibitor, quantified by absorbance at 260 nm and used immediately for cryo-EM or flash-frozen and stored at -80°C. Analysis of a specimen prepared in this way by repeated sucrose gradient fractionations verified that it contained little or no monosomes.

Structural data

Electron density maps are available at EMDB: EMD-0192 (stalled ribosome), EMD-0194 (collided ribosome), EMD-0195 (collided di-ribosome – stalled) and EMD-0197 (collided di-ribosome – collided). Atomic coordinates are available at Protein Data Bank (PDB) 6HCF (stalled ribosome), 6HCJ (collided ribosome), 6HCM (collided di-ribosome-stalled)

Chapter 5: ZNF598 is a quality control sensor of ribosome collisions

In Chapter 4, we showed that ZNF598 can selectively engage closely-packed di-ribosomes. These molecular species arise when a trailing ribosome meets a slower (or stalled) leading ribosome. In agreement with our biochemical data, the structure of di-ribosome revealed a unique, defined conformation whereby the mRNA is fully shielded between the two ribosomes. The positioning of the mRNA explained one of our key previous observations which suggested that di-ribosomes targeted by ZNF598 were characterized by their nuclease resistance. In this chapter, we set out to determine whether our *in vitro* and structural observations are physiologically relevant and therefore of broad importance to cellular homeostasis. For this, we move to an *in vivo* mammalian system, characterizing ZNF598 and ribosome collisions in the HEK 293 cell line.

To confirm whether the structure of the collided di-ribosome represents a physiologically relevant state, we tested if we could detect a similar nuclease-resistant di-ribosome species in cells. For this, we induced ribosome collisions *in vivo* by treating cells with a sub-inhibitory dose of emetine, an irreversible translation elongation inhibitor. We reasoned that this would stochastically inhibit only a subset of ribosomes, resulting in local collision events. As expected based on our *in vitro* data, treatment with a low dose of emetine resulted in the formation of a nuclease-resistant, collided poly-ribosome species which efficiently recruited cytosolic ZNF598.

The structure of the collided di-ribosome revealed the paucity of 60S interactions and invariance of the 40S-40S interface to the rotation state of the stalled ribosome. This suggested that multiple different types of stalls should be tolerated by collided di-ribosome. We therefore treated cells with sub-inhibitory doses of multiple different elongation inhibitors, which stall ribosomes by different mechanisms. In each case, treatment correlated with a dramatic increase in eS10 ubiquitination, indicative of ZNF598 engagement and ubiquitination of ribosomes. Hence, detection of excessively slow ribosomes through ribosome collisions is a general mechanism for recognition of aberrant translation.

We reasoned that if ZNF598 is a *bona fide* sensor of ribosome collisions, it should be the most enriched factor in the fraction of collided di-ribosomes. Indeed, quantitative

mass-spectrometry analysis revealed that ZNF598 was the most enriched ribosome-associated protein under conditions that induced collisions (compared to ~600 other detected ribosome-associated proteins).

Finally, indirect detection of excessively slow ribosomes via collision events implies that the induction of this quality control pathway must necessarily be context dependent. In other words, ZNF598 engagement should rely not only on the strength of the pausing signal, but also on the relative distances between translating ribosomes, a property which is effectively determined by the rate of initiation on that particular mRNA. To test this possibility, we exploited our previously described dual-fluorescence reporter assay. As expected, partial reduction of the initiation rate resulted in increased readthrough of the stall-inducing poly(A). Importantly, this effect was no longer observed in cells depleted of ZNF598. Therefore, the threshold for the induction of quality control is substrate specific, integrating multiple parameters such as the velocities of individual ribosomes as well as relative inter-ribosomal distances.

5.1 Nuclease-resistant poly-ribosomes are observed in cultured cells

ZNF598 does not simply recognize two ribosomes in close proximity, but rather a defined molecular architecture that fully shields translated mRNA. We exploited this property to probe whether a similar ribosomal conformation exists in cultured cells. To induce collisions of ribosomes, we treated cells with a sub-inhibitory dose of the translation elongation inhibitor emetine (Grollman, 1968). Treatment with the low dose of irreversible emetine should result in the stochastic inhibition of only a subset of ribosomes, allowing the remaining, non-inhibited ribosomes to elongate until they encounter a drug induced road-block (Figure 5.1). This is in contrast to a fully inhibitory dose of emetine, which should inhibit the elongation of all ribosomes, thereby preventing collisions completely.

To determine whether these collided ribosome species exist, we isolated cytosolic fractions from cells treated with different concentrations of emetine and treated them with micrococcal nuclease. We then fractionated the resulting reaction mixtures on a high-resolution sucrose gradient and determined relative ribosome abundance by continuously measuring absorbance at 260 nm.

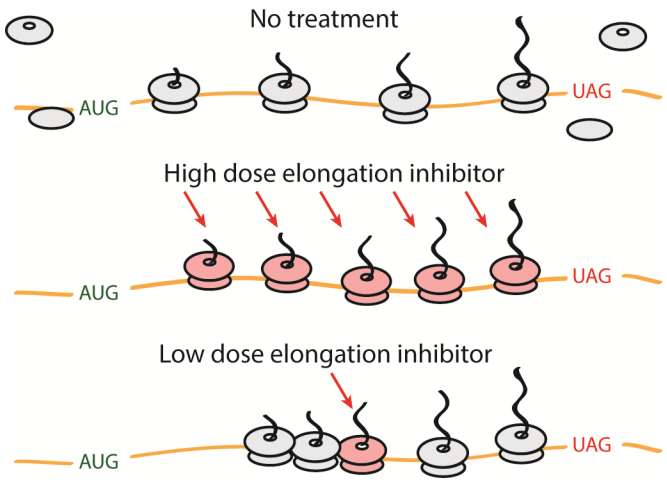

Figure 5.1 Strategy to generate ribosome collisions in cells. Translating polysomes are usually equally distributed on mRNAs. An inhibitory dose of an elongation inhibitor would stall each of the translating ribosomes, preventing collisions from happening. By contrast, a sub-inhibitory dose should affect only a subset of ribosomes, thereby resulting in local collisions.

As expected, nuclease treatment of cytosol from untreated cells or those treated with a high dose of emetine resulted in almost complete collapse of polysomes into monosomes (Figure 5.2A). By contrast, treatment with a low dose of emetine induced the formation of nuclease resistant di-, tri-, tetra- and higher order ribosome complexes, consistent with the supra-molecular arrangement of stalled ribosomes characterized in Chapter 4. The nuclease-resistant, higher-order complexes accumulated to a much greater extent in ZNF598-depleted cells (Figure 5.2A). When we washed out excess emetine after 15 min of treatment and allowed cells to recover for 1h, we observed a significant decrease in the abundance of nuclease resistant species. This was observed in wild type but not ZNF598-deficient cells, where we could observe an additional build-up of tetra-, penta- and higher order poly-ribosomal complexes (Figure 5.2B). Therefore, in cells, just like *in vitro*, ribosome collisions induce the formation of higher-order, nuclease resistant ribosomal complexes, which are substrates for recognition by ZNF598.

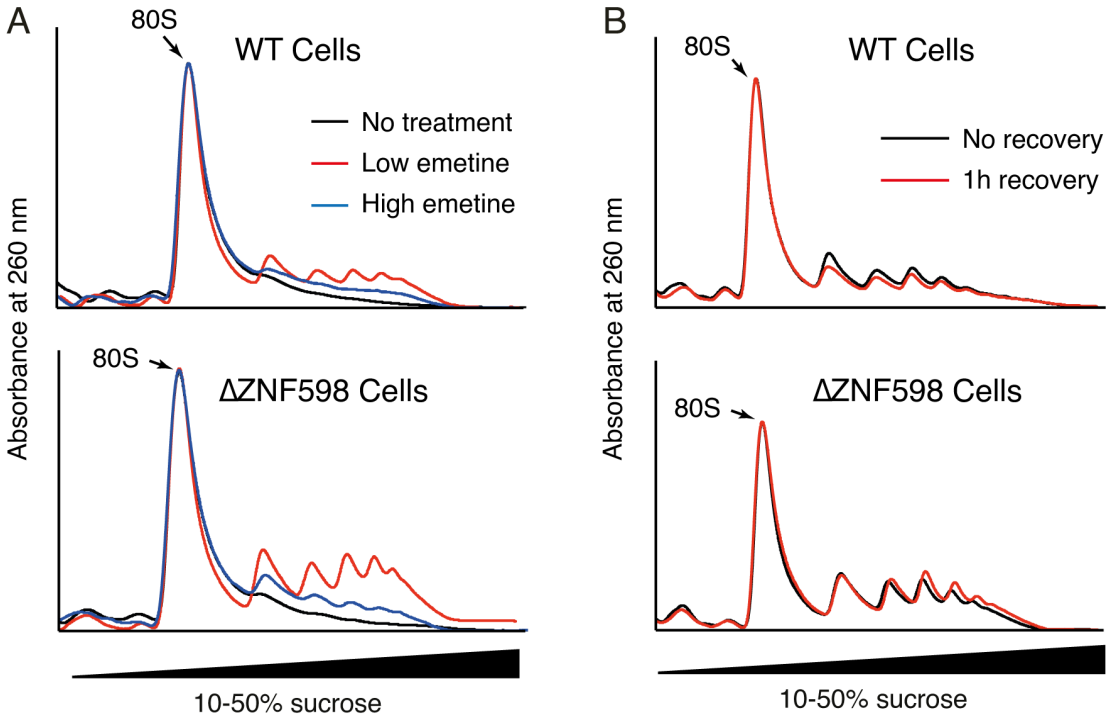

Figure 5.2 Nuclease-resistant, collided di-ribosomes induced in cells are resolved in a ZNF598-dependent manner. (A) Wild type or ZNF598-depleted (ΔZNF598) cells were pre-treated with emetine for 15 min at a low (1.8 µM; red traces) or high dose (360 µM; blue traces). The cytosol was then collected from treated and control cells (black traces), subjected to digestion with S7 nuclease and separated on a sucrose gradient. Continuous profiles of the absorbance at 260 nm across the gradients were plotted and aligned to the 80S-monosome peaks. **(B)** WT or ΔZNF598 cells were treated with a low dose (1.8 µM) of emetine for 15 min. Cells were either immediately harvested (black traces) or emetine was washed out and cells were allowed to recover for 1h in fresh medium (red traces). The cytosol was collected and treated as in (A). All fractionations were performed multiple times and representative results are shown.

5.2 ZNF598 detects ribosome collisions induced by different types of stalls

The major implication of our biochemical and structural analysis of stalled ribosomal-complexes is that ZNF598-mediated recognition should be independent of the primary cause of the stall or conformation of the stalled ribosome. To test this prediction *in vivo*, we treated cells with sub-inhibitory concentrations of three unrelated inhibitors that stall translation at different stages of elongation. As a proxy for efficient recognition of stalls by quality control machinery, we monitored the ubiquitination status of eS10, the primary target of ZNF598. Untreated cells are characterized by very low levels of ubiquitinated eS10 (Figure 5.3A) while the entire pool of cellular ZNF598 remains freely dissociated in the cytosol, as judged by its exclusive migration in non-ribosomal fractions after sucrose gradient separation (Figure 5.3B). When we treated cells with three different translation elongation inhibitors: anisomycin, emetine and didemnin B at low dosage, we

observed markedly elevated levels of eS10 ubiquitination (Figure 5.3A). As illustrated for one of the inhibitors (emetine), ZNF598 was recruited to higher-order ribosomal complexes (Figure 5.3B), consistent with observed ubiquitination patterns (Figure 5.3A). By contrast, treatment with high doses of inhibitors shown little to no increase in eS10 ubiquitination (Figure 5.3A) and no ZNF598 recruitment to the ribosomal complexes (Figure 5.3B).

As noted, each of the three drugs used inhibits elongation differently. Emetine is an irreversible inhibitor of translocation (Jiménez et al., 1977), anisomycin prevents peptidyl transfer (Barbacid et al., 1975) and didemnin B traps eEF1 at the ribosome thereby preventing its dissociation (Shao et al., 2016). In each case, individual ribosomes would be stalled in a relatively different state with a series of characteristics dictated by the drug type used. These include: occupancy of the A-site, occupancy of the GTPase centre, positions of the engaged tRNAs as well as the inter-subunit rotation state. As shown in Figure 5.3A, it is not a particular state as defined by a collection of physical characteristics of the ribosome which is being detected by ZNF598. Instead, it is the consequence of a stall, ribosomal collision, which triggers ZNF598 recruitment.

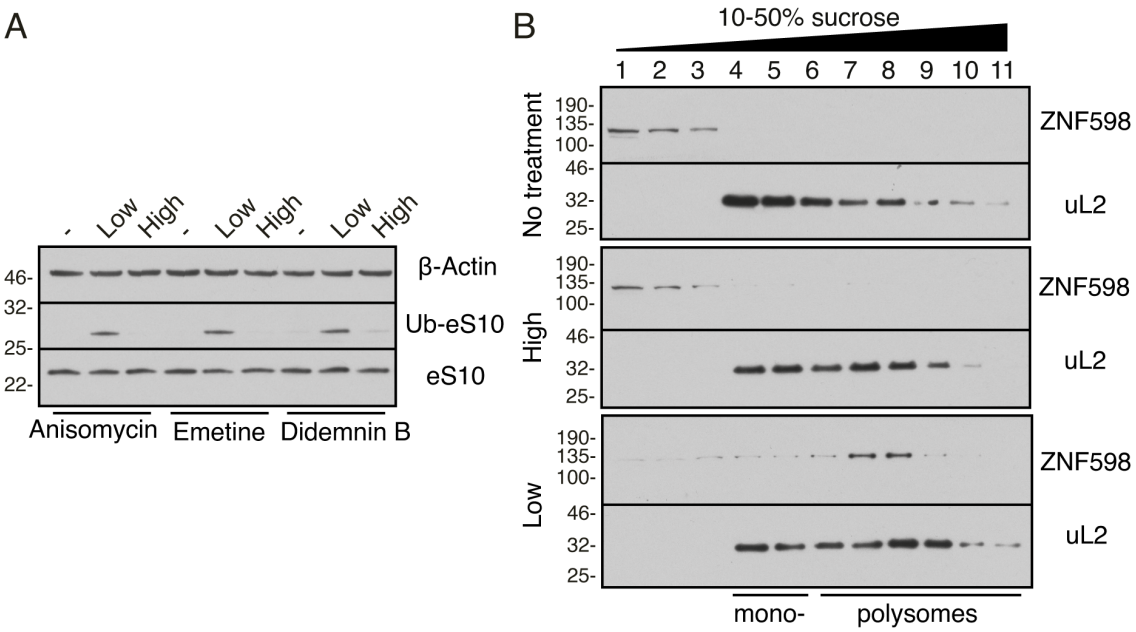

Figure 5.3 ZNF598-mediated recognition of stalled di-ribosomes is agnostic to the primary cause of stall. (A) Cells were treated with nothing or a low or high dose of the indicated translation elongation inhibitor for 15 min and analysed by immunoblotting. Membranes were pre-cut and incubated with a higher concentration of primary antibodies to detect the ubiquitinated version of eS10 with higher sensitivity. **(B)** Cytosol isolated from cells pre-treated for 15 min with nothing or a low or high dose of emetine were separated on a sucrose gradient and analysed by immunoblotting for endogenous ZNF598 and the 60S-ribosomal protein uL2.

5.3 ZNF598 is the most upstream factor involved in recognition of collided ribosomes

To further establish that ZNF598 is the *bona fide* sensor of ribosome collisions, we took an unbiased approach using quantitative mass-spectrometry. We compared the protein composition of actively translating polysomes to those stalled with sub or fully inhibitory concentrations of emetine. For this, we fractionated the cytosol from treated cells on a sucrose gradient and further purified ribosomal complexes from fractions 8-11, which were previously shown to contain heavy polysomes. Those complexes were then analysed by quantitative mass spectrometry using tandem mass tagging (TMT) (Thompson et al., 2003). The abundance ratios of proteins associating with ribosomes were compared in a pair-wise manner (i.e. low emetine vs non-treated; low emetine vs high-emetine and high emetine vs non-treated). ZNF598 was the most enriched protein when ribosome-associated complexes from low emetine treated cells were compared either with complexes from untreated or high emetine treated cells (Figure 5.4). In contrast, there was no relative difference in the abundance of ribosomal proteins between conditions, allowing us to use them as internal controls for quantitation. Of the proteins enriched at least 2-fold (>$\log_2$) in the low emetine condition (i.e. binding specifically to collided ribosomes), we found four potential candidates besides ZNF598. Of those, Sin3a seemed to specifically associate with emetine-stalled ribosomes independently of the dose used, thereby eliminating it from further consideration. As a result, there were three remaining candidate proteins which specifically associated with collided ribosomes: Suppressor of mec-8 and unc-52 protein homolog 1 (SMU1), Zinc finger protein 346 (ZNF346) and Endothelial differentiation-related factor 1 (EDF1). An additional TMT experiment performed in exactly the same way, but using cells depleted from ZNF598, showed that only EDF1, but not SMU1 nor ZNF346 was enriched in the fraction of low-emetine induced, collided poly-ribosomes (data not shown). EDF1 (also known as MBF1) was previously reported to act as a transcriptional co-activator (Kabe et al., 1999). However, the archaeal homolog of this highly conserved protein was recently observed to bind ribosomes (Blombach et al., 2014). We therefore considered the possibility that EDF1 might act upstream of ZNF598, putatively as the most proximal sensor of ribosome collisions.

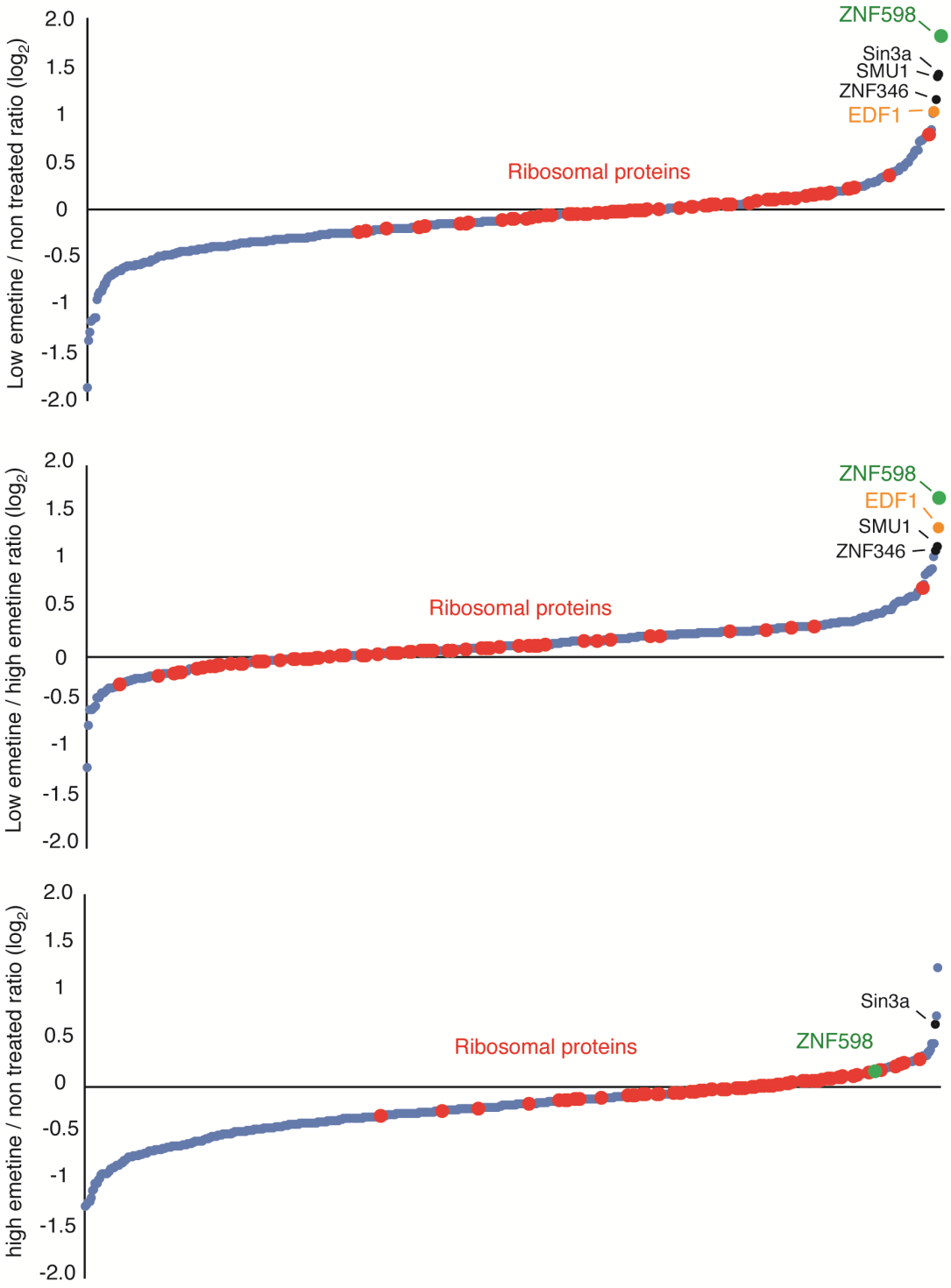

Figure 5.4 ZNF598 is the major factor that engages collided ribosomes in cells. Native polysomes from HEK 293 cells not treated or treated with a low or high dose of emetine were isolated and analysed by quantitative mass spectrometry using TMT. Abundance ratios of proteins associating with polysomes from the three pairwise comparisons (low emetine vs non-treated – top panel; low emetine vs high emetine – middle panel; high emetine vs non-treated – bottom panel) are plotted on a $\log_2$ scale. Note that ZNF598 (marked in green) is the most highly enriched protein selectively in the low emetine condition. Ribosomal proteins (indicated in red) are uniformly not enriched in any of the conditions and serve as an internal control for quantitation. See also Appendix 1. TMT analysis was performed by Sew-Yeu Peak-Chew.

To test this hypothesis, we first decided to confirm the TMT results using an orthogonal strategy. For this, we prepared cytosol from WT cells pre-treated with a low dose of emetine (as in Figure 5.4), separated it on a sucrose gradient, and analysed each fraction by immunoblotting. In our control, non-treated sample, we observed that EDF1 migrated predominantly in the top, non-ribosomal fractions, with very little enrichment in heavy poly-ribosomal fractions (Figure 5.5). In contrast, after treatment with emetine we observed that ~70% of the EDF1 pool shifted to the heavy poly-ribosomal fractions, where we previously saw ZNF598. Importantly, EDF1 binding was specific to collided di-ribosomes as it was effectively depleted from monosome containing fractions.

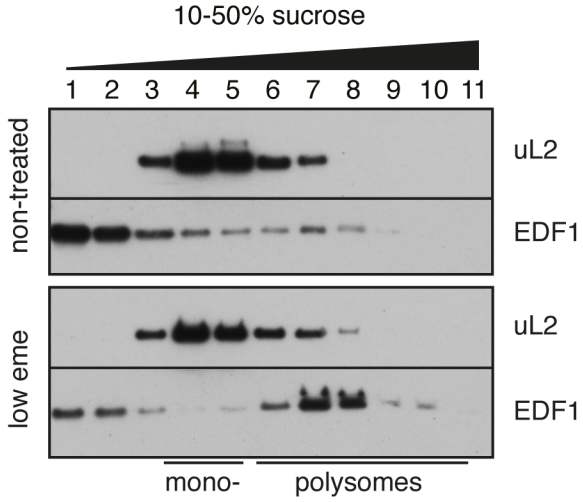

Figure 5.5 EDF1 binds specifically to low dose emetine-induced, collided poly-ribosomes. Cytosol was isolated from cells treated with nothing (top panel) or a low dose (1.8 μM; bottom panel) of emetine and separated on a 10-50% sucrose gradient. Each fraction was then analysed by immunoblotting for ribosomal protein uL2 and EDF1. Positions of mono- and polysomes are indicated.

If EDF1 were the most upstream factor detecting ribosome collisions, ZNF598 function should be dependent on EDF1. To test this possibility, we knocked out EDF1 using the CRIPSR-Cas9-mediated gene disruption strategy (Ran et al., 2013). We generated three independent, EDF1-depleted clones in the previously described $(K^{AAA})_{21}$ reporter cell line (Figure 5.6A). To test whether EDF1 depletion affects ZNF598 function, we treated each EDF1 knockout clone with a low or high dose of emetine and analysed the ubiquitination status of ZNF598 target eS10 (Figure 5.6B). When compared with WT cells, we did not detect any defect in ZNF598-mediated ubiquitination of eS10 in the presence of low emetine doses. We also tested the functional phenotype of an EDF1 deletion in terms of characterizing the capacity to readthrough stall-inducing sequences using our dual fluorescence reporter system (described in Chapter 2). Analysis

of GFP and RFP expression after induction of the $(K^{AAA})_{21}$ stalling reporter in one of the EDF1 knockout clones revealed a small decrease in the RFP:GFP ratio (when compared to WT cells), which could be attributed to slight decrease in RFP expression (Figure 5.6C). This argues strongly against the role of EDF1 in the induction of the RQC pathway. However, the capacity of EDF1 to bind to collided di-ribosome complexes, as well as a translation-related phenotype suggests a potential role in collision-induced, translational modulation.

This unbiased analysis confirms that in cells, as *in vitro*, ZNF598 is the most proximal and direct quality control sensor of ribosome collisions.

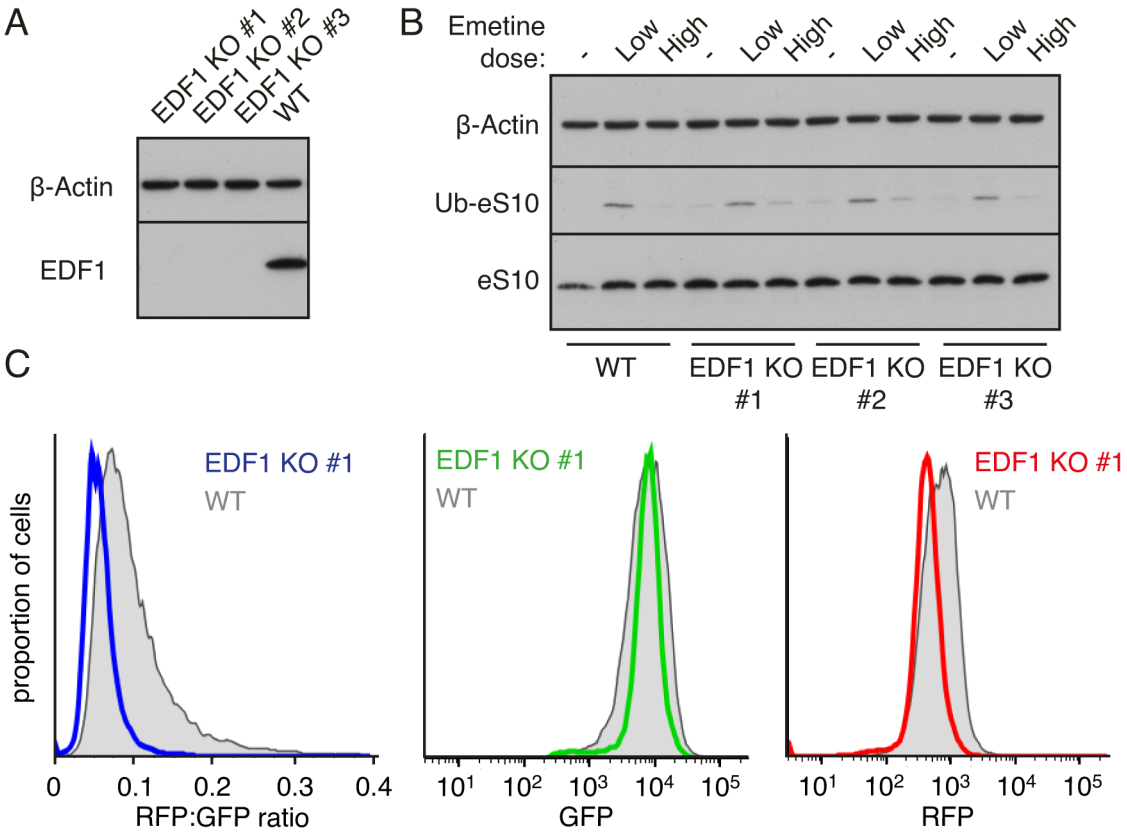

Figure 5.6 EDF1 deletion does not affect ZNF598 function. (A) Total cell lysates from three independent EDF1 knockout clonal cell lines (EDF1 KO #1-3) as well as wild type (WT) cells were analysed by immunoblotting for EDF1 (with β-actin serving as a loading control). **(B)** The same cell lines as in (A) were treated for 15 minutes with nothing (-), low (low; 1.8 µM) or high (high; 360 µM) concentration of emetine and total cell lysates were analyzed by immunoblotting. Note that ubiquitinated eS10 was detected separately with increased concentration of primary antibody. **(C)** One of the EDF1 KO clonal cell lines and WT control cells were induced for the expression of $(K^{AAA})_{21}$ dual-fluorescent reporter construct for 24h and analyzed by flow cytometry. Histograms represent RFP:GFP ratio (left), GFP expression (middle) and RFP expression (right). Control cells are in grey, whereas EDF1 KO cells are in blue (RFP:GFP ratio), green (GFP) and red (RFP).

5.4 RACK1 depletion impairs eS10 ubiquitination

RACK1 is the other protein that could potentially act upstream of the ZNF598, albeit not as an active sensor, but a scaffold. Our structure of the di-ribosome shows that interface 2 is formed by RACK1 of the stalled ribosome and eS10, eS3 and uS10 proteins of the collided ribosome (see Chapter 4, Figure 4.8B). RACK1/Asc1 was also implicated both genetically and functionally in the same pathway as ZNF598/Hel2 (see Chapter 2, Figures 2.6, 2.11) (Kuroha et al., 2010; Sitron et al., 2017; Sundaramoorthy et al., 2017). Hence, we hypothesized that RACK1 might play a role in the formation and structural stabilisation of collided di-ribosome species recognized by ZNF598. In order to test the functional implications of this hypothesis, we knocked down RACK1 with siRNA, induced collisions using low concentrations of emetine and analysed eS10 ubiquitination in a time resolved manner (Figure 5.7A).

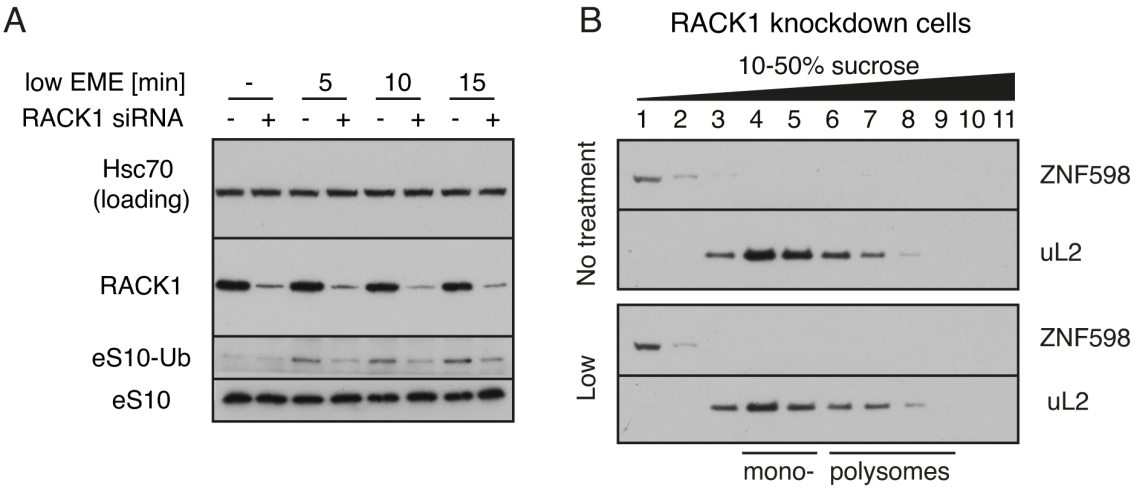

Figure 5.7 RACK1-depleted cells show impaired eS10 ubiquitination. (A) Cells treated with siRNA targeting RACK1 for five days or non-treated cells were subjected to a low dose of emetine for 5-15 min and analysed by immunoblotting for indicated proteins. Note that ubiquitinated eS10 was detected with a higher concentration of primary antibody. **(B)** Cells treated with RACK1 siRNA as in (A) were treated with nothing (upper panel) or with a low dose of emetine (lower panel) for 15 min. The cytosol was isolated and separated on a sucrose gradient. Each fraction was analysed by immunoblotting for ZNF598 and uL2. Positions of mono- and poly-ribosomes are indicated.

When compared with wild type cells, RACK1-depleted cells showed drastically reduced levels of eS10 ubiquitination at every time point analysed (Figure 5.7A). Also, low dose emetine treatment did not induce recruitment of ZNF598 to the ribosomes (Figure 5.7B).

This is in contrast to the situation observed in wild type cells, where the total pool of cellular ZNF598 migrated in high molecular-weight ribosomal fractions when a similar treatment was applied (Figure 5.3B). Our combined *in vitro* and *in vivo* analyses strongly suggest that RACK1 plays a role in a formation and/or stabilisation of the di-ribosome species recognized by ZNF598. In its absence, there is an inability to induce terminal stalling and initiate the RQC pathway.

5.5 Induction of quality control during excessively slow translation is context dependent

A stalled ribosome is not the cue for the initiation of quality control. Rather, it is the consequence of the stall that matters. A major implication of this statement is that the threshold for the induction of quality control should be dependent on translation dynamics. Hence, highly translated mRNAs, which are characterized by shorter average inter-ribosomal distance, will have a relatively low tolerance for ribosomal slowdown. That is because even a minor pause will result in ribosome collision and recognition by ZNF598. In contrast, messages that are translated infrequently should allow for increased readthrough if the same pausing signal is considered. Therefore, it should be possible to increase readthrough of the transient stall by reducing the frequency of translation initiation.

To directly test this model, we employed our dual-fluorescence reporter containing the stall-inducing $(K^{AAA})_{21}$ sequence (described in Chapter 2). As described previously, under normal conditions, translation through this reporter results in a low RFP:GFP ratio due to ribosome stalling and quality control engagement on the poly(A), which precludes synthesis of the downstream RFP. When we partially inhibited translation initiation using a sub-inhibitory dose of pactamycin, we observed an increased RFP:GFP ratio (Figure 5.8A). This was due to increased readthrough of the poly(A), as inferred from the selective increase of the RFP expression without any change to GFP. Importantly, this effect was eliminated in ZNF598-depleted cells (Figure 5.8B), and no appreciable change in RFP:GFP ratio was observed for a reporter lacking the poly(A) stall (Figure 5.8C).

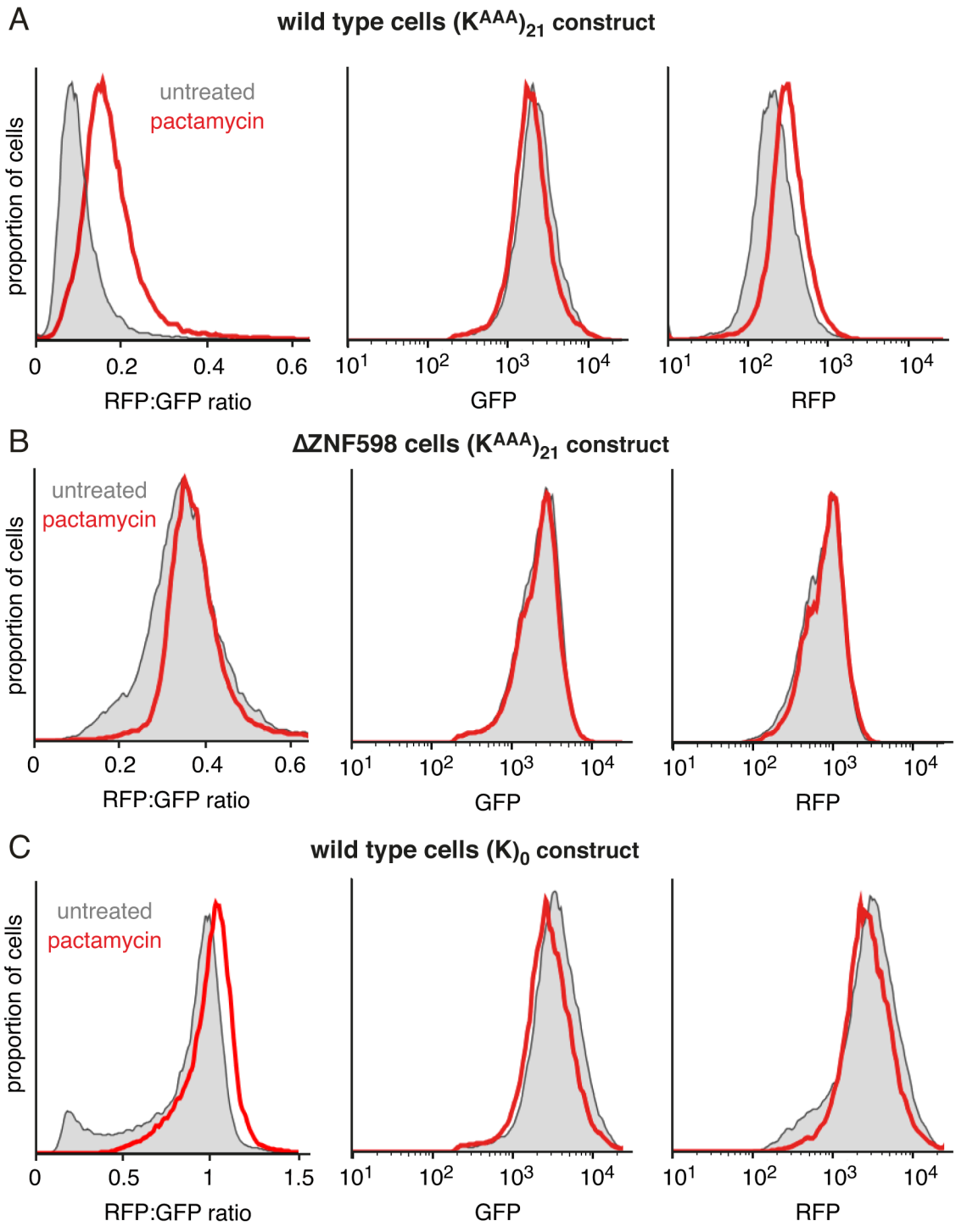

Figure 5.8 Partial inhibition of translation initiation results in increased readthrough of the poly(A). Indicated dual-fluorescence reporters were induced for 22h in the presence of DMSO vehicle (grey) or 10 nM pactamycin (red) and analysed by FACS. Histograms representing RFP:GFP ratio (left), GFP (middle) and RFP (right) are plotted. Panel **(A)** corresponds to wild type cells expressing the $(K^{AAA})_{21}$ stalling reporter; **(B)** ZNF598-deficient cells expressing the $(K^{AAA})_{21}$ stalling reporter; **(C)** wild type cells expressing the $(K)_0$ control reporter.

When we titrated different amounts of pactamycin, we saw a dose-dependent increase in readthrough of poly(A), as judged by increased RFP:GFP ratio (Figure 5.9A). In contrast, the same concentrations of pactamycin had minimal effect on our control non-stalling reporter (Figure 5.9B). Thus, the efficiency of ZNF598-mediated quality control induction during poly(A) translation is influenced by the frequency of translation initiation. This is fully consistent with the predicted function of ZNF598 in a collision-sensing model.

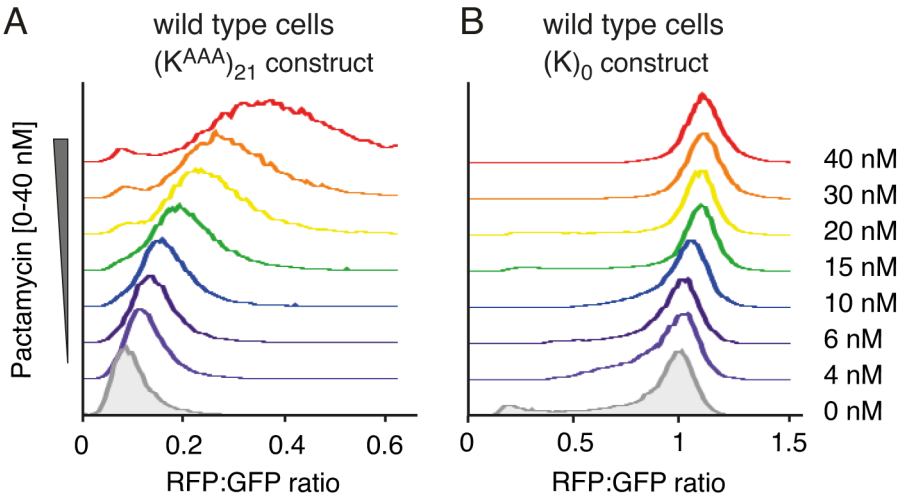

Figure 5.9 Pactamycin increases readthrough of the poly(A) in a dose dependent manner. Wild type cells induced for the expression of **(A)** $(K^{AAA})_{21}$ stalling or **(B)** $(K)_0$ control reporter for 22h in the presence of DMSO vehicle (shaded gray) or different concentrations of pactamcyin (colored traces) were analysed by FACS. Staggered histograms representing RFP:GFP ratios are plotted.

5.6 Discussion

Our *in vivo* analyses fully support the model presented in Chapter 4, which proposes that ZNF598 detects excessively slow translation by identifying ribosome collisions. We have confirmed that nuclease-resistant, di- (as well as poly-) ribosome complexes exist in cells and are enriched under conditions which induce ribosome collisions. We were also able to verify that the most proximal factor responsible for recognition of such events is ZNF598. Moreover, we have shown that ZNF598 is a universal sensor of ribosome collisions induced by different types of stalls. This is in accordance with speculations made regarding the analysis of flexibility and tolerance of the di-ribosome species, which was based on our structural data.

As excessively slow translation is detected indirectly through collisions, our model has profound physiological implications. Most importantly, the collision of ribosomes is an event that integrates not only the strength (or length) of the initial pause, but also the distances between translating ribosomes as well as their relative velocities. A simple modelling exercise can better illustrate this interdependence. Based on the structure of the collided di-ribosome, the distance between two P-sites can be estimated at ~10 codons. The average distance between P-sites of translating ribosomes in mammalian cells is ~66 codons as estimated from ribosome profiling experiments (Ingolia et al., 2011). Assuming the average elongation speed to be ~5.6 codons/s (Ingolia et al., 2011), a trailing ribosome will arrive at the position of the preceding ribosome in 11.6 s. Ribosome collision will only occur if the leading ribosome elongated less than 11 codons in this time. Thus, aberrant translation would be recognized whenever a ribosome cannot elongate at least 11 codons before the trailing ribosome closes the inter-ribosomal distance (Figure 5.10A). More exactly, excessively slow translation can be defined as every 10-codon distance where average elongation speed is ~5-6 times slower than normal, so less than 1 codon/s. The two main parameters determining collisions: the frequency of initiation (which dictates relative inter-ribosomal distances) and speed of translation, are influenced by many intrinsic and extrinsic factors. Things that can have direct differential impact on translation include mRNA properties, different physiological states of the cell or even the stage of differentiation. Moreover, environmental stress can induce various responses, which often modulate translation levels. Hence, the threshold for the induction of quality control during translation can vary for different mRNAs and be further affected by cellular conditions. As an example, mRNA translated infrequently will have a much higher tolerance for transient pausing, which should additionally facilitate efficient synthesis of encoded protein. In contrast, extremely highly translated mRNAs would have very low tolerance for slowdown (Figure 5.10B). This is important, because even relatively few copies of such an aberrant mRNA could potentially generate truncated, toxic nascent polypeptides at a high rate. Preventing this risk is probably more beneficial to the cell than occasional premature engagement with quality control machinery.

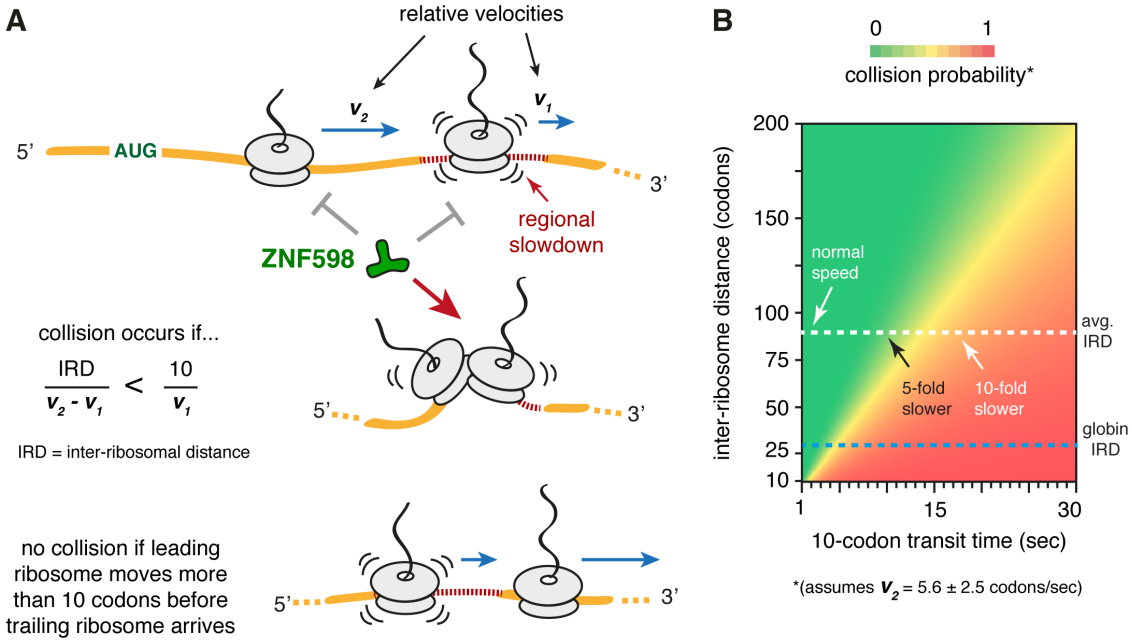

Figure 5.10 Model for ZNF598-mediated sensing of excessively slow translation. (A) Under normal conditions, ZNF598 does not associate with either translating ribosomes, or ribosomes slowing down at stall-inducing sequences (regional slowdown). However, under conditions when relative velocities of leading and trailing ribosomes allow the trailing ribosome to cover the inter-ribosomal distance (IRD) before the leading ribosome moves 10 codons forward, there will be a collision event sufficient to recruit ZNF598. **(B)** Heatmap illustrating probability of ribosomal collision. Slowdown (x axis; represented as a transit time through 10 codons in seconds) is plotted as a function of the inter-ribosomal distance (y axis; represented as codons). The average velocity of the ribosome is calculated as roughly 5.6 ± 2.5 codons/sec. At an average IRD of 66 codons, collisions will only start to occur if the leading ribosome slows down roughly 5-fold over a 10-codon distance. However, for highly translated mRNAs characterized by short IRD, such as globin mRNA, a two-fold slowdown in lead ribosome speed is sufficient to result in collisions. Model, analysis, and heatmap were generated with help from Manu Hegde.

An interesting physiological adaptation is exemplified in reticulocytes, which we used as our initial source of collided ribosomes. Reticulocytes translate globin mRNA at an extremely high rate. We observed that the globin ORF, which contains 140 codons, is on average occupied by 4-6 ribosomes (Chapter 4, Figure 4.7A). This results in an average inter-ribosomal distance of 20-40 codons, which is markedly lower than the average 60-codon distance in normal cells (Ingolia et al., 2011). This means that even relatively minor slowdown during globin synthesis should result in collision events. To facilitate production of haemoglobin at such a high level (almost 200 g/l of cytoplasm), reticulocytes sacrificed quality control fidelity by almost entirely eliminating ZNF598 (see Chapter 4, Figure 4.1). Therefore, native polysomes in rabbit reticulocyte lysate contain naturally occurring collided di-ribosomes. This feature, in hindsight, explains

why nuclease-digested ribosomes from RRL system allowed us to initially identify ZNF598 targets (see Chapter 3, Figures 3.1, 3.2).

5.7 Materials and methods

Constructs, antibodies & siRNAs

Most anitbodies and siRNAs were described in previous chapters. Additionally, the antibody against EDF1 was from Bethyl Laboratories #A304-039A. To generate a CRISPR-Cas9 mediated knockout of EDF1, guide RNA targeting exon 2 of EDF1 (5'-ATCTTAGCGGCACAGAGACG-3') was designed using the CRISPR design tool at crispr.mit.edu and cloned into the px459 plasmid (Ran et al., 2013).

Cell cultures

All cell lines as well as culture conditions were described in Chapter 2. Additionally, treatments with pactamycin were for 22 h (performed at the same time as induction of the reporter expression with doxycycline) at between 4 to 40 nM as indicated in the figure legends. Treatment with elongation inhibitors was for 15 minutes at the following concentrations: emetine low dose at 1.8 μM or high dose at 360 μM; anisomycin low dose at 0.19 μM or high dose at 76 μM; Didemnin B low dose at 0.5 μM or high dose at 100 μM.

Flow cytometry analysis & western blotting

Analysis by flow cytometry and western blotting were as described in Chapter 2. For the detection of ubiquitinated eS10, membranes were cut and the fragment containing ubiquitinated eS10 was incubated with higher concentration of anti-eS10 primary antibody (1:250) followed by incubation with secondary antibody at 1:1,000.

Analysis of ribosome profiles in cells

To analyse nuclease-resistant polysome in cells, one 10 cm dish of cells at around 80% confluency was treated with DMSO (control), low (1.8 μM), or high (360 μM) dose of emetine for 15 min. For the analysis of the recovery after 15 min of emetine treatment, treated cells were washed twice with emetine-free media and either harvested immediately (control) or incubated for 1h in the 37°C incubator and transferred to ice. Harvested cells were washed twice with ice-cold PBS and spun for 5 min at 1,200 rpm

in a tabletop centrifuge. Lysis was performed on ice for 15 min in 300 µl of lysis buffer containing 20 mM HEPES pH 7.4, 100 mM K(OAc), 5 mM $Mg(OAc)_2$, 0.5% Triton X-100, 1 mM DTT and protease inhibitor cocktail (EDTA-free) (Roche). After lysis, lysates were clarified by centrifugation at 15,000g for 15 min at 4°C in a tabletop microcentrifuge. The total concentration of RNA in the lysate was quantified using the Qubit RNA HS Assay Kit (Thermo Fisher). For nuclease digestion, lysate containing 90 µg of RNA was adjusted to 1 mM $CaCl_2$ and 0.5 U of S7 nuclease per µg of RNA in a total reaction volume of 300 µl. Digestion was for 40 min at 25°C. Reactions were terminated by addition of 1.2 µl of 500 mM EGTA. Samples were then layered onto 12 ml of continuous 10%-50% sucrose gradients and separated by centrifugation at 40,000 rpm for 2h at 4°C in an SW40 rotor (Beckman). Fractionation was performed using a piston gradient fractionator system (Biocomp), which continuously monitored UV absorbance at 254 nm across the gradient.

Analysis of ZNF598 interaction with ribosomes in cells

For each condition, two 10 cm plates of cells at around 80% confluency were used. After pre-treatment with a low or high dose of emetine (or just DMSO as a vehicle control), cells were washed with ice-cold PBS and harvested by scraping. After sedimentation at 4°C at 1200 rpm for 5 min, cell pellets were resuspended in 200 µl of RNC buffer (50 mM HEPES, 100 mM K(OAc), 5 mM $Mg(OAc)_2$) containing 40 U/ml of RNAsin (Promega), 0.01% digitonin, 1x protease inhibitor cocktail (EDTA-free cOmplete from ROCHE) and 1 mM DTT. After 15 min incubation on ice, cells were disrupted using a pre-chilled 26G needle appended to a 1 ml syringe. Lysates were clarified by 15 min of centrifugation at 15,000g at 4°C in a tabletop centrifuge. Concentrations of the lysates were adjusted to 150 µg in 20 µl volume, loaded on 10-50% analytical (200 µl) sucrose gradients and spun for 20 min at 55,000 rpm in TLS-55 rotor at 4°C using slowest acceleration and deceleration settings. After fractionation into 11 fractions, samples were analyzed by immunoblotting as described in previous chapters.

Quantitative mass spectrometry of purified polysomes

HEK 293 cells were grown on 10 cm plates. One 10 cm plate was used for each experimental condition, which was performed in duplicate. 90% confluent cells were treated for 15 min with a low dose of emetine (1.8 uM), a high dose of emetine (360 uM)

or with DMSO (control). Prior to harvesting, cells were washed with ice cold PBS twice. Lysis was in 200 ul of digitonin buffer (50 mM HEPES pH 7.6, 100 mM K(OAc), 5 mM $Mg(OAc)_2$, 0.01% purified digitonin, 40 U/ml RNAsin, 1x protease inhibitor cocktail, 1 mM DTT) for 20 min on ice. Cells were ruptured by passing through a 26G needle using a 1 ml syringe (20 passes). Lysates were sedimented by centrifugation for 15 min at 15,000 g at 4°C using a tabletop centrifuge. The resulting supernatant was loaded onto a 10-50% sucrose gradient (2 ml gradient volume) in 1xRNC buffer. Centrifugation was for 1h at 55,000 rpm in the TLS 55 rotor (Beckman) at 4°C using the slowest acceleration and deceleration settings. After the spin, 11 fractions were manually collected from the top of the gradient. Fractions 8-11 were pooled together (previously verified to represent polysomal fractions), diluted with an equal volume of 1xRNC buffer (800 µl) and centrifuged for 1h at 100,000 rpm in the TLA100.3 rotor at 4°C. The polysome pellet was washed once with 200 µl of 1xRNC and resuspended in 20-50 µl of 1xRNC buffer. The concentrations were normalized using absorbance at 260 nm and subjected to quantitative mass spectrometry using Tandem Mass Tagging (TMT) (Thompson et al., 2003).

Chapter 6: Understanding the role of Activating signal cointegrator 1 complex (ASCC) in the RQC

ZNF598 is the most proximal and direct sensor of excessively slow translation as it recognizes ribosome collision events. As an E3 ubiquitin ligase, it marks collided di-ribosomes with ubiquitin in order to induce the downstream events of the RQC pathway. However, the exact role of ZNF598-mediated ubiquitination and how this culminates in splitting of the ribosomal subunits and degradation of truncated nascent polypeptides remain uncharacterized.

The structure of the collided di-ribosome revealed a closed conformation in which inter-ribosomal mRNA is fully shielded and where engagement of translational complexes, including rescue factors Pelota-Hbs1 is not permitted on the trailing ribosome. It also clearly shows that ZNF598-targeted proteins on the trailing ribosome are all positioned at the inter-ribosomal interface, where we speculate ubiquitination occurs. Therefore, it is unlikely that ubiquitin at the interface would directly promote recruitment of the rescue factors to the trailing ribosome, as they cannot be accommodated. Rather, it is reasonable to assume that collided di-ribosome requires additional remodelling before final splitting can occur. Indeed, recent studies in yeast have provided genetic and biochemical data supporting a role for the Ski2-like helicase 1 [Slh1; in mammals Activating signal cointegrator complex 1 subunit 3 (ASCC3)] and its associated components in the early events of RQC (Matsuo et al., 2017; Sitron et al., 2017).

In this chapter, we provide an initial characterization of the mammalian ASCC3 helicase by showing that it is an RQC component which acts downstream of ZNF598. Firstly, we show that ASCC3 binds to the ribosomes as a part of a stable multi-protein complex. Using genetic epistasis analysis, we provide evidence that it acts downstream of ZNF598. Curiously, however, we find that ASCC3, unlike ZNF598, is not enriched in fractions containing collided ribosomes. Moreover, we find that its interaction with ribosomes does not depend on ZNF598. Hence, we speculate that the ASCC3 helicase might continuously sample translating ribosomes but be activated only upon ZNF598-mediated ubiquitination. Afterwards, its ATP-ase activity may be conducive to its

function as an active remodeller of collided di-ribosome species, allowing their downstream processing by splitting factors as well as mRNA surveillance machinery. Our initial characterization of ASCC3 should provide a framework for future biochemical and structural efforts towards understanding its molecular function within the RQC.

6.1 ASCC3 binds to cytosolic ribosomes as a part of a stable, multi-protein complex

As we were working on ZNF598, the Brandman laboratory revisited their original screen looking for factors involved in translational arrest on polybasic sequences (Brandman et al., 2012), and reported the Ski2-like helicase 1 (Slh1) as another putative factor involved at an early stage of the RQC (Sitron et al., 2017). They showed that Slh1 deletion resulted in failure to induce the RQC during translation through stall-inducing CGA codons, a similar phenotype to Asc1 or Hel2 deletion. Additional genetic epistasis experiments allowed the authors to conclude that Slh1 acts upstream of RQC complex assembly, most likely at one of the early steps of translational arrest. Finally, immunoprecipitation experiments with endogenously tagged Slh1 and Hel2 revealed that two other factors, Cue3 and uncharacterized Ykr023w, were highly enriched with the co-purified ribosomes. Deletion of each of these two factors also showed a partial defect in RQC induction when assessing translation through the polybasic reporter.

Around the same time, an independent study from the Inada laboratory found Slh1, Cue3 and Ykr023w as the most highly enriched proteins purified with Hel2-bound ribosomal complexes (Matsuo et al., 2017). This study also demonstrated that depletion of ASCC3, a putative mammalian homolog of Slh1, permits higher readthrough of poly(A) stall-inducing sequences in human cells. Based on these two reports, we reasoned that ASCC3 might act downstream of ZNF598. With its ATP-ase activity we further speculated that it is capable of providing the necessary force to remodel collided di-ribosomes, thereby facilitating efficient splitting of ribosomal subunits.

ASCC3 was first identified as part of a novel complex containing known Activating Signal Cointegrator 1 (ASC-1, also known as TRIP4) along with two other previously uncharacterized proteins, ASCC2 and ASCC1 (Jung et al., 2002). The complex isolated from the nuclei of HeLa cells was very stable, surviving multiple steps

of purification using standard chromatography techniques. Another, later report also suggested nuclear localization of ASCC3 and its function as a DNA helicase involved in the ALKBH3-dependent DNA alkylation damage pathway (Dango et al., 2011). Although previously ASCC3 was primarily analysed in the context of its nuclear function, study from Inada laboratory showed that it can also exist in the cytosol, justifying its proposed function within RQC (Matsuo et al., 2017).

ASCC3 was previously reported to be a human homolog of Slh1 (Matsuo et al., 2017), however the human homologs of Cue3 and Ykr023w are not identified to date. Given the high stability of the ASCC, we considered the possibility that other subunits of the complex might be functional homologs of Cue3 and Ykr023w. Hence, we analysed domain composition of other components of the ASCC and found that ASCC2, similarly to yeast Cue3, also contains the ubiquitin-binding coupling of ubiquitin to ER degradation (CUE) domain (Figure 6.1A), suggesting that the two proteins may be evolutionarily related. Moreover, when we looked for the human homolog of Ykr023w using Ensembl BioMart tool, we found TRIP4/ASC-1 as the closest orthologue with ~17% identity to its yeast counterpart (Flicek et al., 2014). Hence, we suspected that evolutionarily related human ASCC may perform a similar function to yeast Slh1/Cue2/Ykr023w.

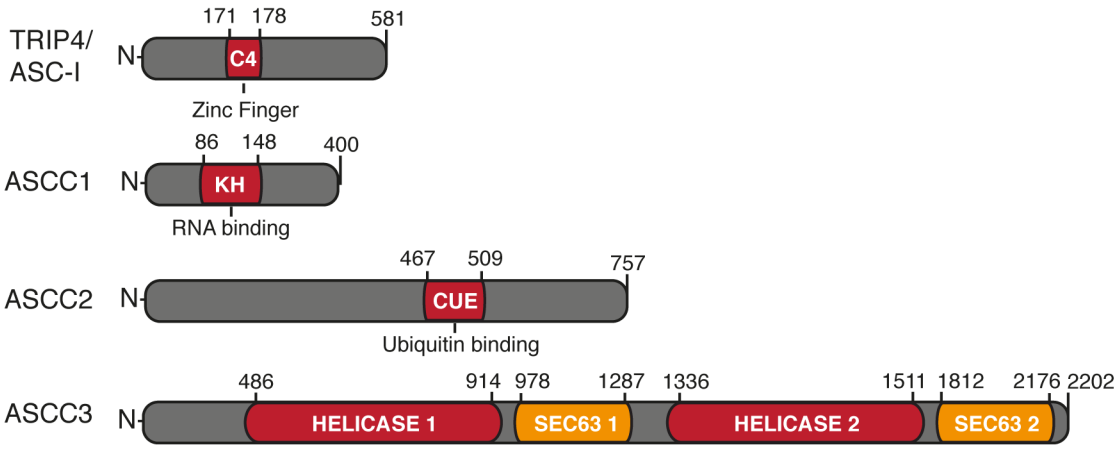

Figure 6.1 Domain architecture of all four subunits of ASCC. Domain prediction is based on the Uniprot database. Note that ASCC2 is distantly related to yeast Cue3 and similarly contains CUE ubiquitin binding domain.

To understand the potential effects of ASCC depletion on translation and possibly the RQC, we first asked if it can directly interact with cytosolic ribosomes. To this end,

we isolated the cytosol from HEK 293 cells and separated it on a 10-50% sucrose gradient (Figure 6.1B). Immunoblotting against ASCC3, ASCC2 and TRIP4/ASC-1 showed co-purification of all three with ribosomal proteins. The individual migration profiles of each subunit were very similar. Hence, we suspected that they interact with ribosomes as a part of the same multi-protein complex, which was previously observed in the nucleus (Jung et al., 2002).

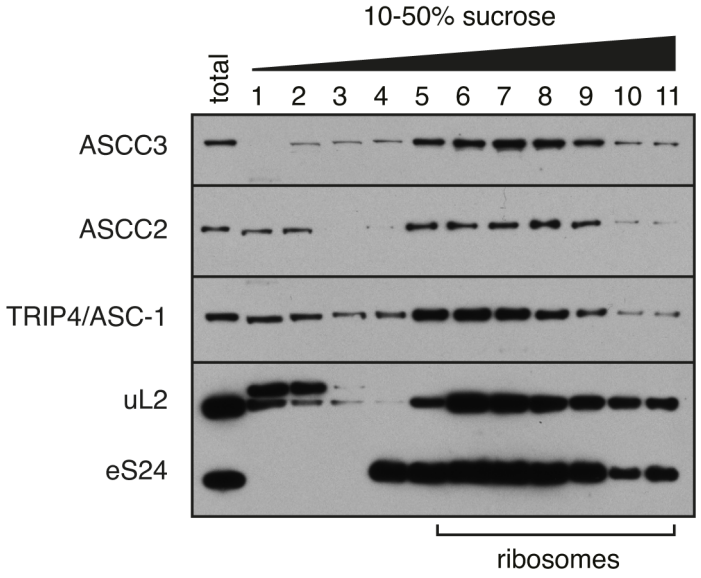

Figure 6.2 ASCC co-fractionates with cytosolic ribosomes. The cytosolic fraction was isolated from HEK 293 cells and separated on a 10-50% sucrose gradient. Each fraction was analysed by immunoblotting for components of the ASCC, 60S-ribosomal protein uL2 and 40S ribosomal protein eS24.

6.2 ASCC3 is the main active component of ASCC involved in the early steps of RQC

Having established a direct interaction of the ASCC with ribosomes, we decided to characterize it in more detail using siRNA-mediated knockdown of individual subunits of the complex. We found that depletion of ASCC3 resulted in destabilization of all other subunits (Figure 6.2A). ASCC2 knockdown additionally destabilized ASCC1, but not TRIP4/ASC-1 or ASCC3. Finally, knockdown of ASCC1 or TRIP4/ASC-1 did not have any effect on other subunits of the complex. From this, we concluded that ASCC3 constitutes the central structural component of the complex, which directly interacts with ASCC2 and TRIP4/ASC-1. Interaction of ASCC1 with the rest of the complex is mediated by either ASCC2 alone or in combination with ASCC3 via a shared interface.

Nevertheless, the overall stability of the complex appears to be highly dependent on a set of inter-subunit interactions.

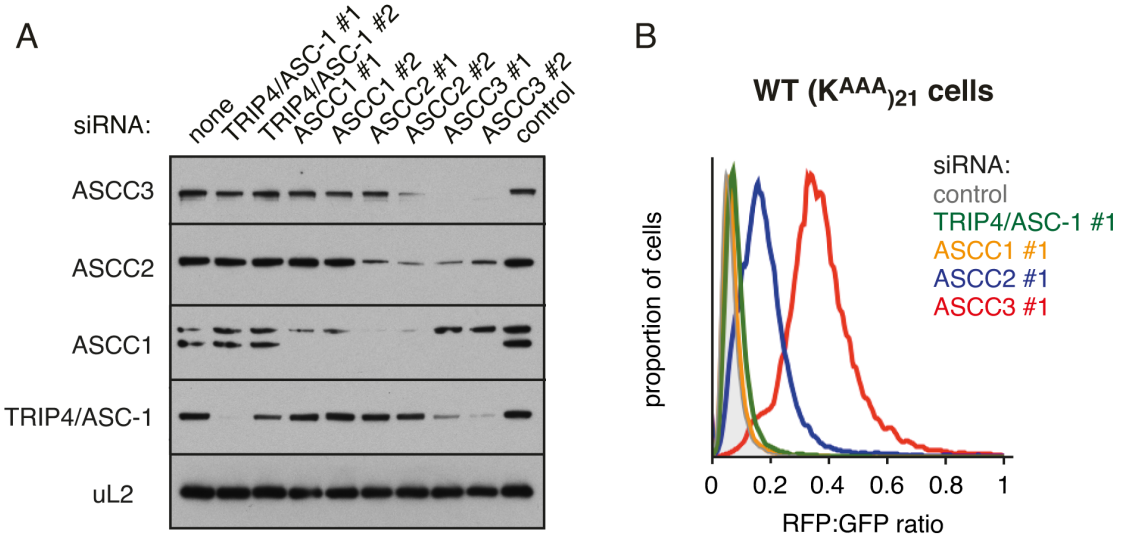

Figure 6.3 Structural and functional analysis of the ASCC using siRNA-mediated gene silencing. (A) HEK 293 cells were treated with siRNAs targeting all components of the ASCC (two different siRNA, #1 and #2, were used per each gene) for three days. Whole cell lysates were then collected and analysed by immunoblotting with antibodies against ASCC components. **(B)** $(K^{AAA})_{21}$ reporter cells were treated as in (A) but induced with doxycycline for 24h and analysed by flow cytometry. The RFP:GFP ratio was then plotted.

Using the same siRNA-mediated knockdown strategy, we set out to probe the function of ASCC components in the context of ribosomal stalling on poly(A) sequences. We utilized our previously described stable cell line expressing the inducible $(K^{AAA})_{21}$ stalling reporter (see Chapter 2). Depletion of ASCC3 resulted in an increased ratio of RFP:GFP, indicative of increased readthrough of the poly(A) sequence (Figure 6.3B). This was generally consistent with the previous observations from the Inada group (Matsuo et al., 2017). Knockdown of ASCC2 showed a minor increase in the RFP:GFP ratio, similar to the phenotype observed upon deletion of yeast Cue3, which resulted in partial increase in readthrough of the mRNA encoding stretch of polybasic amino acids (Matsuo et al., 2017). Curiously, we did not detect any change in the RFP:GFP ratio when we depleted the Ykr023w homolog TRIP4/ASC-1 or ASCC1. We confirmed that knockdown efficiency was greater than 95% (Figure 6.3A). To confirm the siRNA knockdown results, we used CRISPR-Cas9 to disrupt ASCC3 gene in our previously described stable cell line expressing the $(K^{AAA})_{21}$ stalling reporter (Ran et al., 2013). We generated two ΔASCC3 clones, both of which showed decreased levels of ASCC2,

ASCC1 and TRIP4/ASC-1 (Figure 6.4A) consistent with siRNA data (Figure 6.3A). Flow cytometry analysis after induction of the double-fluorescence reporter in one of the ΔASCC3 clones showed increased RFP:GFP ratio. This ratio was driven by a combined increase in RFP expression and decrease in GFP expression (Figure 6.4B). This effect was almost completely reversed when a recombinant, 3xFLAG-tagged version of ASCC3 was re-introduced in the same cells, showing that the phenotype is specific to ASCC3 depletion.

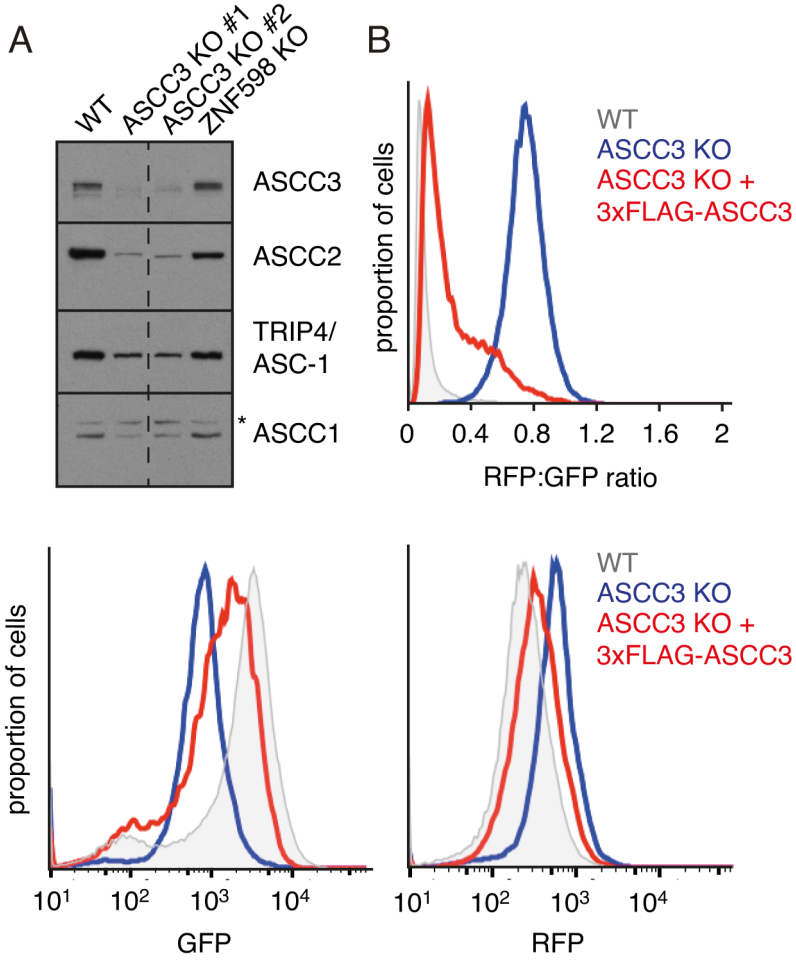

Figure 6.4 ASCC3 is the main component of the ASCC involved in RQC. (A) Total cell lysates from two separate ASCC3 knockout clones (ASCC3 KO #1 and #2) were analysed alongside WT and ZNF598 KO cell lysates by immunoblotting against indicated subunits of the ASCC. Asterisk represents a non-specific band detected by the ASCC1 antibody. Note that middle lanes from the western blot were removed for clarity, whereas remaining parts of the strips were spliced as indicated by the dashed line. **(B)** ASCC3 KO cells with the $(K^{AAA})_{21}$ reporter were transfected with either 3xFLAG-ASCC3 together with BFP (red traces) or just BFP (blue) 24h prior to induction with doxycycline for another 24h. WT $(K^{AAA})_{21}$ cells transfected with BFP only were analysed in the same way as a control. Around 20,000 BFP-positive events were analysed in each condition.

6.3 ASCC3 acts downstream of the ZNF598 E3 ligase

The readthrough phenotype observed upon ASCC3 depletion differed from those previously observed in ΔRACK1 or ΔZNF598 cells. This was because we saw not only increased expression of RFP downstream of the stall-inducing poly(A) but also markedly reduced GFP expression upstream of the poly(A) (Figure 6.4B). This observation was unexpected, and we wondered whether it reflected a more general function of ASCC3. Alternatively, it could be specific only to stall-inducing messages. To address this, we depleted ASCC3 in the cell line expressing the $(K)_0$ control reporter. We found that ASCC3 knockdown had no effect on either GFP or RFP, arguing for a specific role of ASCC3 during translational stalling (Figure 6.5A).

In yeast, the Hel2 deletion is dominant to an Slh1 deletion (Sitron et al., 2017), suggesting that Slh1 likely acts downstream of Hel2. If the same holds in the mammalian system, we should observe a dominant effect of ZNF598 depletion over ASCC3 knockdown. To test this, we simultaneously depleted both ASCC3 and ZNF598 in cells expressing the $(K^{AAA})_{21}$ reporter using combined siRNA treatment. Flow cytometry analysis revealed that decreased GFP expression upon single depletion of ASCC3 was completely abolished when ASCC3 was depleted in conjunction with ZNF598 (Figure 6.5B). Of note, increased RFP expression was due to the dominant effect of the ZNF598 deletion. This phenotype was firmly established and characterised in Chapter 2. Similar to double knockdown in WT cells, deletion of ASCC3 in ΔZNF598 cells did not have an appreciable effect on the expression of the $(K^{AAA})_{21}$ reporter (Figure 6.5C). These observations support the following claims: 1) ASCC3 acts downstream of ZNF598 and 2) the stall-specific decrease in GFP expression observed upon ASCC3 deletion relies on ZNF598 function. The basis for the decreased GFP expression upon ASCC3 depletion is currently unclear. However, we can rule out the most trivial explanations. We checked that general rate of translation is not lower in cells lacking ASCC3, as GFP expression from the $(K)_0$ control reporter is not affected (Figure 6.5A). We can also rule out decreased levels of mRNA containing stall-inducing signal, as qPCR results showed no difference between WT and ASCC3-depleted cells (data not shown).

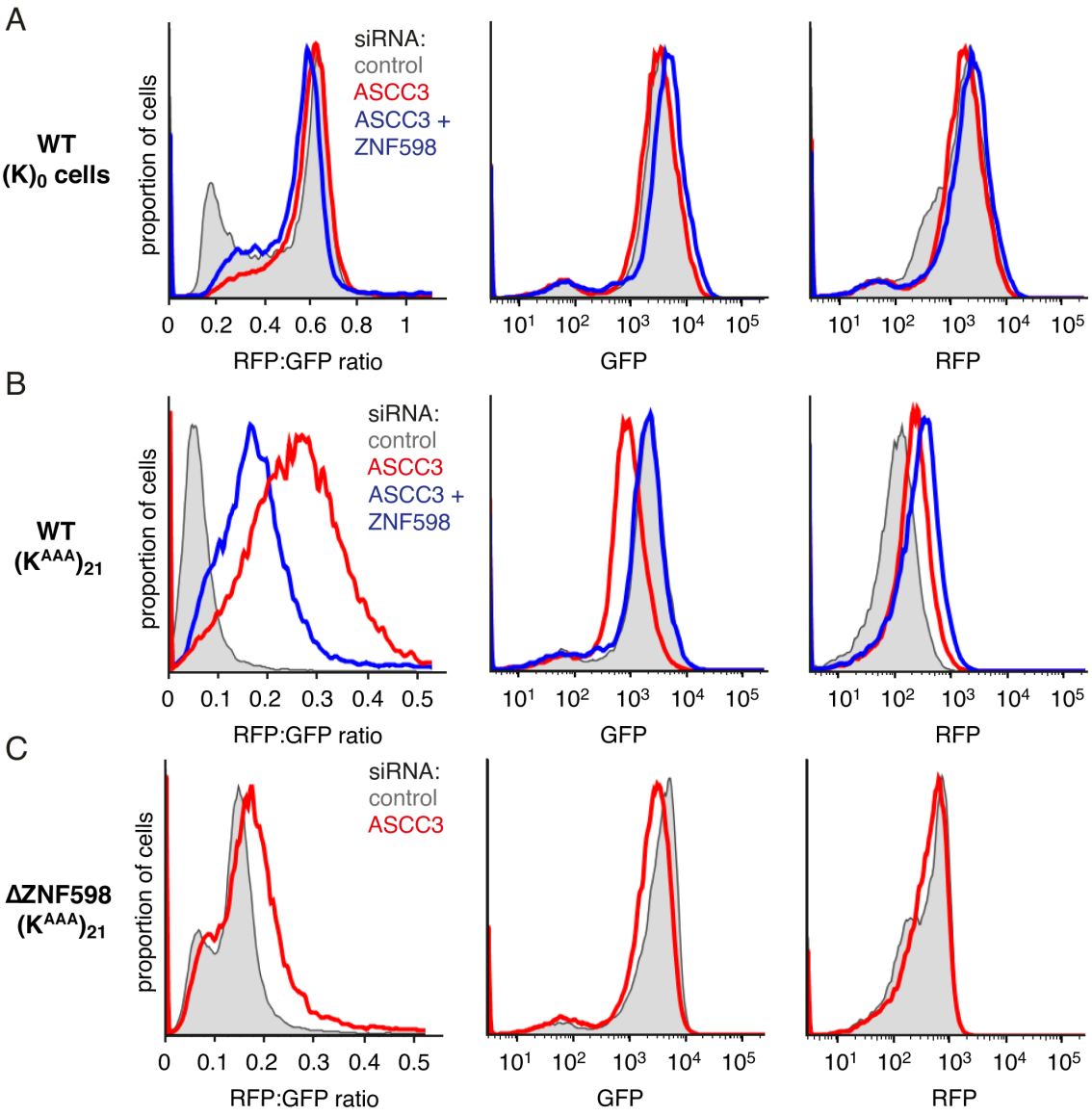

Figure 6.5 ZNF598 acts upstream of ASCC3. (A) WT cells with the $(K)_0$ control reporter **(B)** $(K^{AAA})_{21}$ reporter, **(C)** or ZNF598 KO cells bearing $(K^{AAA})_{21}$ reporter were treated with indicated siRNA for three days. Expression of the respective reporter was induced for another 24h and cells were analysed by flow cytometry. For each condition around 20,000 events were analysed.

6.4 ASCC interaction with ribosomes does not rely on ZNF598

Having established that the function of ASCC3 is dependent on ZNF598 activity, we wondered whether ZNF598 facilitates ASCC recruitment to the ribosomes. To analyse ASCC interaction with ribosomes in the absence of ZNF598, we took advantage of our ΔZNF598 cells. We isolated cytosolic fractions from actively growing WT and ΔZNF598 cells, separated them on 10-50% sucrose gradients and immunoblotted to look for

ASCC3 and ASCC2. When we compared migration profiles of both ASCC3 and ASCC2, we could not detect any appreciable differences between WT and ΔZNF598 cells.

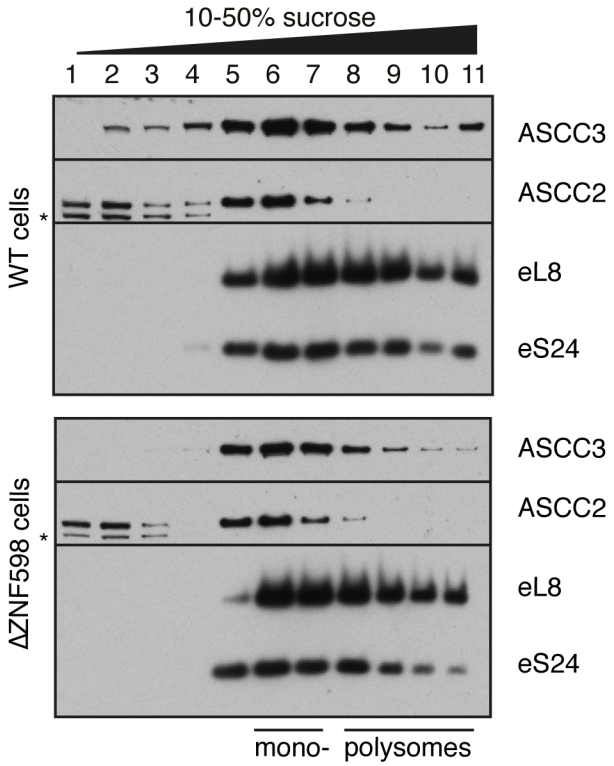

Figure 6.6 ZNF598 depletion does not affect ASCC interaction with ribosomes. Cytosolic fractions from WT (top) or ΔZNF598 (bottom) cells were separated on 10-50% sucrose gradients and each fraction was analysed by immunoblotting against indicated proteins. Positions of mono- and polysomes are indicated below. Asterisk indicates non-specific band detected with anti-ASCC2 antibody.

To analyse ASCC interaction with ribosomes in the context of ribosomal stalling, we used the eRF1^{AAQ} mutant (see Chapter 4 for detailed explanation). We generated translation-competent cytosolic fractions from HEK 293 cells, performed *in vitro* translation in the presence or absence of eRF1^{AAQ}, and analysed reaction mixtures on a sucrose gradient. As in the RRL system, addition of eRF1^{AAQ} resulted in site-specific stalling of ribosomes at the stop codon. This can be inferred from the presence of a smeary autoradiographic signal in the high molecular weight parts of the gel, exclusively in the heaviest (8-10) fractions of the sucrose gradient (Figure 6.7A). This signal corresponded to the heterogenous population of tRNA-associated nascent chains attached to the poly-ribosomes stalled at the stop codon. As expected, endogenous ZNF598 co-migrated in the fractions containing stalled ribosomes. Importantly, in the

control reaction without eRF1^{AAQ}, the entire pool of ZNF598 migrated at the top of the gradient and no interaction with ribosomes was observed (Figure 6.7A, bottom panel). In contrast, when we analysed distribution of ASCC components under the same experimental conditions, we did not observe any difference between the samples lacking or containing eRF1^{AAQ} (Figure 6.7B). This is generally consistent with our TMT mass spec analysis of emetine stalled complexes, which did not show ASCC3 enrichment in any conditions analysed (see Appendix 1). To conclude, our observations cumulatively suggest that ASCC continuously sample the ribosomes and gets selectively activated by ZNF598 only under conditions of ribosome collisions.

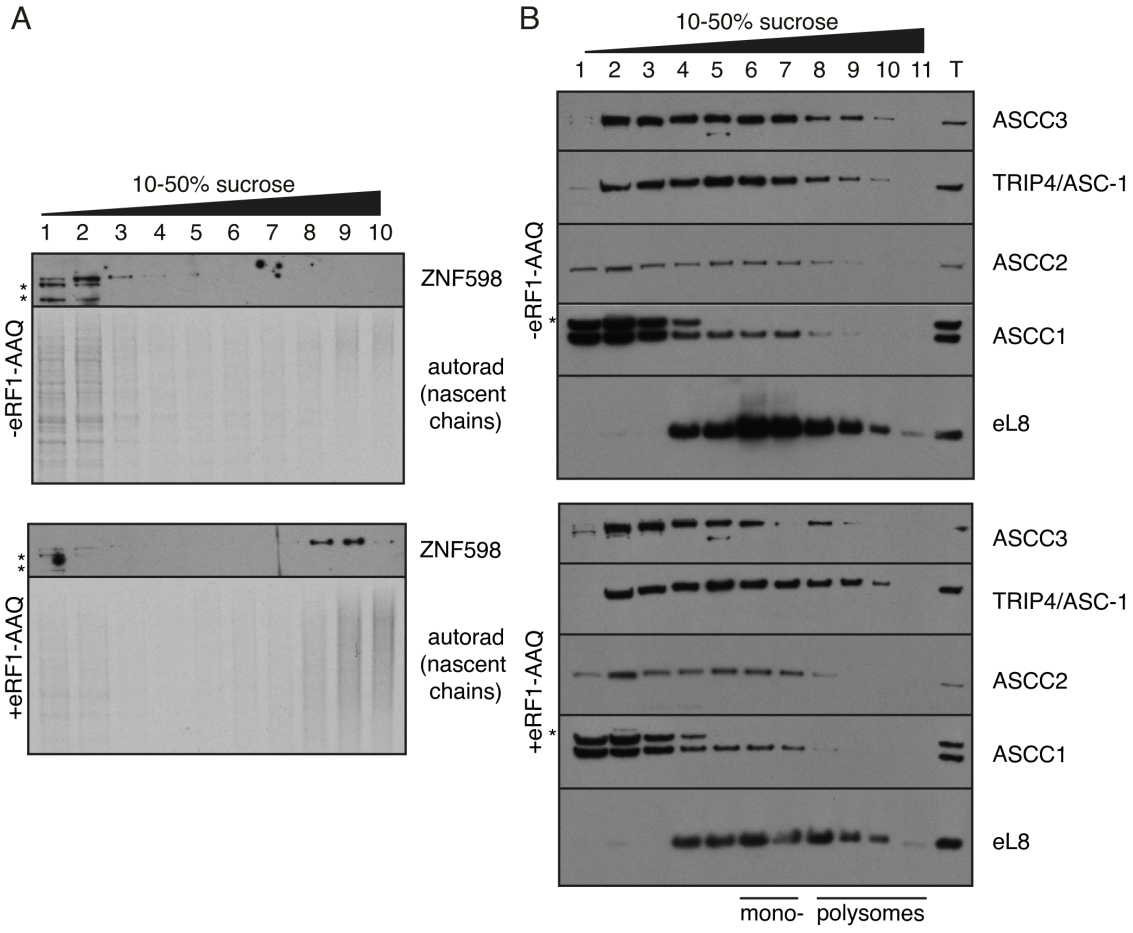

Figure 6.7 ASCC does not preferentially associate with collided di-ribosomes. *In vitro* translation reactions of endogenous mRNAs using translation-competent lysates from HEK 293 cells were performed in the absence (top panels) or presence (bottom panels) of eRF1^{AAQ} with **(A)** or without **(B)** addition of 35S-labelled methionine. Resulting reactions were fractioned on sucrose gradients. Each fraction from the gradient was analysed by autoradiography and/or immunoblotting against indicated proteins. Note the accumulation of tRNA-associated nascent polypeptides and ZNF598 in heavy molecular weight fractions (8-10) containing collided ribosomes due to addition of eRF1^{AAQ} [bottom panel (A)]. 'T' indicates total samples before fractionation, whereas asterisks indicate non-specific bands detected with some of the antibodies.

6.5 ASCC2 depletion affects interaction of ASCC3 with ribosomes

Apart from the ASCC3 helicase, ASCC2 also appears to be important for the functional activity of the ASCC complex within the RQC pathway. This is deduced from the fact that ASCC2 depletion resulted in partially increased readthrough of the poly(A) (Figure 6.3B), which cannot be attributed to decreased levels of ASCC3 (Figure 6.3A). ASCC2 contains the CUE ubiquitin binding domain, which led us to speculate that it may sense ribosome ubiquitination and activate the complex. To test this, we made an ASCC2 knockout cell line in the $(K^{AAA})_{21}$ reporter background using CRISPR-Cas9 mediated gene disruption (Figure 6.8A) (Ran et al., 2013). Consistent with the siRNA data (Figure 6.3B), ΔASCC2 cells showed minimally improved readthrough of the poly(A) stalling sequence (Figure 6.8C).

To test whether the CUE domain is indeed needed for the proper function of ASCC2, we designed a construct in which we mutated the key leucine residues responsible for ubiquitin binding (henceforth referred to as CUE-) (see materials and methods for details). We re-expressed either the WT or mutant ASCC2 at the same level in the ΔASCC2 background (Figure 6.8B) and analysed expression of the dual-fluorescence reporter using flow cytometry. Analysis of the RFP:GFP ratio showed that expression of either the WT or the CUE- mutant fully restored the stalling to levels observed in WT cells (Figure 6.8C). Hence, we concluded that ASCC2 CUE domain may not be involved in the function of the complex within the RQC pathway.

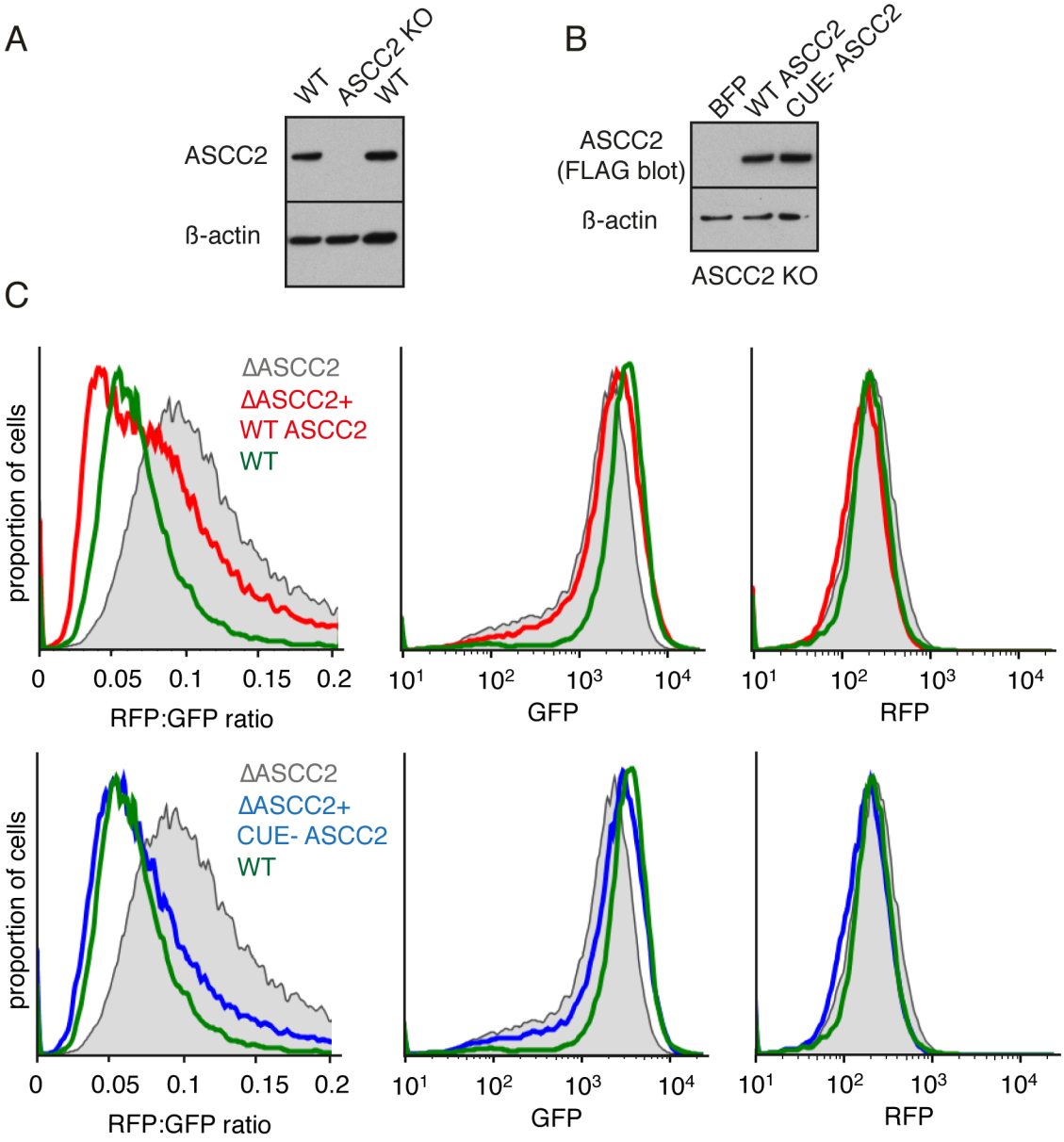

Figure 6.8 The CUE domain of ASCC2 is not required for its function within the RQC pathway. (A) Cell lysates from WT and ASCC2 KO cells were analysed by immunoblotting against ASCC2 and β-actin. **(B)** ΔASCC2 cells with the stably integrated $(K^{AAA})_{21}$ reporter were co-transfected with 3xFLAG-tagged WT or CUE- ASCC2 and BFP (or BFP only) and analysed by immunoblotting against ASCC2 (using the FLAG antibody) and actin. **(C)** The same cells as in (B) as well as WT $(K^{AAA})_{21}$ cells transfected with BFP (green traces) serving as a control were induced for expression of the reporter for 24h prior analysis by flow cytometry. 20,000 BFP positive cells were analysed for each sample. Histograms representing RFP:GFP ratio (left) GFP (middle) or RFP (right) are shown.

We therefore sought an alternative explanation for the observed functional phenotype. Even though ASCC2 deletion did not affect ASCC3 stability, we still considered the possibility that it may affect the ability of the complex to interact with ribosomes. Hence, we isolated the cytosolic fraction from ΔASCC2 cells and analysed it

on a sucrose gradient, alongside cytosol from WT cells. ASCC3 was markedly shifted towards the lighter fractions in ΔASCC2 cells (Figure 6.9). This result suggests that lack of ASCC2 partially destabilizes the interaction between the complex and ribosomes. Of note, we still detected a proportion of ASCC3 comigrating with ribosomes, which probably explains only a partial readthrough phenotype observed in the cells lacking ASCC2 (Figure 6.8C).

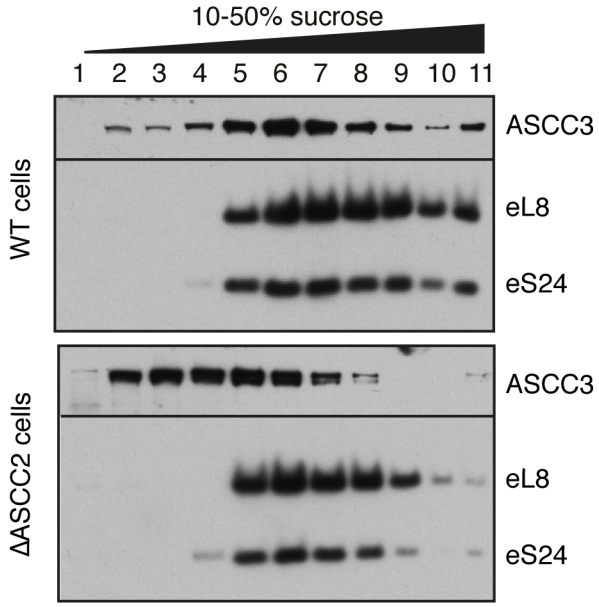

Figure 6.9 ASCC2 deletion destabilizes interaction of ASCC3 with ribosomes. Cytosolic fractions from WT (top) or ΔASCC2 (bottom) cells were separated on 10-50% sucrose gradients and each fraction was analysed by immunoblotting against indicated proteins.

6.6 Discussion

Using genetic analysis in cell cultures we have shown that the ASCC3 helicase, the human orthologue of yeast Slh1, is involved in the early steps of RQC, acting downstream of the ZNF598 E3 ligase. *In vivo*-based biochemistry allowed us to further determine that ASCC3 interacts with mammalian ribosomes as a part of the previously reported multi-protein complex ASCC which also contains ASCC2, ASCC1 and TRIP4/ASC-1. Based on our *in silico* predictions as well as functional analyses, we propose that ASCC2 and TRIP4/ASC1 are functional homologues of yeast Cue3 and Ykr023w, respectively. Of those, only ASCC2 seem to be important for the function of the complex within RQC, as its deletion results in destabilization of the interaction

between the active component ASCC3 and ribosomes (Figure 6.8). As a result of this destabilization, a partial increase in readthrough of the poly(A) stalling sequence is observed in ASCC2-deficient cells (Figures 6.3B, 6.8C). Surprisingly however, TRIP4/ASC-1 does not seem to be functionally important, as its deletion did not have any effect on poly(A)-mediated stalling (Figure 6.3B). This is in contrast with previously reported data in yeast which showed a similar polybasic-readthrough phenotype upon deletion of either Ykr023w or Cue3 (Matsuo et al., 2017; Sitron et al., 2017). This discrepancy between yeast and humans might imply functional divergence of the ASCC in higher eukaryotes.

Closer inspection of the expression of each fluorescent protein from our double fluorescence-reporter revealed an unexpected consequence of ASCC3 depletion. Apart from the expected small increase in RFP expression, there was additional decrease in GFP expression (Figure 6.5B). Our attempts to explain this phenotype as a consequence of decreased mRNA levels or generic translational defect upon ASCC3 deletion was inconclusive. Even though the molecular basis for decreased GFP expression remains to be determined, we can speculate about some possible explanations. An attractive hypothesis is that in the absence of ASCC3 there is a decrease in levels of translation initiation on stall-containing messages, due to overload of the mRNA with ribosomes. This is possible, if we assume that ZNF598-mediated ubiquitination converts excessively slow ribosomes into terminally stalled di-ribosomes. In cells lacking ASCC3, the inability to disassemble stalled complexes would result in a pile-up of ribosomes up to the start codon, which could affect efficient initiation. Consistent with this hypothesis, depletion of both ZNF598 and ASCC3 reversed GFP expression to levels observed in WT (Figure 6.5B) or ZNF598 KO cells (Figure 6.5C).

Biochemical fractionation on sucrose gradients showed constitutive association of ASCC with ribosomes. This interaction was independent of ZNF598 (Figure 6.6) and was not altered under conditions promoting ribosome collisions (Figure 6.7B, Appendix 1). This data suggests a high affinity of the ASCC for ribosomes under steady state conditions, allowing it to continuously sample translating complexes. In contrast, ZNF598 is highly specific in its association with collided di-ribosomes - a feature more characteristic for a quality control sensor. The relative abundance of ASCC3, estimated to be ~5000 copies/cell (Beck et al., 2011), is several orders of magnitude lower than the relative abundance of ribosomes (~ millions copies/cell). In light of this, the high affinity

towards translating ribosomes most likely permits immediate resolution of stalled complexes upon ZNF598 detection. This speed is important to prevent negative consequences of ribosome stalling, such as nascent protein misfolding or ribosome depletion.

In this chapter, we provide a framework for future studies of the role of ASCC within RQC. Biochemical reconstitution experiments using well defined, ubiquitinated di-ribosome complexes, should facilitate efforts towards understanding the molecular function of the ASCC3 helicase. At the same time, the relatively high affinity interaction between ASCC and ribosomes should encourage structural studies of ribosome-ASCC ternary complexes. The combination of genetics, functional biochemistry and structural biology should allow for the near-complete description of the molecular events starting from the initial ubiquitination of the collided di-ribosome up to the splitting of the ribosomal subunits.

6.7 Materials and methods

Constructs, antibodies & siRNAs

Construct for the recombinant expression of ASCC3 was in the pcDNA3.1 vector containing a C-terminal 3xFLAG. ASCC3 ORF was first PCR amplified from commercially available vector at Origene (Cat. No RC216672) and cloned using standard restriction digestion and ligation into the backbone. Expression of WT ASCC2 tagged with 1xFLAG was from commercially available vector at Origene (Cat. No RC203391). The CUE- mutant was designed and generated by Sebastian Kraatz. It contained three point mutations within the LLP motif of the CUE domain: L478A, L479A, P480A. These mutations were designed to abolish critical interactions with mono-ubiquitin as previously described (Shih et al., 2003). For CRISPR-Cas9 mediated knockout of ASCC3 in reporter cell lines, guide RNAs targeting exon 1 and 2 of ASCC3 (5'-TTTTAGATTTGGGCCTGACA-3'; 5'-GAAGGACTCTGTTGGTCACA-3' respectively) were designed using the CRISPR design tool at crispr.mit.edu and cloned into the px330-U6 plasmid (Ran et al., 2013). Guide RNA targeting exon 2 of ASCC2 (5' – TGTCCCCCGCAAATTCGACG- 3') was designed and cloned as described above. Antibodies against ASCC were from Bethyl Laboratories: ASCC1 #A303-871A, ASCC2 #A304-020A, ASC-1/TRIP4 #A300-843A, ASCC3 #A304-015A. Pre-designed,

validated Silencer Select siRNAs were from Life Technologies: ASC-1/TRIP4 #1: s17820, #2 s17822; ASCC1 #1: s27225, #2 s27224; ASCC2: #1: s38590, #2 s23588; ASCC3: #1 s21603, #2 s21604. Other antibodies were described in previous chapters.

In vitro translation in HEK lysate

Translation-competent lysate was generated from WT or HEK 293 cells. Four 15 cm plates of cells at around ~80% confluency were used for a single preparation of the lysate. After two washes with ice cold PBS, cells were scraped and spun for 5 min at 1,000 rpm in 4°C. An additional wash followed by a spin was performed and cells were resuspended in 1 ml of hypotonic buffer (10 mM HEPES pH 7.6, 10 mM K(OAc), 1.5 mM $Mg(OAc)_2$, 2 mM DTT). After swelling for 30 min on ice, cells were ruptured using a pre-chilled 26G needle and 2 ml syringe. Cytosol was extracted by 15 min centrifugation at 15,000 g at 4°C in a tabletop microcentrifuge. The supernatant was dialysed against 500 ml of dialysis buffer (10 mM HEPES pH 7.6, 90 mM K(OAc), 1.5 mM $Mg(OAc)_2$, 1 mM DTT) for 2h at 4°C using a 0.5-3 ml 10,000 MWCO dialysis cassette. The dialysed lysate was spun for 15 min at 15,000 g at 4°C in a tabletop microcentrifuge after which 10x translation buffer was added (20 mM K(OAc), 15 mM MgCl2, DTT 3 mM, HEPES pH 7.6 130 mM, spermidine 4 mM, creatine kinase 0.4 mg/ml, pig liver tRNA 1 mg/ml, creatine phosphate 120 mM, ATP 10 mM, GTP 10 mM, 19 aminoacids 400 µM each). The sample was then mixed well and spun again for 15 min at 15,000 g at 4°C. The resulting supernatant was aliquoted and flash frozen in liquid nitrogen. A typical reaction contained 17 ul of HEK lysate, 1 ul of 35S Methionine (500 µCi/ml), $eRF1^{AAQ}$ (5 µM final concentration) and water to 20 µl, and was allowed to progress for 30-60 min at 32°C.

Analysis of ASCC interaction with ribosomes

Usually, two 10 cm plates of cells at around 80% confluency were used for each genotype. Cells were first washed with ice-cold PBS and harvested by scraping. After sedimentation at 4°C at 1,200 rpm for 5 min, cell pellets were resuspended in 200 µl of RNC buffer (50 mM HEPES, 100 mM K(OAc), 5 mM $Mg(OAc)_2$) containing 40 U/ml of RNAsin (Promega), 0.01% digitonin, 1x protease inhibitor cocktail (EDTA-free cOmplete from ROCHE) and 1 mM DTT. After 15 min incubation on ice, cells were disrupted using a pre-chilled 26G needle appended to 1 ml syringe. Lysates were clarified

by 15 min centrifugation at 15,000g at 4°C in a tabletop centrifuge. Concentrations of the lysates were adjusted to between 75-150 µg (depending on the experiment) in 20 µl volume, loaded on a 10-50% analytical (200 µl) sucrose gradients and spun for 30 min at 55 000 rpm in TLS-55 rotor at 4°C using slowest acceleration and deceleration settings. In the case of *in vitro* translation reactions 0.5 µl of the reaction was saved (as a total sample) and the rest (19.5 µl) was loaded on a gradient and fractionated as described above. After fractionation and collection of 11 fractions, samples were analyzed by immunoblotting.

Cell culture, flow cytometry and western blotting

These and other remaining standard techniques were described in detail in previous chapters**.**

Chapter 7: Perspectives and future work

In this work, we have identified and characterized a novel mechanism responsible for the recognition of excessively slow ribosomes. Initially guided by genetic analyses in mammalian cell culture, we biochemically characterized ZNF598, an E3 ligase and the major factor involved in monitoring translation speed. We showed that ZNF598 site-specifically ubiquitinates ribosomes, and crucially, we show the link between this activity and the induction of a quality control pathway during excessively slow translation. We then went on to reconstitute ZNF598-mediated recognition of aberrantly slow ribosomes using an *in vitro* translation system. Manipulating ZNF598 in our *in vitro* system allowed us to discover the unexpected selectivity of ZNF598 towards closely-packed, collided di-ribosome species. This species arises when a trailing ribosome meets an aberrantly slow leading ribosome. Further biochemical and structural characterization of collided di-ribosome species revealed certain special features, such as resistance to nuclease digestion and a unique ribosome-ribosome interface which allows accommodation of different types of slowdowns. Based on our *in vitro* and *in vivo* characterizations, we propose a general model for sensing aberrantly slow translation through ribosome collisions. The indirect recognition of the consequence of the slowdown, rather than the singular feature of the stalled ribosome itself, has important implications for cellular physiology. Namely, the threshold for the induction of the quality control depends on cellular context, as collisions are dependent on a number of integrated parameters such as the velocities of the lead and trailing ribosomes, and relative inter-ribosomal distances, which are dictated by the efficiency of translation initiation.

ZNF598 is the first example of a factor which selectively engages a distinct, supra-molecular assembly of ribosomes for quality control purposes. However, our TMT mass spectrometry experiment also identified another protein EDF1, which was selectively enriched on collided ribosomes. Even though we showed that EDF1 does not appear to be required for the ribosome-associated quality control pathway, it is still possible that it may play a role responding to ribosome collisions. One attractive possibility is that it prevents frameshifting, which often accompanies ribosomal stalling. Indeed, a recent report used yeast genetics to identify Mbf1, a homolog of EDF1, along with ribosomal proteins uS3 and Asc1 (of note both present at the inter-ribosomal interface of the collided di-ribosome) as suppressors of stall-induced ribosomal

frameshifting (Wang et al., 2018). How ribosome collisions affect frameshifting and the potential molecular role of EDF1 within this process remain to be investigated.

Given the number of previously observed different poly-ribosomal arrangements (Afonina et al., 2014; Brandt et al., 2009, 2010; Christensen and Bourne, 1999; Myasnikov et al., 2014), it is plausible that additional factors might exploit unique features of supra-molecular assemblies of translation complexes. These could be for other, equally important physiological functions not related to quality control, such as translational regulation or translation-related stress responses. Systematic characterization of these various assemblies and their physiological relevance should reveal other underlying principles of translational control.

The direct consequence of ZNF598-mediated recognition of ribosome collisions is the deposition of a ubiquitin molecule on the 40S ribosomal proteins located at the inter-ribosomal interface. Although the exact role of this modification is yet to be determined, we and others have firmly established that this step is crucial for the induction of RQC pathway in both mammals and yeast (Figure 3.4, 3.5) (Garzia et al., 2017; Matsuo et al., 2017; Sundaramoorthy et al., 2017). More recently, Hel2-mediated ubiquitination was also functionally linked to the induction of the NGD mRNA surveillance pathway (Ikeuchi et al., 2019). Hence, Hel2/ZNF598 is a general, most proximal sensor of aberrant translation, triggering both protein and mRNA quality control responses. The details of how these two pathways are integrated at the collided di-ribosome remain to be clarified. However, in both instances, there is ultimately the need to allow disassembly of the ribosomal complexes and endonucleolytic cleavage of the associated mRNA. Factors proposed to be involved in these downstream steps in yeast include Slh1 helicase, ubiquitin-binding protein Cue3 and uncharacterized protein Ykr023w (Matsuo et al., 2017; Sitron et al., 2017). Here, we have demonstrated that mammalian homologs of these proteins: ASCC3, ASCC2 and ASC-1/TRIP-4 respectively, form a complex which interacts with ribosomes. Of these proteins, ASCC3 appears to be the major, active component involved in RQC (Figure 6.3, 6.4), whereas ASCC2 is likely to play a role in stabilization of the ASCC-ribosome interaction (Figure 6.9). ASCC3 was already reported to have unwinding activity towards DNA (Dango et al., 2011), therefore it is tempting to speculate that it may act as an active re-modeller of the di-ribosome complexes, allowing their subsequent processing by ribosome rescue factors and/or mRNA endonuclease. Our initial characterization of the ASCC, which

revealed its direct role in RQC and its ability to stably interact with ribosomes, should encourage further biochemical and structural studies aimed at mechanistically dissecting the downstream steps of di-ribosome disassembly. Significant effort should also be directed towards identifying the mechanism of action of the elusive endonuclease which cleaves stall-inducing, aberrant mRNA. Given that specific endonucleolytic cleavage within the collided di-ribosome appears to be dependent on ribosome ubiquitination (Ikeuchi et al., 2019), the ability to generate fully ubiquitinated collided di-ribosome should pave the way for identification and subsequent characterization of this relevant enzyme.

The next important question which emerges naturally from our work concerns the native substrates for the RQC pathway. So far, we and others have exploited the power of artificially designed model substrates to mechanistically dissect individual steps of this quality control mechanism. Even though we showed that the system can clearly detect a diverse range of problems (see Chapter 5), it is still unclear what sort of substrates are recognized and dealt with in the context of living cells. The nature of this quality control system suggests that it neutralizes aberrancies that occur rather randomly during the process of cellular translation. Even though that might as well be true, it is still possible that the pathway is tailored to cope with only a subset of particularly troublesome, yet extremely highly translated messages in order to prevent otherwise frequent insults against cellular homeostasis. This would therefore justify the energetic cost of maintaining the RQC machinery. Insights from our work, particularly the fact that ribosome slowdown results in collision events which generate nuclease resistant di-ribosome species, should now allow the design of studies aimed at identification of endogenous clients of ZNF598. Sequencing of the mRNA fragments protected by the nuclease resistant di-ribosome species isolated from cells should reveal the identity of messages inducing ribosome collisions. Expanding this study to different cell types and different tissues might highlight some of the unique problems faced by more specialised systems such as neurons.

Finally, our discovery that site-specific ribosome ubiquitination can govern complex cellular response highlights the significance of post-translational modifications (PTMs) in the context of translational control. Historically, the ribosome was viewed as a highly conserved, static and invariable structure. However, more recent evidence suggests that ribosomes can differ in both their protein composition (Genuth and Barna,

2018), as well as the their suit of PTMs (Simsek and Barna, 2017), even within a single species. Eukaryotes are characterized by high versatility of PTMs, which include covalent attachment of modifier proteins such as ubiquitin or UFM1, or more simple chemical modifications of a single amino acid like phosphorylation. Therefore, it is tempting to speculate that evolution might have exploited this functional and structural diversity to achieve additional levels of dynamic regulation at the ribosome. With the advancement of the highly sensitive proteomic methods, a number of new specific PTMs of core ribosomal proteins have been identified in the last couple of years (Higgins et al., 2015; Simsek and Barna, 2017; Simsek et al., 2017). Some of these modifications are of direct relevance for disease states such as hyper-phosphorylation of uS19 observed in specific models of Parkinson's disease (Martin et al., 2014). Systematic classification of ribosome PTMs and more importantly, their physiological relevance, are the next obvious steps in order to fully understand the complexity of eukaryotic translation. In parallel, more focused efforts aimed at identification and characterization of molecular players involved in writing and reading of the PTM code on the ribosome should provide us with necessary understanding of the mechanistic details underlying these regulatory processes.

References

Afonina, Z.A., Myasnikov, A.G., Shirokov, V.A., Klaholz, B.P., and Spirin, A.S. (2014). Formation of circular polyribosomes on eukaryotic mRNA without cap-structure and poly(A)-tail: a cryo electron tomography study. Nucleic Acids Res. *42*, 9461–9469.

Afonina, Z.A., Myasnikov, A.G., Shirokov, V.A., Klaholz, B.P., and Spirin, A.S. (2015). Conformation transitions of eukaryotic polyribosomes during multi-round translation. Nucleic Acids Res. *43*, 618–628.

Alkalaeva, E.Z., Pisarev, A. V, Frolova, L.Y., Kisselev, L.L., and Pestova, T. V (2006). In vitro reconstitution of eukaryotic translation reveals cooperativity between release factors eRF1 and eRF3. Cell *125*, 1125–1136.

Amrani, N., Ganesan, R., Kervestin, S., Mangus, D.A., Ghosh, S., and Jacobson, A. (2004). A faux 3′-UTR promotes aberrant termination and triggers nonsense- mediated mRNA decay. Nature *432*, 112–118.

Araki, Y., Takahashi, S., Kobayashi, T., Kajiho, H., Hoshino, S., and Katada, T. (2001). Ski7p G protein interacts with the exosome and the Ski complex for 3'-to-5' mRNA decay in yeast. EMBO J. *20*, 4684–4693.

Arthur, L.L., Szczesny, P., Djuranovic, S., Pavlovic-Djuranovic, S., Green, R., and Koutmou, K.S. (2015). Translational control by lysine-encoding A-rich sequences. Sci. Adv. *1*, e1500154.

Atkinson, G.C., Baldauf, S.L., and Hauryliuk, V. (2008). Evolution of nonstop, no-go and nonsense-mediated mRNA decay and their termination factor-derived components. BMC Evol. Biol. *8*, 290.

Barbacid, M., Fresno, M., and Vazquez, D. (1975). Inhibitors of polypeptide elongation on yeast polysomes. J. Antibiot. (Tokyo). *28*, 453–462.

Beck, M., Schmidt, A., Malmstroem, J., Claassen, M., Ori, A., Szymborska, A., Herzog, F., Rinner, O., Ellenberg, J., and Aebersold, R. (2011). The quantitative proteome of a human cell line. Mol. Syst. Biol. *7*, 549.

Becker, T., Armache, J.-P., Jarasch, A., Anger, A.M., Villa, E., Sieber, H., Motaal, B.A., Mielke, T., Berninghausen, O., and Beckmann, R. (2011). Structure of the no-go mRNA decay complex Dom34-Hbs1 bound to a stalled 80S ribosome. Nat. Struct. Mol. Biol. *18*, 715–720.

Behrmann, E., Loerke, J., Budkevich, T. V, Yamamoto, K., Schmidt, A., Penczek, P.A., Vos, M.R., Bürger, J., Mielke, T., Scheerer, P., et al. (2015). Structural snapshots of actively translating human ribosomes. Cell *161*, 845–857.

Bengtson, M.H., and Joazeiro, C. a P. (2010). Role of a ribosome-associated E3 ubiquitin ligase in protein quality control. Nature *467*, 470–473.

Berg, M.G., Singh, L.N., Younis, I., Liu, Q., Pinto, A.M., Kaida, D., Zhang, Z., Cho, S., Sherrill-Mix, S., Wan, L., et al. (2012). U1 snRNP determines mRNA length and regulates isoform expression. Cell *150*, 53–64.

Beringer, M., and Rodnina, M. V (2007). The ribosomal peptidyl transferase. Mol. Cell *26*, 311–321.

Blombach, F., Launay, H., Snijders, A.P.L., Zorraquino, V., Wu, H., de Koning, B., Brouns, S.J.J., Ettema, T.J.G., Camilloni, C., Cavalli, A., et al. (2014). Archaeal MBF1 binds to 30S and 70S ribosomes via its helix–turn–helix domain. Biochem. J. *462*, 373–384.

Brandman, O., and Hegde, R.S. (2016). Ribosome-associated protein quality control. Nat. Struct. Mol. Biol. *23*, 7–15.

Brandman, O., Stewart-Ornstein, J., Wong, D., Larson, A., Williams, C.C., Li, G.-W., Zhou, S., King, D., Shen, P.S., Weibezahn, J., et al. (2012). A ribosome-bound quality control complex triggers degradation of nascent peptides and signals translation stress. Cell *151*, 1042–1054.

Brandt, F., Etchells, S.A., Ortiz, J.O., Elcock, A.H., Hartl, F.U., and Baumeister, W. (2009). The native 3D organization of bacterial polysomes. Cell *136*, 261–271.

Brandt, F., Carlson, L.-A., Hartl, F.U., Baumeister, W., and Grünewald, K. (2010). The three-dimensional organization of polyribosomes in intact human cells. Mol. Cell *39*, 560–569.

Brown, A., Shao, S., Murray, J., Hegde, R.S., and Ramakrishnan, V. (2015). Structural basis for stop codon recognition in eukaryotes. Nature *524*, 493–496.

Budkevich, T., Giesebrecht, J., Altman, R.B., Munro, J.B., Mielke, T., Nierhaus, K.H., Blanchard, S.C., and Spahn, C.M.T. (2011). Structure and dynamics of the mammalian ribosomal pretranslocation complex. Mol. Cell *44*, 214–224.

Calfon, M., Zeng, H., Urano, F., Till, J.H., Hubbard, S.R., Harding, H.P., Clark, S.G., and Ron, D. (2002). IRE1 couples endoplasmic reticulum load to secretory capacity by processing the XBP-1 mRNA. Nature *415*, 92–96.

Carter, M.S., Doskow, J., Morris, P., Li, S., Nhim, R.P., Sandstedt, S., and Wilkinson, M.F. (1995). A regulatory mechanism that detects premature nonsense codons in T-cell receptor transcripts in vivo is reversed by protein synthesis inhibitors in vitro. J. Biol. Chem. *270*, 28995–29003.

Carvalho, M.D., Carvalho, J.F., and Merrick, W.C. (1984). Biological characterization of various forms of elongation factor 1 from rabbit reticulocytes. Arch. Biochem. Biophys. *234*, 603–611.

Chakrabarti, O., and Hegde, R.S. (2009). Functional Depletion of Mahogunin by Cytosolically Exposed Prion Protein Contributes to Neurodegeneration. Cell *137*, 1136–1147.

Chang, Y.-F., Imam, J.S., and Wilkinson, M.F. (2007). The Nonsense-Mediated Decay RNA Surveillance Pathway. Annu. Rev. Biochem. *76*, 51–74.

Choe, Y.-J., Park, S.-H., Hassemer, T., Vincenz-Donnelly, L., Körner, R., Hayer-Hartl, M., and Hartl, F.U. (2016). Failure of RQC machinery causes protein aggregation and proteotoxic stress. Nature *531*, 191–195.

Christensen, A.K., and Bourne, C.M. (1999). Shape of large bound polysomes in cultured fibroblasts and thyroid epithelial cells. Anat. Rec. *255*, 116–129.

Chu, J., Hong, N.A., Masuda, C.A., Jenkins, B. V, Nelms, K.A., Goodnow, C.C., Glynne, R.J., Wu, H., Masliah, E., Joazeiro, C.A.P., et al. (2009). A mouse forward genetics screen identifies LISTERIN as an E3 ubiquitin ligase involved in neurodegeneration. Proc. Natl. Acad. Sci. U. S. A. *106*, 2097–2103.

Crick, F.H.C. (1958). On protein synthesis. Symp. Soc. Exp. Biol. *12*, 138–163.

Custodio, N., Carmo-Fonseca, M., Geraghty, F., Periera, H.S., Grosveld, F., and Antoniou, M. (1999). Inefficient processing impairs release of RNA from the site of transcription. EMBO J. *18*, 2855–2866.

Dango, S., Mosammaparast, N., Sowa, M.E., Xiong, L.J., Wu, F., Park, K., Rubin, M., Gygi, S., Harper, J.W., and Shi, Y. (2011). DNA unwinding by ASCC3 helicase is coupled to ALKBH3-dependent DNA alkylation repair and cancer cell proliferation. Mol. Cell *44*, 373–384.

Defenouillère, Q., Yao, Y., Mouaikel, J., Namane, A., Galopier, A., Decourty, L., Doyen, A., Malabat, C., Saveanu, C., Jacquier, A., et al. (2013). Cdc48-associated complex bound to 60S particles is required for the clearance of aberrant translation products. Proc. Natl. Acad. Sci. USA *110 VN*-, 5046–5051.

Defenouillère, Q., Zhang, E., Namane, A., Mouaikel, J., Jacquier, A., and Fromont-Racine, M. (2016). Rqc1 and Ltn1 Prevent C-terminal Alanine-Threonine Tail (CAT-tail)-induced Protein Aggregation by Efficient Recruitment of Cdc48 on Stalled 60S Subunits. J. Biol. Chem. *291*, 12245–12253.

Dimitrova, L.N., Kuroha, K., Tatematsu, T., and Inada, T. (2009). Nascent peptide-dependent translation arrest leads to Not4p-mediated protein degradation by the proteasome. J. Biol. Chem. *284*, 10343–10352.

Dinman, J.D. (2012). Mechanisms and implications of programmed translational frameshifting. Wiley Interdiscip. Rev. RNA *3*, 661–673.

Doerfel, L.K., Wohlgemuth, I., Kothe, C., Peske, F., Urlaub, H., and Rodnina, M. V (2013). EF-P is essential for rapid synthesis of proteins containing consecutive proline residues. Science *339*, 85–88.

Doma, M.K., and Parker, R. (2006). Endonucleolytic cleavage of eukaryotic mRNAs with stalls in translation elongation. Nature *440*, 561–564.

Doma, M.K., and Parker, R. (2007). RNA quality control in eukaryotes. Cell *131*, 660–

668.

van den Elzen, A.M.G., Henri, J., Lazar, N., Gas, M.E., Durand, D., Lacroute, F., Nicaise, M., van Tilbeurgh, H., Seraphin, B., Graille, M., et al. (2010). Dissection of Dom34-Hbs1 reveals independent functions in two RNA quality control pathways. Nat. Struct. Mol. Biol. *17*, 1446-U74.

Flicek, P., Amode, M.R., Barrell, D., Beal, K., Billis, K., Brent, S., Carvalho-Silva, D., Clapham, P., Coates, G., Fitzgerald, S., et al. (2014). Ensembl 2014. Nucleic Acids Res. *42*, 749–755.

Frischmeyer, P.A., Van Hoof, A., O'Donnell, K., Guerrerio, A.L., Parker, R., and Dietz, H.C. (2002). An mRNA surveillance mechanism that eliminates transcripts lacking termination codons. Science *295*, 2258–2261.

Frolova, L.Y., Tsivkovskii, R.Y., Sivolobova, G.F., Oparina, N.Y., Serpinsky, O.I., Blinov, V.M., Tatkov, S.I., and Kisselev, L.L. (1999). Mutations in the highly conserved GGQ motif of class 1 polypeptide release factors abolish ability of human eRF1 to trigger peptidyl-tRNA hydrolysis. RNA *5*, 1014–1020.

Gallo, S., and Manfrini, N. (2015). Working hard at the nexus between cell signaling and the ribosomal machinery: An insight into the roles of RACK1 in translational regulation. Translation *3*, e1120382.

Gamble, C.E., Brule, C.E., Dean, K.M., Fields, S., and Grayhack, E.J. (2016). Adjacent Codons Act in Concert to Modulate Translation Efficiency in Yeast. Cell *166*, 679–690.

Garzia, A., Jafarnejad, S.M., Meyer, C., Chapat, C., Gogakos, T., Morozov, P., Amiri, M., Shapiro, M., Molina, H., Tuschl, T., et al. (2017). The E3 ubiquitin ligase and RNA-binding protein ZNF598 orchestrates ribosome quality control of premature polyadenylated mRNAs. Nat. Commun. *8*, 16056.

Gautier, E.-F., Ducamp, S., Leduc, M., Salnot, V., Guillonneau, F., Dussiot, M., Hale, J., Giarratana, M.-C., Raimbault, A., Douay, L., et al. (2016). Comprehensive Proteomic Analysis of Human Erythropoiesis. Cell Rep. *16*, 1470–1484.

Genuth, N.R., and Barna, M. (2018). The Discovery of Ribosome Heterogeneity and Its Implications for Gene Regulation and Organismal Life. Mol. Cell *71*, 364–374.

Graille, M., Chaillet, M., and van Tilbeurgh, H. (2008). Structure of yeast Dom34: a protein related to translation termination factor Erf1 and involved in No-Go decay. J. Biol. Chem. *283*, 7145–7154.

Grollman, A.P. (1968). Inhibitors of protein biosynthesis. V. Effects of emetine on protein and nucleic acid biosynthesis in HeLa cells. J. Biol. Chem. *243*, 4089–4094.

Gutierrez, E., Shin, B.-S., Woolstenhulme, C.J., Kim, J.-R., Saini, P., Buskirk, A.R., and Dever, T.E. (2013). eIF5A Promotes Translation of Polyproline Motifs. Mol. Cell *51*, 35–45.

Guydosh, N.R., and Green, R. (2014). Dom34 Rescues Ribosomes in 3′ Untranslated

Regions. Cell *156*, 950–962.

Heuer, A., Gerovac, M., Schmidt, C., Trowitzsch, S., Preis, A., Kötter, P., Berninghausen, O., Becker, T., Beckmann, R., and Tampé, R. (2017). Structure of the 40S-ABCE1 post-splitting complex in ribosome recycling and translation initiation. Nat. Struct. Mol. Biol. *24*, 453–460.

Higgins, R., Gendron, J.M., Rising, L., Mak, R., Webb, K., Kaiser, S.E., Zuzow, N., Riviere, P., Yang, B., Fenech, E., et al. (2015). The Unfolded Protein Response Triggers Site-Specific Regulatory Ubiquitylation of 40S Ribosomal Proteins. Mol. Cell *59*, 35–49.

Hilal, T., Yamamoto, H., Loerke, J., Bürger, J., Mielke, T., and Spahn, C.M.T. (2016). Structural insights into ribosomal rescue by Dom34 and Hbs1 at near-atomic resolution. Nat. Commun.

Hinnebusch, A.G. (2014). The scanning mechanism of eukaryotic translation initiation. Annu. Rev. Biochem. *83*, 779–812.

Hinnebusch, A.G., and Lorsch, J.R. (2012). The mechanism of eukaryotic translation initiation: new insights and challenges. Cold Spring Harb. Perspect. Biol. *4*, a011544–a011544.

Le Hir, H., Gatfield, D., Izaurralde, E., and Moore, M.J. (2001). The exon-exon junction complex provides a binding platform for factors involved in mRNA export and nonsense-mediated mRNA decay. EMBO J. *20*, 4987–4997.

Hogg, J.R., and Goff, S.P. (2010). Upf1 Senses 3′UTR Length to Potentiate mRNA Decay. Cell *143*, 379–389.

Van Hoof, A., Frischmeyer, P.A., Dietz, H.C., and Parker, R. (2002). Exosome-mediated recognition and degradation of mRNAs lacking a termination codon. Science (80-.). *295*, 2262–2264.

Hopfield, J.J. (1974). Kinetic proofreading: a new mechanism for reducing errors in biosynthetic processes requiring high specificity. Proc. Natl. Acad. Sci. USA *71*, 4135–4139.

Hosoda, N., Kobayashi, T., Uchida, N., Funakoshi, Y., Kikuchi, Y., Hoshino, S., and Katada, T. (2003). Translation termination factor eRF3 mediates mRNA decay through the regulation of deadenylation. J. Biol. Chem. *278*, 38287–38291.

Ikeuchi, K., Tesina, P., Matsuo, Y., Sugiyama, T., Cheng, J., Saeki, Y., Tanaka, K., Becker, T., Beckmann, R., and Inada, T. (2019). Collided ribosomes form a unique structural interface to induce Hel2-driven quality control pathways. EMBO J. e100276.

Ingolia, N.T., Lareau, L.F., and Weissman, J.S. (2011). Ribosome profiling of mouse embryonic stem cells reveals the complexity and dynamics of mammalian proteomes. Cell *147*, 789–802.

Ishimura, R., Nagy, G., Dotu, I., Zhou, H., Yang, X.-L., Schimmel, P., Senju, S.,

Nishimura, Y., Chuang, J.H., and Ackerman, S.L. (2014). Ribosome stalling induced by mutation of a CNS-specific tRNA causes neurodegeneration. Science *345*, 455–459.

Ito-Harashima, S., Kuroha, K., Tatematsu, T., and Inada, T. (2007). Translation of the poly(A) tail plays crucial roles in nonstop mRNA surveillance via translation repression and protein destabilization by proteasome in yeast. Genes Dev. *21*, 519–524.

Izawa, T., Park, S.-H., Zhao, L., Hartl, F.U., and Neupert, W. (2017). Cytosolic Protein Vms1 Links Ribosome Quality Control to Mitochondrial and Cellular Homeostasis. Cell *171*, 890-903.e18.

Jiménez, A., Carrasco, L., and Vázquez, D. (1977). Enzymic and nonenzymic translocation by yeast polysomes. Site of action of a number of inhibitors. Biochemistry *16*, 4727–4730.

Joazeiro, C.A.P. (2017). Ribosomal Stalling During Translation: Providing Substrates for Ribosome-Associated Protein Quality Control. Annu. Rev. Cell Dev. Biol. *33*, 343–368.

Jung, D.-J., Sung, H.-S., Goo, Y.-W., Lee, H.M., Park, O.K., Jung, S.-Y., Lim, J., Kim, H.-J., Lee, S.-K., Kim, T.S., et al. (2002). Novel transcription coactivator complex containing activating signal cointegrator 1. Mol. Cell. Biol. *22*, 5203–5211.

Juszkiewicz, S., Chandrasekaran, V., Lin, Z., Kraatz, S., Ramakrishnan, V., and Hegde, R.S. (2018). ZNF598 Is a Quality Control Sensor of Collided Ribosomes. Mol. Cell *72*, 469-481.e7.

Kabe, Y., Goto, M., Shima, D., Imai, T., Wada, T., Morohashi, K. i, Shirakawa, M., Hirose, S., and Handa, H. (1999). The role of human MBF1 as a transcriptional coactivator. J. Biol. Chem. *274*, 34196–34202.

Kaida, D., Berg, M.G., Younis, I., Kasim, M., Singh, L.N., Wan, L., and Dreyfuss, G. (2010). U1 snRNP protects pre-mRNAs from premature cleavage and polyadenylation. Nature *468*, 664–668.

Kalderon, D., Richardson, W.D., Markham, A.F., and Smith, A.E. (1984a). Sequence requirements for nuclear location of simian virus 40 large-T antigen. Nature *311*, 33–38.

Kalderon, D., Roberts, B.L., Richardson, W.D., and Smith, A.E. (1984b). A short amino acid sequence able to specify nuclear location. Cell *39*, 499–509.

Karousis, E.D., and Mühlemann, O. (2019). Nonsense-Mediated mRNA Decay Begins Where Translation Ends. Cold Spring Harb. Perspect. Biol. *11*, a032862.

Khoshnevis, S., Gross, T., Rotte, C., Baierlein, C., Ficner, R., and Krebber, H. (2010). The iron-sulphur protein RNase L inhibitor functions in translation termination. EMBO Rep. *11*, 214–219.

Kinniburgh, A.J., Maquat, L.E., Schedl, T., Rachmilewitz, E., and Ross, J. (1982). mRNA-deficient beta o-thalassemia results from a single nucleotide deletion. Nucleic Acids Res. *10*, 5421–5427.

Kobayashi, K., Kikuno, I., Kuroha, K., Saito, K., Ito, K., Ishitani, R., Inada, T., and Nureki, O. (2010). Structural basis for mRNA surveillance by archaeal Pelota and GTP-bound EF1alpha complex. Proc. Natl. Acad. Sci. USA *107*, 17575–17579.

Kostova, K.K., Hickey, K.L., Osuna, B.A., Hussmann, J.A., Frost, A., Weinberg, D.E., and Weissman, J.S. (2017). CAT-tailing as a fail-safe mechanism for efficient degradation of stalled nascent polypeptides. Science *357*, 414–417.

Koutmou, K.S., Schuller, A.P., Brunelle, J.L., Radhakrishnan, A., Djuranovic, S., and Green, R. (2015). Ribosomes slide on lysine-encoding homopolymeric A stretches. Elife *2015*.

Kozak, M. (1986). Point mutations define a sequence flanking the AUG initiator codon that modulates translation by eukaryotic ribosomes. Cell *44*, 283–292.

Kuroha, K., Tatematsu, T., and Inada, T. (2009). Upf1 stimulates degradation of the product derived from aberrant messenger RNA containing a specific nonsense mutation by the proteasome. EMBO Rep. *10*, 1265–1271.

Kuroha, K., Akamatsu, M., Dimitrova, L., Ito, T., Kato, Y., Shirahige, K., and Inada, T. (2010). Receptor for activated C kinase 1 stimulates nascent polypeptide-dependent translation arrest. EMBO Rep. *11*, 956–961.

Kuroha, K., Zinoviev, A., Hellen, C.U.T., and Pestova, T. V. (2018). Release of Ubiquitinated and Non-ubiquitinated Nascent Chains from Stalled Mammalian Ribosomal Complexes by ANKZF1 and Ptrh1. Mol. Cell *72*, 286-302.e8.

Kwon, I., Xiang, S., Kato, M., Wu, L., Theodoropoulos, P., Wang, T., Kim, J., Yun, J., Xie, Y., and McKnight, S.L. (2014). Poly-dipeptides encoded by the C9orf72 repeats bind nucleoli, impede RNA biogenesis, and kill cells. Science *345*, 1139–1145.

Lareau, L.F., Hite, D.H., Hogan, G.J., and Brown, P.O. (2014). Distinct stages of the translation elongation cycle revealed by sequencing ribosome-protected mRNA fragments. Elife *3*, e01257.

Lee, J.W., Beebe, K., Nangle, L.A., Jang, J., Longo-Guess, C.M., Cook, S.A., Davisson, M.T., Sundberg, J.P., Schimmel, P., and Ackerman, S.L. (2006). Editing-defective tRNA synthetase causes protein misfolding and neurodegeneration. Nature *443*, 50–55.

Letzring, D.P., Dean, K.M., and Grayhack, E.J. (2010). Control of translation efficiency in yeast by codon-anticodon interactions. RNA *16*, 2516–2528.

Letzring, D.P., Wolf, A.S., Brule, C.E., and Grayhack, E.J. (2013). Translation of CGA codon repeats in yeast involves quality control components and ribosomal protein L1. RNA *19*, 1208–1217.

Li, G.-W., Burkhardt, D., Gross, C., and Weissman, J.S. (2014). Quantifying absolute protein synthesis rates reveals principles underlying allocation of cellular resources. Cell *157*, 624–635.

Lin, Y.J., Huang, L.H., and Huang, C.T. (2013). Enhancement of Heterologous Gene

Expression in Flammulina velutipes Using Polycistronic Vectors Containing a Viral 2A Cleavage Sequence. PLoS One *8*.

Ling, C., and Ermolenko, D.N. (2016). Structural insights into ribosome translocation. Wiley Interdiscip. Rev. RNA *7*, 620–636.

Ling, J., Reynolds, N., and Ibba, M. (2009). Aminoacyl-tRNA Synthesis and Translational Quality Control. Annu. Rev. Microbiol. *63*, 61–78.

Lu, J., and Deutsch, C. (2008). Electrostatics in the Ribosomal Tunnel Modulate Chain Elongation Rates. J. Mol. Biol. *384*, 73–86.

Lykke-Andersen, J., Shu, M.D., and Steitz, J.A. (2001). Communication of the Position of Exon-Exon Junctions to the mRNA Surveillance Machinery by the Protein RNPS1. Science *293*, 1836–1839.

Lyumkis, D., Oliveira dos Passos, D., Tahara, E.B., Webb, K., Bennett, E.J., Vinterbo, S., Potter, C.S., Carragher, B., and Joazeiro, C.A.P. (2014). Structural basis for translational surveillance by the large ribosomal subunit-associated protein quality control complex. Proc. Natl. Acad. Sci. USA *111*, 15981–15986.

Maquat, L.E., Kinniburgh, A.J., Rachmilewitz, E.A., and Ross, J. (1981). Unstable beta-globin mRNA in mRNA-deficient beta o thalassemia. Cell *27*, 543–553.

Martin, I., Kim, J.W., Lee, B.D., Kang, H.C., Xu, J.-C., Jia, H., Stankowski, J., Kim, M.-S., Zhong, J., Kumar, M., et al. (2014). Ribosomal Protein s15 Phosphorylation Mediates LRRK2 Neurodegeneration in Parkinson's Disease. Cell *157*, 472–485.

Marton, M.J., Vazquez de Aldana, C.R., Qiu, H., Chakraburtty, K., and Hinnebusch, A.G. (1997). Evidence that GCN1 and GCN20, translational regulators of GCN4, function on elongating ribosomes in activation of eIF2alpha kinase GCN2. Mol. Cell. Biol. *17*, 4474–4489.

Matsuo, Y., Ikeuchi, K., Saeki, Y., Iwasaki, S., Schmidt, C., Udagawa, T., Sato, F., Tsuchiya, H., Becker, T., Tanaka, K., et al. (2017). Ubiquitination of stalled ribosome triggers ribosome-associated quality control. Nat. Commun. *8*, 159.

Meaux, S., and Van Hoof, A. (2006). Yeast transcripts cleaved by an internal ribozyme provide new insight into the role of the cap and poly(A) tail in translation and mRNA decay. RNA *12*, 1323–1337.

Mizielinska, S., Grönke, S., Niccoli, T., Ridler, C.E., Clayton, E.L., Devoy, A., Moens, T., Norona, F.E., Woollacott, I.O.C., Pietrzyk, J., et al. (2014). C9orf72 repeat expansions cause neurodegeneration in Drosophila through arginine-rich proteins. Science *345*, 1192–1195.

Moazed, D., and Noller, H.F. (1989). Intermediate states in the movement of transfer RNA in the ribosome. Nature *342*, 142–148.

Muhlrad, D., and Parker, R. (1999). Aberrant mRNAs with extended 3' UTRs are substrates for rapid degradation by mRNA surveillance. RNA *5*, 1299–1307.

Myasnikov, A.G., Afonina, Z.A., Ménétret, J.-F., Shirokov, V.A., Spirin, A.S., and Klaholz, B.P. (2014). The molecular structure of the left-handed supra-molecular helix of eukaryotic polyribosomes. Nat. Commun. *5*, 5294.

Nagy, E., and Maquat, L.E. (1998). A rule for termination-codon position within intron-containing genes: when nonsense affects RNA abundance. Trends Biochem. Sci. *23*, 198–199.

Nissen, P., Hansen, J., Ban, N., Moore, P.B., and Steitz, T.A. (2000). The structural basis of ribosome activity in peptide bond synthesis. Science *289*, 920–930.

Osuna, B.A., Howard, C.J., KC, S., Frost, A., and Weinberg, D.E. (2017). In vitro analysis of RQC activities provides insights into the mechanism and function of CAT tailing. Elife *6*.

Ozsolak, F., Kapranov, P., Foissac, S., Kim, S.W., Fishilevich, E., Monaghan, A.P., John, B., and Milos, P.M. (2010). Comprehensive polyadenylation site maps in yeast and human reveal pervasive alternative polyadenylation. Cell *143*, 1018–1029.

Passos, D.O., Doma, M.K., Shoemaker, C.J., Muhlrad, D., Green, R., Weissman, J., Hollien, J., and Parker, R. (2009). Analysis of Dom34 and its function in no-go decay. Mol. Biol. Cell *20*, 3025–3032.

Pavlov, M.Y., Watts, R.E., Tan, Z., Cornish, V.W., Ehrenberg, M., and Forster, A.C. (2009). Slow peptide bond formation by proline and other N-alkylamino acids in translation. Proc. Natl. Acad. Sci. USA *106*, 50–54.

Perara, E., Rothman, R.E., and Lingappa, V.R. (1986). Uncoupling translocation from translation: implications for transport of proteins across membranes. Science *232*, 348–352.

Pisarev, A. V, Skabkin, M.A., Pisareva, V.P., Skabkina, O. V, Rakotondrafara, A.M., Hentze, M.W., Hellen, C.U.T., and Pestova, T. V (2010). The role of ABCE1 in eukaryotic posttermination ribosomal recycling. Mol. Cell *37*, 196–210.

Pisareva, V.P., Skabkin, M.A., Hellen, C.U.T., Pestova, T. V, and Pisarev, A. V (2011). Dissociation by Pelota, Hbs1 and ABCE1 of mammalian vacant 80S ribosomes and stalled elongation complexes. EMBO J. *30*, 1804–1817.

Presnyak, V., Alhusaini, N., Chen, Y.-H., Martin, S., Morris, N., Kline, N., Olson, S., Weinberg, D., Baker, K.E., Graveley, B.R., et al. (2015). Codon Optimality Is a Major Determinant of mRNA Stability. Cell *160*, 1111–1124.

Proudfoot, N. (2004). New perspectives on connecting messenger RNA 3' end formation to transcription. Curr. Opin. Cell Biol. *16*, 272–278.

Ran, F.A., Hsu, P.D., Wright, J., Agarwala, V., Scott, D.A., and Zhang, F. (2013). Genome engineering using the CRISPR-Cas9 system. Nat. Protoc. *8*, 2281–2308.

Rodrigo-Brenni, M.C., and Hegde, R.S. (2012). Design Principles of Protein Biosynthesis-Coupled Quality Control. Dev. Cell *23*, 896–907.

Saito, S., Hosoda, N., and Hoshino, S. (2013). The Hbs1-Dom34 protein complex functions in non-stop mRNA decay in mammalian cells. J. Biol. Chem. *288*, 17832–17843.

Salas-Marco, J., and Bedwell, D.M. (2004). GTP hydrolysis by eRF3 facilitates stop codon decoding during eukaryotic translation termination. Mol. Cell. Biol. *24*, 7769–7778.

Scheres, S.H., and Nagai, K. (2017). CryoEM structures of spliceosomal complexes reveal the molecular mechanism of pre-mRNA splicing. Curr. Opin. Struct. Biol. *46*, 130–139.

Schmidt, C., Becker, T., Heuer, A., Braunger, K., Shanmuganathan, V., Pech, M., Berninghausen, O., Wilson, D.N., and Beckmann, R. (2016). Structure of the hypusinylated eukaryotic translation factor eIF-5A bound to the ribosome. Nucleic Acids Res. *44*, 1944–1951.

Schwer, B., Mao, X., and Shuman, S. (1998). Accelerated mRNA decay in conditional mutants of yeast mRNA capping enzyme. Nucleic Acids Res. *26*, 2050–2057.

Shao, S., and Hegde, R.S. (2014). Reconstitution of a Minimal Ribosome-Associated Ubiquitination Pathway with Purified Factors. Mol. Cell *55*, 880–890.

Shao, S., von der Malsburg, K., and Hegde, R.S. (2013). Listerin-dependent nascent protein ubiquitination relies on ribosome subunit dissociation. Mol. Cell *50*, 637–648.

Shao, S., Brown, A., Santhanam, B., and Hegde, R.S. (2015). Structure and assembly pathway of the ribosome quality control complex. Mol. Cell *57*, 433–445.

Shao, S., Murray, J., Brown, A., Taunton, J., Ramakrishnan, V., and Hegde, R.S. (2016). Decoding Mammalian Ribosome-mRNA States by Translational GTPase Complexes. Cell *167*, 1229-1240.e15.

Sharma, A., Mariappan, M., Appathurai, S., and Hegde, R.S. (2010). In vitro dissection of protein translocation into the mammalian endoplasmic reticulum. Methods Mol. Biol. *619*, 339–363.

Shen, P.S., Park, J., Qin, Y., Li, X., Parsawar, K., Larson, M.H., Cox, J., Cheng, Y., Lambowitz, A.M., Weissman, J.S., et al. (2015). Rqc2p and 60S ribosomal subunits mediate mRNA-independent elongation of nascent chains. Science *347*, 75–78.

Shih, S.C., Prag, G., Francis, S.A., Sutanto, M.A., Hurley, J.H., and Hicke, L. (2003). A ubiquitin-binding motif required for intramolecular monoubiquitylation, the CUE domain. EMBO J. *22*, 1273–1281.

Shoemaker, C.J., and Green, R. (2011). Kinetic analysis reveals the ordered coupling of translation termination and ribosome recycling in yeast. Proc. Natl. Acad. Sci. U. S. A. *108*, E1392-8.

Shoemaker, C.J., and Green, R. (2012). Translation drives mRNA quality control. Nat. Struct. Mol. Biol. *19*, 594–601.

Shoemaker, C.J., Eyler, D.E., and Green, R. (2010). Dom34:Hbs1 promotes subunit dissociation and peptidyl-tRNA drop off to initiate no-go decay. Science *330*, 369–372.

Shuman, S. (2000). Structure, mechanism, and evolution of the mRNA capping apparatus. Prog. Nucleic Acid Res. Mol. Biol. *66*, 1–40.

Simms, C.L., Hudson, B.H., Mosior, J.W., Rangwala, A.S., and Zaher, H.S. (2014). An Active Role for the Ribosome in Determining the Fate of Oxidized mRNA. Cell Rep. *9*, 1256–1264.

Simms, C.L., Yan, L.L., and Zaher, H.S. (2017). Ribosome Collision Is Critical for Quality Control during No-Go Decay. Mol. Cell *68*, 361-373.e5.

Simsek, D., and Barna, M. (2017). An emerging role for the ribosome as a nexus for post-translational modifications. Curr. Opin. Cell Biol. *45*, 92–101.

Simsek, D., Tiu, G.C., Flynn, R.A., Byeon, G.W., Leppek, K., Xu, A.F., Chang, H.Y., and Barna, M. (2017). The Mammalian Ribo-interactome Reveals Ribosome Functional Diversity and Heterogeneity. Cell *169*, 1051-1065.e18.

Singh, G., Rebbapragada, I., and Lykke-Andersen, J. (2008). A Competition between Stimulators and Antagonists of Upf Complex Recruitment Governs Human Nonsense-Mediated mRNA Decay. PLoS Biol. *6*, e111.

Sitron, C.S., and Brandman, O. (2018). CAT tails drive on- and off-ribosome degradation of stalled polypeptides. BioRxiv 469296.

Sitron, C.S., Park, J.H., and Brandman, O. (2017). Asc1, Hel2, and Slh1 couple translation arrest to nascent chain degradation. RNA *23*, 798–810.

Stapf, C., Cartwright, E., Bycroft, M., Hofmann, K., and Buchberger, A. (2011). The general definition of the p97/valosin-containing protein (VCP)-interacting motif (VIM) delineates a new family of p97 cofactors. J. Biol. Chem. *286*, 38670–38678.

Stolz, A., Hilt, W., Buchberger, A., and Wolf, D.H. (2011). Cdc48: a power machine in protein degradation. Trends Biochem. Sci. *36*, 515–523.

Sundaramoorthy, E., Leonard, M., Mak, R., Liao, J., Fulzele, A., and Bennett, E.J. (2017). ZNF598 and RACK1 Regulate Mammalian Ribosome-Associated Quality Control Function by Mediating Regulatory 40S Ribosomal Ubiquitylation. Mol. Cell *65*, 751-760.e4.

Thompson, A., Schäfer, J., Kuhn, K., Kienle, S., Schwarz, J., Schmidt, G., Neumann, T., and Hamon, C. (2003). Tandem mass tags: A novel quantification strategy for comparative analysis of complex protein mixtures by MS/MS. Anal. Chem. *75*, 1895–1904.

Tsuboi, T., Kuroha, K., Kudo, K., Makino, S., Inoue, E., Kashima, I., and Inada, T. (2012). Dom34:hbs1 plays a general role in quality-control systems by dissociation of a stalled ribosome at the 3’ end of aberrant mRNA. Mol. Cell *46*, 518–529.

Ude, S., Lassak, J., Starosta, A.L., Kraxenberger, T., Wilson, D.N., and Jung, K. (2013). Translation elongation factor EF-P alleviates ribosome stalling at polyproline stretches. Science *339*, 82–85.

Verma, R., Oania, R.S., Kolawa, N.J., and Deshaies, R.J. (2013). Cdc48/p97 promotes degradation of aberrant nascent polypeptides bound to the ribosome. Elife *2013*, 1–17.

Verma, R., Reichermeier, K.M., Burroughs, A.M., Oania, R.S., Reitsma, J.M., Aravind, L., and Deshaies, R.J. (2018). Vms1 and ANKZF1 peptidyl-tRNA hydrolases release nascent chains from stalled ribosomes. Nature *557*, 446–451.

Voorhees, R.M., Schmeing, T.M., Kelley, A.C., and Ramakrishnan, V. (2010). The mechanism for activation of GTP hydrolysis on the ribosome. Science *330*, 835–838.

Wang, J., Zhou, J., Yang, Q., and Grayhack, E.J. (2018). Multi-protein bridging factor 1(Mbf1), Rps3 and Asc1 prevent stalled ribosomes from frameshifting. Elife *7*.

Wilson, D.N., Arenz, S., and Beckmann, R. (2016). Translation regulation via nascent polypeptide-mediated ribosome stalling. Curr. Opin. Struct. Biol. *37*, 123–133.

Wilson, M.A., Meaux, S., and van Hoof, A. (2007). A genomic screen in yeast reveals novel aspects of nonstop mRNA metabolism. Genetics *177*, 773–784.

Wohlgemuth, I., Brenner, S., Beringer, M., and Rodnina, M. V (2008). Modulation of the rate of peptidyl transfer on the ribosome by the nature of substrates. J. Biol. Chem. *283*, 32229–32235.

Wolff, S., Weissman, J.S., and Dillin, A. (2014). Differential scales of protein quality control. Cell *157*, 52–64.

Yanagitani, K., Imagawa, Y., Iwawaki, T., Hosoda, A., Saito, M., Kimata, Y., and Kohno, K. (2009). Cotranslational Targeting of XBP1 Protein to the Membrane Promotes Cytoplasmic Splicing of Its Own mRNA. Mol. Cell *34*, 191–200.

Yanagitani, K., Kimata, Y., Kadokura, H., and Kohno, K. (2011). Translational Pausing Ensures Membrane Targeting and Cytoplasmic Splicing of XBP1u mRNA. Science *331*, 586–589.

Yonashiro, R., Tahara, E.B., Bengtson, M.H., Khokhrina, M., Lorenz, H., Chen, K.C., Kigoshi-Tansho, Y., Savas, J.N., Yates, J.R., Kay, S.A., et al. (2016). The Rqc2/Tae2 subunit of the ribosome-associated quality control (RQC) complex marks ribosome-stalled nascent polypeptide chains for aggregation. Elife *5*, 1–16.

Yoshida, H., Matsui, T., Yamamoto, A., Okada, T., and Mori, K. (2001). XBP1 mRNA is induced by ATF6 and spliced by IRE1 in response to ER stress to produce a highly active transcription factor. Cell *107*, 881–891.

Zaher, H.S., and Green, R. (2009). Fidelity at the molecular level: lessons from protein synthesis. Cell *136*, 746–762.

Zhou, Z., Dang, Y., Zhou, M., Yuan, H., and Liu, Y. (2018). Codon usage biases co-

evolve with transcription termination machinery to suppress premature cleavage and polyadenylation. Elife *7*.

Zurita Rendón, O., Fredrickson, E.K., Howard, C.J., Van Vranken, J., Fogarty, S., Tolley, N.D., Kalia, R., Osuna, B.A., Shen, P.S., Hill, C.P., et al. (2018). Vms1p is a release factor for the ribosome-associated quality control complex. Nat. Commun. *9*, 2197.

Appendix 1

The table shows tandem mass tag (TMT) mass spectrometry data. The quantitative value for each protein in each sample (in duplicate) is indicated in the first set of columns. Last three columns contain the Log2 values of the ratios between averaged values for indicated conditions.

L eme = treatment with 1.8 µM emetine for 15 min

H eme = treatment with 360 µM emetine for 15 min

Unt = untreated cells (using DMSO vehicle only) for 15 min

Ribosomal proteins are highlighted in light orange and shown at the end of the table

The non-ribosomal protein data are sorted in descending order by the "Log2(AvgL/Unt)" column

Accession	Gene name	L Eme 1	L Eme 2	H Eme 1	H Eme 2	Unt 1	Unt 2	Log2 (AvgL/ AvgUnt)	Log2 (AvgL/ AvgH)	Log2 (AvgH/ AvgUnt)
Q86UK7	ZNF598	69.7	66.3	19.6	23.6	22	17.3	1.79	1.65	0.14
Q96ST3	SIN3A	112.5	190.2	103.3	77.2	57.1	58.4	1.39	0.75	0.64
Q2TAY7	SMU1	208.6	562.9	190.2	163	121.3	178.1	1.37	1.13	0.24
Q9UL40-2	ZNF346	253	517.1	195.6	164	148	203.6	1.13	1.1	0.03
O60869	EDF1	5930.7	5090.5	2424.3	1917.5	2772	2695.2	1.01	1.34	-0.33
Q15393	SF3B3	184.8	349.6	143.4	150	110.5	155.2	1.01	0.87	0.14
O60832	DKC1	215.3	520.6	196	207.6	233.7	186.9	0.81	0.87	-0.06
Q6Y7W6	GIGYF2	3033.2	2872.8	1591.8	1548.1	1753.4	1697.5	0.78	0.91	-0.14
O75179	ANKRD17	107.2	165.1	97.3	86.4	84.5	78.5	0.74	0.57	0.17
P06576	ATP5B	189.8	180	128.4	111.9	97.8	124.1	0.74	0.62	0.11
P49755	TMED10	145.9	291.5	112.9	99.8	143.2	118.8	0.74	1.04	-0.3
Q53RG0	EIF4E	849.6	748.1	579.1	460.1	467	509.4	0.71	0.62	0.09
Q659C4	LARP1B	230.7	389	252.7	206	188.4	194	0.7	0.43	0.26
P79522	PRR3	145.4	182.5	134.4	104	97.6	104.3	0.7	0.46	0.24
P13639	EEF2	30443.7	27558.9	41287.3	43158.7	15940	20074	0.69	-0.54	1.23
Q06265-2	EXOSC9	459.7	753.9	501.4	372.6	353.9	448	0.6	0.47	0.12
P52434-4	POLR2H	107.2	60.9	56.7	59.6	53.3	57.4	0.6	0.53	0.07
V9GZ56	LSM4	231.6	366.6	236.3	191.8	185.4	212.6	0.59	0.48	0.11
P38935	IGHMBP2	222.4	307	186.5	166	188.7	173.8	0.55	0.59	-0.04
Q9NRA8-3	EIF4ENIF1	518.7	675.8	505.5	486.7	405.8	413.1	0.54	0.27	0.28
Q6P158	DHX57	1940.6	1958.3	1793.9	1727.8	1321.9	1395.4	0.52	0.15	0.37
Q7Z460	CLASP1	119.4	137.9	128.8	80.7	83.3	101.7	0.48	0.3	0.18
Q9BTD8	RBM42	571.4	1181.6	654.3	640.8	623.2	636.6	0.48	0.44	0.04
Q9BQG0-2	MYBBP1A	343.3	551.7	368.1	391.8	230.6	420.9	0.46	0.24	0.22
P30153	PPP2R1A	135.5	184.7	133.9	115.5	90.8	143.8	0.45	0.36	0.09
Q9NZM5	GLTSCR2	106	99.1	97.8	75	61.5	91.2	0.43	0.25	0.18
Q9UNQ2	DIMT1	819.4	1146	909	763.1	687	773.1	0.43	0.23	0.2
P55010	EIF5	903.7	924.8	849.4	620.6	627.4	736.9	0.42	0.31	0.11
O75531	BANF1	808.3	847.8	557.7	584.8	680.1	587.7	0.39	0.54	-0.15
Q9UII4	HERC5	547.2	685.3	505.5	461.1	440.2	499	0.39	0.35	0.04

F8VZG9	RBFOX1	157.2	194.6	180.7	151.1	125.2	142.4	0.39	0.08	0.31
F8WB05	ATXN2	39.5	40.2	33.9	29.8	26.9	34.5	0.38	0.32	0.05
P81605-2	DCD	944.6	1185.3	1228.4	876.9	885.5	767.4	0.37	0.02	0.35
Q13618	CUL3	187.8	250.6	177.3	186.9	177.7	164.4	0.36	0.27	0.09
Q13144	EIF2B5	1653.3	2331.8	1711.2	1511.7	1384.5	1727.8	0.36	0.31	0.05
Q9H074	PAIP1	64.8	61.6	79.9	84.2	42	57.8	0.34	-0.38	0.72
J3KTA4	DDX5	1010.7	1617.7	912.6	799.8	1116.2	963.9	0.34	0.62	-0.28
Q9H0A0	NAT10	146.1	143.1	126.1	97.8	101.4	128.8	0.33	0.37	-0.04
O43172	PRPF4	301.9	413.3	275.2	248.5	297.1	276	0.32	0.45	-0.13
A0A024RA52	PSMA2	65.2	57	44.5	35.7	46.1	52.4	0.31	0.61	-0.3
Q8WU90	ZC3H15	389.4	750.1	357	342.9	433.4	487.2	0.31	0.7	-0.4
Q9GZS3	WDR61	111.3	111.9	101.4	92.6	84.7	97.2	0.3	0.2	0.09
Q9Y3Z3	SAMHD1	69.8	90.5	90.3	88.8	68.3	64	0.28	-0.16	0.44
P19388	POLR2E		227.7		153		189.3	0.27	0.57	-0.31
Q13523	PRPF4B	135.7	132.2	100.8	103.5	115.6	106.6	0.27	0.39	-0.12
Q9UBI9	HECA	71	80.9	65.1	54.5	61.5	65.7	0.26	0.34	-0.09
O00505	KPNA3	66.9	71.9	42.5	44.8	51.1	65	0.26	0.67	-0.41
P35250	RFC2	883.2	896.2	749.3	673	682.2	806.5	0.26	0.32	-0.07
Q96T21	SECISBP2	81.4	71	78.1	71.5	61.2	66.1	0.26	0.03	0.23
P08579	SNRPB2	314.4	128.1	238.2	173.2	208.2	162.7	0.25	0.11	0.15
E7EQR4	EZR	204.9	237.7	297.8	165.3	184.1	189.6	0.24	-0.07	0.31
Q15363	TMED2	74.1	80.6	59.3	51.9	57	74.1	0.24	0.48	-0.24
Q9H7E2-3	TDRD3	413.2	609.9	475.6	402.2	408.7	463.1	0.23	0.22	0.01
Q8TDN6	BRIX1	146.1	227.5	150.4	157.4	166.5	152.6	0.23	0.28	-0.05
Q6PGP7	TTC37	293.7	242	278.7	262.9	236.2	219.6	0.23	-0.02	0.25
P31942	HNRNPH3	75.3	95	72.5	65.8	67.6	78.5	0.22	0.3	-0.08
A0A024R4E5	HDLBP	95.3	119.9	102.7	97.9	102.3	82.8	0.22	0.1	0.12
A0A0D9SGE8	PHF6	49.1	35.2	41.4	32.3	31.8	40.5	0.22	0.19	0.03
Q9UKZ1	CNOT11	289.2	393.8	275.7	259.6	285.2	306.7	0.21	0.35	-0.15
Q7L2E3-2	DHX30	3037.5	3466.7	2819.3	2475.7	2679.6	2949	0.21	0.3	-0.09
Q8N3C0	ASCC3	382.8	424.7	353	324.2	361.4	342.9	0.2	0.25	-0.06
O14654	IRS4	247.3	222.5	215.1	168.8	167.2	240.6	0.2	0.29	-0.09
P26368	U2AF2	32.8	51.8	38.9	30.7	37.8	36.4	0.19	0.28	-0.09
P41208	CETN2	169.2	149	117	117.5	122.9	157.2	0.18	0.44	-0.26
P26641	EEF1G	2231.4	3289.5	2182.7	2175.2	2531.6	2332.3	0.18	0.34	-0.16
P60842	EIF4A1	1877.1	2679.9	2268	2114.2	1885.5	2143.1	0.18	0.06	0.12
Q15773	MLF2	174.6	163.5	150	114.3	151.9	147.3	0.18	0.36	-0.18
Q9BYG3	NIFK	610.9	586.4	510.2	523.8	560.3	504.2	0.17	0.21	-0.04
Q9HAN9	NMNAT1	501.8	619.8	484	458.8	484.4	509.8	0.17	0.25	-0.08
P46063	RECQL	336.1	383.4	325	308.1	313.7	330.3	0.16	0.18	-0.02
A0A087WYN9	DHX29	576	628.7	562.9	437.8	560.7	514.7	0.16	0.27	-0.1
Q9NZT1	CALML5	90.6	98.8	118.4	84.7	61.8	107.5	0.16	-0.1	0.26
Q7L2H7	EIF3M	1968.5	2174.7	2068	1922.1	1647.9	2068	0.16	0.05	0.1
Q8N163	CCAR2	596.8	609.6	536.6	451.5	605.6	481.7	0.15	0.29	-0.14
P09661	SNRPA1	594.5	742.9	593.5	520.6	590.1	614.4	0.15	0.26	-0.11
P13010	XRCC5	3512.6	4304.7	3382.1	3312.4	3801.6	3250.9	0.15	0.22	-0.08
P08195-4	SLC3A2	167	190.6	167.6	132.8	173.4	150.1	0.14	0.25	-0.11
E7EQ64	PRSS1	1566.9	1058.4	1173.4	945.9	876.9	1504.7	0.14	0.31	-0.17
Q9Y4Y9	LSM5	462.9	457.2	420.5	367.6	377.9	454.3	0.14	0.22	-0.08
B3KSH1	EIF3F	2244.3	2371.2	2250.8	2165.1	2012.6	2211.2	0.13	0.06	0.06
B0QY89	EIF3L	5940.7	6929.1	6244.8	5870.4	5787.8	5972.7	0.13	0.09	0.04
Q9NUQ6-3	SPATS2L	319.1	323.7	266.7	276.3	315.8	272.9	0.13	0.24	-0.12
P11586	MTHFD1	6027.8	4984.7	5353.8	3800.3	4974.3	5168.6	0.12	0.27	-0.15
Q5SW79	CEP170	302.7	346.6	267.8	237.5	302	295	0.12	0.36	-0.24

P78527	PRKDC	11795.8	13662.4	12348.3	11104.6	11657	11774	0.12	0.12	0
Q00839	HNRNPU	11517.1	12481.6	12530.5	12328.6	11533	10545	0.12	-0.05	0.17
Q9UQ80	PA2G4	14643.4	14444	18177.7	18038.4	13070	13656	0.12	-0.32	0.44
P51149	RAB7A	139.8	174.1	147.1	103.3	180.1	109.7	0.12	0.33	-0.21
P25786-2	PSMA1	445.4	671.4	324.9	274.2	678.9	353.5	0.11	0.9	-0.79
Q7L2J0	MEPCE	269.4	263.8	226.2	229.7	266.4	231	0.1	0.23	-0.13
Q9GZR7	DDX24	1628.8	1918.2	1501.4	1326.8	1666	1649.7	0.1	0.33	-0.23
P05198	EIF2S1	1689.1	2005.2	2050.7	1992.5	1717.1	1729.2	0.1	-0.13	0.23
Q9Y5Q9	GTF3C3	123.4	121.7	113.2	92.1	116.3	112.1	0.1	0.26	-0.15
Q96HR8	NAF1	106	119.6	119.3	119.4	87.1	122.7	0.1	-0.08	0.19
Q12905	ILF2	5608.8	5772.9	5510.8	5131.2	5717.3	4928.1	0.1	0.1	0
Q13347	EIF3I	2956.2	3707.3	2876.2	2662.3	3297	2973.8	0.09	0.27	-0.18
Q13868	EXOSC2	125.5	122.6	118.3	109.9	101.1	131.3	0.09	0.12	-0.03
O43390	HNRNPR	5055.7	5560.1	4881.5	4874.8	5031.3	4942.4	0.09	0.12	-0.03
Q12986	NFX1	268.6	236.9	229.3	186.7	223	250.3	0.09	0.28	-0.19
A0A0A0MRR7	SNRPC	356.5	443.7	412.8	293.8	365.7	383.9	0.09	0.18	-0.09
Q08211	DHX9	7799.5	8759.6	7525.2	6563	8008.9	7672.2	0.08	0.23	-0.15
P18621-3	RPL17	21528.1	23144.7	23118.1	23071	19317	22903	0.08	-0.05	0.13
P42285	SKIV2L2	1342	1661.3	1320	1175.3	1494	1356.8	0.08	0.27	-0.19
O43823	AKAP8	264.8	231.8	213.4	199.1	249.7	224.4	0.07	0.27	-0.2
A5YKK6	CNOT1	4541.6	5587.4	4021.1	3652.8	4710.9	4939.8	0.07	0.4	-0.33
Q9UIV1	CNOT7	372.3	557.9	379.4	347.7	426	457.8	0.07	0.36	-0.28
P42166	TMPO	136.8	159.2	150.4	107.5	123.3	158.1	0.07	0.2	-0.13
Q9UN86	G3BP2	1562.4	1576.3	1455.9	1374.7	1533	1462.3	0.07	0.15	-0.08
P38919	EIF4A3	4623.4	4999.9	4772.1	3957.2	4622.9	4607.4	0.06	0.14	-0.08
Q1KMD3	HNRNPUL2	2468.3	2674.7	2520.6	2174.3	2433.9	2503	0.06	0.13	-0.07
Q53GS9	USP39	404.1	462.9	350.4	316.1	397	436	0.06	0.38	-0.32
P62736	ACTA2	522.8	430.4	465.6	343.7	475	446.1	0.05	0.24	-0.19
O43760-2	SYNGR2	269.1	245	230.8	203.5	283.3	213.5	0.05	0.24	-0.19
Q9UN81	L1RE1	180	145.7	166.9	135.5	155.9	159.6	0.05	0.11	-0.06
Q9UHI6	DDX20	1583	1909.3	1578	1393.4	1610.3	1758.4	0.05	0.23	-0.18
P35998	PSMC2	188.7	202.7	164.3	130.8	219.7	159.9	0.04	0.41	-0.36
P63261	ACTG1	540.4	490.5	492	415.1	545.4	458.1	0.04	0.18	-0.15
P53396	ACLY	280.4	282.1	330.8	324.9	276	270.3	0.04	-0.22	0.26
A0A0D9SF53	DDX3X	109.3	97.2	100.2	86.7	85.1	116	0.04	0.14	-0.11
Q14152	EIF3A	11399.3	13202.2	11916.2	11484.7	12535	11435	0.04	0.07	-0.03
A0A087WUT6	EIF5B	1681.6	1551.4	1449.7	1242.2	1672	1474.5	0.04	0.26	-0.23
P52272	HNRNPM	9991.9	9756.4	10628.1	9969.8	10294	8975.8	0.04	-0.06	0.1
H0YAR2	PABPC1	61.3	55.5	58.3	48.8	55.1	58.5	0.04	0.13	-0.09
Q9UJA5	TRMT6	878.6	890	842.2	827.3	903.2	813	0.04	0.08	-0.04
P68363	TUBA1B	1043	1022.7	960	796.2	1081.8	927.3	0.04	0.23	-0.19
P63104	YWHAZ	2104	1998.5	2571.1	2250.3	1978.1	2046.6	0.03	-0.23	0.26
Q01780	EXOSC10	298.9	312.7	240.5	209	319.1	278.6	0.03	0.44	-0.41
P62847-4	RPS24	5803.1	5607.9	5775	5591.2	5685.5	5463.8	0.03	0.01	0.03
Q9BZE4	GTPBP4	2784.7	2964.2	2930.9	2633.3	2914.1	2700.4	0.03	0.05	-0.01
Q9Y2X3	NOP58	121.7	150.5	139	104.9	126.8	140.3	0.03	0.16	-0.13
P26196	DDX6	2978.8	3479.7	3299.4	3066.9	3289.1	3034.5	0.03	0.02	0.01
O75940	SMNDC1	148.1	131.6	143.3	113.6	112.5	160.6	0.03	0.12	-0.09
P47813	EIF1AX	589.6	629	633.5	544.2	608.6	591.9	0.02	0.05	-0.03
D3DQV9	EIF4G2	2025.3	2449.3	2660.6	2426.6	2060.5	2365.8	0.02	-0.19	0.2
Q12906-7	ILF3	11046.9	11755.2	10817.2	10576.3	12366	10180	0.02	0.09	-0.08
A0A087X2G6	NOP16	387.9	299	344.9	277.4	308.8	367.4	0.02	0.14	-0.12
P20290	BTF3	157.8	172.7	139.2	138.8	151.4	174.6	0.02	0.25	-0.23
A0A087WV05	4	672.8	715.5	648.3	681.5	712.7	658.7	0.02	0.06	-0.04

P12956	XRCC6	3451.2	3990.8	3920.9	3652.1	3991.8	3361.9	0.02	-0.03	0.04
O00148	DDX39A	362.8	410.4	337	275.2	428.1	337.5	0.01	0.34	-0.32
A0A0A0MRX1	ELAVL2	525.5	653.6	539.6	470.3	585.4	582.2	0.01	0.22	-0.21
Q99613	EIF3C	5658.4	6790.9	5955.6	5921.3	6513.1	5862.9	0.01	0.07	-0.06
F8W930	IGF2BP2	1278.3	1446.2	1284.6	1173.8	1438.4	1264.5	0.01	0.15	-0.14
Q13823	GNL2	655	741.6	637.9	506	638.6	748.6	0.01	0.29	-0.28
O00567	NOP56	105.7	105.3	110.4	79.8	105	105.2	0.01	0.15	-0.14
O75643	SNRNP200	4420.3	4732.3	4080.2	3402.8	4565.2	4553.2	0.01	0.29	-0.29
P31946	YWHAB	1024.9	1017.1	1235.1	1130.4	953.6	1081.5	0	-0.21	0.22
Q92600	RQCD1	818.4	919.9	736	711.6	791.3	945.7	0	0.26	-0.26
A0A0U1RQC9	TP53	84.3	94.8	84.7	59.5	83.9	95.6	0	0.31	-0.32
Q14677-3	CLINT1	2505.7	3356.4	2582.7	2508.8	3147.7	2708.2	0	0.2	-0.2
Q04637-8	EIF4G1	7933.4	9550.8	10727.4	10647.8	8554.9	8965.2	0	-0.29	0.29
A0A087WXF8	ZCCHC17	114.5	104.5	95.2	86	112.9	106.4	0	0.27	-0.28
Q8IZL8	PELP1	1015.2	1266.6	1041.9	838.3	1095.9	1188.6	0	0.28	-0.28
Q9UKV8	AGO2	645.4	649.7	630.3	525.6	697.2	598.1	0	0.16	-0.16
Q96A72	MAGOHB	1909.8	2248.9	2230.2	1916.8	1978.7	2192	0	0	-0.01
Q7Z2T5	TRMT1L	1528.3	1671.4	1484.3	1534.4	1808.6	1395.1	0	0.08	-0.09
P60228	EIF3E	3045.5	3152.5	3063.8	2961.6	3211.5	3038.7	-0.01	0.04	-0.05
O15234	CASC3	197.6	205.7	232.2	215.8	196.9	209.7	-0.01	-0.15	0.14
P63244	RACK1	26080.9	25408.6	25428	24771.1	26467	25415	-0.01	0.04	-0.05
M0R2Z9	SUGP2	408.8	375	352.9	289.2	378.4	410	-0.01	0.29	-0.3
Q9H0U9	TSPYL1	148.1	157.5	147.8	123.4	176.6	130.1	-0.01	0.17	-0.18
P61981	YWHAG	544.1	583.5	718.1	630.2	582.8	559.2	-0.02	-0.26	0.24
O95793	STAU1	9706.2	9464.9	9017.8	9089.3	9893.4	9513.2	-0.02	0.08	-0.1
Q9BVP2	GNL3	5299.8	5830.8	5391.2	4897.5	5982.5	5335.6	-0.02	0.11	-0.14
Q9UQ80-2	PA2G4	577	369.4	683.5	507.4	428.4	530.2	-0.02	-0.33	0.31
P14678-3	SNRPB	281.2	384.7	250	202.1	389.7	283.4	-0.02	0.56	-0.57
Q92615	LARP4B	6111.8	6654.1	5945.7	5909.2	6895	6037.7	-0.02	0.11	-0.13
Q9HCS7	XAB2	206.8	176.6	190.8	185.4	204.1	184.1	-0.02	0.03	-0.05
Q99471	PFDN5	102.2	97	81.2	86.4	89.7	112.8	-0.02	0.25	-0.27
A0A087WVQ6	CLTC	10445.7	11006.2	9756.3	9118.1	11254	10585	-0.03	0.18	-0.21
E9PAV3	NACA	895.2	787	759.5	688.3	746.9	971.3	-0.03	0.22	-0.25
A0A0C4DG89	DDX46	319.9	269.5	282.2	219.1	311.7	288.8	-0.03	0.23	-0.26
D6RF23	RACK1	469.4	414.8	501.3	345.7	388.6	512.4	-0.03	0.06	-0.09
Q96PK6	RBM14	436.5	367.1	393.4	306.5	455	365.4	-0.03	0.2	-0.23
P49458	SRP9	897.1	1068.5	849.7	808.4	1109.6	899.9	-0.03	0.25	-0.28
Q5R363	SRPK1	3168.8	3574.3	3181.1	3130.8	3205.8	3684.7	-0.03	0.1	-0.13
Q7KZF4	SND1	483.4	424.9	460.4	409.8	498	428.2	-0.03	0.06	-0.09
Q08J23	NSUN2	4705.3	5689.4	5392.6	5174.6	5424.9	5151.7	-0.03	-0.02	0
A0A0B4J220	C11orf98	963.2	710.7	848.6	649.7	915	804.5	-0.04	0.16	-0.2
Q92522	H1FX	652.4	661.7	721.2	542.6	682.4	666.4	-0.04	0.06	-0.09
Q9NW64	RBM22	293.7	270.4	246.4	202.2	282.5	298.5	-0.04	0.33	-0.37
Q9H4L4	SENP3	135.4	194.1	140.5	120.2	165.3	172.3	-0.04	0.34	-0.37
Q99832	CCT7	733.5	683.7	639.4	582.4	792.4	665.7	-0.04	0.21	-0.26
B3KY60	2	2038.7	2040.4	1883.6	1739.4	2114.9	2093.9	-0.05	0.17	-0.22
P55884-2	EIF3B	6349.2	6602.5	6213.7	6044.7	6752.3	6647.2	-0.05	0.08	-0.13
Q9BY77	POLDIP3	735.6	700.8	585.2	534.2	689.4	802.3	-0.05	0.36	-0.41
A0A0U1RRM4	PTBP1	2118.2	2046.5	2006.8	1948.3	2259.7	2041	-0.05	0.07	-0.12
Q9NY93	DDX56	95.7	75.5	78.1	69.8	99.7	78.1	-0.05	0.21	-0.27
Q9BRT6	LLPH	563	454.3	533.7	441.8	572	484.1	-0.05	0.06	-0.11
Q5T1Z8	PUM1	1184.6	1498.8	1143.3	1095.5	1466.6	1302.9	-0.05	0.26	-0.31
P62820	RAB1A	521.6	697	510.7	396.4	756.8	502.3	-0.05	0.43	-0.47
Q14232	EIF2B1	534.9	449.7	517.8	487.6	459.4	559	-0.05	-0.03	-0.02

E7ERK9	EIF2B4	287.7	220.6	268	239.7	251.7	274.5	-0.05	0	-0.05
O75821	EIF3G	2284.3	2523.2	2414.6	2323	2618.1	2403.5	-0.06	0.02	-0.08
Q08945	SSRP1	182.7	178.5	178.3	151.1	177.9	199.7	-0.06	0.13	-0.2
O75934	BCAS2	460.5	461.2	499.4	380.5	489.8	472	-0.06	0.07	-0.13
P40937	RFC5	218.7	235.5	232.7	197.3	248.2	223.8	-0.06	0.08	-0.13
Q00577	PURA	1548.7	1507.9	1546.1	1466.9	1671.3	1514.5	-0.06	0.02	-0.08
P08621	SNRNP70	897.6	973.2	786.4	795.3	966.5	982.5	-0.06	0.24	-0.3
P62258	YWHAE	2938.5	3431.9	4003.3	3546.9	3516.3	3186.6	-0.07	-0.25	0.17
Q9UBQ5	EIF3K	1716.1	1644.1	2166.2	1700.4	1791.5	1724.4	-0.07	-0.2	0.14
P13807	GYS1	23407.6	14315	10704.4	9560.2	22156	17557	-0.07	0.9	-0.97
A0A0G2JIW1	HSPA1B	1144.9	1248.1	1100.7	903.3	1397.8	1119.1	-0.07	0.26	-0.33
Q15717-2	ELAVL1	2798.7	2878.3	2800.1	2604.4	3115.4	2862.9	-0.07	0.07	-0.15
O43399-7	TPD52L2	493.1	411.5	448.5	315	442.7	505.8	-0.07	0.24	-0.31
Q09161	NCBP1	322.7	328.4	394.9	341.1	331.2	354.2	-0.07	-0.18	0.1
Q9BZI7	UPF3B	290.7	271.1	315.8	289.5	299.4	289.4	-0.07	-0.11	0.04
O75533	SF3B1	880.3	965	867.3	717	905.7	1027.9	-0.07	0.22	-0.29
P62979	RPS27A	2706.4	2460.6	2595	2505.5	2971.5	2462.3	-0.07	0.02	-0.09
Q96KR1	ZFR	1392.4	1320.3	1507.8	1138.9	1561	1293.9	-0.07	0.04	-0.11
Q9H2U1	DHX36	961.5	1048	1000.8	994.3	1047.8	1073.1	-0.08	0.01	-0.09
P62913-2	RPL11	96.5	87.3	122.6	124.7	76	118.4	-0.08	-0.43	0.35
B3KT93	2	17550.3	17843	19173.5	18743.9	19450	17895	-0.08	-0.1	0.02
P35249	RFC4	685.7	587.9	570.5	514.3	653.7	689.2	-0.08	0.23	-0.31
E9PAU2	RAVER1	363.8	460.3	363	305.3	503	366.6	-0.08	0.3	-0.38
Q6NZY4	ZCCHC8	59.6	52.7	63.3	61.9	54.6	64	-0.08	-0.16	0.08
P04406	GAPDH	2974.4	1505.2	1365.3	1122.2	3101.8	1652.3	-0.09	0.85	-0.93
O60506	SYNCRIP	19778.1	22737.4	22672.9	23328.6	23133	22275	-0.09	-0.11	0.02
A0A0A0MR39	MYEF2	151.3	176.8	174.4	145.1	178.7	169.5	-0.09	0.04	-0.12
Q9UMS4	PRPF19	2617.4	2781.5	2639	2310.8	3047.3	2694.6	-0.09	0.13	-0.21
Q8NI27	THOC2	593.8	687.9	618.2	525.9	649	710.5	-0.09	0.16	-0.25
C9J6P4	ZC3HAV1	948	1076.8	956.8	926.7	1101.8	1054.8	-0.09	0.1	-0.2
Q9NUD5	ZCCHC3	565.8	596	589.7	510.1	631.1	601.9	-0.09	0.08	-0.16
A0A0U1RQK7	EIF4G3	745.6	599.3	678.7	544.3	687.2	749.6	-0.1	0.14	-0.23
Q13243	SRSF5	129	141.5	133	119.8	155.6	133.9	-0.1	0.1	-0.2
Q9Y224	C14orf166	3034.5	3582.1	3746.4	3518.4	3422.1	3673.3	-0.1	-0.13	0.03
P60709	ACTB	662.4	587.7	630	475	745	605.1	-0.11	0.18	-0.29
Q7Z6E9	RBBP6	96.3	83.4	91.7	76	91.9	102.1	-0.11	0.1	-0.21
P84090	ERH	1535.3	1756.7	1437.9	1064.9	1911.3	1645.5	-0.11	0.4	-0.51
P11142	HSPA8	1859.2	2174.6	1953.7	1673.3	2345.9	2007.9	-0.11	0.15	-0.26
Q13151	HNRNPA0	1400.9	1361	1403.8	1147.6	1594.6	1391.5	-0.11	0.11	-0.23
P52597	HNRNPF	526.6	546.1	459.8	403.3	631.7	528	-0.11	0.31	-0.43
Q9BUJ2	HNRNPUL1	213.8	195.4	229.3	260.4	242.2	198.6	-0.11	-0.26	0.15
Q8N5L8	RPP25L	80.8	75.6	103	77.6	77.8	91.1	-0.11	-0.21	0.1
P12277	CKB	696.6	534.8	544.4	411.8	733.4	606	-0.12	0.36	-0.49
P06730-2	EIF4E	1189	1073.5	1307.2	1224.4	1255.3	1201.2	-0.12	-0.16	0.04
Q15366-3	PCBP2	1047.8	1184.2	1187.3	1054.1	1282.2	1151	-0.12	-0.01	-0.12
Q13428-4	TCOF1	2465.9	2181.8	2112.7	1942.5	2713.1	2323.5	-0.12	0.2	-0.31
O75494	SRSF10	344.1	351.8	326.6	287.6	372.5	384.2	-0.12	0.18	-0.3
Q6P2Q9	PRPF8	3340.2	3499.9	3009.8	2660	4068.4	3433.1	-0.13	0.27	-0.4
P78371	CCT2	776.2	804.1	716.5	600.2	931.2	794.1	-0.13	0.26	-0.39
Q9Y2W1	THRAP3	1317.4	1461.2	1251.2	989.2	1672.5	1367.9	-0.13	0.31	-0.44
O43395	PRPF3	156.5	173.2	152.3	127.2	194.6	165.2	-0.13	0.24	-0.36
P27348	YWHAQ	161.1	184	210.3	185.6	176.3	204.6	-0.14	-0.2	0.06
S4R3H4	ACIN1	1556.7	1916.1	1433.9	1309.7	2034.3	1795	-0.14	0.34	-0.48
Q9H9A5	CNOT10	691.5	702.5	626.6	594.9	767.6	770.1	-0.14	0.19	-0.33

O00425	IGF2BP3	6977.5	8049.1	7092	6867.5	8726.4	7857.9	-0.14	0.11	-0.25
O60306	AQR	159.3	111.3	139.4	114.7	151.2	147.6	-0.14	0.09	-0.23
Q07666	KHDRBS1	767.9	903.1	719.6	649.6	1006.6	835.9	-0.14	0.29	-0.43
Q5JSZ5	PRRC2B	1069.4	1005.4	1085.6	1045.5	1190.8	1091.7	-0.14	-0.04	-0.1
O75817	POP7	195.7	153.8	128.6	174.7	221	164.4	-0.14	0.2	-0.35
Q9Y4W2	LAS1L	402.8	380.9	364.3	302.3	424.9	441.2	-0.14	0.23	-0.38
Q15287	RNPS1	462.5	388	384.5	348.3	431.9	507.4	-0.14	0.21	-0.36
Q15427	SF3B4	61.1	61.8	53.4	52.6	70.3	65	-0.14	0.21	-0.35
Q15650	TRIP4	143.9	122.4	138.9	137.6	152	142.6	-0.15	-0.05	-0.09
O15371	EIF3D	3605.3	3761.1	3838.8	3770.7	4346	3845.9	-0.15	-0.05	-0.11
O14893	GEMIN2	762.3	737.8	729.9	645.2	824.9	845.2	-0.15	0.13	-0.28
P57678	GEMIN4	1703.8	1665.7	1717.6	1527.5	1763.5	1983.4	-0.15	0.05	-0.21
P52292	KPNA2	241.6	271.7	229.1	205.2	345	225.4	-0.15	0.24	-0.39
O43143	DHX15	714.3	724.9	669.6	600.3	848.3	747.1	-0.15	0.18	-0.33
Q9UKM9	RALY	1509.3	1646.4	1439.8	1240.5	1910.5	1582.6	-0.15	0.24	-0.38
Q9Y3B4	SF3B6	142.3	125.9	128.6	120.6	138	160.3	-0.15	0.11	-0.26
P40227	CCT6A	1039.3	1140.6	902.4	788.9	1454	968.8	-0.15	0.37	-0.52
Q96FX7	TRMT61A	75.1	69	81.7	87.2	78.4	81.5	-0.15	-0.23	0.08
Q5BKZ1	ZNF326	186.7	199.4	182.9	149.9	227.8	203.1	-0.16	0.21	-0.37
Q99453	PHOX2B	131.8	94.3	110.6	80.5	131.2	120.8	-0.16	0.24	-0.4
Q9NVU7	SDAD1	229.1	254.1	283.2	224.4	282.1	259.5	-0.16	-0.07	-0.09
Q13435	SF3B2	1030.5	1112.3	921.4	822	1371.2	1025.5	-0.16	0.3	-0.46
B3KMB1	SMC	252.8	211.5	226.7	163.8	269.5	248.9	-0.16	0.25	-0.41
Q9NXF1	TEX10	879.8	939.9	813.5	682.4	997.4	1041.1	-0.16	0.28	-0.45
Q8IZH2	XRN1	373.6	393	331.3	310.1	464.4	399.3	-0.17	0.26	-0.43
Q99700	ATXN2	1031.5	1091.6	1086.5	1074	1229.7	1152.4	-0.17	-0.03	-0.14
P80723	BASP1	102.7	82.8	91.6	58.4	107.4	100.8	-0.17	0.31	-0.47
A0A0A0MTC5	STAU2	1215.2	1109	1047.7	1012.9	1431.1	1178.4	-0.17	0.17	-0.34
Q9H840	GEMIN7	110.6	89.4	102.2	89.4	89.6	136	-0.17	0.06	-0.24
P14866	HNRNPL	4729.1	7455.5	4428.8	4277.4	8027.3	5691.1	-0.17	0.48	-0.66
X6RAL5	SAP18	397	429.2	405.6	334.7	523.8	406.5	-0.17	0.16	-0.33
A8MXP9	MATR3	6844.2	7045.9	5990.7	5363.4	8395.9	7271.6	-0.17	0.29	-0.46
B1AHD1	SNU13	125.2	133.2	147.6	120.1	145.7	145.2	-0.17	-0.05	-0.12
Q15154	PCM1	1806.1	1862.6	1575.2	1369.7	2275.5	1841	-0.17	0.32	-0.48
Q9NSD9	FARSB	1072.7	1259.9	1645	1407.4	1219	1398.7	-0.17	-0.39	0.22
O76021	RSL1D1	1266.5	1262.8	1348.3	1340.1	1546.2	1299.7	-0.17	-0.09	-0.08
P62136-2	PPP1CA	143.9	170.2	157.9	158.9	171.6	185.4	-0.18	-0.01	-0.17
Q8WYQ5	DGCR8	292.2	280.3	337.8	260	363.1	285	-0.18	-0.06	-0.12
Q9BU76	MMTAG2	252.9	176.6	182.8	163.5	236.1	249.7	-0.18	0.31	-0.49
A0A087WX23	PEG10	264.8	286.9	251.3	240.5	327.6	296.7	-0.18	0.17	-0.34
Q9Y265	RUVBL1	1612.6	1758.2	1529.7	1351.2	2079.4	1736.4	-0.18	0.23	-0.41
P35030	PRSS3	1006.9	669.8	635.9	540.3	954.9	947	-0.18	0.51	-0.69
O75152	ZC3H11A	759	914.8	791.2	675.3	1029.3	869.8	-0.18	0.19	-0.37
Q13310-3	PABPC4	11484.3	10938.1	12617.7	12777.5	13718	11812	-0.19	-0.18	-0.01
Q13427	PPIG	197.3	184.7	197	148.3	220.2	214.7	-0.19	0.15	-0.33
Q8ND56	LSM14A	1233.6	1199.7	1273.3	1216.1	1527.8	1250	-0.19	-0.03	-0.16
P48634	PRRC2A	2184.8	2411.5	2309.2	2331.2	2867.3	2359.1	-0.19	-0.01	-0.17
P22087	FBL	2408	2248.5	2058.4	1899.7	2807.1	2504.3	-0.19	0.23	-0.42
P51991	HNRNPA3	1223.9	1481	1393.9	1299.4	1715.2	1395.3	-0.2	0.01	-0.21
P78362-2	SRPK2	374.8	393.8	422.4	332.2	456.3	425.9	-0.2	0.03	-0.23
O00410-3	IPO5	63.8	86.1	77.4	73.4	66.8	105.2	-0.2	-0.01	-0.19
P07195	LDHB	198.4	192	122.3	117.4	294.9	154.5	-0.2	0.7	-0.91
Q13573	SNW1	395.6	416.1	361.9	337.9	494.5	440.7	-0.2	0.21	-0.42
U3KQP1	ASNSD1	150.6	190.7	142.8	134.5	207.8	186	-0.21	0.3	-0.51

Q96CT7	CCDC124	1725.8	1886.8	1621.4	1410.1	2166.5	2018.3	-0.21	0.25	-0.47
Q14694-2	USP10	2155.8	2302.4	2386.7	2222.7	2532.8	2623.1	-0.21	-0.05	-0.16
Q15365	PCBP1	445.7	413.9	459.3	401	453	540.9	-0.21	0	-0.21
Q9H6S0	YTHDC2	942.5	1026.2	972.5	955.2	1132.2	1148.9	-0.21	0.03	-0.24
Q6ZN17	LIN28B	454.5	439.5	518.6	513.3	558.8	475.4	-0.21	-0.21	0
Q96MX6	WDR92	118.7	65.8	62.9	57.5	149.6	64.3	-0.21	0.62	-0.83
P16989	YBX3	2800.7	2880.6	2791.4	2699.7	3610.7	2940.7	-0.21	0.05	-0.25
P22626	HNRNPA2B1	2343.6	2618.3	2748.6	2051.2	3170.2	2607.8	-0.22	0.05	-0.27
Q9NZI8	IGF2BP1	11122	11393	11873	11237	13833	12400	-0.22	-0.04	-0.18
Q99729-3	HNRNPAB	3043.2	4163.1	4257.4	4068.8	4400.4	3985	-0.22	-0.21	-0.01
Q9NZB2-6	FAM120A	3763.8	4218.8	3863.2	3503.8	4950.8	4357.3	-0.22	0.12	-0.34
Q9H307	PNN	1309.2	1277.4	1202.8	1114.5	1551.5	1459.8	-0.22	0.16	-0.38
H3BLZ8	DDX17	208.7	261.4	245.8	204.1	270.3	275.6	-0.22	0.06	-0.28
Q96GQ7	DDX27	402.1	427.2	419.3	365.1	506	462.5	-0.22	0.08	-0.3
J3QS41	HELZ	714.6	628.4	647.8	604.6	811	754.9	-0.22	0.1	-0.32
P49756	RBM25	488.3	472.5	411	371.3	613.9	507.8	-0.22	0.3	-0.52
Q15459	SF3A1	419.8	419.7	361.9	312.3	510	470.7	-0.22	0.32	-0.54
P26640	VARS	198.7	201.5	222.9	196.5	235	230.4	-0.22	-0.07	-0.15
A0A087WW66	PSMD1	40.3	30.2	34.3	32.4	40.9	41.5	-0.23	0.08	-0.3
H7C2Q8	EBNA1BP2	229.1	367.2	337.7	295.9	327.3	374.3	-0.23	-0.09	-0.15
P46976	GYG1	2435.7	1994	1599.4	1312.3	2862.3	2345.7	-0.23	0.61	-0.84
P05556-3	ITGB1	197.8	227.5	224.2	158	307.9	189.3	-0.23	0.15	-0.38
Q9NW13	RBM28	1111.8	1096.9	1439.7	1393.5	1367.9	1221.9	-0.23	-0.36	0.13
Q12874	SF3A3	157.8	132.7	126.3	128.8	172.5	168.6	-0.23	0.19	-0.42
P51116	FXR2	1987.1	1892	1917.4	1883	2479.7	2095.6	-0.24	0.03	-0.27
Q71RC2-4	LARP4	2910.6	2827	2936.5	2752.4	3618.3	3147.5	-0.24	0.01	-0.25
P09496-2	CLTA	1007.4	929.9	989.2	1064.2	1128.4	1153.8	-0.24	-0.08	-0.15
Q8NCA5	FAM98A	1655.5	1641.7	1733.6	1529.3	1985.6	1911.2	-0.24	0.02	-0.26
Q6I9Y2	THOC7	286	277.3	231.2	237.6	355	309.8	-0.24	0.26	-0.5
O75396	SEC22B	135.1	139.8	103.2	81.9	175.4	148.9	-0.24	0.57	-0.81
Q9NYF8	BCLAF1	1602.6	1454.8	1704.1	1224.9	1968.1	1673.9	-0.25	0.06	-0.31
P20645	M6PR	1081.7	846.4	915.1	761	1252.4	1048.1	-0.25	0.2	-0.46
P10412	HIST1H1E	3565.5	3363.4	2620.9	2012.9	4651.1	3564.8	-0.25	0.58	-0.83
P07910-2	HNRNPC	10380	12010.3	9763.2	8738.7	15286	11288	-0.25	0.28	-0.52
Q8IY81	FTSJ3	99.5	79.9	80.7	66.4	106.9	105.9	-0.25	0.29	-0.53
Q99436	PSMB7	564.5	403.2	391	340.5	662.2	487.8	-0.25	0.4	-0.65
P09651	HNRNPA1	689.8	751.2	753.3	664.7	882	848.5	-0.26	0.02	-0.29
Q14103	HNRNPD	1369.2	1854.9	2068.7	2008.4	1986.6	1877.5	-0.26	-0.34	0.08
Q8WWM7-3	ATXN2L	3945.4	4494.6	4206.8	4178.9	5445	4644	-0.26	0.01	-0.27
F8VZQ9	SARNP	235.3	194.2	197.1	167.1	287.4	228.5	-0.26	0.24	-0.5
Q06787	FMR1	1857.7	1749.4	1966.2	1860	2266.1	2042.9	-0.26	-0.09	-0.17
Q15029	EFTUD2	4360.6	3523.9	3338.8	2808.4	5743.4	3783.4	-0.27	0.36	-0.63
E9PRY8	EEF1D	179.9	170.7	193.8	172.2	203.8	218.8	-0.27	-0.06	-0.21
P41091	EIF2S3	1600.8	1766.8	2074	2078.8	2193.2	1878	-0.27	-0.3	0.03
Q8TEQ6	GEMIN5	2365.5	2445.1	2406.1	2205.8	2944.9	2860.8	-0.27	0.06	-0.33
F8W8D3	SLBP	79.6	60	61.8	70.3	86.9	81.1	-0.27	0.08	-0.35
O75569	PRKRA	458.9	447.4	496.9	463	591.2	498.8	-0.27	-0.08	-0.18
O14979-2	HNRNPDL	1180.2	1453	1704.6	1576.6	1611.9	1566.4	-0.27	-0.32	0.05
P61978-2	HNRNPK	2895.2	3384.1	3117.6	2930	4258.8	3328.3	-0.27	0.05	-0.33
Q14157-5	UBAP2L	1984.6	1765.8	2086.9	2149.1	2453.6	2082.3	-0.27	-0.18	-0.1
Q6PKG0	LARP1	12117.3	10728.2	11533.2	11264.4	14547	12952	-0.27	0	-0.27
Q9NPI6	DCP1A	301	367.1	268.2	240.7	401	403.9	-0.27	0.39	-0.66
P84103	SRSF3	1031.9	1238	962.9	803.6	1444.5	1294.8	-0.27	0.36	-0.63
B3KS98	EIF3H	1266.5	1245	1452.8	1467.9	1751.3	1296.5	-0.28	-0.22	-0.06

Q9BQ67	GRWD1	283.6	271.9	296.3	272.4	352.4	322.5	-0.28	-0.03	-0.25
Q9H361	PABPC3	578.1	482	624.2	613.8	729.3	557.8	-0.28	-0.22	-0.06
P14618	PKM	2576.7	1585.4	1463.6	1199.3	3261.3	1785	-0.28	0.64	-0.92
E7EQZ4	SMN1	614.7	534.3	559.2	543	728.1	663.3	-0.28	0.06	-0.34
Q13769	THOC5	146.9	135.4	118.9	104.6	187.9	154.3	-0.28	0.34	-0.61
P49770	EIF2B2	224.8	230.6	275.3	292.3	258.5	294.7	-0.28	-0.32	0.04
P06733	ENO1	4317.2	2636	2499.8	2178.2	5260.9	3246.5	-0.29	0.57	-0.86
P05023	ATP1A1	1023.7	999.4	1204.9	903.6	1375.2	1096.5	-0.29	-0.06	-0.23
Q9Y3I0	RTCB	3869.7	4002.5	5084.3	4174	4930.7	4668.8	-0.29	-0.23	-0.05
Q8N6T3-2	ARFGAP1	202.2	165.4	199.3	156.2	243.6	209.5	-0.3	0.05	-0.35
Q9Y3Y2-3	CHTOP	800.9	854.2	821	708.1	1075	957.3	-0.3	0.11	-0.41
O94906	PRPF6	1265.6	1210.6	1114.7	993.6	1612.3	1441.7	-0.3	0.23	-0.53
Q9HCE1	MOV10	2408.6	2290.6	2399.6	2274.7	3027.1	2742.8	-0.3	0.01	-0.3
Q13247	SRSF6	354.9	295.4	305.5	275.9	473.1	326.6	-0.3	0.16	-0.46
Q92499	DDX1	3714.9	3849.3	4193.5	4047.6	4758.7	4630.3	-0.31	-0.12	-0.19
A0A0J9YX62	DNAJB6	75.9	59.6	79.8	61.2	87.7	80.4	-0.31	-0.06	-0.25
G8JLB6	HNRNPH1	1013.1	1033	1044.4	946.5	1419.8	1119.8	-0.31	0.04	-0.35
O15173-2	PGRMC2	190.3	206.8	220.6	168.8	259.2	232.1	-0.31	0.03	-0.34
Q9Y520-7	PRRC2C	6710.4	7803.3	6496	6353.4	9223.1	8764.1	-0.31	0.18	-0.49
J3KTL2	SRSF1	1269.3	1269.5	1335.7	949.3	1738.3	1413.8	-0.31	0.15	-0.46
Q5VZU9	TPP2	5134.4	4578.4	4262.1	3452.7	6388.5	5614	-0.31	0.33	-0.64
P08670	VIM	4719.5	5116.2	4745.3	3940.9	7189.2	4979.5	-0.31	0.18	-0.49
Q9H0D6	XRN2	1142.3	1131.2	1224.3	1092	1503.2	1331.4	-0.32	-0.03	-0.29
Q9Y3X0	CCDC9	379	350.3	392.9	380.6	544.4	365.8	-0.32	-0.08	-0.23
P55265-4	ADAR	1989.4	1720.9	1753.7	1344.7	2539.5	2097	-0.32	0.26	-0.58
P06748	NPM1	4324.8	4503.5	5225.7	4811.3	5634.4	5374.4	-0.32	-0.19	-0.13
Q9Y3C6	PPIL1	113.5	99.5	117.3	81.6	137.7	128.4	-0.32	0.1	-0.42
Q9Y5S9	RBM8A	1394.9	1767.8	1638.5	1627.3	2167.5	1779.2	-0.32	-0.05	-0.27
P54709	ATP1B3	163.4	144.8	191	118.9	193.4	190.2	-0.32	-0.01	-0.31
Q13200	PSMD2	216.3	139.4	155.4	130.4	242.9	203.1	-0.33	0.32	-0.64
P20042	EIF2S2	2888	3104.6	4226.9	4415.7	4019.8	3521.8	-0.33	-0.53	0.2
P62805	HIST1H4A	50.7	75.8	60.9	60.8	78.4	81.1	-0.33	0.06	-0.39
Q9UHX1	PUF60	136.3	120.4	110	85.7	182.3	139.7	-0.33	0.39	-0.72
Q9BUQ8	DDX23	663.3	559.3	580.5	531.1	799.7	739.8	-0.33	0.14	-0.47
Q9BZK3	NACAP1	145.5	148.5	147.5	155.2	195.3	173.1	-0.33	-0.04	-0.28
P35251	RFC1	327.9	311.2	341.9	315.5	451.7	349	-0.33	-0.04	-0.28
P38159	RBMX	1721.5	1996.1	1573.9	1534.3	2840.9	1819.6	-0.33	0.26	-0.58
A9Z1X7	SRRM1	841.6	850.9	820	696.1	1126.1	1006.2	-0.33	0.16	-0.49
P68104	EEF1A1	1106.8	1190.6	1185.7	1189.9	1647.7	1265.1	-0.34	-0.05	-0.29
Q6P2E9	EDC4	3938.9	4364.5	3152.4	2812.9	5373.3	5120.6	-0.34	0.48	-0.81
O15226-2	NKRF	483.1	429.1	436	404.5	687.7	467	-0.34	0.12	-0.46
Q9BWF3	RBM4	172.4	157.9	167.2	143.2	244.7	174.2	-0.34	0.09	-0.43
P37108	SRP14	786.9	1004.2	968.4	958.9	1310.2	960.7	-0.34	-0.11	-0.24
P62158	CALM1	634.6	693.7	675.7	511.4	887.9	802.5	-0.35	0.16	-0.51
Q96I24	FUBP3	109.6	93.4	99.8	99.3	137.3	120.9	-0.35	0.03	-0.37
P05455	SSB	2426.7	2495.9	2718.7	2664.8	3042.4	3235.2	-0.35	-0.13	-0.22
Q15758	SLC1A5	384.3	328.8	388.9	359.3	537.4	373.2	-0.35	-0.07	-0.28
P62191	PSMC1	163.2	131.1	249.8	121.3	203.2	175.5	-0.36	-0.33	-0.03
Q9NX58	LYAR	154.4	139	139.7	116.7	220.8	156.3	-0.36	0.19	-0.56
P09497-2	CLTB	345.4	392.3	358.8	368.7	549.7	397.5	-0.36	0.02	-0.38
Q9BXP5	SRRT	232.7	236.8	239.4	233	326.6	275.7	-0.36	-0.01	-0.35
P62306	SNRPF	162.9	204.2	191.9	175.4	250.3	219.4	-0.36	0	-0.35
E9PB61	ALYREF	2040.7	1978.8	2070.8	1930.1	2839.5	2326.5	-0.36	0.01	-0.37
P62987	UBA52	42.2	42.3	63.5	60.2	42.1	66.2	-0.36	-0.55	0.19

Q9BRJ6	C7orf50	875.6	947.2	1068.1	1010.8	1224.4	1115	-0.36	-0.19	-0.17
P27797	CALR	277.5	198.4	223.3	172.7	300.8	313.7	-0.37	0.27	-0.63
Q3KQU3	MAP7D1	151.9	147.9	159.1	138.4	228.1	160.5	-0.37	0.01	-0.39
O43660	PLRG1	86.4	72.8	72.8	78.2	115.9	90.3	-0.37	0.08	-0.45
Q9BX40	LSM14B	220	189.3	209.9	212.5	289.9	238	-0.37	-0.05	-0.32
P62316	SNRPD2	577.7	503.5	519.9	487.2	759.3	639	-0.37	0.1	-0.47
P23246	SFPQ	281.4	241.7	242.6	199.3	363.4	313.3	-0.37	0.24	-0.61
Q8WWY3	PRPF31	61.5	59.2	55.6	46.8	94.5	61	-0.37	0.24	-0.6
B3KTL8	YTHDF1	295.6	343.6	348.5	348.6	469.7	361.5	-0.38	-0.13	-0.25
P07355-2	ANXA2	377.4	354.2	394.2	333	499.6	453.6	-0.38	0.01	-0.39
O14828	SCAMP3	264	271	266.1	205.9	415.8	280.7	-0.38	0.18	-0.56
Q9BV38	WDR18	302.2	303.2	310.3	262	451.8	335.8	-0.38	0.08	-0.46
Q9BZJ0	CRNKL1	572.7	543.3	533.5	472.2	812	645.6	-0.39	0.15	-0.54
Q9H0U4	RAB1B	436	437.4	417.6	326.2	752.5	394	-0.39	0.23	-0.62
P48643	CCT5	618.3	718	604.5	523.4	1175.8	575.4	-0.39	0.24	-0.63
O43290	SART1	499.7	503.6	527.8	469.2	684.2	632.5	-0.39	0.01	-0.4
P51114	FXR1	361.1	283.2	318.6	333.4	447.8	400	-0.4	-0.02	-0.38
Q7Z417	NUFIP2	4079.8	3968.9	4382.7	4337.1	5907	4741.9	-0.4	-0.12	-0.29
Q9NR30	DDX21	3614.2	3368.6	3665	3314.3	5321.8	3860.3	-0.4	0	-0.4
Q9BPZ3	PAIP2	93	89.8	127.6	116	127.6	113.3	-0.4	-0.41	0.02
Q96DH6	MSI2	1537.5	1521.2	1789.3	1591.8	2066.5	1970.8	-0.4	-0.14	-0.26
Q9Y295	DRG1	784.7	740.9	770.7	607.5	906.2	1117.5	-0.41	0.15	-0.55
P47897	QARS	6732.9	6555.4	5913.9	5319.9	9017.1	8648.4	-0.41	0.24	-0.65
Q3MHD2-2	LSM12	134.4	171.3	157.7	141	256.1	150.3	-0.41	0.03	-0.44
O75400	PRPF40A	78.9	86.5	101.4	93.2	111.4	108.7	-0.41	-0.23	-0.18
H7C2I1	PRMT1	443.1	408.4	450.8	345.9	621.7	511.9	-0.41	0.1	-0.51
A0A087WWS1	THOC1	534.3	489.2	503.7	411.2	755.1	608.8	-0.41	0.16	-0.58
Q15649	ZNHIT3	116.7	114.8	143.3	130	188.8	119.6	-0.41	-0.24	-0.17
J3KR35	CCDC12	119.5	154.3	134.2	144.5	177.5	188.4	-0.42	-0.03	-0.39
Q15024	EXOSC7	452.2	460.9	517.2	456.5	622.5	602.1	-0.42	-0.09	-0.33
U3KQK0	HIST1H2BN	100.1	103	103.8	94.5	141.5	130.1	-0.42	0.03	-0.45
P24534	EEF1B2	1251.3	1148.4	1473	1366.7	1638.3	1593.1	-0.43	-0.24	-0.19
P16403	HIST1H1C	476	361	315.3	249.5	654.6	470.9	-0.43	0.57	-0.99
P56192	MARS	6531	6777.7	5784.2	5616.6	9189.3	8705.5	-0.43	0.22	-0.65
Q13283	G3BP1	6921.2	7986.4	9619.4	9933.5	10194	9860.7	-0.43	-0.39	-0.04
P29558	RBMS1	497.8	465.4	547.3	614.4	746.1	554.2	-0.43	-0.27	-0.16
P50991	CCT4	1194.4	1018.2	971.3	911.1	1862.6	1119.5	-0.43	0.23	-0.66
O75175	CNOT3	594.5	588.5	510.3	442.1	837	763.1	-0.44	0.31	-0.75
Q92879	CELF1	312.9	291.5	345.2	293.2	511.6	311.1	-0.44	-0.08	-0.37
P67809	YBX1	6401.1	6309.9	6998.9	7739.5	10018	7265.2	-0.44	-0.21	-0.23
Q8NC51	SERBP1	18689.7	18964.1	21323.5	21763.8	28824	22192	-0.44	-0.19	-0.24
Q9Y230	RUVBL2	732.8	787.9	725.7	614.9	1231.3	826.4	-0.44	0.18	-0.62
O95816	BAG2	172.5	193.5	201.8	170	302	198.8	-0.45	-0.02	-0.43
Q96F86	EDC3	833.6	750.2	744	580.1	1138.9	1031.6	-0.45	0.26	-0.71
A0A0U1RRH7	Histone H2A	676.5	670.9	589.6	511	832.2	1009	-0.45	0.29	-0.74
P50990	CCT8	3523.1	3055.4	2964.3	2611.4	5598.1	3397.4	-0.45	0.24	-0.69
Q6PJT7	ZC3H14	215.4	219.3	201.3	171.2	343.9	250.8	-0.45	0.22	-0.67
P11387	TOP1	147.3	151.4	166.5	156.9	262.9	148.8	-0.46	-0.11	-0.35
P41252	IARS	10590.3	10960.2	9641.6	8960.9	14881	14713	-0.46	0.21	-0.67
P62995	TRA2B	389.2	408.2	472.4	399.4	598.8	501.5	-0.46	-0.13	-0.34
Q13155	AIMP2	2468.1	2146.4	2084.4	1920.7	3381.3	2989.2	-0.47	0.2	-0.67
P61221	ABCE1	935	971.2	862.1	686.9	1398	1251.3	-0.47	0.3	-0.77
Q10567	AP1B1	180	168.5	174.3	157.6	306	181.1	-0.48	0.07	-0.55
Q9C0B0	UNK	187.6	177	228.9	211.8	260	249	-0.48	-0.27	-0.21

Q16563	SYPL1	192.2	200.2	240	183.8	308.6	239.2	-0.48	-0.11	-0.37
P54136	RARS	10431.3	9725.4	9613	8729.6	14630	13675	-0.49	0.14	-0.63
Q6IBR2	FARSLA	345.5	328.1	522.8	469.8	464.8	481.6	-0.49	-0.56	0.07
Q9NWZ8	GEMIN8	226.9	180	220.7	217.5	297.5	275.8	-0.49	-0.11	-0.39
P08238	HSP90AB1	1024.3	817.7	944.9	742.4	1523.7	1066.1	-0.49	0.13	-0.62
Q13148	TARDBP	354.5	379.9	368.2	318.8	628.2	406.6	-0.49	0.1	-0.59
P09012	SNRPA	265	218.5	270	226	419.9	257.6	-0.49	-0.04	-0.45
P16520	GNB3	171.5	178.8	208.9	165.2	307.2	190.9	-0.51	-0.09	-0.41
E5RJR5	SKP1	190.4	183.2	192.4	196.7	318.9	213.5	-0.51	-0.06	-0.45
P49368	CCT3	1139.1	914	1005.4	949.2	1791.5	1123	-0.51	0.07	-0.58
Q96QR8	PURB	362.6	336.1	342.9	355.9	556.4	441.8	-0.51	0	-0.51
P51148-2	RAB5C	67.5	56.3	69.2	46	96	81.4	-0.52	0.1	-0.62
P31689	DNAJA1	233	159.7	191.3	151.4	360	206.8	-0.53	0.2	-0.73
P14868	DARS	5221.3	5135.1	4667.4	4393.8	7975.9	7109.8	-0.54	0.19	-0.74
Q13838-2	DDX39B	1478.6	1581.8	1486.7	1221.7	2760.7	1675.5	-0.54	0.18	-0.71
P17987	TCP1	1683.9	1492.2	1396.3	1276.5	3028.8	1593.5	-0.54	0.25	-0.79
O95985	TOP3B	19.7	22.4	25.3	22.4	34.2	28.1	-0.57	-0.18	-0.39
O00139-4	KIF2A	96.6	100.6	101.1	90.4	176.1	116.8	-0.57	0.04	-0.61
Q9P2J5	LARS	13031.7	12489.2	11419.5	11104.1	19787	18073	-0.57	0.18	-0.75
P49006	MARCKSL1	95.1	71.8	84.3	72	154.5	93.5	-0.57	0.09	-0.67
Q08170	SRSF4	737.1	650.4	722.8	593	1229	833.4	-0.57	0.08	-0.65
P19338	NCL	3600.5	4200.2	5290.7	4492.9	6207	5469.4	-0.58	-0.33	-0.26
Q15836	VAMP3	188.5	193.6	197.4	160.3	353.3	219.4	-0.58	0.1	-0.68
Q12904	AIMP1	4214	3963.9	3698.5	3638.1	6584.3	5744.7	-0.59	0.16	-0.75
Q15046	KARS	4744.1	4666.5	4657	4240.6	7425.8	6701.6	-0.59	0.08	-0.67
P52298	NCBP2	98.8	104.1	119.9	128.6	203.5	101.6	-0.59	-0.29	-0.3
Q13263	TRIM28	3582.3	3657.5	3998.2	3190	6165.5	4753.5	-0.59	0.01	-0.6
P07814	EPRS	19073.2	17421.8	16728.5	16370.7	29685	25801	-0.6	0.14	-0.75
Q9Y3F4-2	STRAP	1103.9	1246.5	1271.9	1243.4	1933.2	1637.2	-0.6	-0.1	-0.51
P16989-2	YBX3	427.2	374.3	495.7	525.8	702.2	512	-0.6	-0.35	-0.25
Q9UQ35	SRRM2	1004.8	983.7	1014.2	862.8	1761.5	1245.5	-0.6	0.08	-0.68
Q16576-2	RBBP7	79.4	81.6	88.9	74	133.4	111.8	-0.61	-0.02	-0.59
Q92900	UPF1	5099.5	5043.2	4096.8	3508.6	8584.7	6924.6	-0.61	0.42	-1.03
Q5JWF2	GNAS	360.9	312.7	421.6	277.3	624	409.3	-0.62	-0.05	-0.56
Q8IU60	DCP2	245	239.5	182.9	164.5	403.1	342.6	-0.62	0.48	-1.1
Q5SY16	NOL9	105.4	95.7	92.2	78.9	172.2	139	-0.63	0.23	-0.86
P60903	S100A10	206.2	213.7	269.7	202.3	382.5	277.7	-0.65	-0.17	-0.48
Q9UHC7	MKRN1	91.3	112.2	131	143.1	179.4	142	-0.66	-0.43	-0.23
O43324	EEF1E1	1015.9	1084.4	1032.9	985.2	1760.5	1568.2	-0.66	0.06	-0.72
E7ERS3	ZC3H18	49.4	53.2	40.1	39.3	109.5	53	-0.66	0.37	-1.03
P35613	BSG	563.7	497.3	720.6	473.4	1096.6	599.1	-0.68	-0.17	-0.51
Q9Y5A9	YTHDF2	1099.6	1118.2	1326.7	1313.1	2108.6	1437.6	-0.68	-0.25	-0.43
Q92843-2	BCL2L2	613.6	609.3	752.6	687	1121	852	-0.69	-0.24	-0.45
Q14444	CAPRIN1	7271.4	7618	10728.8	11188.6	12759	11383	-0.7	-0.56	-0.14
Q15428	SF3A2	55.7	61.5	48.6	51.9	119.2	71.2	-0.7	0.22	-0.92
Q16629	SRSF7	204.6	199.6	196.3	176.7	387.7	284.2	-0.73	0.12	-0.85
P62314	SNRPD1	100	83.9	94.3	94.2	179.2	132.9	-0.76	-0.04	-0.73
Q7RTV0	PHF5A	69.6	60.6	51.3	46.5	131.2	94.8	-0.8	0.41	-1.21
Q969S3	ZNF622	129.9	129.1	155.6	118.3	248.3	204.2	-0.8	-0.08	-0.72
P20618	PSMB1	118.5	78	89.4	56.6	244.4	105	-0.83	0.43	-1.26
P07237	P4HB	235.1	200.1	232.3	189.2	480.3	316.4	-0.87	0.05	-0.92
Q5RKV6	EXOSC6	33.8	46.9	70	62.9	86	62.5	-0.88	-0.72	-0.16
Q13242	SRSF9	50.4	61.8	73.3	56.8	124.8	86.7	-0.91	-0.21	-0.7
P62318	SNRPD3	166.5	225	205.1	200.8	493.7	266.2	-0.96	-0.05	-0.9

P56537	EIF6	705.6	672.2	887.1	774.5	1609.2	1431.7	-1.14	-0.27	-0.87
O75822	EIF3J	361.3	308.1	371.4	285.3	911.3	569.9	-1.15	0.03	-1.17
Q9NU22	MDN1	47.9	65.3	66.9	52.5	152.8	101.2	-1.17	-0.08	-1.09
P53985	SLC16A1	109.7	66.8	129.7	79.9	282.7	118.9	-1.19	-0.25	-0.94
P18583-9	SON	31.8	41.8	42.4	33.5	117.7	63	-1.3	-0.04	-1.25
P12532-2	CKMT1A	158	204.4	231	172.8	519.4	428.3	-1.39	-0.16	-1.23
O75534-4	CSDE1	3.5	10.1	16.5	14.1	33.8	16.4	-1.88	-1.17	-0.71
F8W727	RPL32	11814.8	25359.9	10912.2	11786.7	10292	11722	0.76	0.71	0.04
P62263	RPS14	13019.6	9455	9675.6	8695.3	8202.9	9526.4	0.34	0.29	0.05
P83731	RPL24	12200.6	17699.9	12312	13672.6	13642	12212	0.21	0.2	0.01
P05386	RPLP1	7847.4	6690.8	6883.5	7615.4	5214.2	7441	0.2	0	0.2
Q9Y3U8	RPL36	3481.9	3859.8	3282	2800	3225.4	3163.9	0.2	0.27	-0.07
P62081	RPS7	9111.2	9649.1	9259.6	8889.6	8316.3	8496.6	0.16	0.05	0.11
P62829	RPL23	13407.4	14274.7	13867.3	13590.4	10749	14278	0.15	0.01	0.13
P61353	RPL27	7740.5	7811.4	6560.1	5949.2	7394.2	6594.3	0.15	0.31	-0.16
Q02878	RPL6	15467.9	17081.3	14824.1	14045.9	14658	14654	0.15	0.17	-0.02
P60866	RPS20	3848.2	4100.5	3963.6	3745.9	3338.2	3872.8	0.14	0.04	0.1
P62854	RPS26	2747.7	3485.8	3071.3	2947.8	3065.2	2591.9	0.14	0.05	0.09
P62891	RPL39	272.3	273.7	218.8	240.3	247.2	249.4	0.14	0.25	-0.11
P62244	RPS15A	6606.3	7156.1	6640.7	6107.6	6427.6	6211.4	0.12	0.11	0.01
P15880	RPS2	28189.5	28781	28466.3	27520.4	26272	27012	0.1	0.03	0.07
P62851	RPS25	5108.8	6065.8	5116.2	5399	5283.4	5107.4	0.1	0.09	0.02
P46782	RPS5	11840	13179.2	13744.9	14556.2	10666	12749	0.1	-0.18	0.27
P35268	RPL22	5031	5652.4	5243.7	5296.8	4650.8	5410.7	0.09	0.02	0.07
P62269	RPS18	9419.9	8865.8	9088.5	8814.5	8719.4	8620.3	0.08	0.03	0.05
P05387	RPLP2	13786.8	14069.7	12650.3	12506.9	13250	13122	0.08	0.15	-0.07
P62750	RPL23A	20655.2	20663.5	20142.1	19804.9	19065	19902	0.08	0.05	0.04
P62277	RPS13	9704.2	9369.8	9677.5	9420.5	8978.8	9169.1	0.07	0	0.07
P05388	RPLP0	19355.7	18330.9	19869.1	20413.9	17437	18545	0.07	-0.1	0.16
P50914	RPL14	7139.6	7575.8	8242.3	8368.6	6393.6	7821.7	0.05	-0.17	0.22
P42677	RPS27	2888.7	2948.4	2824.7	2781.3	2866.2	2824.7	0.04	0.06	-0.02
P61247	RPS3A	19862	19224.3	18226.6	17869.3	19571	18554	0.04	0.11	-0.08
A0A0C4DG17	RPSA	18424.7	16877.5	17090.5	16593.3	16798	17598	0.04	0.07	-0.03
P18124	RPL7	22687.7	20918.4	21346.9	21091.5	20680	21796	0.04	0.04	0
P25398	RPS12	13465.8	12986.9	14073.5	14961.8	11980	13925	0.03	-0.13	0.16
P62906	RPL10A	10668.3	11777.4	12739.6	13153.1	9222	12833	0.03	-0.21	0.23
P46778	RPL21	9877.8	9645	9086.1	9010	9767.9	9419.3	0.03	0.11	-0.08
P27635	RPL10	11217.8	10459	10288.9	10201.5	10904	10424	0.02	0.08	-0.06
P36578	RPL4	31631.5	32004.4	32104.1	32908.5	29803	32905	0.02	-0.03	0.05
P62249	RPS16	10647.6	11062	10863.6	10355.9	11740	9776.3	0.01	0.03	-0.02
P32969	RPL9	10054.5	9968.7	10454.9	10452.8	9280.9	10573	0.01	-0.06	0.07
P46776	RPL27A	4614.5	4500.4	4318.7	4199.8	4772	4340.4	0	0.1	-0.1
P46781	RPS9	12744.5	13758.3	14582.8	13719	14163	12657	-0.02	-0.09	0.08
P62917	RPL8	10638.4	9877.7	10404.6	9965.3	10246	10617	-0.02	0.01	-0.03
P39019	RPS19	18881.9	19481.6	19012.1	21021.4	20178	18866	-0.03	-0.06	0.04
P63220	RPS21	1745.5	1438.6	1534.6	1468.4	1737.9	1511.4	-0.03	0.08	-0.11
P26373	RPL13	7258.7	6756.9	6569.2	6830.7	7359	6944.8	-0.03	0.06	-0.09
J3QQ67	RPL18	9047.8	8581.8	9741	9243	8508.1	9502.6	-0.03	-0.11	0.08
Q02543	RPL18A	7011.1	7067.1	7407.9	7244.3	6678.1	7669.7	-0.03	-0.06	0.03
P46783	RPS10	10865.3	9770.1	9959	9116.7	11234	9946.1	-0.04	0.11	-0.15
P08708	RPS17	12475	10974.9	11813	12232.1	12103	11982	-0.04	-0.04	0
P23396	RPS3	24242.1	25025.7	25482.3	24753.3	26685	24004	-0.04	-0.03	-0.01
P62913	RPL11	9509	9829.4	10103.3	10293.4	9227.5	10618	-0.04	-0.08	0.04

P39023	RPL3	21637.6	19817.8	21032.7	21489.1	20810	21925	-0.04	-0.04	-0.01
P62888	RPL30	8605.6	9109.6	8721.2	8354.6	9361.2	8882.4	-0.04	0.05	-0.1
P62280	RPS11	10815.8	11288.3	11168.1	11263.9	12369	10457	-0.05	-0.02	-0.03
P62273	RPS29	1351.6	1140.5	1252.2	1158	1403.1	1180.3	-0.05	0.05	-0.1
P40429	RPL13A	12235.7	11502.5	11944.9	11797.1	12511	12077	-0.05	0	-0.05
P62424	RPL7A	19357	17693	18965.6	18544.6	18470	19932	-0.05	-0.02	-0.03
P62753	RPS6	17457.8	16635.3	17075.8	17414.7	18597	16933	-0.06	-0.02	-0.04
P47914	RPL29	2209	2028.7	1910.4	1761.8	2406.2	2013.6	-0.06	0.21	-0.27
K7ELC2	RPS15	10077.3	7757.3	8660.7	9000.9	9593.3	9130	-0.07	0.01	-0.08
P62701	RPS4X	20290.6	19780.2	21628.1	20819	21612	20346	-0.07	-0.08	0.02
P61313	RPL15	7102.8	6730.7	6991.6	7191.5	7285.5	7248.2	-0.07	-0.04	-0.04
P62899	RPL31	7337.4	6700.9	7192.3	7147.2	7357.1	7400.6	-0.07	-0.03	-0.04
F8W7C6	RPL10	2229.1	2148	2105.2	2185.8	2304.6	2315.2	-0.08	0.03	-0.11
P46779	RPL28	6906.8	5556.3	6073.9	5986.2	7006.4	6179.2	-0.08	0.05	-0.13
P42766	RPL35	5352.7	5424.5	5116.2	5107.2	6411.4	5002	-0.08	0.08	-0.16
P61254	RPL26	5566.6	4779.2	4937.7	4668.6	6069.1	4912.9	-0.09	0.11	-0.19
P30050	RPL12	9327.4	8684.5	9465.1	9284.8	9949.3	9323.1	-0.1	-0.06	-0.04
P61513	RPL37A	5061.3	4793.8	5465.5	5110.1	5239	5427.7	-0.11	-0.1	-0.01
P46777	RPL5	16668	15663.4	16912.7	17151.7	17017	17870	-0.11	-0.08	-0.03
P63173	RPL38	11076.3	9089.8	9315.6	9232.5	12163	9698.2	-0.12	0.12	-0.24
P84098	RPL19	7527.4	6625.6	7071.6	6824.5	7873.6	7584.2	-0.13	0.03	-0.15
J3KQN4	RPL36A	4425.1	3349.1	3603	3333.6	5099.7	3552.9	-0.15	0.16	-0.32
P62241	RPS8	19161.6	18699.1	19101.6	18981.8	22808	19380	-0.16	-0.01	-0.15
P61927	RPL37	3038.2	2615.4	3046.1	3043.9	3179.6	3133.2	-0.16	-0.11	-0.05
P62857	RPS28	3506.4	2883.9	3320.7	3638.7	3665.5	3610.3	-0.19	-0.12	-0.06
P62266	RPS23	7551	7297.7	8263.3	8398	8943.3	8087.4	-0.2	-0.17	-0.03
P49207	RPL34	8646.9	8208.6	8313.4	9258.5	11014	8664.8	-0.22	-0.06	-0.16
E9PR30	FAU	4059.3	3605	4060.3	4552.1	5152.4	3899.3	-0.24	-0.17	-0.07
P18077	RPL35A	10735.6	10933.5	12708.4	14043.9	12420	13305	-0.25	-0.3	0.06